

Novel SMAC Mimetics as Peptide-based Small Molecule Inhibitors of IAPs to Induce Apoptosis in Cancer Cells

By: Kyle McClymont

Thesis submitted to the
Faculty of Graduate and Postdoctoral Studies
in fulfilment of the requirements for the
Masters of Science degree in Chemistry at the University of Ottawa

Candidate

Supervisor

Kyle S. McClymont

Robert N. Ben

© Kyle McClymont, Ottawa, Canada, 2015

Dedication

To my friends and family, for all their help and support over these past two years

Table of Contents

List of Figures.....	v
List of Tables.....	vi
List of Schemes.....	vi
Abstract.....	viii
Acknowledgements.....	ix
List of Abbreviations.....	x
Chapter 1: Apoptosis and Cancer	1
1.1 Cancer and Human Disease.....	1
1.1.1 The Origins of Cancer	1
1.1.2 Treatment Strategies	2
1.2 Apoptosis.....	2
1.2.1 General Overview	2
1.2.2 Caspases: The Effectors of Apoptosis	4
1.2.3 Caspase Activation: Comparing the Intrinsic and Extrinsic Pathways of Apoptosis ...	6
1.2.4 Apoptotic Regulation: The role of IAPs and SMAC	10
1.3 SMAC Mimetics	14
1.3.1 Background	14
1.3.2 Mechanism of Action	16
1.4 Concluding Remarks.....	18
1.5 References.....	18
Chapter 2: The Development of SMAC Mimetics to Treat Cancer.....	28
2.1 Early SAR Work.....	28
2.2 Classes of SMAC Mimetics	31
2.2.1 Monovalent SMAC Mimetics	31
2.2.2 Bivalent SMAC mimetics	37
2.3 SMAC Mimetics: A Bright Future.....	44
2.4 Goals and Objectives: Logical Design of Novel SMAC Mimetics.....	45
2.4.1 General Approach	45
2.4.2 Modifications to P2 - Monomers	46
2.4.3 Exploring P2 Linker Strategies	47

2.4.4 Exploring P4 Linker Strategies	47
2.5 References.....	50
Chapter 3: Synthesis and Testing of Monovalent and Divalent SMAC Mimetics in MDA-MB-231 Breast Cancer Cells.....	56
3.2 Modifications to P2 – Monomers 33-36.....	56
3.3 P2 Linker Strategies– Compounds 56, 58, 64, 66.....	61
3.4 Exploring P4 Linker Strategies.....	65
3.4.1 Triazole P4 Linkers – Compounds 79 and 82	66
3.4.2 C-linked P4 linkers – Compounds 84, 86, 88 and 91	68
3.4.3 Oxidized P4 Linkers – Compounds 94 and 97	71
3.4.4 Dimerization at the P4 residue – Compounds 99, 101 and 103	75
3.5 Caspase-3/7 Activation – Confirmation of Apoptosis as a Mechanism of Cell Death.....	78
3.6 Results Summary	79
3.7 Future Work.....	82
3.8 References.....	83
Experimental Protocols and Characterization Data.....	87
General Materials and Methods for Chemical Synthesis.....	87
General Peptide Coupling Procedure	88
General Boc-deprotection Procedure	88
General Methods and Materials for Cell Based Viability Assays	88
General Cell Culture.....	88
AlamarBlue® Viability Assay.....	89
Apo-ONE® Homogeneous Caspase-3/7 Assay	89
Data Plotting and IC₅₀ Calculations	90
Statistical Analysis	90
Cryopreservation of Cell line	90
Experimental Protocols and Characterization Data for Chemical Compounds	91
References.....	131
Appendix I: Cellular morphology Images.....	134
Supplementary Spectral Data	136

List of Figures

Figure 1. Comparative histology of apoptotic vs. necrotic cells.....	3
Figure 2. (A) General scheme of apoptotic activation (B) General representation of initiator procaspase 8/9.....	4
Figure 3. Structural representation of executioner caspase 7 homodimer	5
Figure 4. A schematic representation of cytochrome C release from the mitochondria promoted by the activity of the BH3 proteins of the Bcl-2 family.....	7
Figure 5. Schematic representation of the modes of extrinsic apoptotic activation.....	9
Figure 6. A linear representation of the human IAP proteins	11
Figure 7. Representation of the XIAP BIR2 two point binding model.	11
Figure 8. (A) SMAC homolog used by Jiang to probe the mechanism of SMAC-XIAP interaction (B) Structural model of SMAC homodimer	12
Figure 9. Close up view of the interaction between the N-terminal AVPI sequence of SMAC (green) and the BIR3 IBM binding groove of XIAP	15
Figure 10. (A) SMAC mimetics promote cIAP self-degradation. (B) SMAC mimetic TNFR1 mediated caspase 8 activation	17
Figure 11. Examples of early SMAC peptidomimetics.....	30
Figure 12. A general scheme for SMAC mimetic design.....	30
Figure 13. Examples of potent, bicyclic monovalent SMAC mimetics	33
Figure 14. Some examples of potent non-constrained SMAC monomers.....	36
Figure 15. Examples of non-peptide based SMAC mimetics.....	37
Figure 16. Results showing that siRNA inactivation of either TNF- α or caspase-8 significantly hampers induction of cell death by 20	38
Figure 17. Examples of potent P4 linked SMAC mimetic dimers reported by Wang.....	39
Figure 18. Some examples of potent P4 linked SMAC mimetics.....	41
Figure 19. Some potent bivalent SMAC mimetics linked at P2.	42
Figure 20. Some examples of unusual SMAC dimers from the recent literature linked at P3.....	43
Figure 21. SMAC mimetic scaffold used in the design of our compound series.	45
Figure 22. Monovalent P2 modification targets 33-36	46
Figure 23. P2 linked bivalent targets 56, 64 and 66	47
Figure 24. 1,2,3 triazoles as isosteres for an amide linkage.....	49
Figure 25. Functional antagonism of SMAC mimetics 33-36 and 50 against MDA-MB-231 breast cancer cells in a dose-responsive manner	60
Figure 26. Functional antagonism of SMAC mimetics 56, 58, 64 and 66 against MDA-MB-231 breast cancer cells in a dose-responsive manner.....	64
Figure 27. Functional antagonism of SMAC mimetics 79 and 82 against MDA-MB-231 breast cancer cells in a dose-responsive manner	68
Figure 28. Functional antagonism of SMAC mimetics 84, 86, 88 and 91 against MDA-MB-231 breast cancer cells in a dose-responsive manner.....	71

Figure 29. Functional antagonism of SMAC mimetics 94 and 97 against MDA-MB-231 breast cancer cells in a dose-responsive manner	74
Figure 30. Functional antagonism of SMAC mimetics 99 , 101 and 103 against MDA-MB-231 breast cancer cells in a dose-responsive manner.....	77
Figure 31. Functional activation of Caspase-3/7 by the denoted compounds at 10 μ M in MDA-MB-231 breast cancer cells assessed using an Apo-ONE assay.....	78
Figure 32. Proposed targets for future synthesis and testing.....	82

List of Tables

Table 1. Comparison of binding affinities for cIAP selective (6) and pan selective (7) SMAC mimetics.....	34
Table 2. Experimental conditions for the thiolation of 38	57
Table 3. Properties of compounds 33-36 and 50	59
Table 4. Properties of bivalent SMAC mimetics 56 , 58 , 64 , 66	63
Table 5. Properties of P4 triazole-linked monovalent SMAC mimetics 79 and 82	67
Table 6. Properties of C-linked monovalent SMAC mimetics 84 , 86 , 88 and 91	70
Table 7. Properties of P4 oxidized linker SMAC mimetics 94 and 96	73
Table 8. Properties of P4 linked SMAC mimetics 99 , 101 and 103	76
Table 9. List of compounds tested with IC ₅₀ values against MDA-MB-231 breast cancer cells... 80	
Table 10. Images of MDA-MB-231 breast cancer cells treated with denoted compound at either 10 μ M or 10 nM.	134

List of Schemes

Scheme 1. P4 linker modification targets from common precursor 67	48
Scheme 2. Synthesis of aryl sulfide 39 <i>via</i> direct substitution of prolinol 37	56
Scheme 3. Phosphonium salt proposed by Hata and co-workers.....	56
Scheme 4. Synthesis of SMAC monomers 33 , 34 and 36	58
Scheme 5. Synthesis of 35	58
Scheme 6. Synthesis of P3 glycine insert 50 as negative control.	59
Scheme 7. Synthesis of bivalent SMAC mimetic 56	61
Scheme 8. Synthesis of bivalent SMAC mimetic 58	61
Scheme 9. Synthesis of bivalent SMAC mimetic 64 bearing a saturated alkyl linker.....	62
Scheme 10. Synthesis of bivalent SMAC mimetic 66 possessing a long, rigid linker	63
Scheme 11. Ohira-Bestman reagent.....	65
Scheme 12. Synthesis of intermediate 67	66

Scheme 13. Synthesis of triazoles 79 and 82	67
Scheme 14. Synthesis of C-linked analogues 84, 86, 88, 91	69
Scheme 15. Synthesis of bivalent sulfone 94	72
Scheme 16. Mercury nitrate mediated oxidation of internal alkynes.	72
Scheme 17. Synthesis of ketone 97 + side product 95	73
Scheme 18. Synthesis of P4 linked bivalent SMAC mimetic 99 and 6-bromo monomer 101	75
Scheme 19. Synthesis of P4 linked negative control 103	75

Abstract

SMAC mimetics (Secondary Mitochondria-derived Activator of Caspases) have generated significant interest as potential chemotherapeutic compounds *via* their ability to promote apoptosis in cancer cells. These molecules target several Inhibitor of Apoptosis Proteins (IAPs) including XIAP (X-linked Inhibitor of Apoptosis Protein) and cIAP-1/2 (Cellular Inhibitor of Apoptosis Proteins 1 & 2) whose elevated expression is ubiquitous with tumorigenesis. We report the design, synthesis and evaluation of novel SMAC based peptidomimetics which appear to mirror the anti-IAP of SMAC *in vitro*. We combined elements of reported SMAC mimetics with unique structural features in an attempt to design novel, efficacious IAP antagonists. Our approach included modifications to the 2nd and 4th residues of the AVPI peptide sequence, which is known to be the motif responsible for SMAC 's interaction with its native substrates. Cell-based compound testing against MDA-MB-231 breast cancer cells identified several promising lead structures possessing nanomolar cytotoxic effects. Apoptotic activity was confirmed *via* the detection of capsase-3/7 activation, a hallmark of regulated cell death. Our experimental data suggests we have developed selective, potent anti-cancer compounds which can be further developed in the pursuit of new anti-cancer therapeutics.

Acknowledgements

There are so many people to thank who have helped make my time at uOttawa an incredible experience.

To my lab mates, thank you for creating such a collegial environment and for keeping those long days in the lab entertaining. I'll miss our group lunches, lab parties and coffee runs to Timmies.

Thank you to the other students in the department who were always willing to lend a reagent or give advice when it was needed.

To the office staff Jose, Annette and Linda, who kept things running smoothly and made sure I was always paid on time.

Thank you to the incredible professors in the Department of Chemistry with whom I have had the pleasure of interacting. They have been great teachers and have contributed enormously to my growth as a chemist over these past two years.

To my supervisor, Dr. Robert Ben for his support and mentorship. Thank you for taking that chance back when I was in my 3rd year of undergrad and giving me a summer lab job, I think it ended up working out ok.

Thank you to my friends with whom I shared many pints and who put up with my chemistry ideas/stories... for the most part.

Most of all thank you to my parents and my sister for their patience and love. And to my mom for always having me home for Sunday dinner.

List of Abbreviations

α	alpha
β	beta
γ	gamma
δ	delta
μL	microliter
^1H	proton
^{13}C	carbon
Ac	acetyl
ACD	accidental cell death
Ac_2O	acetic anhydride
Ala	alanine
$\text{BF}_3 \cdot \text{OEt}_2$	boron trifluoride diethyl etherate
BIR	baculovirus IAP repeat
Bn	benzyl
Boc	<i>tert</i> -butyloxycarbonyl
Boc_2O	Di- <i>tert</i> -butyl dicarbonate
br	broad
CaCl_2	calcium chloride
Cat.	catalytic
CDCl_3	deuterated chloroform
CD_3OD	deuterated methanol
CH_3CN	acetonitrile
CH_2Cl_2	dichloromethane
CI	confidence interval
cIAP	cellular inhibitor of apoptosis protein

cLogP	calculated logP
CN	nitrile
CuI	copper iodide
Cu ₂ SO ₄	copper(II) sulfate
d	doublet
D ₂ O	deuterium oxide
dppb	1,4-Bis(diphenylphosphino)butane
DD	death domain
dd	doublet of doublets
DED	death effector domain
DIAD	Diisopropyl azidodicarboxylate
DISC	Death Inducing Signalling Complex
DIPEA	diisopropylethylamine
DMF	dimethyl formamide
DMSO	dimethyl sulfoxide
DR	death receptor
dt	doublet of triplets
ESI	electrospray ionization
Et	ethyl
Et ₂ O	diethyl ether
EtOAc	ethyl acetate
EtOH	ethanol
FADD	Fas Adaptor Death Domain
FBS	fetal bovine serum
Fmoc	9-fluorenylmethyloxycarbonyl
Gly	glycine
HCl	hydrochloric acid

HCTU	2-(6-chloro-1H-benzotriazole-1-yl)-1,1,3,3-tetramethylammonium hexafluorophosphate
HPLC	high performance liquid chromatography
HRMS	high resolution mass spectrometry
hrs	hours
IAP	inhibitor of apoptosis protein
IBM	IAP binding motif
IPAc	isopropyl acetate
kDa	kiloDaltons
LRMS	low resolution mass spectrometry
m	multiplet
M	molar
M ⁺	parent molecular ion
Me	Methyl
MeOH	methanol
MHz	megahertz
mM	millimolar
MS	mass spectrometry
NaH	sodium hydride
Na ₂ SO ₄	sodium sulfate
NaHCO ₃	sodium hydrogen carbonate
NaOH	sodium hydroxide
NaOMe	sodium methoxide
Nap-SH	2-naphthalenethiol
(Nap-S) ₂	2-naphthyl disulfide
NF-κB	nuclear factor kappa B
O/N	overnight

PEG	poly ethylene glycol
pen/strep	penicillin/streptomycin
PG	protecting group
Pd/C	palladium on carbon
Pd ₂ (dba) ₃	tris(dibenzylideneacetone)dipalladium
Pd(PPh ₃) ₄	tetrakis(triphenylphosphine)palladium
pKa	acid dissociation constant
Pra	propargylglycine
Pro	proline
PSA	polar surface area
q	quartet
RCD	regulated cell death
Rf	retention factor
RIPK1	receptor-interacting serine/threonine protein kinase 1
RPM	revolutions per minute
RT	room temperature
SAR	structure activity relationship
s	singlet
SEM	scanning electron microscopy
SM	starting material
SMAC	second mitochondria-derived activator of caspases
SPPS	solid phase peptide synthesis
t	triplet
TBAF	<i>tert</i> -butylammonium fluoride
TBS	<i>tert</i> -butyldimethylsilyl
TEA	triethylamine
TEM	transmission electron microscopy

TFA	trifluoroacetic acid
THF	tetrahydrofuran
TMS	trimethylsilyl
TNF α	tumor necrosis factor alpha
TNFR1	tumor necrosis factor receptor 1
TRAIL	TNF related apoptosis inducing ligand
TRADD	TNF type I-associated death domain protein
VT-NMR	Variable temperature nuclear magnetic resonance
XIAP	X-linked inhibitor of apoptosis protein

This page was intentionally left blank

Chapter 1: Apoptosis and Cancer

1.1 Cancer and Human Disease

1.1.1 The Origins of Cancer

Cancer has grown to be a pervasive problem for humanity, and an often challenging condition for medical professionals to treat. Contrary to the common belief that the incidence of cancer has increased over time due to industrialization and increased exposure to man-made toxins many studies have clearly identified humanity's ever increasing lifespan as the catalyst for oncogenesis.¹² A recent study by the NIH has helped to de-convolute the mechanism of age related carcinogenesis and found that age associated DNA methylation at specific sites produced a reduced threshold for malignant transformation.¹³ While age plays a significant role, several risk factors for cancer have been identified over many decades of research. Ezzati and colleagues published a 2005 study in *The Lancet* identifying the top nine environmental risk factors for cancer which are responsible for 1 in 3 cancer related deaths.¹⁴ The major risk factors reported were: Obesity, low fruit/vegetable intake, physical inactivity, smoking, alcohol abuse, unprotected sex, urban air pollution, second hand smoke, contaminated injections leading to hepatitis.

The mechanism by which age and environmental/behavioral risk factors produce cancer is complicated however a general trend is clear, genotoxic stress leads to cancer. Accumulated mutations from transcriptional error, viral infection or DNA electrophiles can de-regulate genetic expression and trigger oncogene activation. Tumorigenesis generally materializes through the over- or under-expression of several well characterized genes and can be grouped into mutations leading to either autocrine growth-factor secretion, anti-proliferative signal insensitivity and the evasion of apoptotic signalling.¹⁵

In the context of apoptotic evasion, several key proteins have been identified for the potentiation of anti-apoptotic phenotypes. Suppression or deletion of genes encoding tumor suppressor proteins such as p53¹⁶ and p16¹⁷ are well known to potentiate uncontrolled cell growth. In addition, over-expression of pro-survival genes can help cells circumvent the process of

apoptosis. Ras (rat sarcoma) protein is mutated in 20-30% of all cancers¹⁸ and is a common tumor promoting protein. Ras can activate Akt/PKB (protein kinase B) activity through PI3K (phosphoinositide 3 kinase) activation which produces several downstream effects.¹⁹ Akt/PKB is a pro-survival protein with several mechanisms of action; it can phosphorylate and inactivate BAD leading to inhibition of the intrinsic apoptotic pathway.²⁰ Additionally, Akt/PKB activity activates proteins which promote NF- κ B gene activation and the expression of IAPs as well as other pro-survival proteins.²¹

1.1.2 Treatment Strategies

Despite the accumulation of detailed knowledge surrounding cancer biology and our relative understanding of the precise mechanisms governing its pathology we continue to treat cancer with a shotgun approach. Our current arsenal of chemotherapeutics such as microtubule destabilizing agents and topoisomerase inhibitors exhibit only modest selectivity for cancer cells by targeting those which are replicating fastest. This produces serious clinical side effects in patients receiving treatments and can make cancer therapy nearly as dangerous as the disease itself.²² There is a clear need for future therapeutics to employ our vast knowledge of cancer biology and design selective inhibitors of tumor proliferation which target specific pathways exclusively de-regulated in cancer cells. Fortunately, a new class of anti-cancer compounds known as SMAC mimetics promise to do exactly this. SMAC mimetics are proposed to function by artificially mimicking the pro-apoptotic activity of the endogenous protein SMAC *via* its AVPI IBM binding motif.²³ Although they are a relatively new class of compounds, having only been first reported in the early 2000s they hold the potential to become the first clinically approved tumor-selective cancer therapy.²⁴

1.2 Apoptosis

1.2.1 General Overview

Apoptosis can be defined as the process of regulated – or programmed – cell death (RCD) whereby a cell “commits suicide” by dismantling itself in a highly controlled fashion.²⁵ In contrast to the process of necrosis – or accidental cell death – (ACD), which is characterized by rapid cellular membrane compromise and inflammation.²⁶ Apoptosis is characterized by several

biochemical and morphological changes including: cell shrinkage, nuclear condensation and DNA fragmentation (laddering), as well as protein cross-linking and degradation.²⁷ The apoptotic cell dismantles itself, releasing its cellular components as membrane-bound fragments (apoptotic bodies) *via* a process termed ‘blebbing’ (Figure 1). Flipases move phosphatidyl serine from the apical surface to the outer surface of the plasma membrane, which promotes recognition and phagocytosis of these apoptotic bodies by nearby macrophages.²⁸ This mechanism circumvents the initiation of an inflammatory response by preventing the leakage of cellular content into the interstitium thus protecting nearby cells from associated damage.²⁹ Apoptosis has proven an essential process for tissue management in multicellular organisms. It has been implicated in the atrophic tailoring of limbs in embryonic development³⁰, destruction of pre-cancerous cells following DNA damage^{31,31b}, infection control^{32,32b} and cell death following exposure to toxic substances.³³

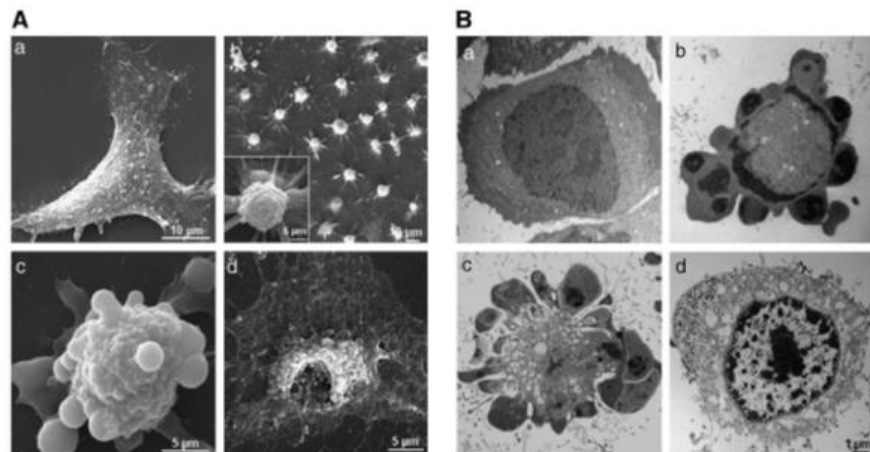


Figure 1. Comparative histology of apoptotic vs. necrotic cells.³⁴ **(A)** SEM images of HeLa human cervical carcinoma cells. (a) Healthy cell in interphase. (b) Cells undergoing early stage apoptosis. (c) Single cell undergoing late stage apoptosis, note the apoptotic bodies blebbing from the parent cell. (d) Single, late stage necrotic cell, note the swollen cellular footprint and loss of membrane definition. **(B)** TEM images of HeLa cells. (a) Healthy cell. (b) Early stage apoptotic cell. (c) Late stage apoptotic cell. (d) Late stage necrotic cell.

Horvitz and colleagues³⁵ reported the first empirical results specifically describing the mechanism of apoptosis in a living organism.³⁶ They examined the tightly controlled growth cycle of nematodes (*C. elegans*) and noted specific cellular attrition events, conserved between individuals, eluding to a pre-programmed cell death process. Their work triggered a cascade of investigations into the mechanism of apoptosis as well as its role in disease. Three decades of

research have shed considerable light on the cellular biochemistry comprising regulated cell death (RCD) while also revealing its considerable complexity. Central to the process of RCD are cysteine proteases known as caspases which act as the executioners of apoptosis by proteolytically degrading cellular proteins for absorption by nearby phagocytotic cells.³⁷ Apoptosis was initially thought to be the only means of RCD, however it has since been joined by numerous other unique forms of RCD which exist on a continuum between RCD and accidental cell death (ACD) possessing characteristics of each (e.g. necroptosis, pyroptosis).³⁸ Despite these revelations apoptosis remains the most well characterized form of RCD and constitutes a tightly linked network of cellular proteins which regulate the delicate balance between cellular life and death in the tissues of higher organisms.

1.2.2 Caspases: The Effectors of Apoptosis

Caspases are the drivers of apoptosis. Their name is a direct derivation of their catalytic activity, they are cysteine proteases which cleave proteins at the aspartic acid residue (c-asp-ase).³⁹ Caspases can be partitioned into two classes: initiator caspases (namely casp-8/9) and executioner caspases (namely casp-3/6/7). Caspases exist as inactive zymogens (procaspases) in healthy cells, the initiation of apoptosis depends on the activation of initiator caspases which

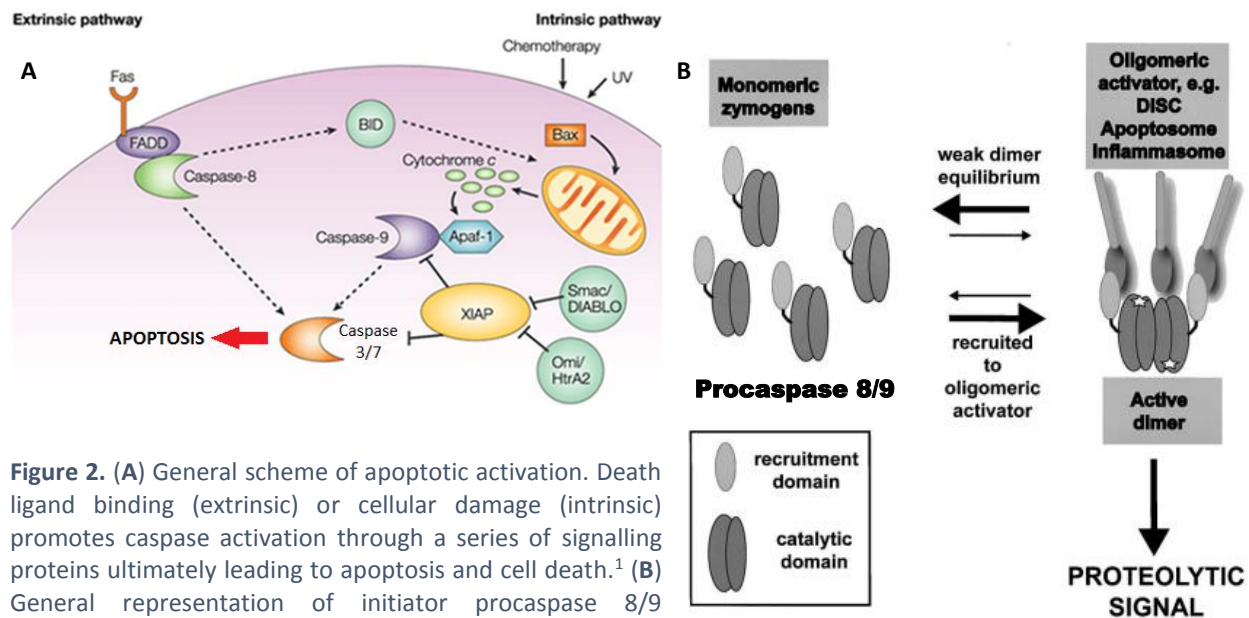


Figure 2. (A) General scheme of apoptotic activation. Death ligand binding (extrinsic) or cellular damage (intrinsic) promotes caspase activation through a series of signalling proteins ultimately leading to apoptosis and cell death.¹ (B) General representation of initiator procaspase 8/9 recruitment and dimerization to yield proteolytically active caspase 8/9.⁸

subsequently modify effector caspases to render them catalytically active and promote

apoptosis(Figure 2A).⁴⁰ Initiator (or apical) procaspases exist as inactive monomers with access to their active-site cysteine residues conformationally restricted. Structurally, they are composed of a large and small subunit as well as a recruitment domain: death effector domain (DED) for caspase 8⁴¹ and caspase activation recruitment domain (CARD) for caspase 9⁴² (*vida infra*). These recruitment domains serve to bring the procaspase monomers into close proximity during activation. This increase in local procaspase concentration triggers a dimerization event according to the induced proximity model proposed by Salvesen and Dixit.⁴³ Monomeric procaspase dimerization yields initiator caspase homodimers with exposed cysteine residues. These caspase dimers are catalytically active and capable of propagating the apoptotic pathway *via* downstream proteolytic cleavage of executioner caspases (Figure 2B).⁸

Executioner caspases are also composed of a large and small subunit, however they lack the recruitment domains seen in their apical counterparts. They exist as homodimers in their inert

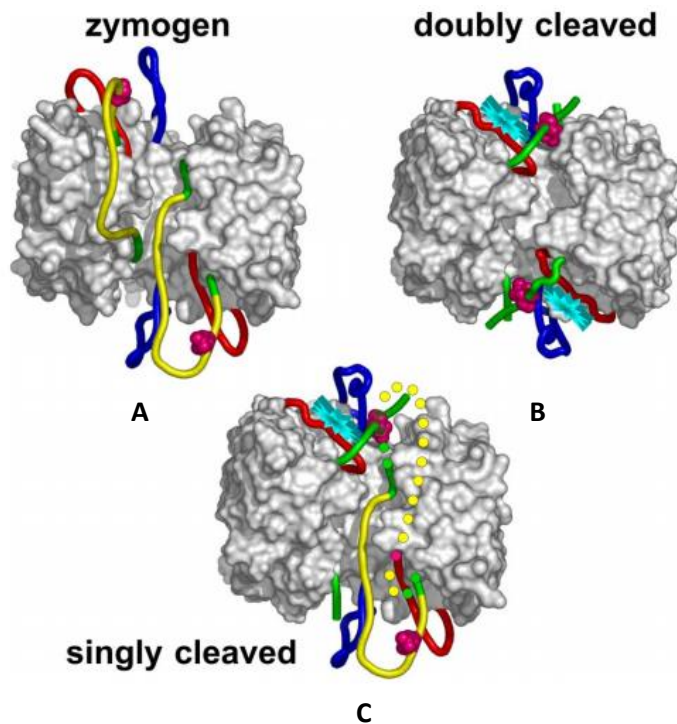


Figure 3. Structural representation of executioner caspase 7 homodimer in its zymogen (procaspase) and cleaved (caspase) forms. Red and blue loops constitute the determinants of catalytic activity and substrate binding specificity respectively. The yellow/green loop represents the trans-subunit linker and the magenta ball the site of Asp-192 cleavage. The cyan star denotes the substrate binding site and position of Cys-285.⁴

zymogenic form with each monomer arranged in a head to tail orientation relative to the other. Substantial study towards the structural biology of executioner caspase activation has revealed significant amino acid sequence homology between caspases 3,6 and 7 and provided a mechanism for their activation.^{44,45,46} In procaspase 7, the active site Cys-285 residue is sequestered by a series of 4 polypeptide loop structures which are conformationally situated to prevent substrate binding.⁴⁵ A trans-subunit 'linker' loop connects the large and small subunits of each monomer plays the critical role of maintaining this inactive

conformation. Initiator caspases (caspase 8/9) cleave Asp-192 of the linker loop in procaspase 7 leading to a conformational rearrangement of the 4 polypeptide loops to form a catalytically active substrate binding pocket termed the 'loop bundle' (Figure 3).⁴⁴ Following executioner procaspase activation to the active caspase form, a caspase cascade is initiated whereby executioner caspases cleave nearby executioner procaspases to rapidly increase the concentration of active caspase proteases within the cell. The executioner caspases begin dismantling the cell *via* proteolytic cleavage of both structural and functional proteins as well as activate caspase-dependent deoxyribonucleases which fragment the nuclear DNA.³⁷ In this way, the executioner caspases 3,6 and 7 befit their name by serving as the undertakers of cells experiencing apoptosis. Their activation constitutes an irreversible cascade which results in complete destruction of the cell *via* the controlled process of apoptosis.

1.2.3 Caspase Activation: Comparing the Intrinsic and Extrinsic Pathways of Apoptosis

While there are numerous cellular events capable of triggering apoptosis the initiation event is governed by two pathways: auto-initiated cell death (intrinsic) or initiation from and external stimulus (extrinsic). While these pathways proceed *via* unique signalling cascades they share the common outcome of executioner caspases 3 and 7 activation.³⁶ Additionally, these two pathways are not mutually exclusive, and stimulation of one pathway does not preclude activation of the other.

1.2.3.A The Intrinsic Pathway

The intrinsic apoptotic pathway is initiated by the cell itself, often following DNA damage or oncogene activation. Central to the ability of a cell to intrinsically initiate apoptosis is the permeabilization of the mitochondrial membrane and release of cytochrome C.^{47,48} This event of mitochondrial membrane permeabilization is governed by several regulatory agents and the Bcl-2 family of proteins represents one of the most important players in the modulation of this process.⁴⁹

The Bcl-2 family of proteins is very large and can be sub-divided into three categories: (1) BH3 (Bcl-2 Homology 3) domain proteins which promote apoptosis, (2) The executioner proteins Bax (Bcl-2 associated x-protein) and Bak (Bcl-2 antagonist killer) which associate with the mitochondrial membrane to permeabilize it and (3) the anti-apoptotic proteins, which includes

Bcl-2 itself.⁵⁰ Numerous BH3 based pro-apoptotic proteins, such as BID (BH3 interacting-domain death agonist) are up-regulated by the p53 tumor suppression gene following cellular or genotoxic stress.⁵¹ The mitochondrial permeabilization event constitutes a multi-pronged effort by the BH3 subgroup of proteins.⁵⁰ Activator BH3 proteins bind to various Bcl-2 anti-apoptotic proteins, disrupting their association with the executioner proteins Bax and Bak (indirect activation).^{52,53} Additionally, BH3 proteins have been proposed to bind directly Bax/Bak (direct activation).⁵⁴ Bax is a cytosolic protein while Bak is embedded in the mitochondrial membrane; the BH3 mediated activation event leads to oligomerization of Bax/Bak to form a mitochondrial pore which allows the release of cytochrome C as well as other pro-apoptotic factors such as SMAC (second mitochondria-derived activator of caspases) (Figure 4).⁵⁵

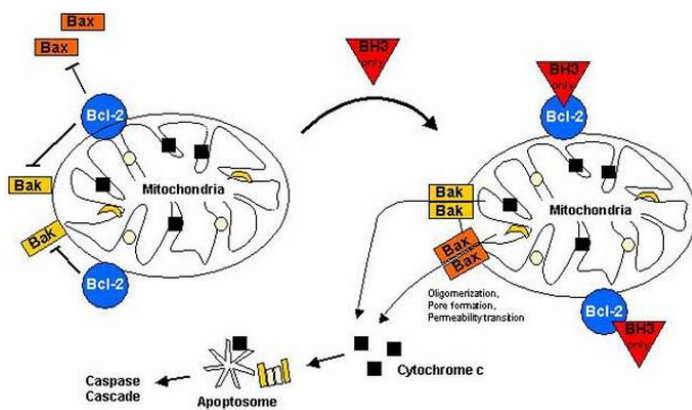


Figure 4. A schematic representation of cytochrome C release from the mitochondria promoted by the activity of the BH3 proteins of the Bcl-2 family. Bcl-2 and related inhibitory proteins (blue) inhibit Bak and Bax association (yellow & orange respectively). Up-regulation of BH3 proteins (red) following cellular stress promotes Bak/Bax association at the mitochondrial outer membrane *via* direct activation as well as sequestration of inhibitory Bcl-2 proteins by means of direct competitive binding.⁵⁶

Cytochrome C release from the inner mitochondrial membrane indicates a significant cellular event and signals the key initiation step towards intrinsic apoptosis. The released cytochrome c binds the cytosolic protein Apaf-1 (apoptotic protease activating factor 1) in an ATP dependent process.⁴² Although it was initially suggested that ATP hydrolysis was required prior to cytochrome c binding, later findings demonstrated that this association can occur in absence of ATP.⁵⁷ Experiments have shown that ATP plays a crucial role in altering the conformation of apaf-1; following ATP association and hydrolysis to ADP the apaf-1 protein rearranges to expose a caspase recruitment domain (CARD). Subsequent exchange of ADP for another molecule of ATP promotes the association of apaf-1 CARD domains into a concentric apoptosome complex.⁵⁸ The active apoptosome recruits procaspase-9 *via* its CARD domains and promotes procaspase-9 dimerization and activation to generate caspase-9.⁵⁹ Once activated, caspase-9 can cleave

downstream executioner procaspases-3/7 to initiate a caspase cascade and effect cell death, as described previously.

1.2.3.B Extrinsic Pathway

The extrinsic apoptotic pathway is modulated by extracellular ligand binding to transmembrane proteins on the cell surface. Numerous cell-surface death receptors (DRs) under the tumor necrosis factor (TNF) super family are known to initiate apoptosis in this way and include: (ligand/receptor) FasL(CD95)/FasR, TNF- α /TNFR1, TRAIL (TNF related apoptosis inducing ligand)/DR4 & DR5; although the Fas and TNF receptor-ligand interactions remain the most well characterized to date.³⁶ These DRs and their ligands can be divided into two categories, each possessing a slightly different mechanism of apoptotic activation.

The first category includes FasR and DR4/5 with their respective ligands, FasL and TRAIL. FasL is a transmembrane protein found on the cell surface of cytotoxic T-lymphocytes and requires direct cell-cell interaction between FasL and FasR (the receptor) to initiate a response.⁶⁰ Conversely, TRAIL is a cytokine secreted by numerous cell types to induce nearby cell death, it comes in two sub-types TRAIL-1 and TRAIL-2 which bind DR4 & DR5 respectively at the cell surface.⁶¹ Ligand-DR binding initiates an intracellular response which recruits an adaptor protein FADD (fas-associated protein with death domain) to the DR at the inner surface of the plasma membrane. This association allows the DED (death effector domain) of FADD to recruit procaspase-8 *via* its respective DED. Upon association of caspase-8 to FADD a DISC (death inducing signalling complex) is formed.⁶² Procaspase-8 dimerizes and auto-cleaves to generate active caspase-8 which propagates downstream apoptotic activity (Figure 5A). In addition, caspase-8 processes BID into its active truncated form (t-BID) which is subsequently able to activate an intrinsic apoptotic response *via* mitochondrial membrane permeabilization and cytochrome c release.⁶³

The second category is largely represented by the TNFR1 receptor and exhibits a much more complex mode of activation compared to the Fas/TRAIL controlled receptors. The TNFR1 receptor binds TNF- α , which can exist either as either a membrane bound or free floating protein.^{64,65} TNF- α binding elicits numerous different protein binding events and leads to the formation of multiple different complexes at the apical cellular interface depending on the background expression of

certain regulatory proteins (*vida infra*). For clarity, a simplified picture of TNF- α mediated cell death involves ligand binding to the TNFR1 DR followed by binding of the adaptor protein TRADD (TNFR1-associated death domain protein) along with several regulatory proteins⁶⁶, including RIPK1 (Receptor-interacting serine/threonine-protein kinase 1) whose significance will be discussed later. The TNFR1-TRADD complex is internalized *via* a clathrin mediated membrane contraction whereupon a conformational change causes TRADD to shed its associated regulatory proteins.⁶⁷ This event liberates TRADD to recruit FADD which attracts procaspase-8 through DED association to form a DISC, procaspase-8 is then activated to caspase-8 and the caspase cascade ensues (Figure 5B).⁶⁸

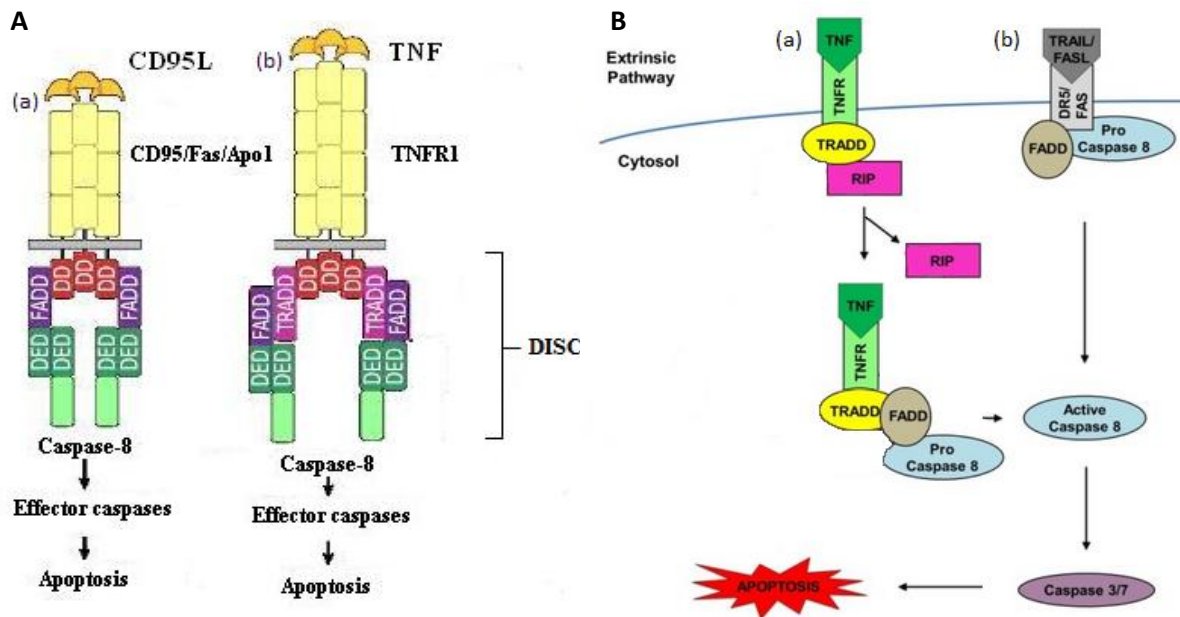


Figure 5. Schematic representation of the modes of extrinsic apoptotic activation. (A) Representative DISCs for Fas/Trail (a) and TNF- α (b). Ligand (gold) to the DR (beige) triggers adaptor protein recruitment FADD/TRADD *via* death domains, FADD recruits procaspase-8 (pale green) using death effector domain and procaspase proximity promotes dimerization and caspase-8 activation *via* the death inducing signalling complex (DISC). (B) Ligand binding to death receptors promoting downstream caspase activation. (a) TNF- α binds TNFR receptor and promotes internalization, a conformational change allows TRADD (yellow) to bind FADD (grey) allowing procaspase-8 recruitment and conversion to active caspase-8. (b) TRAIL or FasL bind their respective receptors (DR4/5 & FasR), FADD is recruited followed by procaspase-8 leading to DISC formation and caspase-8 activation.^{7,10}

To summarize, regardless of whether apoptosis is initiated through the intrinsic or extrinsic pathway the general mechanism of activation is consistent: An apoptotic stimulus, such as DNA

damage or killer T-cell binding, initiates a protein cascade triggering the activation of initiator caspases (caspases-8/9) which subsequently activate effector caspases (caspases-3/7) which modulate cell death.

1.2.4 Apoptotic Regulation: The role of IAPs and SMAC

As in any cellular process, especially one producing lethal effects, tight protein regulation is employed by cells to prevent unwanted effects. Certain regulatory proteins, known as inhibitor of apoptosis proteins (IAPs), play a key role in the repression of RCD to safeguard against unwarranted apoptosis.⁶⁹ Conversely, certain pro-apoptotic proteins exist which in some cases counteract the activity of IAPs to promote apoptosis. Through a delicate balance of apoptotic stimulation and repression cells achieve a homeostatic balance while maintaining the ability to “self-destruct” should conditions prove necessary.

IAPs are a large class of proteins responsible for the repression of apoptosis. They include XIAP (X-chromosome-linked inhibitor of apoptosis protein), cIAP-1/2 (cellular inhibitor of apoptosis proteins 1 & 2), ML-IAP (melanoma IAP), ILP2 (IAP-like protein 2), survivin, apollon and NAIP (neuronal apoptosis inhibitory protein).⁵ While these proteins function through different means they all share common BIR (baculoviral IAP repeat) domains of which there are 3 subtypes (BIR1-3) (Figure 6).^{70,71} BIR domains possess a zinc finger motif with four highly conserved amino acid residues which contribute to their structural homology.⁷² The BIR domains are essential for IAP activity and frequently mediate the direct binding of IAPs to caspases as well as other pro-apoptotic proteins causing their deactivation.^{73,74} Many IAPs also contain a C-terminal RING finger domain⁷⁵ with specific activity towards ubiquitin recruitment which can lead to auto-ubiquitination and self-degradation or ubiquitin transfer to other proteins.⁷⁶ Although every IAP plays an important role in the suppression of apoptosis, several “classical” IAPs have been studied extensively and are particularly important in IAP de-regulation and disease.⁵ The activity of XIAP and c-IAP 1/2 will be discussed below, information on the activity of other IAPs may be found in the adjoining references.⁷⁷

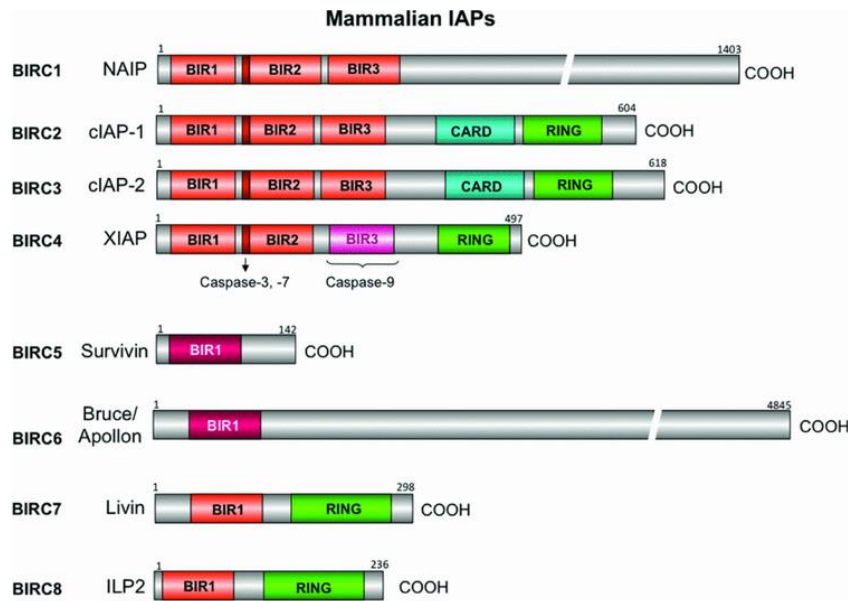


Figure 6. A linear representation of the human IAP proteins. Each poses at least one BIR domain (red/magenta) and may also contain a CARD (cyan) and RING domain (green). The caspase-3/7 binding site of XIAP between BIR1 and BIR2 is denoted.³

1.2.4.A XIAP: Anti-apoptotic activity and regulation by SMAC

The IAP protein XIAP is a potent modulator of apoptotic activity.⁷⁸ As its name suggests, it is encoded by the XIAP gene located on the X-chromosome and is constitutively expressed in many cells and can be important for cell survival.⁷⁹ XIAP works by intercepting and binding executioner caspases-3/7 as well as initiator caspase-9; this associative interaction inhibits caspase activity and can potentially arrest apoptosis.⁸⁰ XIAP can be divided into three separate domains: BIR1/2, BIR3 and RING the first two of which are essential for its anti-caspase activity. The BIR1 and BIR2 domains of XIAP are found adjacent to each other at the N-terminus of the protein and are responsible for XIAP's ability to bind caspases-3/7.⁸¹ This association is proposed to proceed *via* a two point binding model where (1) the linker region between BIR1 and BIR2 forms an interaction at the caspase substrate binding groove⁸² and (2) the BIR2 domain IBM (IAP binding motif) interacting groove (a negatively charged groove conserved among BIR domains) binds the N-terminus of the caspase 3/7 small subunit (Figure 7).⁸³ The BIR3 domain of XIAP binds initiator procaspase-9 *via* an association between the IBM binding groove of



Figure 7. Representation of the XIAP BIR2 two point binding model. The BIR2 IBM interacting groove (yellow) and BIR1-2 linker binding site (red) are shown.

BIR3 and the homodimerization domain of procaspase-9.⁸⁴ In this way, XIAP sequesters caspase-9 activity by blocking the ability of procaspase monomers to associate.

XIAP itself is regulated by several pro-apoptotic proteins. For example, the mitochondrial protein HTRA2 is released to the cytosol following initiation of the intrinsic apoptotic pathway.⁸⁵ It functions as a serine protease and using a 4 amino acid AVPS (alanine-valine-proline-serine) IBM, binds XIAP *via* the IBM binding groove of BIR3 and degrades it; this in-turn protects caspases 3,7 and 9 from XIAP inhibition.⁸⁶ Another key regulator of XIAP is SMAC (second mitochondria-derived activator of caspases), also known as DIABLO (direct IAP binding-protein with low pI), which was first reported in July 2000.⁸⁷ SMAC is a homo-dimeric protein containing a total of two N-terminal AVPI (alanine-valine-proline-isoleucine) IBMs which form tight associations with the BIR2 and BIR3 IBM binding grooves of XIAP,

inhibiting its caspase binding activity.⁶ Although initially thought to bind two separate molecules of XIAP *via* its adjacent N-terminal IBMs, later work identified that SMAC in-fact forms a tight 2:1 SMAC-BIR2/3 complex ($K_d = 0.3$ nM) whereby the two AVPI sequences of the SMAC dimer simultaneously bind the BIR2 and BIR3 IBM binding grooves of a single XIAP molecule (Figure 8B).⁹ Interestingly, SMAC is also able to displace already-bound caspases 3,7 and 9 from XIAP through competitive binding. A study by the Jiang group in 2007 used a SMAC homolog composed of two AVPI sequences spaced by a PEG linker (Figure 8A) to simulate a dimeric SMAC protein.² They found that their SMAC analogue was able to re-initiate caspase-3/9 activity and proposed divergent mechanisms for this observation. While it was accepted that SMAC displaced caspase-9 from XIAP *via* competitive binding at the BIR3 domain⁸⁸ less was known about the mechanism

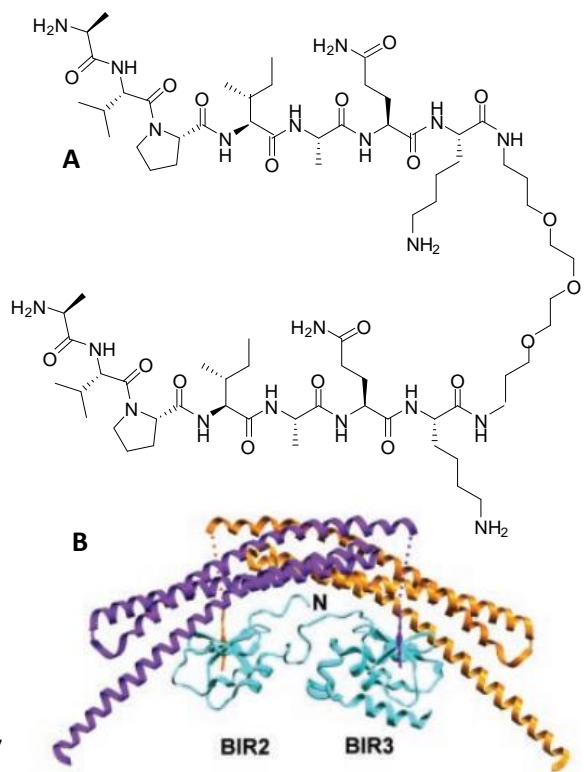


Figure 8. (A) SMAC homolog used by Jiang to probe the mechanism of SMAC-XIAP interaction and caspase displacement.² (B) Structural model of SMAC homodimer (purple and gold monomers) N-termini simultaneously binding the BIR2/BIR3 domains of XIAP (cyan).⁹

of caspase-3/7 liberation. Jiang and colleagues found that initial binding of one SMAC IBM to the BIR3 of XIAP was followed by a second SMAC BIR2 association which inhibited the ability of the BIR1-2 linker of XIAP to retain caspase3/7, allowing its release. Thus SMAC regulates XIAP through direct binding and is an activator of apoptosis through both direct and indirect liberation of caspase activity.⁸⁹

1.2.4.B cIAP 1 & 2: Regulation anti-apoptotic activity and attenuation of SMAC

The cellular apoptosis proteins are two functionally similar proteins with anti-apoptotic properties. They have BIR1-3 domains as in XIAP (Figure 6) and while they exhibit poor binding towards caspases⁹⁰ they show a high affinity for SMAC and are able to inhibit its pro-apoptotic activity through binding.⁵ Both cIAP-1 and 2 also have a RING domain which holds E3 ubiquitin ligase activity and can mark SMAC, as well as other pro-apoptotic proteins, for proteasomal degradation.⁹¹ In addition to directly binding and degrading pro-apoptotic proteins, c-IAPs also play an integral role in activation of the extrinsic apoptotic pathway and the regulation of pro-survival genes, particularly *via* the NF- κ B signalling pathway.⁹² TNF binding to the TNFR1 receptor can produce a myriad of responses depending on the conditions of the internal cellular environment. Upon TNF binding, TRADD, RIPK1, TRAF2 (TNF-receptor associated factor 2) and cIAP-1/2 are recruited to the apical surface of the TNFR1 receptor to form a protein aggregate known as complex I. In healthy cells, RIPK1 is ubiquitinated by the E3 ubiquitin ligase activity of cIAPs-1/2⁹³ or TRAF2⁹⁴ which leads to downstream activation of the I κ B kinase (IKK complex) which in-turn phosphorylates I κ B, leading to its degradation.⁹⁵ Loss of I κ B liberates p50 and transcription factor RELA (REL-associated protein) which translocate to the nucleus and activate NF- κ B genes, promoting the expression of various anti-apoptotic proteins including cIAPs, TRAFs and c-FLIP.^{5,96} Complex I stabilization by c-FLIP (cellular FADD-like IL-1 β -converting enzyme inhibitory protein) is lost following a decrease in either protein synthesis or NF- κ B gene expression leading to c-FLIP degradation.⁹⁷ Following c-FLIP loss, and prior RIPK1 ubiquitination, the TRADD bound TNFR1 receptor is phagocytized into the cell where FADD and caspase-8 associate to form complex IIa which is able to promote apoptosis.⁹⁸

If instead SMAC is released from the mitochondria and cIAP-1/2 levels drop (SMAC binds c-IAPs *via* BIR3 domain)⁹⁹ RIPK1 survives at the apical surface of the TNFR1 receptor. Intact RIPK1 is then

able to dissociate from the TNFR1 receptor and serves as a scaffold for RIPK3, FADD and caspase-8 recruitment to form pro-apoptotic complex IIb.^{68,38} In summary, cIAPs-1 & 2 inhibit apoptosis through the binding and inhibition of SMAC as well as ubiquitination of RIPK1 leading to activation of NF- κ B pro-survival genes. However, cIAPs also play a role in the extrinsic mediated cell death pathways.

1.3 SMAC Mimetics

1.3.1 Background

The IAP binding protein SMAC/Diablo was first reported in July 2000 by two separate research groups^{89,6} and its therapeutic potential was quickly recognized. Two subsequent studies also examined the structural basis for the interaction between SMAC and XIAP in-depth.^{82a,100} Through the use of both X-ray and NMR techniques the structure of SMAC, as well as its binding interactions with the BIR2 and BIR3 domains of XIAP were mapped (Figure 9A). Site-directed mutagenesis of the SMAC protein found that the N-terminal portion was essential for activity, specifically the first four residues: alanine, valine, proline and isoleucine termed the AVPI IAP binding motif (IBM). Amino acid substitution experiments on the AVPI IBM were conducted and found that the positive charge and methyl substituent of the N-terminal alanine were also essential for strong BIR 2/3 binding. The other residues of the AVPI peptide sequence were found to stabilize the SMAC-XIAP interaction through a combination of amide hydrogen bonds and side-chain hydrophobic interactions. Substitution of these three residues generally resulted in a drop in BIR2/BIR3 binding efficiency, although Fesik noted that substitution of phenylalanine for isoleucine resulted in a modest increase in binding efficiency, an observation which would later be exploited.⁸⁹ Several groups recognized preferential binding by native SMAC for the BIR3 domain of XIAP and noted a weaker interaction at BIR2. A later study by would show that SMAC is in fact able to simultaneously occupy both the BIR2 & 3 domains of XIAP in its dimeric state.⁹ An x-ray crystal structure⁶ combined with detailed NMR data⁸⁹ provided a clear picture of the interaction between the AVPI sequence of SMAC and the IBM binding groove of XIAP BIR3 (Figure 9B). To summarize, Leu 307 and Trp 310 create a hydrophobic pocket in which the methyl

substituent of the AVPI alanine sits. Glu 314 makes the essential charge stabilized hydrogen bond with the N-terminal alanine nitrogen. The valine residue is stabilized by hydrogen bonds to its nitrogen and carbonyl components by Gly 306 and Thr 308 respectively. In addition, the hydrophobic side chain of valine forms an association with the methyl group of Thr 308. Trp 323 engages in hydrogen bond interactions with the AVPI alanine, valine and proline, with which it also forms a hydrophobic stack. Finally, Gly 306 along with the hydrophobic portions of Lys 297 and 299 provide a channel for the docking of the AVPI isoleucine residue. Fesik noted that these key binding residues in BIR3 were also present in the BIR3 domain of cIAP-1 confirming the relatively ubiquitous ability of the AVPI sequence to bind IAP BIR3 domains. In BIR2 of XIAP, the

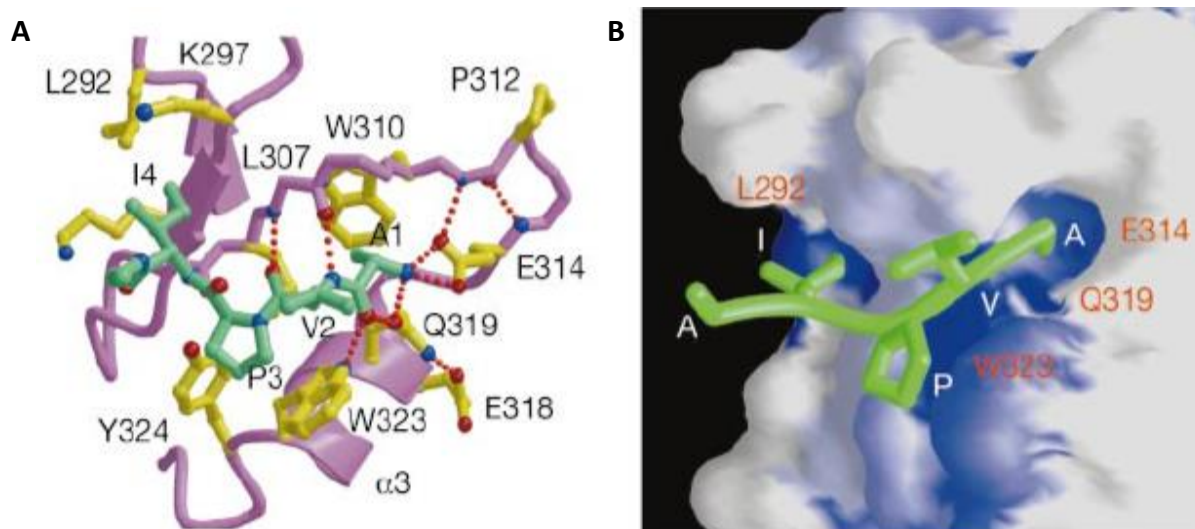


Figure 9. (A) Close up view of the interaction between the N-terminal AVPI sequence of SMAC (green) and the BIR3 IBM binding groove of XIAP (purple, key interacting residues in yellow). Hydrogen bonds are shown as red dotted lines, blue balls represent nitrogen atoms, red balls are oxygen. (B) A surface representation of the N-terminal AVPI sequence of SMAC (green) interacting with the XIAP BIR3 IBM binding groove. Areas of blue and white represent the most and least hydrophobic surfaces respectively.⁶

equivalent to Gly 306 is replaced and a histidine residue substitutes Trp 323. They suggested these modifications may explain the reduced affinity of SMAC for BIR2 ($K_D = 2.3 \mu\text{M}$) compared to BIR3 ($K_D = 0.42 \mu\text{M}$).⁸⁹

This early work gave medicinal chemists a detailed picture of the biochemical interaction between SMAC and its native substrates. Knowledge that both XIAP and cIAP-1/2 are frequently overexpressed in human cancers¹⁰¹ kick-started a race to develop a small molecule analogue of

the AVPI SMAC peptide sequence, which was itself already a moderate inhibitor of XIAP BIR3 *in-vitro* ($K_D = 0.48 \mu\text{M}$).¹⁰²

1.3.2 Mechanism of Action

In the 14 years that SMAC mimetics have existed significant research has been conducted on their mode of action. Work by both chemists and biologists has progressively de-convoluted how SMAC mimetics activate apoptosis in tumor cells while sparing non-cancerous cells. De-regulation of IAPs is known to play a role in cancer and was suspected to act *via* the suppression of caspases.¹⁰³ Medicinal chemists have successfully described the synthesis of peptide-derived small molecules mimicking the protein SMAC which are able to inhibit IAPs by binding them at highly conserved BIR domains using an interaction which mimics that of SMAC's N-terminal AVPI sequence.¹⁰⁴ Numerous studies have reported SMAC mimetics with potent binding affinities for the BIR domains of common IAPs: XIAP (BIR2 and BIR3), cIAP-1 (BIR3), cIAP-2 (BIR3), ML-IAP (BIR3)^{105,106,107} as well as described caspase-3,7,8 & 9 activation following treatment in cells.^{108,109,110} SMAC mimetics have been shown to induce apoptosis in cancer cells through the activation of two caspase pathways.

1.3.2.A Caspase-9 activation

Potent, cell permeable SMAC mimetics are able to interact with the BIR2 and BIR3 IBM binding motifs of XIAP, this binding event is known to relieve XIAP-caspase interaction and liberate caspases to promote apoptosis.^{101,2} XIAP inhibition is important for activation of the intrinsic apoptotic pathway (refer to 1.2.4.A) by initiating caspase-9 activation which in-turn promotes procaspase-3/7 cleavage and RCD.³⁶ Both SMAC mimetic monomers and dimers (*vide infra*) may bind to XIAP, although dimeric SMAC mimetics have been shown to interact with both the BIR2 and BIR3 domains of XIAP yielding significantly higher binding affinities.¹¹¹ The early SMAC literature placed heavy emphasis on the inhibition of XIAP as the primary means of re-activating apoptosis in cancer cells, however recent findings suggest that the relief of caspase-8 inhibition may be a more significant target.¹⁰⁷ Despite these findings, it has been shown by several research groups that "pan-selective" antagonists, which target cIAP-1/2 in addition to XIAP, yield the most potent activators of apoptosis.¹¹²

1.3.2.B Caspase-8 Activation

Caspase-8 activation was initially an afterthought in the early design of SMAC mimetics.¹¹³ Medicinal chemists believed that IAP antagonists produced their effects by inhibiting XIAP to re-activating caspase 9 through the intrinsic pathway. Data from two 2007 Cell publications altered this view dramatically.^{114,115} These studies showed that caspase-8 activation through TNF- α /TNFR1 signalling could be achieved by the inhibition of the IAPs cIAP-1 & 2 which served as the barrier to TNFR1 mediated apoptosis and that TNF signalling is essential for SMAC mimetic induced apoptosis.¹¹⁶ cIAP-1/2 proteins contain both a BIR3 and RING domain, the latter possessing ubiquitin ligase activity. Upon TNF- α binding to the TNFR1 receptor in cancer cells cIAPs ubiquitinate RIPK1 leading to downstream activation of NF- κ B genes and synthesis of pro-survival proteins, which include IAPs (refer to 1.2.4.B). In their inactive state, cIAPs sequester their RING domain; SMAC mimetics can bind the BIR3 domains of cIAP-1/2 which induces a conformational change and exposes these RING domains which in-turn promotes dimerization with nearby cIAPs through their exposed domains.⁵ RING dimerization activates E3 ubiquitin ligase activity causing ubiquitination of nearby proteins, in addition to the dimerized cIAPs themselves (Figure 10A). This burst of ubiquitin transfer activity causes initial RIPK1 degradation

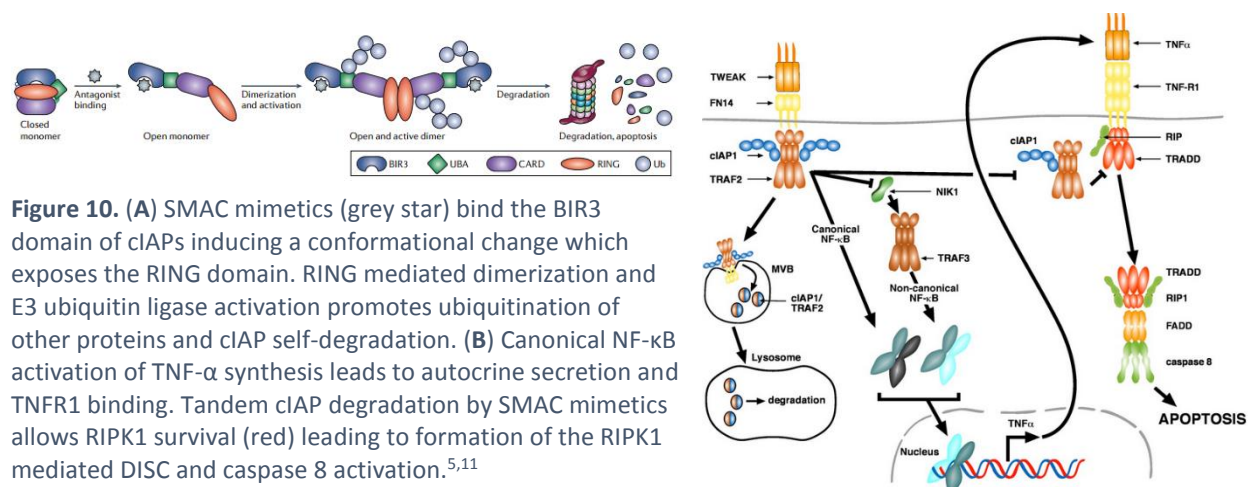


Figure 10. (A) SMAC mimetics (grey star) bind the BIR3 domain of cIAPs inducing a conformational change which exposes the RING domain. RING mediated dimerization and E3 ubiquitin ligase activation promotes ubiquitination of other proteins and cIAP self-degradation. **(B)** Canonical NF- κ B activation of TNF- α synthesis leads to autocrine secretion and TNFR1 binding. Tandem cIAP degradation by SMAC mimetics allows RIPK1 survival (red) leading to formation of the RIPK1 mediated DISC and caspase 8 activation.^{5,11}

and activation of the NF- κ B pathway, which promotes autocrine TNF- α secretion in certain cells.¹¹⁷ The secreted TNF- α protein binds TNFR1 receptors, however due to cIAP-1/2 depletion from SMAC mimetic activity cIAP-1/2 is degraded and cannot mark RIPK1 for ubiquitination, thus it survives. RIPK1 is able to associate with FADD and caspase-8 to form the RIP-dependent DISC complex and activate caspase-8 to promote apoptosis through effector caspases 3/7 (Figure

10B).¹¹⁸ The inability of SMAC mimetics to induce apoptosis in certain cell types has been predicted to stem from a lack of autocrine TNF- α secretion in those cells.¹¹⁴

1.3.2.C Tumor Selectivity

These mechanistic studies have raised an interesting question. If TNF- α mediated cell death is the primary actor in SMAC mimetic treated cancer cells then why do so many studies report minimal toxicity of SMAC mimetics toward non-cancerous cells *in-vitro* and in animal models? If IAP antagonists are indiscriminately promoting autocrine TNF- α secretion and down-regulating NF- κ B pro-survival genes then why should healthy cells be immune? Numerous others have posed the same questions and the answer continues to elude researchers.¹¹⁹ It has been suggested that cellular transformation from healthy to cancerous may modify surface receptor behaviour of cells to shift from pro-survival to pro-death, however this is unproven.¹¹⁹ A recent Nature article suggests that SMAC mimetics may activate cytokine secretion in tumor cells, marking them for destruction by the immune system.¹²⁰ It is commonly accepted that IAP antagonists lower the threshold for apoptosis through inhibition of caspase activity and reduction in pro-survival gene expression¹²¹ but more research is required to uncover the exact mechanism behind the selective tumor killing effects observed with SMAC mimetics.¹²²

1.4 Concluding Remarks

Our goal was to design novel SMAC mimetics capable of inducing apoptosis selectively in cancer cells. We drew inspiration from other successful strategies employed in the synthesis of reported SMAC mimetics and sought to design, synthesize and test a novel library of IAP antagonists.

1.5 References

1. suite, E. B. http://mol-biol4masters.masters.grkraj.org/html/Co_and_Post_Translational_Events5-Cellular_Protein_Traffic_files/image078.png.

2. Gao, Z. T., Y.; Wang, J.; Yin, Q.; Wu, H.; Li, Y.M.; and; Jiang, X., A Dimeric Smac/Diablo Peptide Directly Relieves Caspase-3 Inhibition by XIAP: Dynamic and Cooperative Regulation of XIAP by Smac/Diablo. *The journal of biological chemistry* **2007**, *282* (42), 30718-30728.
3. RIBE, E. M.; SERRANO-SAIZ, E.; AKPAN, N.; TROY, C. M., Mechanisms of neuronal death in disease: defining the models and the players. *Biochemical Journal* **2008**, *415*, 165-182.
4. Denault, J.-B.; Békés, M.; Scott, F. L.; Sexton, K. M. B.; Bogyo, M.; Salvesen, Guy S., Engineered Hybrid Dimers: Tracking the Activation Pathway of Caspase-7. *Molecular Cell* **2006**, *23* (4), 523-533.
5. Fulda, S.; Vucic, D., Targeting IAP proteins for therapeutic intervention in cancer. *Nat Rev Drug Discov* **2012**, *11* (2), 109-124.
6. Wu, G.; Chai, J.; Suber, T. L.; Wu, J.-W.; Du, C.; Wang, X.; Shi, Y., Structural basis of IAP recognition by Smac/DIABLO. *Nature* **2000**, *408* (6815), 1008-1012.
7. Volkova, T. O.; Poltorak, A. N. Cellular Caspases: New Targets for the Action of Pharmacological Agents 2012. <http://www.intechopen.com/books/apoptosis-and-medicine/cellular-caspases-new-targets-for-the-action-of-pharmacological-agents>.
8. Boatright, K. M.; Renatus, M.; Scott, F. L.; Sperandio, S.; Shin, H.; Pedersen, I. M.; Ricci, J.-E.; Edris, W. A.; Sutherlin, D. P.; Green, D. R.; Salvesen, G. S., A Unified Model for Apical Caspase Activation. *Molecular Cell* **2003**, *11* (2), 529-541.
9. Huang, Y.; Rich, R. L.; Myszka, D. G.; Wu, H., Requirement of Both the Second and Third BIR Domains for the Relief of X-linked Inhibitor of Apoptosis Protein (XIAP)-mediated Caspase Inhibition by Smac. *Journal of Biological Chemistry* **2003**, *278* (49), 49517-49522.
10. Marquez, R. T.; Tsao, B. W.; Faust, N. F.; Xu, L., Drug Resistance and Molecular Cancer Therapy: Apoptosis Versus Autophagy. **2012**.
11. Vince, J. E.; Chau, D.; Callus, B.; Wong, W. W.-L.; Hawkins, C. J.; Schneider, P.; McKinlay, M.; Benetatos, C. A.; Condon, S. M.; Chunduru, S. K.; Yeoh, G.; Brink, R.; Vaux, D. L.; Silke, J., TWEAK-FN14 signaling induces lysosomal degradation of a cIAP1–TRAF2 complex to sensitize tumor cells to TNF α . *The Journal of Cell Biology* **2008**, *182* (1), 171-184.
12. Armitage, P.; Doll, R., The Age Distribution of Cancer and a Multi-stage Theory of Carcinogenesis. *British Journal of Cancer* **1954**, *8* (1), 1-12.
13. Xu, Z.; Taylor, J. A., Genome-wide age-related DNA methylation changes in blood and other tissues relate to histone modification, expression, and cancer. *Carcinogenesis* **2013**.
14. Danaei, G.; Vander Hoorn, S.; Lopez, A. D.; Murray, C. J. L.; Ezzati, M., Causes of cancer in the world: comparative risk assessment of nine behavioural and environmental risk factors. *The Lancet* *366* (9499), 1784-1793.
15. Hanahan, D.; Weinberg, R. A., The Hallmarks of Cancer. *Cell* **2000**, *100* (1), 57-70.
16. Hollstein, M.; Sidransky, D.; Vogelstein, B.; Harris, C., p53 mutations in human cancers. *Science* **1991**, *253* (5015), 49-53.
17. Igaki, H.; Sasaki, H.; Kishi, T.; Sakamoto, H.; Tachimori, Y.; Kato, H.; Watanabe, H.; Sugimura, T.; Terada, M., Highly Frequent Homozygous Deletion of the p16 Gene in Esophageal Cancer Cell Lines. *Biochemical and Biophysical Research Communications* **1994**, *203* (2), 1090-1095.
18. Bos, J. L., ras Oncogenes in Human Cancer: A Review. *Cancer Research* **1989**, *49* (17), 4682-4689.

19. Franke, T. F.; Kaplan, D. R.; Cantley, L. C.; Toker, A., Direct Regulation of the Akt Proto-Oncogene Product by Phosphatidylinositol-3,4-bisphosphate. *Science* **1997**, *275* (5300), 665-668.
20. Datta, S. R.; Dudek, H.; Tao, X.; Masters, S.; Fu, H.; Gotoh, Y.; Greenberg, M. E., Akt Phosphorylation of BAD Couples Survival Signals to the Cell-Intrinsic Death Machinery. *Cell* **1997**, *91* (2), 231-241.
21. Madrid, L. V.; Mayo, M. W.; Reuther, J. Y.; Baldwin, A. S., Akt Stimulates the Transactivation Potential of the RelA/p65 Subunit of NF- κ B through Utilization of the I κ B Kinase and Activation of the Mitogen-activated Protein Kinase p38. *Journal of Biological Chemistry* **2001**, *276* (22), 18934-18940.
22. Budman, D. R., Book Review. *New England Journal of Medicine* **2006**, *355* (18), 1942-1942.
23. Bai, L.; Smith, D. C.; Wang, S., Small-molecule SMAC mimetics as new cancer therapeutics. *Pharmacology & Therapeutics* **2014**, *144* (1), 82-95.
24. McKinlay, M. A. SMAC Mimetics: a new class of targeted agents that activate apoptotic cell death and block pro-survival signalling in cancer cells. 2011. <http://www.ddw-online.com/therapeutics/p149034-smac-mimetics:-a-new-class-of-targeted-agents-that-activate-apoptotic-cell-death-and-block-pro-survival-signalling-in-cancer-cells-fall-11.html>.
25. Green, D. R., *Means to an End: Apoptosis and Other Cell Death Mechanisms*. Cold Spring Harbor Laboratory Press: 2011.
26. Majno, G.; Joris, I., Apoptosis, oncosis, and necrosis. An overview of cell death. *The American Journal of Pathology* **1995**, *146* (1), 3-15.
27. Kerr, J. F. W., A. H; Currie, A.R., Apoptosis: a basic biological phenomenon with wide-range implications in tissue kinetics. *British Journal of Cancer* **1972**, *26* (4), 239-257.
28. Fadoka, V. A.; Bratton, D. L.; Frasch, S. C.; Warner, M. L.; Henson, P. M., The role of phosphatidylserine in recognition of apoptotic cells by phagocytes. *Cell Death and Differentiation* **1998**, *5* (7), 551-562.
29. Savill, J.; Fadok, V., Corpse clearance defines the meaning of cell death. *Nature* **2000**, *407* (6805), 784-788.
30. Entezari, M.; Zakeri, Z.; Lockshin, R. A., Apoptosis in Developmental Processes. In *eLS*, John Wiley & Sons, Ltd: 2001.
31. (a) Evan, G.; Littlewood, T., A Matter of Life and Cell Death. *Science* **1998**, *281* (5381), 1317-1322; (b) Sharma, V.; Singh, P.; Pandey, A. K.; Dhawan, A., Induction of oxidative stress, DNA damage and apoptosis in mouse liver after sub-acute oral exposure to zinc oxide nanoparticles. *Mutation Research/Genetic Toxicology and Environmental Mutagenesis* **2012**, *745* (1-2), 84-91.
32. (a) Rojas, M.; Olivier, M.; Gros, P.; Barrera, L. F.; García, L. F., TNF- α and IL-10 Modulate the Induction of Apoptosis by Virulent Mycobacterium tuberculosis in Murine Macrophages. *The Journal of Immunology* **1999**, *162* (10), 6122-6131; (b) Cummins, N. W.; Badley, A. D., Mechanisms of HIV-associated lymphocyte apoptosis: 2010. *Cell Death and Dis* **2010**, *1*, e99.
33. Twiner, M. J.; Hanagriff, J. C.; Butler, S.; Madhkoor, A. K.; Doucette, G. J., Induction of Apoptosis Pathways in Several Cell Lines following Exposure to the Marine Algal Toxin Azaspiracid. *Chemical Research in Toxicology* **2012**, *25* (7), 1493-1501.

34. Acedo, P.; Stockert, J. C.; Canete, M.; Villanueva, A., Two combined photosensitizers: a goal for more effective photodynamic therapy of cancer. *Cell Death Dis* **2014**, *5*, e1122.
35. Ellis, H. M.; Horvitz, H. R., Genetic control of programmed cell death in the nematode *C. elegans*. *Cell* **1986**, *44* (6), 817-829.
36. Elmore, S., Apoptosis: A Review of Programmed Cell Death. *Toxicologic pathology* **2007**, *35* (4), 495-516.
37. Shi, Y., Mechanisms of Caspase Activation and Inhibition during Apoptosis. *Molecular Cell* **2002**, *9* (3), 459-470.
38. Pasparakis, M.; Vandenabeele, P., Necroptosis and its role in inflammation. *Nature* **2015**, *517* (7534), 311-320.
39. Alnemri, E. S.; Livingston, D. J.; Nicholson, D. W.; Salvesen, G.; Thornberry, N. A.; Wong, W. W.; Yuan, J., Human ICE/CED-3 Protease Nomenclature. *Cell* **1996**, *87* (2), 171.
40. Mcllwain, D. R.; Berger, T.; Mak, T. W., Caspase Functions in Cell Death and Disease. *Cold Spring Harbor Perspectives in Biology* **2013**, *5* (4).
41. Chang, D. W.; Xing, Z.; Capacio, V. L.; Peter, M. E.; Yang, X., *Interdimer processing mechanism of procaspase-8 activation*. 2003; Vol. 22, p 4132-4142.
42. Zou, H.; Li, Y.; Liu, X.; Wang, X., An APAF-1-Cytochrome c Multimeric Complex Is a Functional Apoptosome That Activates Procaspase-9. *Journal of Biological Chemistry* **1999**, *274* (17), 11549-11556.
43. Salvesen, G. S.; Dixit, V. M., Caspase activation: The induced-proximity model. *Proceedings of the National Academy of Sciences* **1999**, *96* (20), 10964-10967.
44. Chai, J.; Wu, Q.; Shiozaki, E.; Srinivasula, S. M.; Alnemri, E. S.; Shi, Y., Crystal Structure of a Procaspase-7 Zymogen: Mechanisms of Activation and Substrate Binding. *Cell* **2001**, *107* (3), 399-407.
45. Riedl, S. J.; Fuentes-Prior, P.; Renatus, M.; Kairies, N.; Krapp, S.; Huber, R.; Salvesen, G. S.; Bode, W., Structural basis for the activation of human procaspase-7. *Proceedings of the National Academy of Sciences of the United States of America* **2001**, *98* (26), 14790-14795.
46. Fuentes-Prior, P.; Salvesen, Guy S., The protein structures that shape caspase activity, specificity, activation and inhibition. *Biochemical Journal* **2004**, *384* (Pt 2), 201-232.
47. Ghosh, A. K.; Majumder, M.; Steele, R.; Liu, T.-J.; Ray, R. B., MBP-1 mediated apoptosis involves cytochrome c release from mitochondria. *Oncogene* **2002**, *21* (18), 10.
48. Tsujimoto, Y.; Shimizu, S., Bcl-2 family: Life-or-death switch. *FEBS Letters* **2000**, *466* (1), 6-10.
49. Vander Heiden, M. G.; Thompson, C. B., Bcl-2 proteins: regulators of apoptosis or of mitochondrial homeostasis? *Nat Cell Biol* **1999**, *1* (8), E209-E216.
50. Shamas-Din, A.; Kale, J.; Leber, B.; Andrews, D. W., Mechanisms of Action of Bcl-2 Family Proteins. *Cold Spring Harbor Perspectives in Biology* **2013**, *5* (4).
51. Sax, J. K.; Fei, P.; Murphy, M. E.; Bernhard, E.; Korsmeyer, S. J.; El-Deiry, W. S., BID regulation by p53 contributes to chemosensitivity. *Nat Cell Biol* **2002**, *4* (11), 842-849.
52. Chen, L.; Willis, S. N.; Wei, A.; Smith, B. J.; Fletcher, J. I.; Hinds, M. G.; Colman, P. M.; Day, C. L.; Adams, J. M.; Huang, D. C. S., Differential Targeting of Prosurvival Bcl-2 Proteins by Their BH3-Only Ligands Allows Complementary Apoptotic Function. *Molecular Cell* **2005**, *17* (3), 393-403.

53. Willis, S. N.; Chen, L.; Dewson, G.; Wei, A.; Naik, E.; Fletcher, J. I.; Adams, J. M.; Huang, D. C. S., Proapoptotic Bak is sequestered by Mcl-1 and Bcl-xL, but not Bcl-2, until displaced by BH3-only proteins. *Genes & Development* **2005**, *19* (11), 1294-1305.
54. Kim, H.; Rafiuddin-Shah, M.; Tu, H.-C.; Jeffers, J. R.; Zambetti, G. P.; Hsieh, J. J. D.; Cheng, E. H. Y., Hierarchical regulation of mitochondrion-dependent apoptosis by BCL-2 subfamilies. *Nat Cell Biol* **2006**, *8* (12), 1348-1358.
55. Westphal, D.; Dewson, G.; Czabotar, P. E.; Kluck, R. M., Molecular biology of Bax and Bak activation and action. *Biochimica et Biophysica Acta (BBA) - Molecular Cell Research* **2011**, *1813* (4), 521-531.
56. Gewies, A., Introduction to Apoptosis. In *ApoReview*, 2003.
57. Purring-Koch, C.; McLendon, G., Cytochrome c binding to Apaf-1: The effects of dATP and ionic strength. *Proceedings of the National Academy of Sciences of the United States of America* **2000**, *97* (22), 11928-11931.
58. Kim, H.-E.; Du, F.; Fang, M.; Wang, X., Formation of apoptosome is initiated by cytochrome c-induced dATP hydrolysis and subsequent nucleotide exchange on Apaf-1. *Proceedings of the National Academy of Sciences of the United States of America* **2005**, *102* (49), 17545-17550.
59. Acehan, D.; Jiang, X.; Morgan, D. G.; Heuser, J. E.; Wang, X.; Akey, C. W., Three-Dimensional Structure of the Apoptosome: Implications for Assembly, Procaspase-9 Binding, and Activation. *Molecular Cell* **2002**, *9* (2), 423-432.
60. Waring, P.; Mullbacher, A., Cell death induced by the Fas/Fas ligand pathway and its role in pathology. *Immunol Cell Biol* **1999**, *77* (4), 312-317.
61. Song, J. J.; Lee, Y. J., Differential cleavage of Mst1 by caspase-7/-3 is responsible for TRAIL-induced activation of the MAPK superfamily. *Cellular Signalling* **2008**, *20* (5), 892-906.
62. Peter, M. E.; Kramer, P. H., The CD95(APO-1//Fas) DISC and beyond. *Cell Death Differ* **2000**, *10* (1), 26-35.
63. Li, H.; Zhu, H.; Xu, C.-j.; Yuan, J., Cleavage of BID by Caspase 8 Mediates the Mitochondrial Damage in the Fas Pathway of Apoptosis. *Cell* **1998**, *94* (4), 491-501.
64. Gupta, S.; Gollapudi, S., Molecular mechanisms of TNF- α -induced apoptosis in aging human T cell subsets. *The International Journal of Biochemistry & Cell Biology* **2005**, *37* (5), 1034-1042.
65. Ding, W.-X.; Yin, X.-M., Dissection of the multiple mechanisms of TNF- α -induced apoptosis in liver injury. *Journal of Cellular and Molecular Medicine* **2004**, *8* (4), 445-454.
66. Wilson, N. S.; Dixit, V.; Ashkenazi, A., Death receptor signal transducers: nodes of coordination in immune signaling networks. *Nat Immunol* **2009**, *10* (4), 348-355.
67. Schutze, S.; Tchikov, V.; Schneider-Brachert, W., Regulation of TNFR1 and CD95 signalling by receptor compartmentalization. *Nat Rev Mol Cell Biol* **2008**, *9* (8), 655-662.
68. Wang, L.; Du, F.; Wang, X., TNF- α Induces Two Distinct Caspase-8 Activation Pathways. *Cell* **2008**, *133* (4), 693-703.
69. Reed, J. C., Apoptosis-based therapies. *Nat Rev Drug Discov* **2002**, *1* (2), 111-121.
70. Hinds, M. G.; Norton, R. S.; Vaux, D. L.; Day, C. L., Solution structure of a baculoviral inhibitor of apoptosis (IAP) repeat. *Nat Struct Mol Biol* **1999**, *6* (7), 648-651.
71. Vaux, D. L., Inhibitor of Apoptosis (IAP) and BIR-containing Proteins. In *eLS*, John Wiley & Sons, Ltd: 2001.

72. Birnbaum, M. J.; Clem, R. J.; Miller, L. K., An apoptosis-inhibiting gene from a nuclear polyhedrosis virus encoding a polypeptide with Cys/His sequence motifs. *Journal of Virology* **1994**, *68* (4), 2521-2528.
73. Duckett, C. S.; Li, F.; Wang, Y.; Tomaselli, K. J.; Thompson, C. B.; Armstrong, R. C., Human IAP-Like Protein Regulates Programmed Cell Death Downstream of Bcl-x(L) and Cytochrome c. *Molecular and Cellular Biology* **1998**, *18* (1), 608-615.
74. Eckelman, B. P.; Drag, M.; Snipas, S. J.; Salvesen, G. S., The mechanism of peptide-binding specificity of IAP BIR domains. *Cell Death Differ* **2008**, *15* (5), 920-928.
75. Joazeiro, C. A. P.; Weissman, A. M., RING Finger Proteins: Mediators of Ubiquitin Ligase Activity. *Cell* **2000**, *102* (5), 549-552.
76. Salvesen, G. S.; Duckett, C. S., IAP proteins: blocking the road to death's door. *Nat Rev Mol Cell Biol* **2002**, *3* (6), 401-410.
77. (a) Shin, H.; Renatus, M.; Eckelman, Brendan P.; Nunes, Viviane A.; Sampaio, Claudio A M.; Salvesen, Guy S., The BIR domain of IAP-like protein 2 is conformationally unstable: implications for caspase inhibition. *Biochemical Journal* **2005**, *385* (Pt 1), 1-10; (b) Altieri, D. C., Validating survivin as a cancer therapeutic target. *Nat Rev Cancer* **2003**, *3* (1), 46-54; (c) Lage, S. L.; Longo, C.; Branco, L. M.; da Costa, T. B.; Buzzo, C. d. L.; Bortoluci, K. R., Emerging Concepts about NAIP/NLRC4 Inflammasomes. *Frontiers in Immunology* **2014**, *5*, 309; (d) Kasof, G. M.; Gomes, B. C., Livin, a Novel Inhibitor of Apoptosis Protein Family Member. *Journal of Biological Chemistry* **2001**, *276* (5), 3238-3246; (e) Hao, Y.; Sekine, K.; Kawabata, A.; Nakamura, H.; Ishioka, T.; Ohata, H.; Katayama, R.; Hashimoto, C.; Zhang, X.; Noda, T.; Tsuruo, T.; Naito, M., Apollon ubiquitinates SMAC and caspase-9, and has an essential cytoprotection function. *Nat Cell Biol* **2004**, *6* (9), 849-860.
78. Deveraux, Q. L.; Reed, J. C., IAP family proteins—suppressors of apoptosis. *Genes & Development* **1999**, *13* (3), 239-252.
79. (a) Rigaud, S.; Fondaneche, M.-C.; Lambert, N.; Pasquier, B.; Mateo, V.; Soulas, P.; Galicier, L.; Le Deist, F.; Rieux-Laucat, F.; Revy, P.; Fischer, A.; de Saint Basile, G.; Latour, S., XIAP deficiency in humans causes an X-linked lymphoproliferative syndrome. *Nature* **2006**, *444* (7115), 110-114; (b) Holcik, M.; Korneluk, R. G., XIAP, the guardian angel. *Nat Rev Mol Cell Biol* **2001**, *2* (7), 550-556.
80. Deveraux, Q. L.; Takahashi, R.; Salvesen, G. S.; Reed, J. C., X-linked IAP is a direct inhibitor of cell-death proteases. *Nature* **1997**, *388* (6639), 300-304.
81. Eckelman, B. P.; Salvesen, G. S.; Scott, F. L., Human inhibitor of apoptosis proteins: why XIAP is the black sheep of the family. *EMBO Reports* **2006**, *7* (10), 988-994.
82. (a) Chai, J.; Shiozaki, E.; Srinivasula, S. M.; Wu, Q.; Dataa, P.; Alnemri, E. S.; Shi, Y., Structural Basis of Caspase-7 Inhibition by XIAP. *Cell* **2001**, *104* (5), 769-780; (b) Huang, Y.; Park, Y. C.; Rich, R. L.; Segal, D.; Myszka, D. G.; Wu, H., Structural Basis of Caspase Inhibition by XIAP: Differential Roles of the Linker versus the BIR Domain. *Cell* **2001**, *104* (5), 781-790; (c) Riedl, S. J.; Renatus, M.; Schwarzenbacher, R.; Zhou, Q.; Sun, C.; Fesik, S. W.; Liddington, R. C.; Salvesen, G. S., Structural Basis for the Inhibition of Caspase-3 by XIAP. *Cell* **2001**, *104* (5), 791-800.
83. Scott, F. L.; Denault, J.-B.; Riedl, S. J.; Shin, H.; Renatus, M.; Salvesen, G. S., XIAP inhibits caspase-3 and -7 using two binding sites: evolutionarily conserved mechanism of IAPs. *The EMBO Journal* **2005**, *24* (3), 645-655.

84. Shiozaki, E. N.; Chai, J.; Rigotti, D. J.; Riedl, S. J.; Li, P.; Srinivasula, S. M.; Alnemri, E. S.; Fairman, R.; Shi, Y., Mechanism of XIAP-Mediated Inhibition of Caspase-9. *Molecular Cell* **2003**, *11* (2), 519-527.
85. Vande Walle, L.; Lamkanfi, M.; Vandenabeele, P., The mitochondrial serine protease HtrA2/Omi: an overview. *Cell Death Differ* **2008**, *15* (3), 453-460.
86. Hegde, R.; Srinivasula, S. M.; Zhang, Z.; Wassell, R.; Mukattash, R.; Cilenti, L.; DuBois, G.; Lazebnik, Y.; Zervos, A. S.; Fernandes-Alnemri, T.; Alnemri, E. S., Identification of Omi/HtrA2 as a Mitochondrial Apoptotic Serine Protease That Disrupts Inhibitor of Apoptosis Protein-Caspase Interaction. *Journal of Biological Chemistry* **2002**, *277* (1), 432-438.
87. (a) Verhagen, A. M.; Ekert, P. G.; Pakusch, M.; Silke, J.; Connolly, L. M.; Reid, G. E.; Moritz, R. L.; Simpson, R. J.; Vaux, D. L., Identification of DIABLO, a Mammalian Protein that Promotes Apoptosis by Binding to and Antagonizing IAP Proteins. *Cell* **2000**, *102* (1), 43-53; (b) Du, C.; Fang, M.; Li, Y.; Li, L.; Wang, X., Smac, a Mitochondrial Protein that Promotes Cytochrome c-Dependent Caspase Activation by Eliminating IAP Inhibition. *Cell* **2000**, *102* (1), 33-42.
88. Riedl, S. J.; Shi, Y., Molecular mechanisms of caspase regulation during apoptosis. *Nat Rev Mol Cell Biol* **2004**, *5* (11), 897-907.
89. Liu, Z.; Sun, C.; Olejniczak, E. T.; Meadows, R. P.; Betz, S. F.; Oost, T.; Herrmann, J.; Wu, J. C.; Fesik, S. W., Structural basis for binding of Smac/DIABLO to the XIAP BIR3 domain. *Nature* **2000**, *408* (6815), 1004-1008.
90. Eckelman, B. P.; Salvesen, G. S., The Human Anti-apoptotic Proteins cIAP1 and cIAP2 Bind but Do Not Inhibit Caspases. *Journal of Biological Chemistry* **2006**, *281* (6), 3254-3260.
91. (a) Hu, S.; Yang, X., Cellular Inhibitor of Apoptosis 1 and 2 Are Ubiquitin Ligases for the Apoptosis Inducer Smac/DIABLO. *Journal of Biological Chemistry* **2003**, *278* (12), 10055-10060; (b) Samuel, T.; Welsh, K.; Lober, T.; Togo, S. H.; Zapata, J. M.; Reed, J. C., Distinct BIR Domains of cIAP1 Mediate Binding to and Ubiquitination of Tumor Necrosis Factor Receptor-associated Factor 2 and Second Mitochondrial Activator of Caspases. *Journal of Biological Chemistry* **2006**, *281* (2), 1080-1090.
92. (a) Graber, T. E.; Holcik, M., Distinct roles for the cellular inhibitors of apoptosis proteins 1 and 2. *Cell Death and Dis* **2011**, *2*, e135; (b) Scheidereit, C., I[κ]B kinase complexes: gateways to NF-[κ]B activation and transcription. *Oncogene* **2000**, *25* (51), 6685-6705.
93. Mahoney, D. J.; Cheung, H. H.; Mrad, R. L.; Plenchette, S.; Simard, C.; Enwere, E.; Arora, V.; Mak, T. W.; Lacasse, E. C.; Waring, J.; Korneluk, R. G., Both cIAP1 and cIAP2 regulate TNF α -mediated NF- κ B activation. *Proceedings of the National Academy of Sciences* **2008**, *105* (33), 11778-11783.
94. Wertz, I. E.; Dixit, V. M., Signaling to NF- κ B: Regulation by Ubiquitination. *Cold Spring Harbor Perspectives in Biology* **2010**, *2* (3).
95. (a) Ea, C.-K.; Deng, L.; Xia, Z.-P.; Pineda, G.; Chen, Z. J., Activation of IKK by TNF α Requires Site-Specific Ubiquitination of RIP1 and Polyubiquitin Binding by NEMO. *Molecular Cell* **2006**, *22* (2), 245-257; (b) Wu, C.-J.; Conze, D. B.; Li, T.; Srinivasula, S. M.; Ashwell, J. D., Sensing of Lys 63-linked polyubiquitination by NEMO is a key event in NF-[κ]B activation. *Nat Cell Biol* **2006**, *8* (4), 398-406; (c) Naudé, P. J. W.; den Boer, J. A.; Luiten, P. G. M.; Eisel, U. L. M., Tumor necrosis factor receptor cross-talk. *FEBS Journal* **2011**, *278* (6), 888-898.

96. Yang, S.; Wang, B.; Tang, L. S.; Siednienko, J.; Callanan, J. J.; Moynagh, P. N., Pellino3 targets RIP1 and regulates the pro-apoptotic effects of TNF- α . *Nat Commun* **2013**, *4*.
97. Safara, A. R., c-FLIP, a master anti-apoptotic regulator. *Experimental Oncology* **2012**, *3*, 176-184.
98. Micheau, O.; Tschopp, J., Induction of TNF Receptor I-Mediated Apoptosis via Two Sequential Signaling Complexes. *Cell* **2003**, *114* (2), 181-190.
99. Yang, Q.-H.; Du, C., Smac/DIABLO Selectively Reduces the Levels of c-IAP1 and c-IAP2 but Not That of XIAP and Livin in HeLa Cells. *Journal of Biological Chemistry* **2004**, *279* (17), 16963-16970.
100. Srinivasula, S. M.; Hegde, R.; Saleh, A.; Datta, P.; Shiozaki, E.; Chai, J.; Lee, R.-A.; Robbins, P. D.; Fernandes-Alnemri, T.; Shi, Y.; Alnemri, E. S., A conserved XIAP-interaction motif in caspase-9 and Smac/DIABLO regulates caspase activity and apoptosis. *Nature* **2001**, *410* (6824), 112-116.
101. Wright, C. W.; Duckett, C. S., Reawakening the cellular death program in neoplasia through the therapeutic blockade of IAP function. *Journal of Clinical Investigation* **2005**, *115* (10), 2673-2678.
102. Kipp RA, C. M., Wist AD, Cresson CM, Carrell M, Griner E, Wiita A, Albinia PA, Chai J, ShiY, Semmelhack MF, McLendon GL, Molecular targeting of inhibitors of apoptosis proteins based on small molecule mimics of natural binding partners. *Biochemistry* **2002**, *41*, 7344-7349.
103. Jäger, R.; Zwacka, R. M., The Enigmatic Roles of Caspases in Tumor Development. *Cancers* **2010**, *2* (4), 1952-1979.
104. Deshayes, K.; Murray, J.; Vucic, D., The Development of Small-Molecule IAP Antagonists for the Treatment of Cancer. In *Protein-Protein Interactions*, Wendt, M. D., Ed. Springer Berlin Heidelberg: 2012; Vol. 8, pp 81-103.
105. Flygare, J. A.; Beresini, M.; Budha, N.; Chan, H.; Chan, I. T.; Cheeti, S.; Cohen, F.; Deshayes, K.; Doerner, K.; Eckhardt, S. G.; Elliott, L. O.; Feng, B.; Franklin, M. C.; Reisner, S. F.; Gazzard, L.; Halladay, J.; Hymowitz, S. G.; La, H.; LoRusso, P.; Maurer, B.; Murray, L.; Plise, E.; Quan, C.; Stephan, J.-P.; Young, S. G.; Tom, J.; Tsui, V.; Um, J.; Varfolomeev, E.; Vucic, D.; Wagner, A. J.; Wallweber, H. J. A.; Wang, L.; Ware, J.; Wen, Z.; Wong, H.; Wong, J. M.; Wong, M.; Wong, S.; Yu, R.; Zobel, K.; Fairbrother, W. J., Discovery of a Potent Small-Molecule Antagonist of Inhibitor of Apoptosis (IAP) Proteins and Clinical Candidate for the Treatment of Cancer (GDC-0152). *Journal of Medicinal Chemistry* **2012**, *55* (9), 4101-4113.
106. Sheng, R.; Sun, H.; Liu, L.; Lu, J.; McEachern, D.; Wang, G.; Wen, J.; Min, P.; Du, Z.; Lu, H.; Kang, S.; Guo, M.; Yang, D.; Wang, S., A Potent Bivalent Smac Mimetic (SM-1200) Achieving Rapid, Complete, and Durable Tumor Regression in Mice. *Journal of Medicinal Chemistry* **2013**, *56* (10), 3969-3979.
107. Condon, S. M.; Mitsuuchi, Y.; Deng, Y.; LaPorte, M. G.; Rippin, S. R.; Haimowitz, T.; Alexander, M. D.; Kumar, P. T.; Hendi, M. S.; Lee, Y.-H.; Benetatos, C. A.; Yu, G.; Kapoor, G. S.; Neiman, E.; Seipel, M. E.; Burns, J. M.; Graham, M. A.; McKinlay, M. A.; Li, X.; Wang, J.; Shi, Y.; Feltham, R.; Bettjeman, B.; Cumming, M. H.; Vince, J. E.; Khan, N.; Silke, J.; Day, C. L.; Chunduru, S. K., Birinapant, a Smac-Mimetic with Improved Tolerability for the Treatment of Solid Tumors and Hematological Malignancies. *Journal of Medicinal Chemistry* **2014**, *57* (9), 3666-3677.
108. Sun, H.; Liu, L.; Lu, J.; Bai, L.; Li, X.; Nikolovska-Coleska, Z.; McEachern, D.; Yang, C.-Y.; Qiu, S.; Yi, H.; Sun, D.; Wang, S., Potent Bivalent Smac Mimetics: Effect of the Linker on Binding

to Inhibitor of Apoptosis Proteins (IAPs) and Anticancer Activity. *Journal of Medicinal Chemistry* **2011**, *54* (9), 3306-3318.

109. Hennessy, E. J.; Adam, A.; Aquila, B. M.; Castriotta, L. M.; Cook, D.; Hattersley, M.; Hird, A. W.; Huntington, C.; Kamhi, V. M.; Laing, N. M.; Li, D.; MacIntyre, T.; Omer, C. A.; Oza, V.; Patterson, T.; Repik, G.; Rooney, M. T.; Saeh, J. C.; Sha, L.; Vasbinder, M. M.; Wang, H.;

Whitston, D., Discovery of a Novel Class of Dimeric Smac Mimetics as Potent IAP Antagonists Resulting in a Clinical Candidate for the Treatment of Cancer (AZD5582). *Journal of Medicinal Chemistry* **2013**, *56* (24), 9897-9919.

110. Chauhan, D.; Neri, P.; Velankar, M.; Podar, K.; Hideshima, T.; Fulciniti, M.; Tassone, P.; Raje, N.; Mitsiades, C.; Mitsiades, N.; Richardson, P.; Zavel, L.; Tran, M.; Munshi, N.; Anderson, K. C., Targeting mitochondrial factor Smac/DIABLO as therapy for multiple myeloma (MM). *Blood* **2007**, *109* (3), 1220-1227.

111. Cossu, F.; Milani, M.; Mastrangelo, E.; Vachette, P.; Servida, F.; Lecis, D.; Canevari, G.; Delia, D.; Drago, C.; Rizzo, V.; Manzoni, L.; Seneci, P.; Scolastico, C.; Bolognesi, M., Structural Basis for Bivalent Smac-Mimetics Recognition in the IAP Protein Family. *Journal of Molecular Biology* **2009**, *392* (3), 630-644.

112. Ndubaku, C.; Varfolomeev, E.; Wang, L.; Zobel, K.; Lau, K.; Elliott, L. O.; Maurer, B.; Fedorova, A. V.; Dynek, J. N.; Koehler, M.; Hymowitz, S. G.; Tsui, V.; Deshayes, K.; Fairbrother, W. J.; Flygare, J. A.; Vucic, D., Antagonism of c-IAP and XIAP Proteins Is Required for Efficient Induction of Cell Death by Small-Molecule IAP Antagonists. *ACS Chemical Biology* **2009**, *4* (7), 557-566.

113. Sun, H.; Nikolovska-Coleska, Z.; Yang, C.-Y.; Qian, D.; Lu, J.; Qiu, S.; Bai, L.; Peng, Y.; Cai, Q.; Wang, S., Design of Small-Molecule Peptidic and Nonpeptidic Smac Mimetics. *Accounts of Chemical Research* **2008**, *41* (10), 1264-1277.

114. Petersen, S. L.; Wang, L.; Yalcin-Chin, A.; Li, L.; Peyton, M.; Minna, J.; Harran, P.; Wang, X., Autocrine TNF α Signaling Renders Human Cancer Cells Susceptible to Smac-Mimetic-Induced Apoptosis. *Cancer Cell* **2007**, *12* (5), 445-456.

115. Varfolomeev, E.; Blankenship, J. W.; Wayson, S. M.; Fedorova, A. V.; Kayagaki, N.; Garg, P.; Zobel, K.; Dynek, J. N.; Elliott, L. O.; Wallweber, H. J. A.; Flygare, J. A.; Fairbrother, W. J.; Deshayes, K.; Dixit, V. M.; Vucic, D., IAP Antagonists Induce Autoubiquitination of c-IAPs, NF- κ B Activation, and TNF α -Dependent Apoptosis. *Cell* **2007**, *131* (4), 669-681.

116. Silke, J.; Meier, P., Inhibitor of Apoptosis (IAP) Proteins—Modulators of Cell Death and Inflammation. *Cold Spring Harbor Perspectives in Biology* **2013**, *5* (2).

117. Gaither, A.; Porter, D.; Yao, Y.; Borawski, J.; Yang, G.; Donovan, J.; Sage, D.; Slisz, J.; Tran, M.; Straub, C.; Ramsey, T.; Iourgenko, V.; Huang, A.; Chen, Y.; Schlegel, R.; Labow, M.; Fawell, S.; Sellers, W. R.; Zavel, L., A Smac Mimetic Rescue Screen Reveals Roles for Inhibitor of Apoptosis Proteins in Tumor Necrosis Factor- α Signaling. *Cancer Research* **2007**, *67* (24), 11493-11498.

118. Geserick, P.; Hupe, M.; Moulin, M.; Wong, W. W.-L.; Feoktistova, M.; Kellert, B.; Gollnick, H.; Silke, J.; Leverkus, M., Cellular IAPs inhibit a cryptic CD95-induced cell death by limiting RIP1 kinase recruitment. *The Journal of Cell Biology* **2009**, *187* (7), 1037-1054.

119. Fulda, S., Novel Promising IAP Antagonist on the Horizon for Clinical Translation. *Journal of Medicinal Chemistry* **2012**, *55* (9), 4099-4100.

120. Lecis, D.; De Cesare, M.; Perego, P.; Conti, A.; Corna, E.; Drago, C.; Seneci, P.; Walczak, H.; Colombo, M. P.; Delia, D.; Sangaletti, S., Smac mimetics induce inflammation and necrotic tumour cell death by modulating macrophage activity. *Cell Death Dis* **2013**, *4*, e920.
121. Kearney, C. J.; Sheridan, C.; Cullen, S. P.; Tynan, G. A.; Logue, S. E.; Afonina, I. S.; Vucic, D.; Lavelle, E. C.; Martin, S. J., Inhibitor of Apoptosis Proteins (IAPs) and Their Antagonists Regulate Spontaneous and Tumor Necrosis Factor (TNF)-induced Proinflammatory Cytokine and Chemokine Production. *Journal of Biological Chemistry* **2013**, *288* (7), 4878-4890.
122. Wu, H.; Tschopp, J.; Lin, S.-C., Smac Mimetics and TNF α : A Dangerous Liaison? *Cell* *131* (4), 655-658.

Chapter 2: The Development of SMAC Mimetics to Treat Cancer

2.1 Early SAR Work

Initial efforts in the design of SMAC mimetics focused substituting peptides in the short AVPI peptide sequence, which was known to mediate binding to IAPs.¹ The Abbott laboratories research group, under the direction of Dr. Fesik, filed the first patent for an IAP antagonist in 2001 claiming rights to several AVPI derived short peptide sequences.² A key study by McLendon and colleagues examined the contribution that each residue of the AVPI sequence made to binding affinity; this early work provided an essential framework for the structure activity relationship (SAR) strategies employed by other research groups.³ They obtained dissociation constant values from the interaction between their peptides and the purified BIR3 domain of XIAP and their results can be easily summarized: Alanine (P1) proved to be the least amenable to modification, which is not surprising considering it possesses 5 hydrogen bonds between the AVPI sequence and XIAP. Substitution of A for either glycine or serine reduced binding affinity, however the substitution of a 2-amino butyric acid residue (ethyl side chain) halved the K_D (relative to AVPI) to 0.24 μM . Valine (P2) was reasonably open to substitution and fared best when hydrophobic branched residues (leu, ile, phe) or basic amino acids (his, lys) were substituted. Substitution of the proline residue (P3) produced small decreases in binding efficiency which became more pronounced in more potent analogues and was deemed to be unmodifiable. The fourth isoleucine position (P4) was the most easily modified, non-polar amino acids such as phenylalanine and tryptophan provided the best results. This was consistent with observations by Shi that the isoleucine residue of SMAC occupies a hydrophobic channel in the BIR3 binding groove.⁴ N-methylation of the AVPI amide nitrogens was largely not tolerated, with the exception of N-methylation at the fourth residue when phenylalanine was substituted for isoleucine. A study by Genentech employing a phage-display peptide library screen to identify novel BIR3 binding motifs achieved similar results, and corroborated McLendon's findings.⁵

Although these peptide based SMAC analogues displayed promising binding affinities for XIAP they were predicted to suffer from poor cell permeability as well as proteolytic instability.⁶ The first peptidomimetics were reported in 2004 and these adhered to the AVPI scaffold but

possessed more “drug like” properties. Shaomeng Wang from the University of Michigan published the first such article in a JACS communication where he briefly described several novel SMAC derived peptidomimetics, including **1**, able to bind XIAP BIR3 with low nanomolar affinities and enhance etoposide mediated cell death.⁷ Two follow-up publications described his group’s efforts in greater detail.^{8,9} Wang’s early work focussed on modifying the P4 position isoleucine residue of the AVPI motif with various hydrophobic moieties. The most potent analogue from this series, **2** (Figure 11) possessed a P4 diphenylmethyl amide with an N-terminal 2-amino butyrate residue and exhibited a K_i of 24 nM versus the BIR3 domain of XIAP.⁸ Another paper by Wang described novel, conformationally constrained 6,5-bicyclic SMAC mimetics where the position 2 (P2) valine was substituted with a six-membered ring tethered to the position 3 (P3) proline.¹⁰ This compound series exhibited weaker potency than his earlier report however his most potent compound **2** was able to enhance apoptosis in PC-3 prostate tumor cells (from 9 to 23%) when combined with cisplatin and a carrier peptide.

Oost and Fesik of Abbott pharmaceuticals released a landmark publication which contributed immensely the current understanding of SMAC SAR.¹¹ They tested AVPI peptide-substitution analogues for binding affinity with the XIAP BIR3 domain and disclosed that bulky tert-leucine (tle) and cyclohexylglycine residues at P2 conferred the highest potency; these residues are now ubiquitous among many SMAC mimetics. Through amino acid substitution they also found that L-stereochemistry along the AVPI sequence was imperative for effective BIR3 binding. N-methylation of the P1 alanine was explored and the authors observed no ill-effects on binding affinity, although N,N-di-methylation proved detrimental. They tested numerous aromatic P4 residues and found that peptidomimetic **3** (Figure 11) with an (*R*)-linked tetrahydronaphthyl moiety at P4, a P2 cyclohexylglycine and N-methylation of alanine gave good BIR3 binding affinity ($K_D = 16$ nM). Crucially, they demonstrated the ability of their peptidomimetics to induce cell death, unaided, in several cancer cell lines. This, combined with results demonstrating tumor regression of MDA-MB-231 breast cancer cells in a mouse-xenograft model proved SMAC mimetics could act as stand-alone therapeutics.

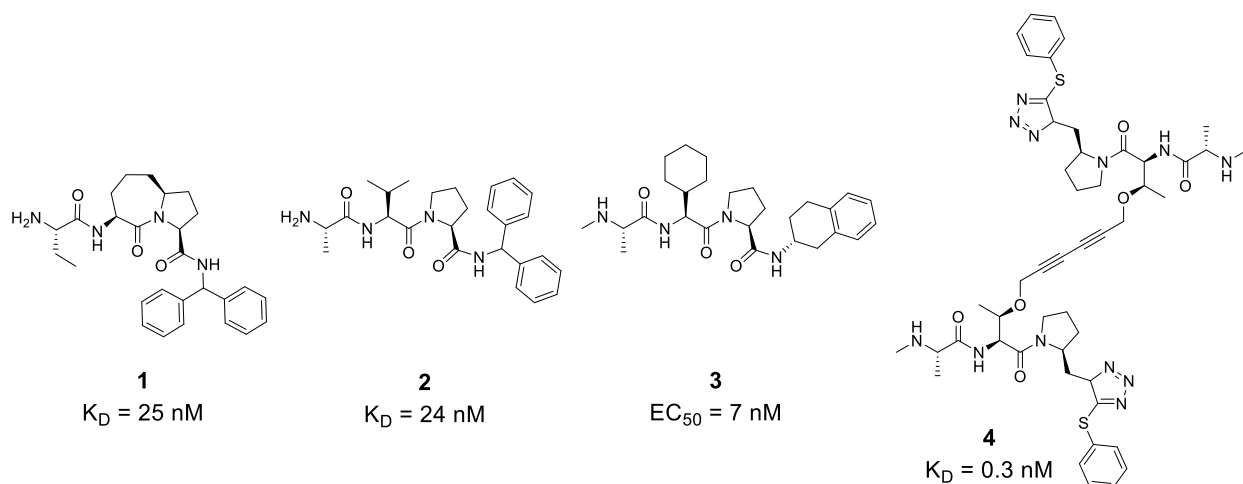


Figure 11. Examples of early SMAC peptidomimetics. Compounds **1** and **2** by the Wang group show high binding affinities for the BIR3 domain of XIAP, **1** was reported in the 2004 JACS publication as an improved version of their initial 6,5-bicycle. Compound **3** the most potent among a series of compounds tested against cells by Abbott pharmaceuticals, it showed low nanomolar toxicity against BT-549 breast cancer cells.

Another significant early report in the SMAC mimetic literature was that of dimerization. The dimeric SMAC mimetic **4** (Figure 11) was discovered serendipitously by the Li/Harran groups as a side product from a copper catalysed reaction; it resulted from the combination of two monomers at the P2 propargylic residue *via* a Glaser coupling.^{12,13} Testing of dimer **4** in a caspase 3-activation assay and found that it significantly outperformed its monomeric counterpart. They reasoned that it was able to simultaneously interact with the BIR2 and BIR3 domains of XIAP in its dimeric state, a feature already known to exist in XIAP's native interaction with the SMAC protein.¹⁴

These early reports effectively laid the groundwork for the strategy of SMAC mimetic design. Through detailed SAR studies it was determined that the P1 (alanine) and P3 (positions) of the AVPI motif should remain largely unaltered, that P2 (valine) and P4 (isoleucine) are open to modification with bulky hydrophobic moieties and that inhibitor dimerization may allow small molecule mimetics to

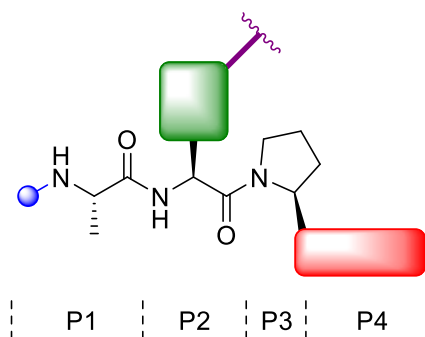


Figure 12. A general scheme for SMAC mimetic design. N-methylation of P1 (blue) improves cell permeability, bulky hydrophobic residues (green and red) at the P2 side chain and P4 improve compound potency. The P2 side chain serves as an effective linker site for dimeric SMAC mimetics (purple).

replicate the 2-point binding mode of SMAC for XIAP (Figure 12). Subsequent work in the filed draws heavily from these early findings.

2.2 Classes of SMAC Mimetics

SMAC mimetics can largely be divided into two categories: monovalent and bivalent IAP antagonists. Each has its own inherent strengths/weaknesses and both have been pursued equally through SAR work since the dichotomy was first established by Li and Harran in 2004. Monomeric (or monovalent) SMAC mimetics benefit from good physiochemical properties and largely do not violate Lipinski's rule¹⁵ however they exhibit less potency relative to their dimeric counterparts.¹ Conversely, dimeric (or bivalent) SMAC mimetics can be highly efficient inhibitors of IAPs and often exceed the potency of their monovalent cousins by 2-3 orders of magnitude.⁶ However, they are large molecules which are not orally bioavailable and must be given intravenously, which could complicate their development as therapeutics.¹

2.2.1 Monovalent SMAC Mimetics

Numerous publications have reported monomeric SMAC mimetics from groups of both industrial and academic origin. In general, 3 strategies for monovalent SMAC mimetics have been adopted in the literature: (1) the use of a conformationally restricted bicyclic mimetic wherein the P3 proline forms a bicycle with an adjoining ring at P2 or P4, (2) non-constrained mimetics with a bulky P2 residue and heavy modification to the P4 and its short linker, (3) non-peptidomimetics composed of heterocyclic rings in place of amide bonds.

2.2.1.A Constrained Bicyclic SMAC mimetics

A 2006 Genentech publication described the synthesis of several 7,5-bicyclic SMAC mimetics linked bearing a P2-P3 ring junction.¹⁶ Computational analysis was used to design the 7-membered ring and pyrazole P4 residue. Additional, modifications to the proline ring included the incorporation of a sulfur atom and di-methylation to yield their most potent analogue **5** (Figure 13). Several compounds had nanomolar binding affinities to IAPs which included XIAP as well as cIAP-1/2 and in addition, were able to induce apoptosis through confirmed caspase-3/7 activation in cell based assays. Another Genentech study explored inhibitory effects of a P3-P4 azabicyclooctane SMAC mimetic on IAP activity.¹⁷ X-ray studies suggested that the cis-fused bicyclic core was able to re-orient the direction of the P3-P4 amide linkage and constrain the

molecular conformation such that the lipophilic P4 moiety maximized its interaction with the BIR domain hydrophobic pocket. Compound **6** (Figure 13) was the most efficient IAP inhibitor of those tested, it was able to bind the BIR3 domains of XIAP and cIAP-1 with binding affinities of 140 nM and 33 nM respectively. **6** activated caspase-3/7 and killed MDA-MB-231 breast cancer cells with an $EC_{50} = 980$ nM. Interestingly, it was not cytotoxic to non-cancerous human mammary epithelial cells (HMECs) and demonstrated no caspase activation in that particular assay. This result demonstrated the ability of SMAC mimetics to re-activate caspase activity and apoptosis in cancerous cells by binding IAPs without inducing apoptosis in healthy cells. A mouse xenograft experiment showed that **6** was able to elicit tumor shrinkage at a dose of 50 mg/kg.

The Wang group continued their bicyclic SMAC mimetic work, releasing an article in 2006 detailing modifications made to compound **1**. They described that N-methylation of the alanine nitrogen improved cell-based growth inhibition 500 fold over the original compound in MDA-MB-231 breast cancer cells (new $IC_{50} = 100$ nM) without comprising its affinity for XIAP BIR3.¹⁸ An ensuing publication described modifications to this new, N-methyl derivative of **1**.¹⁹ A phenyl group was added to the top of the 7-membered ring to form a tricyclic mimetic, this compound experienced a 5 fold drop in potency versus MDA-MB-231 breast cancer cells. Expansion of the proline ring by one carbon to form a 7,6-bicyclic monomer caused a massive drop in potency (EC_{50} of 1.2 μ M). Molecular modeling showed that the expanded proline ring distorted its interaction with Trp 323, although all the original hydrogen bonds remained intact. Substitution of the diphenylmethyl P4 moiety in **1** for the (R)-tetrahydronaphthyl used by Fesik¹¹ significantly enhanced potency leading to the 7,5-bicyclic compound **7** (Figure 13), with an $EC_{50} = 68$ nM in their cell based assay.

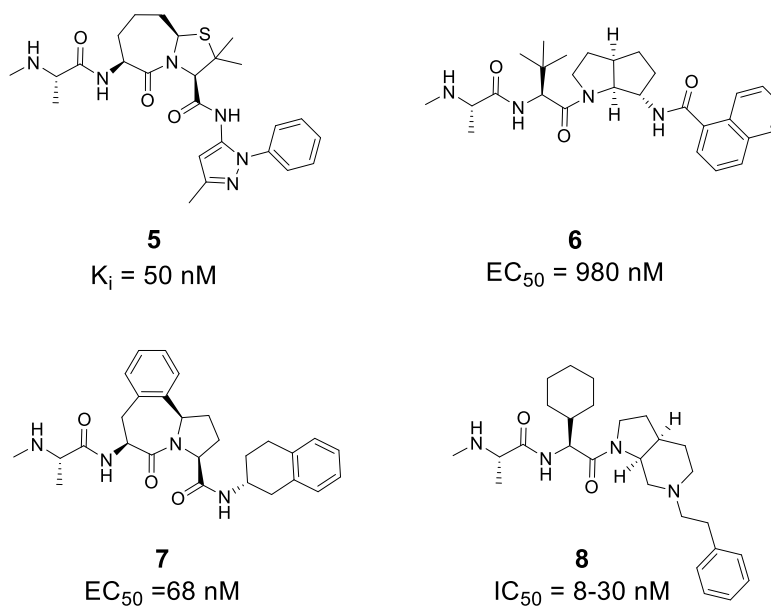


Figure 13. Examples of potent, bicyclic monovalent SMAC mimetics

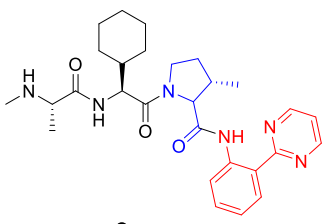
Novartis developed a P3-P4 bicyclic monovalent SMAC monomer (LBW242) **8** (Figure 13) with potent activity against multiple myeloma (MM) cancer cells.²⁰ Their compound was toxic to bortezomib resistant MM cells with an $IC_{50} = 8\text{-}30 \mu\text{M}$ (reported as a range); PARP (Poly ADP ribose polymerase) cleavage (a hallmark of apoptosis)²¹ was detected, which suggested that they were activating caspases and promoting apoptosis. Further analysis determined that **8** was activating caspase-3,8 and 9 in MM cells and testing in healthy lymphocytes produced no toxic effects below $10 \mu\text{M}$, demonstrating a degree of selectivity towards cancer cells.

2.2.1.B Non-Constrained SMAC Mimetics

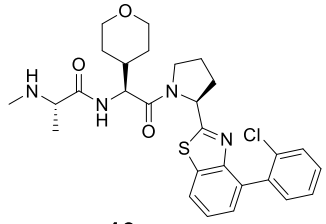
Several groups have produced potent monovalent SMAC peptidomimetics which do not incorporate bicyclic structures. The early goal of SMAC mimetic design was to create potent inhibitors of XIAP.⁶ Later work recognized the co-relation between cIAP-1 & 2 inhibition and enhanced potency however little was understood of the contribution cIAP made to the overall induction of apoptosis by SMAC mimetics. Salvesen and colleagues mapped the peptide binding interactions between various IAP BIR domains and a library of short peptides, however they did not disclose any IAP selective peptidomimetic agonists.²² A team from Genentech released an article in 2009 which detailed their efforts to design a selective inhibitor of cIAP-1 capable of

inducing apoptosis.²³ Using X-ray crystal structure data of the XIAP and cIAP-1 BIR3 IBM binding grooves, they constructed analogues which exploited differences between the two to achieve selective inhibition (Table 1). The XIAP BIR3 binding groove was more congested than that of cIAP-1; a Tyr 234 residue near the proline binding position and Thr 308 in the P4 hydrophobic binding pocket of XIAP created potential steric interaction sites not found in cIAP-1. Compound **9** was synthesized to bind cIAP-1 selectively, a methyl group on the proline ring clashed with the phenolic oxygen of Tyr 308 while a 2-pyrimidinyl heterocycle engaged in lone pair repulsion with the hydroxyl of Thr 308 in the XIAP BIR3 binding groove. Compound **10** lacked these modifications and engaged in high affinity binding with both BIR domains. Through various assays the authors were able to demonstrate that cIAP-1/2 activation was sufficient to induce apoptosis in cancer cells however they stated that “pan-selectivity” for both XIAP and cIAP produced significantly more potent inhibitors.

Table 1. Comparison of binding affinities for cIAP selective (**6**) and pan selective (**7**) SMAC mimetics. The methylated proline (blue) 2, pyramidal heterocyclic P4 (red) were found to impart selective cIAP BIR 3 binding.



9
IC₅₀ = 15 nM



10
IC₅₀ = 150 nM

Antagonist	K _i (μM)			Selectivity (X/c1)
	cIAP-1 BIR3	cIAP-2 BIR3	XIAP BIR3	
9	0.016	0.085	>34	>2000
10	0.036	0.096	0.033	~1

Recently, Genentech reported the development of a new monomeric SMAC mimetic (GDC-0152) **11** (Figure 14) which was advanced to Phase I clinical trials.²⁴ They developed their compound through SAR optimization primarily *via* substitution of bulky hydrophobic residues at the P2 and

P4 residues consistent with work by other groups. They took an interesting approach to P1 however, which is usually left unmodified, and extended the classical N-methyl group with various functionalities. Addition of a cyclopropyl methyl group and a 2,3-dihydroxypropyl group led to no enhancement in IAP binding affinity over the original P1 N-methyl derivative. Their lead compound exhibited nanomolar K_i values with high binding affinities to several IAPs: ML-IAP BIR3 = 14 nM, XIAP BIR3 = 28 nM, XIAP BIR2 = 112 nM, cIAP-1 BIR3 = 17 nM, cIAP-2 BIR 3 = 43 nM. Testing of **11** against MDA-MB-231 breast cancer cells demonstrated cell killing below 100 nM and a caspase-3/7 activation assay showed positive results. Mice, treated orally with **11** showed tumor size reduction in a human-tumor xenograft model. Pre-clinical data gathered on GDC-0152 suggested a favourable PK (pharmacokinetic) profile and it was advanced to phase I clinical trials.²⁵ A 2nd generation analogue GDC-0197 **12** was also entered into clinical trials.²⁶

Novartis developed compound **14** (LCL161) (Figure 14) with a cyclohexyl moiety at P2 and a *p*-fluoro-benzoyl thiazole linked P4 residue.^{27,28} Testing of **14** alone was conducted in tyrosine kinase resistant leukemia cell lines with IC_{50} values ranging from 50 nM to 3 μ M depending on cell type. A combination therapy consisting of LCL161 and nilotinib was administered to mice with BCR-ABL expressing leukemia for 5 weeks (n=10). The investigators found that the combination therapy reduced tumor load below that of nilotinib alone to an almost undetectable level and, following treatment cessation, showed an 80% survival rate past day 100 compared to nilotinib alone which had no survivors past day 80.

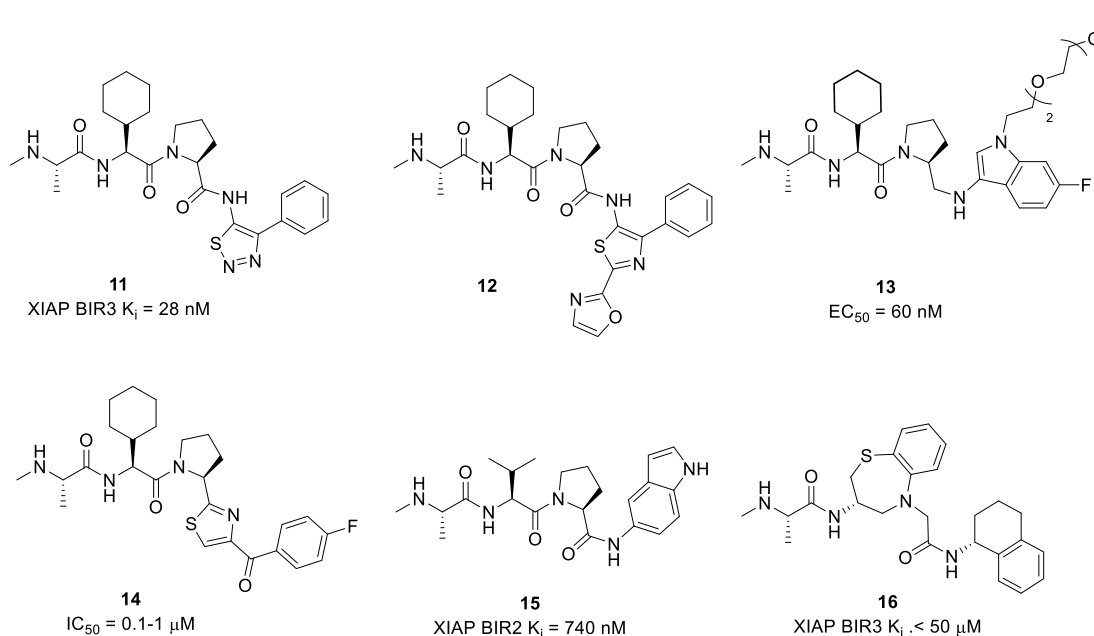


Figure 14. Some examples of potent non-constrained SMAC monomers. **13** was reported in a patent by Tetralogic pharmaceuticals and explored the hydrophobic P4 binding pocket with a large PEG chain.²⁹ **15** was reported as a XIAP BIR2 selective binding agent.³⁰ **16** was described in a patent by Agera pharmaceuticals in which analogues had their P2 and P3 residues combined into a single 7-membered ring.³¹

2.2.1.C Non-peptide based SMAC Mimetics

Some research groups have deviated from the amide-linked peptidomimetic scaffold and have favoured the use of polycyclic heterocycles, common in medicinal chemistry³², to mimic the effects of the SMAC AVPI motif in BIR domain binding. The McLendon group attempted to replace the P2-P3 amide linkage with an oxazole ring **17** (Figure 15) in order to enhance proteolytic stability and cell permeability.³³ Binding studies showed it was 50 times less potent at binding XIAP BIR3 ($K_i = 11$ μ M) relative to the AVPI sequence, however in a cell-based assay against MDA-MB-231 breast cancer cells it induced 25% cell death at 30 μ M while AVPI did not, even at 500 μ M. Crystal structure overlay of **17** in the XIAP BIR3 IBM binding groove showed that it lost a net 2-hydrogen bonds, however it maintained the essential P1 nitrogen Glu 314 charge stabilized hydrogen bond.

Another research group used *in-silico* modeling of the XIAP BIR3 IBM binding groove to computationally design potent SMAC mimetics using a library of “drug like” substituents. Several

lead compounds were synthesized and tested for their XIAP BIR3 binding affinities, compound **18** (Figure 15) had a $K_i = 2.5 \mu\text{M}$ and performed well in an assay against MDA-MB-231 cells inhibiting growth with an $\text{IC}_{50} = 16 \mu\text{M}$.³⁴

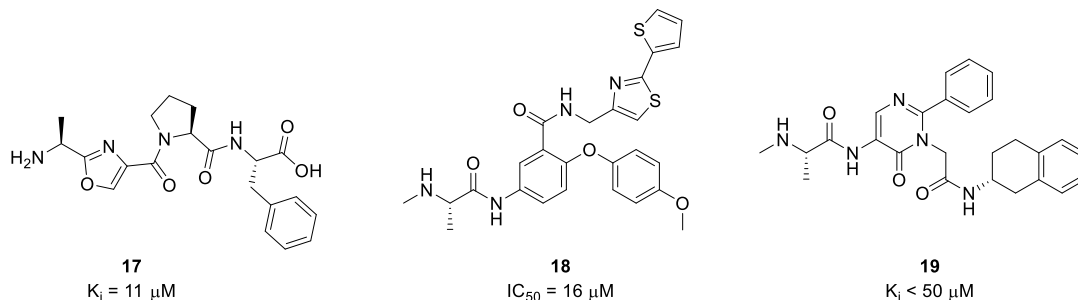


Figure 15. Examples of non-peptide based SMAC mimetics. Compound **19** was disclosed in a Novartis patent.³⁵

2.2.2 Bivalent SMAC mimetics

Since Li and Harran first reported their dimeric SMAC mimetic **4** numerous groups have applied the same strategy to generate a rich class of bivalent IAP inhibitors.⁶ The general SAR strategies applied to the synthesis of bivalent SMAC mimetics mirror those used in the design of their monovalent relatives (section 2.3.1) and are often simply the product of a cross-linking reaction. Most experimentation has been in the placement and properties of the linker connecting the two monomeric fragments in the bivalent mimetic. SMAC mimetics have generally been linked *via* the P2 and P4 residues employing a diverse array of linkers. In addition, some groups have experimented with unusual strategies such as P3 linkage, hetero-dimerization and homo-trimerization, achieving mixed results.

2.2.2.A P4-Linked Homodimeric SMAC mimetics

Although the first bivalent SMAC mimetic was reported as a P2 dimer¹³ subsequent publications focussed on dimerization at P4. Perhaps spurred by the results of Jiang³⁶, which showed that two AVPI residues connected by a flexible linker at the C-terminus could concurrently bind the BIR2 and BIR3 domains of XIAP, many groups employed a P4 tethering strategy. Genentech showed that a bivalent SMAC mimetic (BV6) **21** joined by a flexible P4 linker was able to bind IAP BIR3 domains with high affinity: K_i XIAP = 1.3 nM, K_i cIAP-1 = 0.46 nM.³⁷ Western analysis showed rapid degradation (minutes) of cIAP-1 in cells treated with **21** and the

dimer showed a significantly enhanced potency over the monomer (**20**, MV1) with IC_{50} values of 14 nM and 5 μ M respectively. In an elegant experiment, they were able to show using siRNA that SMAC mimetic treated cells were undergoing TNF- α dependent caspase-8 activation, suggesting that caspase-8 activation rather than caspase-9 was responsible for inducing apoptosis (Figure 16). They proposed that their compounds were able to antagonize cIAP-1/2 in cells leading to TNRF1 mediated caspase-8 activation and apoptosis.

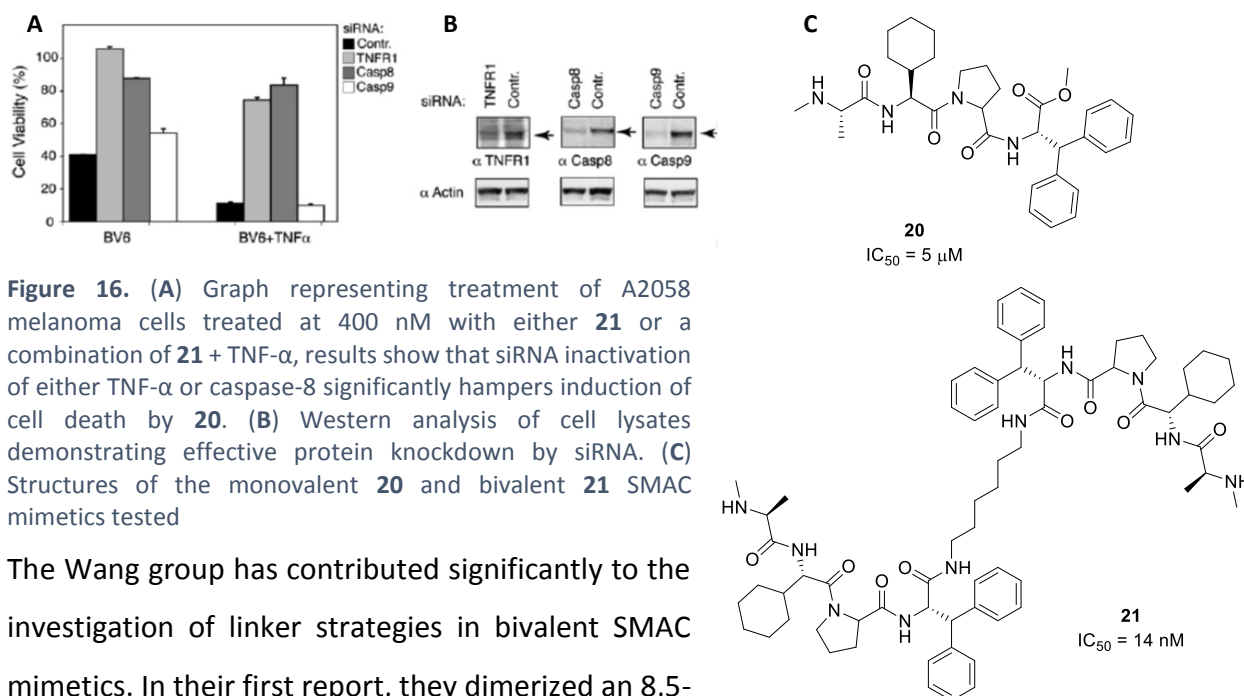


Figure 16. (A) Graph representing treatment of A2058 melanoma cells treated at 400 nM with either **21** or a combination of **21** + TNF- α , results show that siRNA inactivation of either TNF- α or caspase-8 significantly hampers induction of cell death by **20**. (B) Western analysis of cell lysates demonstrating effective protein knockdown by siRNA. (C) Structures of the monovalent **20** and bivalent **21** SMAC mimetics tested

The Wang group has contributed significantly to the investigation of linker strategies in bivalent SMAC mimetics. In their first report, they dimerized an 8,5-

bicyclic version of their earlier 7,5-bicyclic monomer **1**. They used computational modeling to show that one of the phenyl rings in their biphenyl methyl P4 substituent sat outside of the P4 BIR hydrophobic binding pocket and predicted that this could serve as a reasonable attachment point;³⁸ in a later study they confirmed this prediction to be true using an X-ray crystallography.⁹ To their delight dimer **22** (SM-164) (Figure 17), connected through a flexible alkyl-aryl linker, showed superior cell growth inhibition ($IC_{50} = 1$ nM) in HL-60 leukemia cells with minimal non-apoptotic cell death. A study evaluating its mechanism of apoptotic induction showed that **22** potently inhibited cIAP-1/2 ($K_i = 0.3, 1.1$ nM respectively) as well as XIAP. They concluded that their compound was inducing TNF- α mediated apoptosis through caspase-8 activation but stressed that XIAP inhibition was still essential for effective apoptosis by protecting the caspase-

3 from XIAP binding.³⁹ In a 2011 paper they revealed how chemical modification to the linker connecting bivalent SMAC mimetics can modulate their activity against IAPs (Figure 17).⁴⁰ They noticed that compounds like **22** with long lipophilic linkers garnered enhanced anti-tumor cell potency while maintaining relatively constant IAP inhibition compared to compounds with polar PEG based **23** or shortened linkers **24**. They developed a technique to measure the relative cellular concentration of their compounds in MDA-MB-231 breast cancer cells and found that compounds such as **22** with longer, lipophilic linkers were present in cells at higher concentrations. Thus, they concluded that the observed enhancement in potency of **22** over compounds such as **23** and **24** was a function of cellular permeability, and not IAP inhibition.

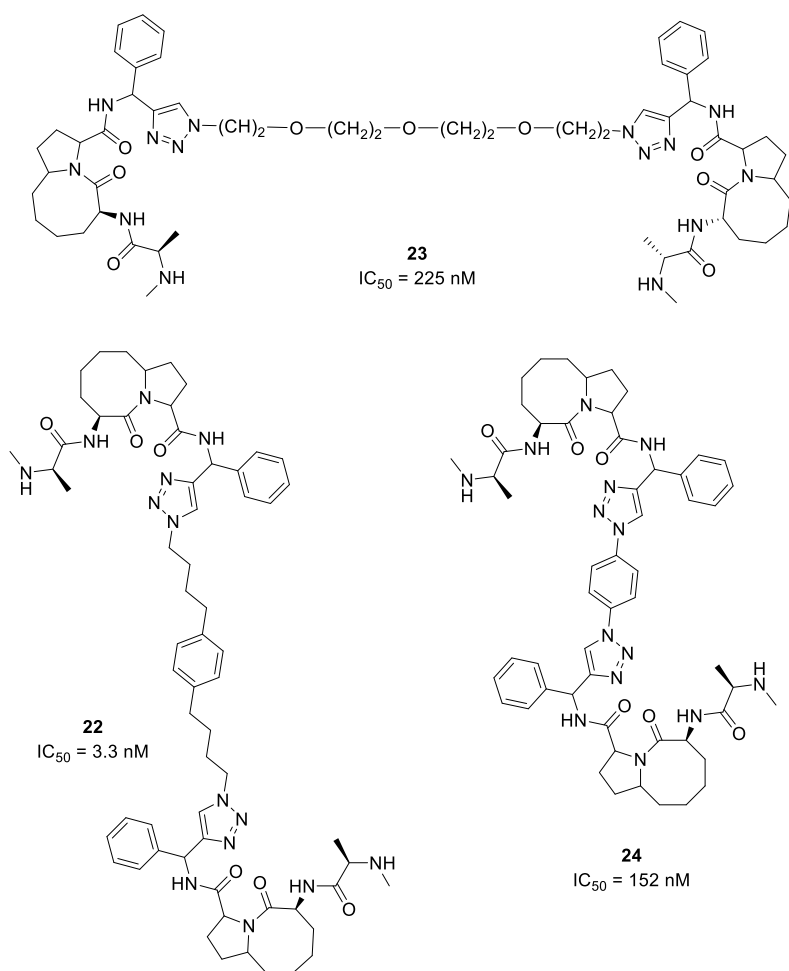


Figure 17. Examples of potent P4 linked SMAC mimetic dimers reported by Wang. IC₅₀ values were obtained following incubation of compounds in MDA-MB-231 breast cancer cells.

Other groups have reported similar results in P4 linker optimization. AstraZeneca disclosed its first attempts at designing bivalent SMAC mimetics in a 2013 *J. Med. Chem.* article.⁴¹ Their SAR work adhered to previously reported strategies, substituting the P2 and P4 positions with bulky lipophilic groups. They also attempted to modify the P3 proline ring through the addition of a cyclopropane as well as heteroatom substitution, however the unaltered proline moiety performed best. Using P2 cyclohexyl and P4 indanyl groups in their

monomers, they explored several dimerization strategies through a P4 linkage. Consistent with the findings of Wang, they noted that linker length/flexibility had minimal effects on IAP binding affinity but translated to marked differences in cellular growth inhibition. Compound **25** (AZD5582) (Figure 18), with a bis-alkyne linker reminiscent of the first bivalent SMAC mimetic **4**, was chosen as a lead for advanced clinical development. It demonstrated excellent growth inhibition in MDA-MB-231 breast cancer cells ($GI_{50} = 0.1$ nM) and was well tolerated in a mouse xenograft efficacy model, promoting tumor shrinkage and growth suppression for 40 days post-treatment.

Birinapant **26** (Figure 18) was patented in 2009 by Tetralogic⁴² however the first detailed account of its biological activity did not surface until 2014;⁴³ an earlier publication described the activity of another, less efficient analogue.⁴⁴ Birinapant is a bivalent SMAC mimetic connected through a short bis-indole linkage at P4. It is the most advanced SMAC mimetic to date and is engaged in/has completed several clinical trials for cancer treatment at the phase I/II level (refer to clinicaltrials.gov). Unlike other SMAC mimetics, **26** lacks a bulky substituent at P2, having been replaced with a non-branched ethyl group. They found that a reduction in β -branching at the P2 position resulted in weakened affinity for the BIR3 domains of XIAP and cIAP-2 while maintaining affinity for cIAP-1. Using previous research which showed that both XIAP^{-/-}/cIAP-1^{-/-} and cIAP-2^{-/-}/cIAP-1^{-/-} double knockout mutant mice suffered mid-embryonic lethality⁴⁵ they predicted that simultaneous inhibition of cIAP-1 with either cIAP-2 or XIAP depletion may lead to the poor patient tolerability associated observed in their pan-selective antagonist **27**. They showed that the heightened XIAP antagonism by **27** promoted XIAP dependent NOD-mediated NF- κ B deactivation which is known to produce clinical manifestations of inflammatory tissue damage.⁴⁶ Compound **26** did not antagonize XIAP sufficiently to initiate this pathway and this is predicted to be one source of its improved tolerability profile in human studies.⁴³

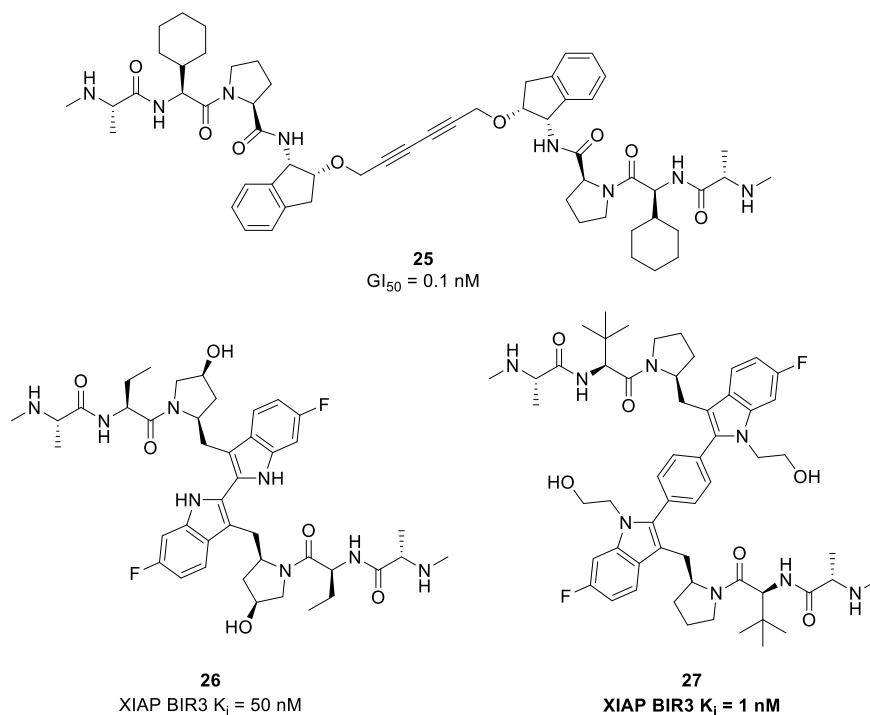


Figure 18. Some examples of potent P4 linked SMAC mimetics.

2.2.2.B P2 Linked Homodimeric SMAC Mimetics

X-ray crystal structures of non-constrained SMAC peptidomimetics bound to the IBM binding grooves of many IAPs show that the P2 residue side chain is solvent exposed and thus an appropriate site for dimerization.⁶ Aegera Therapeutics reported a potent P2 dimer from a series of compounds disclosed in a 2006 patent.⁴⁷ Their most potent analogue **28** (Figure 19) had high affinities for the BIR3 domains of XIAP (K_i = 100 nM), cIAP-1 (K_i = 17 nM) and cIAP-2 (K_i = 34 nM).⁴⁸ Cell based assays demonstrated the potency of **28** which promoted ~25% cell death in SKOV3 ovarian cancer cells at a 5 nM dose after 24 hours of exposure. Using immunoprecipitation they found that their compounds induced caspase-3/8 activation while promoting XIAP and cIAP-1/2 degradation. In addition, RIPK1 ubiquitination decreased while TNF- α production increased. Taken together they concluded that their compound was inducing apoptosis through cIAP degradation and autocrine TNF mediated apoptosis (see section 2.2.2).

The Wang group published a recent report describing the synthesis of a novel P2 linked bivalent SMAC mimetic **29** (SM-1200) (Figure 19) capable of causing apoptosis in MDA-MB-231 breast

cancer cells with an $IC_{50} = 11$ nM. They tested several linkers and found that, unlike in the case of their 2011 P4 linker screen, P2 linker modification resulted in moderate changes in IAP binding affinity in addition to cell-growth inhibition potency. Generally, long hydrophobic linkers produced potent compounds, however the authors noted they had poor PK properties in mice. A urea style attachment site on either side of the linker was required for improved IAP binding and cell permeability over an endo single-nitrogen amide-based linker attachment point. Linker length was also important, the researchers found that shorter aromatic linkers yielded the most potent compounds while short, cyclic aliphatic linkers performed poorly. Compound **29** showed excellent properties in a mouse xenograft model; over an 80 day treatment period consisting of three doses at 10 mg/kg (last treatment at day 40) tumors were quickly eliminated and did not return by the 80th day. In addition animal body weight remained relatively constant throughout the treatment indicating compound **29** was not promoting wasting effects.

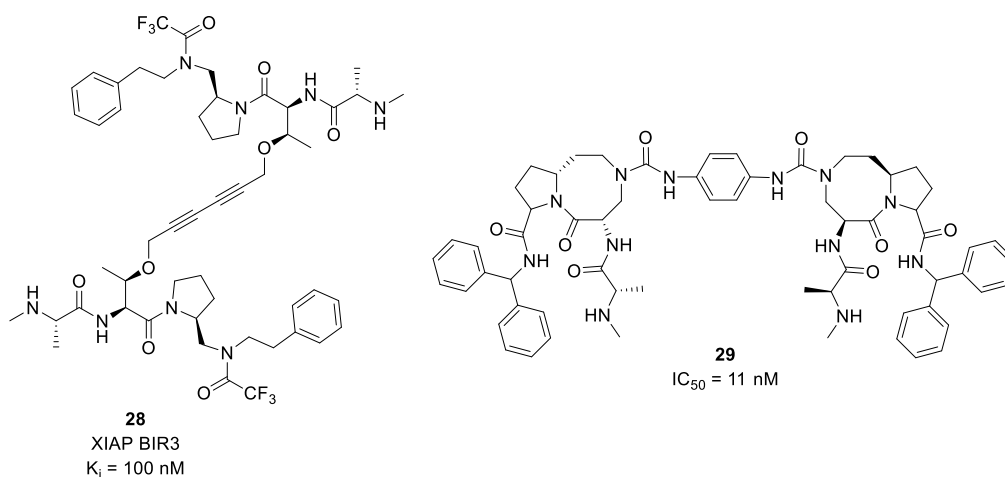


Figure 19. Some potent bivalent SMAC mimetics linked at P2.

2.2.2.C SMAC Mimetics using divergent strategies

SMAC mimetics linked through the proline residue are less common however some groups have reported potent P3 linked analogues (Figure 20). Genentech released a patent describing several analogues including **30** which is dimerized through a benzyl bis-alkyne linker and has a $K_i < 10$ μ M against XIAP BIR3.⁴⁹ Joyant pharmaceuticals filed a patent which tested several P3 linker strategies, their most potent compound **31** contained a unique adamantyl based

linker and induced apoptosis in HCC 461 hepatocellular carcinoma cells with an $IC_{50} = 5$ nM. They also disclosed several unique homo-trimeric structures **32** however no inhibitory data was provided. Bristol-Meyers-Squibb has focused on heterodimeric SMAC mimetics lined through P3.⁵⁰ Their most recent paper⁵¹ described attempts at modifying the linker which connects the two unique monomeric fragments. Several linker lengths and polarities were tested giving results consistent with other groups.⁴⁰ Somewhat surprisingly however, the most efficient inhibitor of IAPs proved to be a direct linker between the two monomers similar to that of Birinapant **26**. Compound **33** was a pan-selective IAP antagonist and promoted apoptosis in MDA-MB-231 breast cancer cells with an $IC_{50} = 0.8$ nM. Studies in a lung cancer xenograft mouse model demonstrated good tolerability and efficacy of tumor destruction.

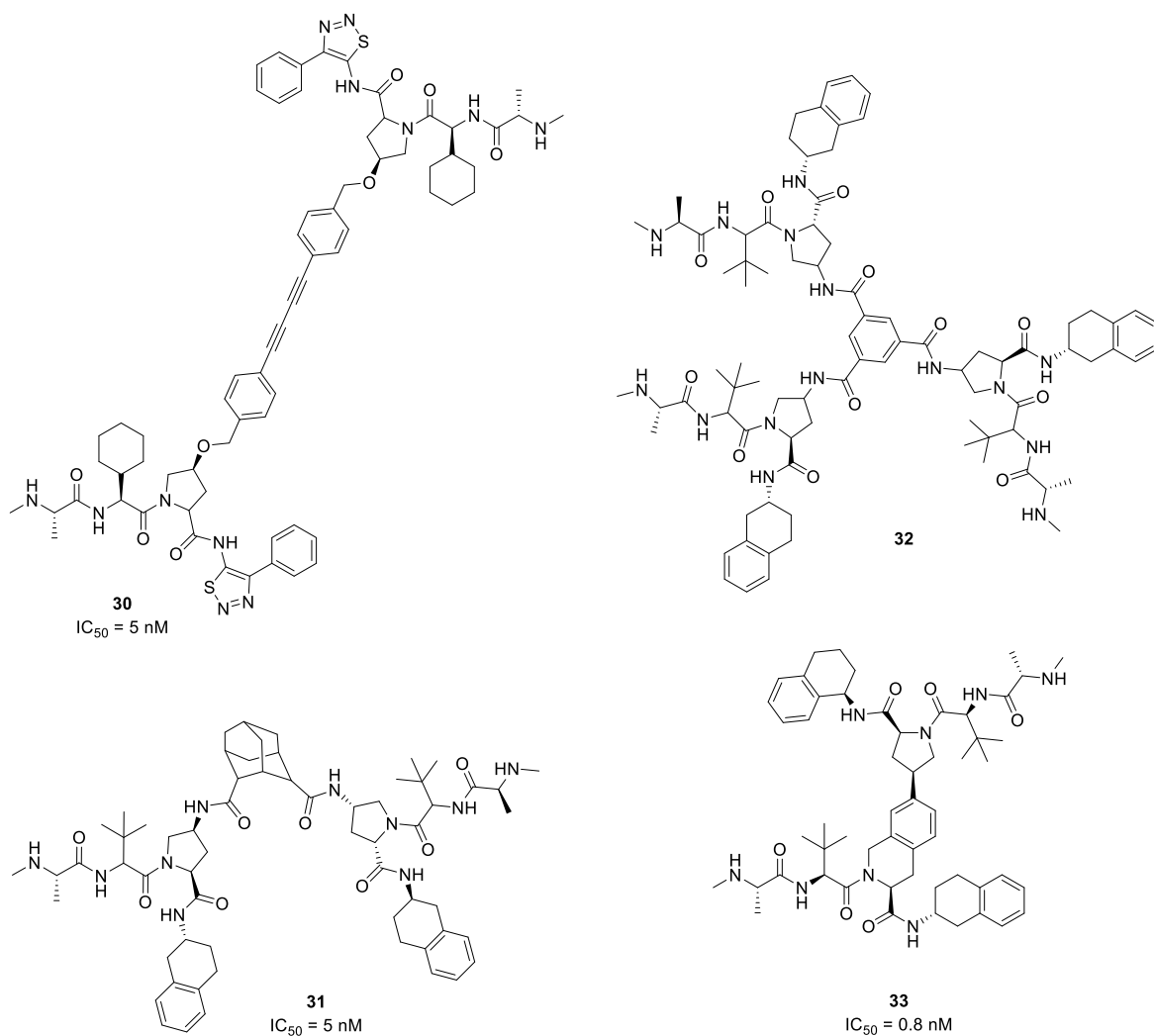


Figure 20. Some examples of unusual SMAC dimers from the recent literature linked at P3.

2.3 SMAC Mimetics: A Bright Future

Clearly, a tremendous amount of scientific research has been invested into the development of SMAC mimetics as cancer therapeutics and some compounds have begun to find their way into the clinic. Birinapant **26** currently leads the way, it has successfully completed a phase II study examining its effects when dosed with irinotecan for patients with relapsed colorectal cancer and is recruiting for a phase II study on the effects of birinipant combined with azacitidine for the treatment of myelomonocytic leukemia. Novartis's LCL161 **14** is entering phase II clinical trials to examine the its efficacy at treating patients with relapsed multiple myeloma and Genentech's GDC-0197/CUDC-427 is recruiting patients for a phase I safety and efficacy study for patients with refractory solid tumors or lymphomas.

While SMAC mimetics have proven their ability to act as single-agent therapeutics they also hold significant potential for use in combination therapies with other chemotherapeutics.⁵² One such study by Dr. John Bell at the Ottawa Hospital Research Institute combined LCL161 with an oncolytic virus to promote apoptosis in various cancer cell lines.⁵³

The future for SMAC mimetics is promising, hopefully, further research will eventually yield a clinically approved, tumor selective chemotherapeutic compound which will help save lives.

2.4 Goals and Objectives: Logical Design of Novel SMAC Mimetics

2.4.1 General Approach

Given the depth of the current SMAC Mimetic literature we chose to model our lead compound after other successful SMAC mimetics using previously studied SAR strategies derived from modification of the AVPI peptide sequence (see sections 2.3-2.4). In the spirit of classical SAR, we established a core SMAC scaffold and identified sites of potential chemical variation (Figure 21).

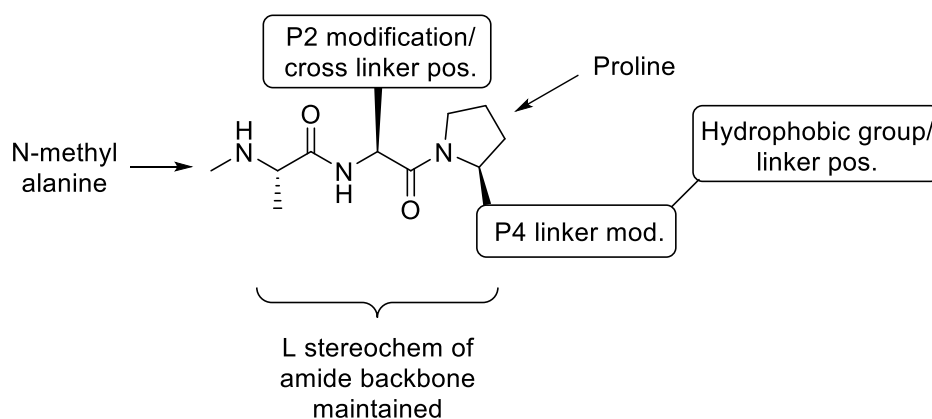


Figure 21. SMAC mimetic scaffold used in the design of our compound series.

The P1 alanine and P3 proline residues from the AVPI motif were kept as well as the N-terminal methylation, these fragments have previously demonstrated their importance for effective IAP inhibition.¹¹ Additionally, the natural L stereochemistry of the peptide backbone was maintained to promote optimal IAP binding.¹

A compound library was generated with the goal of discovering novel SMAC mimetic compounds with potent cytotoxic effects against tumor cells. Modifications were made at P2 to evaluate the effects of hybridization of unbranched P2 moieties, something which has not been explored in the literature to our knowledge. We also tested P2 dimerization strategies to assess the effects of linker flexibility and length on compound potency. Our work also explored how changes to the P4 linker region affect potency without modifying the P4 hydrophobic moiety itself. Finally, we probed the effects of dimerization at the P4 position.

2.4.2 Modifications to P2 - Monomers

We began by decorating the P2 position of our SMAC mimetic scaffold with different non-branched alkyl chains of varying hybridization, in addition to glycine, to generate monomeric SMAC mimetics **33-36** (Figure 22). In order to accurately assess the degree to which our changes were affecting potency we left all other positions constant. This included P4 and its respective P3-P4 linker, which were chosen to exist as a naphthalene moiety connected through a sulfide linker. The rationale for the naphthyl residue stemmed from success by other groups using tetrahydronaphthyl group as their P4 substituent.^{11,19} We reasoned that a naphthylene residue could mimic some of the hydrophobic interactions of the tetrahydronaphthyl group and adequately fill the P4 binding pocket whilst serving as a synthetically basic placeholder which could be substituted for other functionalities in later studies. The sulfide linker was inspired from to a relative absence of sulfur linked P4 substituents in the literature, most reported SMAC mimetics rely on either an amide bond or an α -amine.

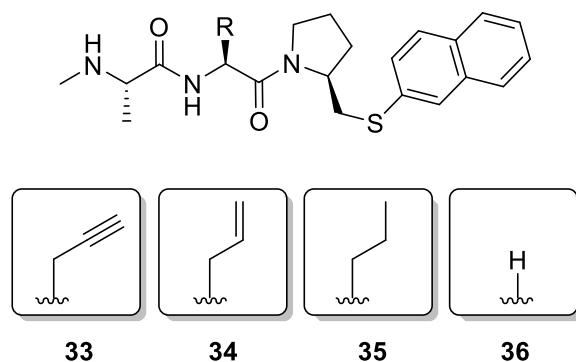


Figure 22. Monovalent P2 modification targets **33-36**.

2.4.3 Exploring P2 Linker Strategies

SMAC mimetic dimers are significantly more active than monomers at inducing apoptosis in cells through enhanced IAP binding.⁶ Different linker types and positions have been explored extensively by medicinal chemists.^{13,40,37} We designed P2 linked compounds **56**, **64**, **66** possessing hydrophobic linkers, a property shown by Wang to be essential for cellular penetration (Figure 23).⁴⁰ By varying linker length and flexibility we gauged the effects of P2 linker variation on IAP binding by bivalent SMAC mimetics.

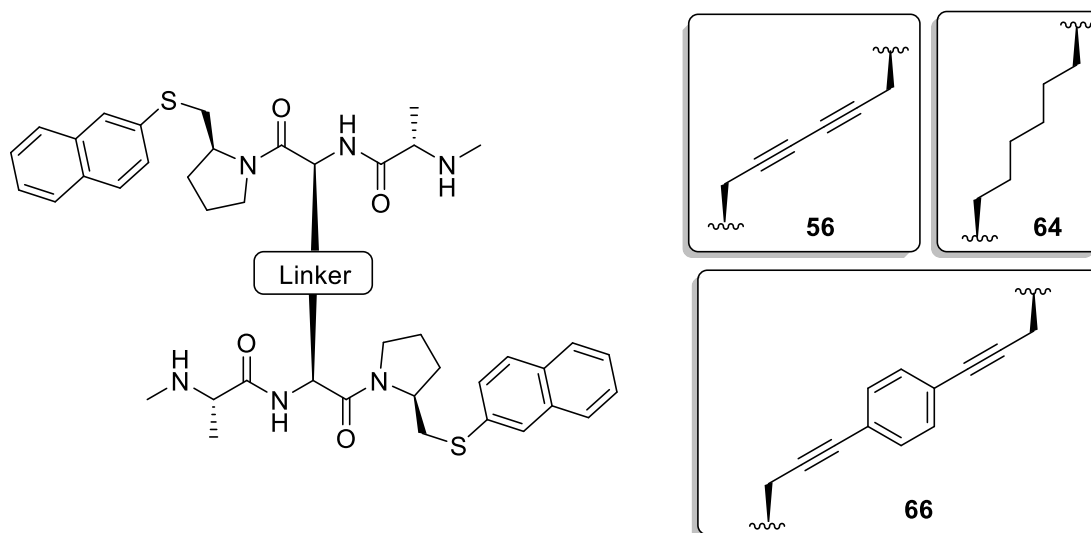
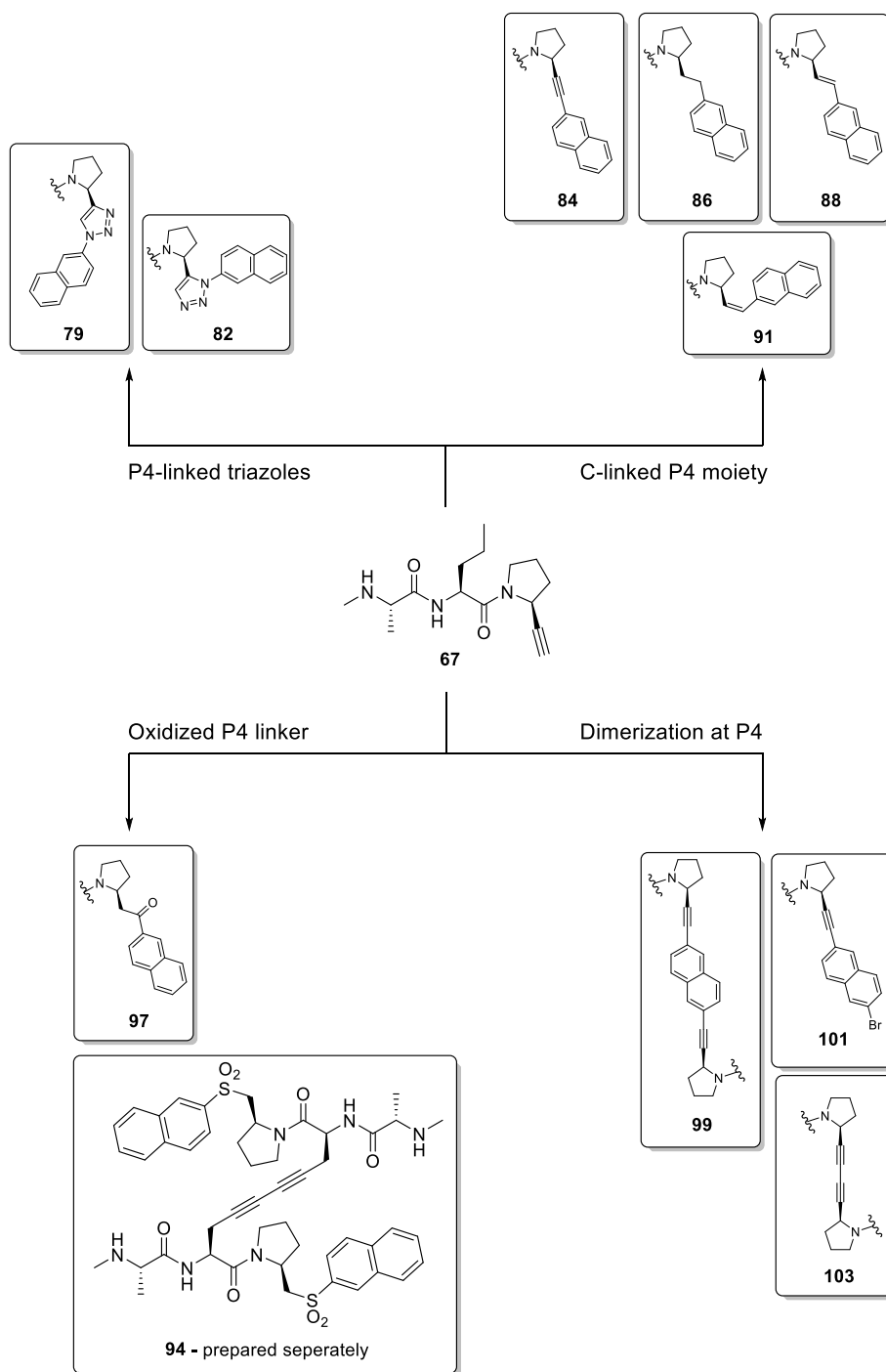


Figure 23. P2 linked bivalent targets **56**, **64** and **66**.

2.4.4 Exploring P4 Linker Strategies.

Next, we turned our attention towards exploring the chemical space of the P4 hydrophobic pocket in the IBM binding groove (see section 1.3.1). Many SMAC mimetics have simply employed an amide to connect the rest of the molecule to the P4 residue²⁴, others have used single heteroatoms²⁹ and some have used heterocycles attached directly to the proline ring.²⁸ Evidently, an amide isostere or some other functionality possessing moderate polar character is required at this position for efficient binding with IAPs. In the interest of generating numerous compounds in the most efficient manner possible our goal was to design a key intermediate compound which could serve as a stepping stone to several P4 linked derivatives in 1-2 steps. Ultimately, compound **67** was selected (Scheme 1) possessing a terminal alkyne residue at the “c-terminus” of P3. Terminal alkynes are rich handles for functionalization and can undergo several different cycloadditions to produce a diverse array of heterocycles.^{54,55,56} In

addition, they can be subjected to different cross coupling reactions⁵⁷ and hydroaminations⁵⁸ among others.⁵⁹ A nor-valine substituent was selected for P2 in **67** since it would be synthetically inert.



Scheme 1. P4 linker modification targets from common precursor **67**.

2.4.4.A Triazole P4 Linkers

Triazoles have found common use by medicinal chemists as amide bond isosteres.⁶⁰ They effectively mimic the relative bond distance/polarity of an amide and are proteolytically stable.⁶¹ We predicted that the 1,3-substituted 1,2,3-triazole (Figure 24B) would more accurately mimic the amide linkage of SMAC than its 1,5-substituted counterpart (Figure 24C) spatially. Compounds **79** and **82** were made from alkyne **67** bearing 1,3- and 1,5- substituted 1,2,3-triazole linkers respectively.

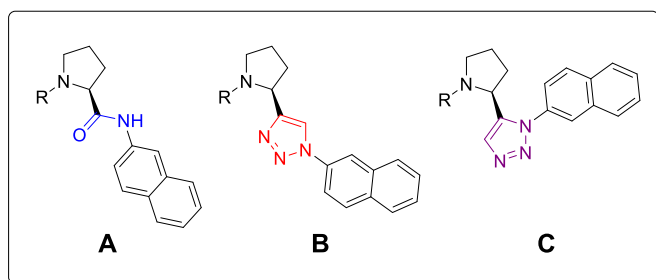


Figure 24. 1,2,3 triazoles as isosteres for an amide linkage. (A) P4 linked through an amide (blue), (B) P4 linked through a 1,3-substituted triazole (red), (C) P4 linked through a 1,5-triazole (purple).

2.4.4.B C-linked P4 Linkers

Several C-linked SMAC mimetic monomers were prepared (Scheme 1). In order to gauge the importance of an amide isostere at P4, we prepared **86** and **91** bearing (E) and (Z) olefins respectively. Double bonds are known to serve as effective amide isosteres⁶² and offer proteolytic stability in addition to higher lipophilicity which we hypothesized could help enhance cell permeability. Compounds **84** and **88** were prepared to assess the impact that flexibility and electronic character have on IAP inhibition for the C-linked series (Scheme 1).

2.4.4.C Oxidized P4 Linkers

We predicted that the introduction of a carbonyl at the P4 linker position may prove beneficial by adding a hydrogen bond acceptor and creating the potential for a novel hydrogen bond in the IAP IBM binding groove which would offer significant stabilizing effects. We designed variants of **56** and **86** in which a sulfone **94** and ketone **97** functionality were installed respectively (Scheme 1).

2.4.4.D P4 Linked Dimers

Several other successful bivalent SMAC mimetics have utilized the P4 residue as their cross-linking site.^{41,43} We explored the ability of our intermediate scaffold **67** to serve as an effective precursor for dimerization. As with the other compounds tested, the naphthalene P4 moiety was held constant. Two compounds **99** and **103** were prepared, **103** was a negative control to assess the effects of linker length and hydrophobicity at the P4 position as well as to determine how the lack of a hydrophobic P4 residue would affect IAP inhibition (Scheme 1).

2.5 References

1. Flygare, J. A.; Fairbrother, W. J., Small-molecule pan-IAP antagonists: a patent review. *Expert Opinion on Therapeutic Patents* **2010**, *20* (2), 251-267.
2. P, B. S.; W, F. S.; Zhihong, L.; P, M. R.; T, O. E.; Chaohong, S., Peptides derived from smac (diablo) and methods of use therefor. Google Patents: 2002.
3. Kipp RA, C. M., Wist AD, Cresson CM, Carrell M, Griner E, Wiita A, Albinak PA, Chai J, ShiY, Semmelhack MF, McLendon GL., Molecular targeting of inhibitors of apoptosis proteins based on small molecule mimics of natural binding partners. *Biochemistry* **2002**, *41*, 7344-7349.
4. Wu, G.; Chai, J.; Suber, T. L.; Wu, J.-W.; Du, C.; Wang, X.; Shi, Y., Structural basis of IAP recognition by Smac/DIABLO. *Nature* **2000**, *408* (6815), 1008-1012.
5. Franklin, M. C.; Kadkhodayan, S.; Ackerly, H.; Alexandru, D.; Distefano, M. D.; Elliott, L. O.; Flygare, J. A.; Mausisa, G.; Okawa, D. C.; Ong, D.; Vucic, D.; Deshayes, K.; Fairbrother, W. J., Structure and Function Analysis of Peptide Antagonists of Melanoma Inhibitor of Apoptosis (ML-IAP)‡. *Biochemistry* **2003**, *42* (27), 8223-8231.
6. Sun, H.; Nikolovska-Coleska, Z.; Yang, C.-Y.; Qian, D.; Lu, J.; Qiu, S.; Bai, L.; Peng, Y.; Cai, Q.; Wang, S., Design of Small-Molecule Peptidic and Nonpeptidic Smac Mimetics. *Accounts of Chemical Research* **2008**, *41* (10), 1264-1277.
7. Sun, H. S., J.A.; Nikolovska-Coleska, Z.; C-Y.; Xu, L.; Llu, M.; Tomita, Y.; Pan, H; Yoshioka, Y.; Krajewski, K.; Roller, P. P; Wang, S., Structure-based design of potent, conformationally constrained Smac mimetics. *Journal of the American Chemical Society* **2004**, *126*, 16686-16687.
8. Sun, H.; Nikolovska-Coleska, Z.; Chen, J.; Yang, C.-Y.; Tomita, Y.; Pan, H.; Yoshioka, Y.; Krajewski, K.; Roller, P. P.; Wang, S., Structure-based design, synthesis and biochemical testing of novel and potent Smac peptido-mimetics. *Bioorganic & Medicinal Chemistry Letters* **2005**, *15* (3), 793-797.
9. Sun, H.; Stuckey, J. A.; Nikolovska-Coleska, Z.; Qin, D.; Meagher, J. L.; Qiu, S.; Lu, J.; Yang, C.-Y.; Saito, N. G.; Wang, S., Structure-Based Design, Synthesis, Evaluation, and Crystallographic Studies of Conformationally Constrained Smac Mimetics as Inhibitors of the X-linked Inhibitor of Apoptosis Protein (XIAP)†. *Journal of Medicinal Chemistry* **2008**, *51* (22), 7169-7180.

10. Sun, H.; Nikolovska-Coleska, Z.; Yang, C.-Y.; Xu, L.; Tomita, Y.; Krajewski, K.; Roller, P. P.; Wang, S., Structure-Based Design, Synthesis, and Evaluation of Conformationally Constrained Mimetics of the Second Mitochondria-Derived Activator of Caspase That Target the X-Linked Inhibitor of Apoptosis Protein/Caspase-9 Interaction Site. *Journal of Medicinal Chemistry* **2004**, *47* (17), 4147-4150.
11. Oost, T. K.; Sun, C.; Armstrong, R. C.; Al-Assaad, A.-S.; Betz, S. F.; Deckwerth, T. L.; Ding, H.; Elmore, S. W.; Meadows, R. P.; Olejniczak, E. T.; Oleksijew, A.; Oltersdorf, T.; Rosenberg, S. H.; Shoemaker, A. R.; Tomaselli, K. J.; Zou, H.; Fesik, S. W., Discovery of Potent Antagonists of the Antiapoptotic Protein XIAP for the Treatment of Cancer. *Journal of Medicinal Chemistry* **2004**, *47* (18), 4417-4426.
12. Balaraman, K.; Kesavan, V., Efficient Copper(II) Acetate Catalyzed Homo- and Heterocoupling of Terminal Alkynes at Ambient Conditions. *Synthesis* **2010**, *2010* (20), 3461-3466.
13. Li, L.; Thomas, R. M.; Suzuki, H.; De Brabander, J. K.; Wang, X.; Harran, P. G., A Small Molecule Smac Mimic Potentiates TRAIL- and TNF α -Mediated Cell Death. *Science* **2004**, *305* (5689), 1471-1474.
14. Huang, Y.; Rich, R. L.; Myszka, D. G.; Wu, H., Requirement of Both the Second and Third BIR Domains for the Relief of X-linked Inhibitor of Apoptosis Protein (XIAP)-mediated Caspase Inhibition by Smac. *Journal of Biological Chemistry* **2003**, *278* (49), 49517-49522.
15. Lipinski, C. A.; Lombardo, F.; Dominy, B. W.; Feeney, P. J., Experimental and computational approaches to estimate solubility and permeability in drug discovery and development settings¹. *Advanced Drug Delivery Reviews* **2001**, *46* (1-3), 3-26.
16. Zobel, K.; Wang, L.; Varfolomeev, E.; Franklin, M. C.; Elliott, L. O.; Wallweber, H. J. A.; Okawa, D. C.; Flygare, J. A.; Vucic, D.; Fairbrother, W. J.; Deshayes, K., Design, Synthesis, and Biological Activity of a Potent Smac Mimetic That Sensitizes Cancer Cells to Apoptosis by Antagonizing IAPs. *ACS Chemical Biology* **2006**, *1* (8), 525-533.
17. Cohen, F.; Aliche, B.; Elliott, L. O.; Flygare, J. A.; Goncharov, T.; Keteltas, S. F.; Franklin, M. C.; Frankovitz, S.; Stephan, J.-P.; Tsui, V.; Vucic, D.; Wong, H.; Fairbrother, W. J., Orally Bioavailable Antagonists of Inhibitor of Apoptosis Proteins Based on an Azabicyclooctane Scaffold ∞ . *Journal of Medicinal Chemistry* **2009**, *52* (6), 1723-1730.
18. Sun, H.; Nikolovska-Coleska, Z.; Lu, J.; Qiu, S.; Yang, C.-Y.; Gao, W.; Meagher, J.; Stuckey, J.; Wang, S., Design, Synthesis, and Evaluation of a Potent, Cell-Permeable, Conformationally Constrained Second Mitochondria Derived Activator of Caspase (Smac) Mimetic. *Journal of Medicinal Chemistry* **2006**, *49* (26), 7916-7920.
19. Zhang, B.; Nikolovska-Coleska, Z.; Zhang, Y.; Bai, L.; Qiu, S.; Yang, C.-Y.; Sun, H.; Wang, S.; Wu, Y., Design, Synthesis, and Evaluation of Tricyclic, Conformationally Constrained Small-Molecule Mimetics of Second Mitochondria-Derived Activator of Caspases. *Journal of Medicinal Chemistry* **2008**, *51* (23), 7352-7355.
20. Chauhan, D.; Neri, P.; Velankar, M.; Podar, K.; Hideshima, T.; Fulciniti, M.; Tassone, P.; Raje, N.; Mitsiades, C.; Mitsiades, N.; Richardson, P.; Zavel, L.; Tran, M.; Munshi, N.; Anderson, K. C., Targeting mitochondrial factor Smac/DIABLO as therapy for multiple myeloma (MM). *Blood* **2007**, *109* (3), 1220-1227.
21. Thornberry, N. A. a. L., Y., Caspases: enemies within. *Science* **1998**, *281*, 1312-1316.

22. Eckelman, B. P.; Drag, M.; Snipas, S. J.; Salvesen, G. S., The mechanism of peptide-binding specificity of IAP BIR domains. *Cell Death Differ* **2008**, *15* (5), 920-928.
23. Ndubaku, C.; Varfolomeev, E.; Wang, L.; Zobel, K.; Lau, K.; Elliott, L. O.; Maurer, B.; Fedorova, A. V.; Dynek, J. N.; Koehler, M.; Hymowitz, S. G.; Tsui, V.; Deshayes, K.; Fairbrother, W. J.; Flygare, J. A.; Vucic, D., Antagonism of c-IAP and XIAP Proteins Is Required for Efficient Induction of Cell Death by Small-Molecule IAP Antagonists. *ACS Chemical Biology* **2009**, *4* (7), 557-566.
24. Flygare, J. A.; Beresini, M.; Budha, N.; Chan, H.; Chan, I. T.; Cheeti, S.; Cohen, F.; Deshayes, K.; Doerner, K.; Eckhardt, S. G.; Elliott, L. O.; Feng, B.; Franklin, M. C.; Reisner, S. F.; Gazzard, L.; Halladay, J.; Hymowitz, S. G.; La, H.; LoRusso, P.; Maurer, B.; Murray, L.; Plise, E.; Quan, C.; Stephan, J.-P.; Young, S. G.; Tom, J.; Tsui, V.; Um, J.; Varfolomeev, E.; Vucic, D.; Wagner, A. J.; Wallweber, H. J. A.; Wang, L.; Ware, J.; Wen, Z.; Wong, H.; Wong, J. M.; Wong, M.; Wong, S.; Yu, R.; Zobel, K.; Fairbrother, W. J., Discovery of a Potent Small-Molecule Antagonist of Inhibitor of Apoptosis (IAP) Proteins and Clinical Candidate for the Treatment of Cancer (GDC-0152). *Journal of Medicinal Chemistry* **2012**, *55* (9), 4101-4113.
25. Erickson, R. I.; Tarrant, J.; Cain, G.; Lewin-Koh, S.-C.; Dybdal, N.; Wong, H.; Blackwood, E.; West, K.; Steigerwalt, R.; Mamounas, M.; Flygare, J. A.; Amemiya, K.; Dambach, D.; Fairbrother, W. J.; Diaz, D., Toxicity Profile of Small-Molecule IAP Antagonist GDC-0152 Is Linked to TNF- α Pharmacology. *Toxicological Sciences* **2013**, *131* (1), 247-258.
26. Wong, H.; Gould, S. E.; Budha, N.; Darbonne, W. C.; Kadel, E. E.; La, H.; Alicke, B.; Halladay, J. S.; Erickson, R.; Portera, C.; Tolcher, A. W.; Infante, J. R.; Mamounas, M.; Flygare, J. A.; Hop, C. E. C. A.; Fairbrother, W. J., Learning and Confirming with Preclinical Studies: Modeling and Simulation in the Discovery of GDC-0917, an Inhibitor of Apoptosis Proteins Antagonist. *Drug Metabolism and Disposition* **2013**, *41* (12), 2104-2113.
27. Weisberg, E.; Ray, A.; Barrett, R.; Nelson, E.; Christie, A. L.; Porter, D.; Straub, C.; Zavel, L.; Daley, J. F.; Lazo-Kallanian, S.; Stone, R.; Galinsky, I.; Frank, D.; Kung, A. L.; Griffin, J. D., Smac mimetics: implications for enhancement of targeted therapies in leukemia. *Leukemia* **2010**, *24* (12), 2100-2109.
28. Thakur, J.; Yang, D.; Feng, L., Solid oral formulations and crystalline forms of an inhibitor of apoptosis protein. Google Patents: 2011.
29. Aggen, J.; Griffin, J. H.; Mammen, M.; Marquess, D.; Moran, E. J.; Oare, D., Muscarinic receptor antagonists. Google Patents: 2008.
30. González-López, M.; Welsh, K.; Finlay, D.; Ardecky, R. J.; Ganji, S. R.; Su, Y.; yuan, H.; Teriete, P.; Mace, P. D.; Riedl, S. J.; Vuori, K.; Reed, J. C.; Cosford, N. D. P., Design, synthesis and evaluation of monovalent Smac mimetics that bind to the BIR2 domain of the anti-apoptotic protein XIAP. *Bioorganic & Medicinal Chemistry Letters* **2011**, *21* (14), 4332-4336.
31. James, J., Bir domain binding compounds. Google Patents: 2007.
32. Patani, G. A.; LaVoie, E. J., Bioisosterism: A Rational Approach in Drug Design. *Chemical Reviews* **1996**, *96* (8), 3147-3176.
33. Wist, A. D.; Gu, L.; Riedl, S. J.; Shi, Y.; McLendon, G. L., Structure-activity based study of the Smac-binding pocket within the BIR3 domain of XIAP. *Bioorganic & Medicinal Chemistry* **2007**, *15* (8), 2935-2943.
34. Huang, J.-W.; Zhang, Z.; Wu, B.; Cellitti, J. F.; Zhang, X.; Dahl, R.; Shiao, C.-W.; Welsh, K.; Emdadi, A.; Stebbins, J. L.; Reed, J. C.; Pellecchia, M., Fragment-Based Design of Small Molecule

X-Linked Inhibitor of Apoptosis Protein Inhibitors. *Journal of Medicinal Chemistry* **2008**, *51* (22), 7111-7118.

35. Chen, Z.; Wang, R. M. D.; Chen, M.; Straub, C. S.; Zawel, L., 6-oxo.-1, 6-dihydropyrimidin-2-yls in the treatment of proliferative diseases. Google Patents: 2008.

36. Gao, Z. T., Y.; Wang, J.; Yin, Q.; Wu, H.; Li, Y.M.; and; Jiang, X., A Dimeric Smac/Diablo Peptide Directly Relieves Caspase-3 Inhibition by XIAP: Dynamic and Cooperative Regulation of XIAP by Smac/Diablo. *The journal of biological chemistry* **2007**, *282* (42), 30718-30728.

37. Varfolomeev, E.; Blankenship, J. W.; Wayson, S. M.; Fedorova, A. V.; Kayagaki, N.; Garg, P.; Zobel, K.; Dynek, J. N.; Elliott, L. O.; Wallweber, H. J. A.; Flygare, J. A.; Fairbrother, W. J.; Deshayes, K.; Dixit, V. M.; Vucic, D., IAP Antagonists Induce Autoubiquitination of c-IAPs, NF- κ B Activation, and TNF α -Dependent Apoptosis. *Cell* **2007**, *131* (4), 669-681.

38. Sun, H.; Nikolovska-Coleska, Z.; Lu, J.; Meagher, J. L.; Yang, C.-Y.; Qiu, S.; Tomita, Y.; Ueda, Y.; Jiang, S.; Krajewski, K.; Roller, P. P.; Stuckey, J. A.; Wang, S., Design, Synthesis, and Characterization of a Potent, Nonpeptide, Cell-Permeable, Bivalent Smac Mimetic That Concurrently Targets Both the BIR2 and BIR3 Domains in XIAP. *Journal of the American Chemical Society* **2007**, *129* (49), 15279-15294.

39. Lu, J.; Bai, L.; Sun, H.; Nikolovska-Coleska, Z.; McEachern, D.; Qiu, S.; Miller, R. S.; Yi, H.; Shangary, S.; Sun, Y.; Meagher, J. L.; Stuckey, J. A.; Wang, S., SM-164: A Novel, Bivalent Smac Mimetic That Induces Apoptosis and Tumor Regression by Concurrent Removal of the Blockade of cIAP-1/2 and XIAP. *Cancer Research* **2008**, *68* (22), 9384-9393.

40. Sun, H.; Liu, L.; Lu, J.; Bai, L.; Li, X.; Nikolovska-Coleska, Z.; McEachern, D.; Yang, C.-Y.; Qiu, S.; Yi, H.; Sun, D.; Wang, S., Potent Bivalent Smac Mimetics: Effect of the Linker on Binding to Inhibitor of Apoptosis Proteins (IAPs) and Anticancer Activity. *Journal of Medicinal Chemistry* **2011**, *54* (9), 3306-3318.

41. Hennessy, E. J.; Saeh, J. C.; Sha, L.; MacIntyre, T.; Wang, H.; Larsen, N. A.; Aquila, B. M.; Ferguson, A. D.; Laing, N. M.; Omer, C. A., Discovery of aminopiperidine-based Smac mimetics as IAP antagonists. *Bioorganic & Medicinal Chemistry Letters* **2012**, *22* (4), 1690-1694.

42. Condon, S. M.; Laporte, M. G.; Deng, Y.; Rippin, S. R., Dimeric IAP inhibitors. Google Patents: 2009.

43. Condon, S. M.; Mitsuuchi, Y.; Deng, Y.; LaPorte, M. G.; Rippin, S. R.; Haimowitz, T.; Alexander, M. D.; Kumar, P. T.; Hendi, M. S.; Lee, Y.-H.; Benetatos, C. A.; Yu, G.; Kapoor, G. S.; Neiman, E.; Seipel, M. E.; Burns, J. M.; Graham, M. A.; McKinlay, M. A.; Li, X.; Wang, J.; Shi, Y.; Feltham, R.; Bettjeman, B.; Cumming, M. H.; Vince, J. E.; Khan, N.; Silke, J.; Day, C. L.; Chunduru, S. K., Birinapant, a Smac-Mimetic with Improved Tolerability for the Treatment of Solid Tumors and Hematological Malignancies. *Journal of Medicinal Chemistry* **2014**, *57* (9), 3666-3677.

44. Vince, J. E.; Wong, W. W.-L.; Khan, N.; Feltham, R.; Chau, D.; Ahmed, A. U.; Benetatos, C. A.; Chunduru, S. K.; Condon, S. M.; McKinlay, M.; Brink, R.; Leverkus, M.; Tergaonkar, V.; Schneider, P.; Callus, B. A.; Koentgen, F.; Vaux, D. L.; Silke, J., IAP Antagonists Target cIAP1 to Induce TNF α -Dependent Apoptosis. *Cell* *131* (4), 682-693.

45. Moulin, M.; Anderton, H.; Voss, A. K.; Thomas, T.; Wong, W. W. L.; Bankovacki, A.; Feltham, R.; Chau, D.; Cook, W. D.; Silke, J.; Vaux, D. L., *IAPs limit activation of RIP kinases by TNF receptor 1 during development*. 2012; Vol. 31, p 1679-1691.

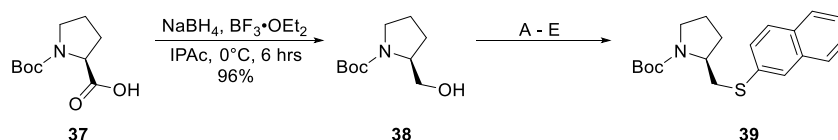
46. Damgaard, R. B.; Fiil, B. K.; Speckmann, C.; Yabal, M.; Stadt, U. z.; Bekker-Jensen, S.; Jost, P. J.; Ehl, S.; Mailand, N.; Gyrd-Hansen, M., *Disease-causing mutations in the XIAP BIR2 domain impair NOD2-dependent immune signalling*. 2013; Vol. 5, p 1278-1295.
47. Laurent, A.; Hewitt, K. E.; Morris, S.; Bureau, P.; Boudreault, A.; Jarvis, S.; Jaquith, J., IAP BIR domain binding compounds. Google Patents: 2009.
48. Bertrand, M. J. M.; Milutinovic, S.; Dickson, K. M.; Ho, W. C.; Boudreault, A.; Durkin, J.; Gillard, J. W.; Jaquith, J. B.; Morris, S. J.; Barker, P. A., cIAP1 and cIAP2 Facilitate Cancer Cell Survival by Functioning as E3 Ligases that Promote RIP1 Ubiquitination. *Molecular Cell* **2008**, *30* (6), 689-700.
49. Flygare, J. A.; Cohen, F.; Deshayes, K.; Koehler, M. F. T.; Gazzard, L. J.; Wang, L.; Ndubaku, C., Inhibitors of iap. Google Patents: 2008.
50. Kim, K. S.; Zhang, L.; Williams, D.; Perez, H. L.; Stang, E.; Borzilleri, R. M.; Posy, S.; Lei, M.; Chaudhry, C.; Emanuel, S.; Talbott, R., Discovery of tetrahydroisoquinoline-based bivalent heterodimeric IAP antagonists. *Bioorganic & Medicinal Chemistry Letters* **2014**, *24* (21), 5022-5029.
51. Perez, H. L.; Chaudhry, C.; Emanuel, S. L.; Fanslau, C.; Fagnoli, J.; Gan, J.; Kim, K. S.; Lei, M.; Naglich, J. G.; Traeger, S. C.; Vuppugalla, R.; Wei, D. D.; Vite, G. D.; Talbott, R. L.; Borzilleri, R. M., Discovery of Potent Heterodimeric Antagonists of Inhibitor of Apoptosis Proteins (IAPs) with Sustained Antitumor Activity. *Journal of Medicinal Chemistry* **2015**, *58* (3), 1556-1562.
52. (a) Beug, S. T.; LaCasse, E. C.; Korneluk, R. G., Smac mimetics combined with innate immune stimuli create the perfect cytokine storm to kill tumor cells. *Oncoimmunology* **2014**, *3*, e28541; (b) Lu, J.; McEachern, D.; Sun, H.; Bai, L.; Peng, Y.; Qiu, S.; Miller, R.; Liao, J.; Yi, H.; Liu, M.; Bellail, A.; Hao, C.; Sun, S.-Y.; Ting, A. T.; Wang, S., Therapeutic Potential and Molecular Mechanism of a Novel, Potent, Nonpeptide, Smac Mimetic SM-164 in Combination with TRAIL for Cancer Treatment. *Molecular Cancer Therapeutics* **2011**, *10* (5), 902-914; (c) Lecis, D.; Drago, C.; Manzoni, L.; Seneci, P.; Scolastico, C.; Mastrangelo, E.; Bolognesi, M.; Anichini, A.; Kashkar, H.; Walczak, H.; Delia, D., Novel SMAC-mimetics synergistically stimulate melanoma cell death in combination with TRAIL and Bortezomib. *Br J Cancer* **2010**, *102* (12), 1707-1716; (d) Dineen, S. P.; Roland, C. L.; Greer, R.; Carbon, J. G.; Toombs, J. E.; Gupta, P.; Bardeesy, N.; Sun, H.; Williams, N.; Minna, J. D.; Brekken, R. A., Smac Mimetic Increases Chemotherapy Response and Improves Survival in Mice with Pancreatic Cancer. *Cancer Research* **2010**, *70* (7), 2852-2861.
53. Beug, S. T.; Tang, V. A.; LaCasse, E. C.; Cheung, H. H.; Beauregard, C. E.; Brun, J.; Nuyens, J. P.; Earl, N.; St-Jean, M.; Holbrook, J.; Dastidar, H.; Mahoney, D. J.; Ilkow, C.; Le Boeuf, F.; Bell, J. C.; Korneluk, R. G., Smac mimetics and innate immune stimuli synergize to promote tumor death. *Nat Biotech* **2014**, *32* (2), 182-190.
54. Cano, I.; Álvarez, E.; Nicasio, M. C.; Pérez, P. J., Regioselective Formation of 2,5-Disubstituted Oxazoles Via Copper(I)-Catalyzed Cycloaddition of Acyl Azides and 1-Alkynes. *Journal of the American Chemical Society* **2011**, *133* (2), 191-193.
55. Park, E. J.; Kim, S. H.; Chang, S., Copper-Catalyzed Reaction of α -Aryldiazoesters with Terminal Alkynes: A Formal [3 + 2] Cycloaddition Route Leading to Indene Derivatives. *Journal of the American Chemical Society* **2008**, *130* (51), 17268-17269.
56. Yu, R. T.; Rovis, T., Enantioselective Rhodium-Catalyzed [2+2+2] Cycloaddition of Alkenyl Isocyanates and Terminal Alkynes: Application to the Total Synthesis of (+)-Lasubine II. *Journal of the American Chemical Society* **2006**, *128* (38), 12370-12371.

57. Eckhardt, M.; Fu, G. C., The First Applications of Carbene Ligands in Cross-Couplings of Alkyl Electrophiles: Sonogashira Reactions of Unactivated Alkyl Bromides and Iodides. *Journal of the American Chemical Society* **2003**, *125* (45), 13642-13643.
58. Yim, J. C. H.; Schafer, L. L., Efficient Anti-Markovnikov-Selective Catalysts for Intermolecular Alkyne Hydroamination: Recent Advances and Synthetic Applications. *European Journal of Organic Chemistry* **2014**, *2014* (31), 6825-6840.
59. Chinchilla, R.; Nájera, C., Chemicals from Alkynes with Palladium Catalysts. *Chemical Reviews* **2014**, *114* (3), 1783-1826.
60. Angell, Y. L.; Burgess, K., Peptidomimetics via copper-catalyzed azide-alkyne cycloadditions. *Chemical Society Reviews* **2007**, *36* (10), 1674-1689.
61. Valverde, I. E.; Bauman, A.; Kluba, C. A.; Vomstein, S.; Walter, M. A.; Mindt, T. L., 1,2,3-Triazoles as Amide Bond Mimics: Triazole Scan Yields Protease-Resistant Peptidomimetics for Tumor Targeting. *Angewandte Chemie International Edition* **2013**, *52* (34), 8957-8960.
62. Hann, M. M.; Sammes, P. G.; Kennewell, P. D.; Taylor, J. B., On the double bond isostere of the peptide bond: preparation of an enkephalin analogue. *Journal of the Chemical Society, Perkin Transactions 1* **1982**, (0), 307-314.

Chapter 3: Synthesis and Testing of Monovalent and Divalent SMAC Mimetics in MDA-MB-231 Breast Cancer Cells

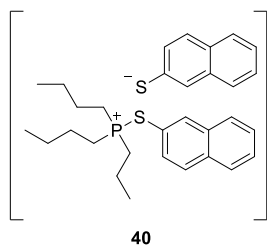
3.2 Modifications to P2 – Monomers 33-36

To prepare the P2 modified monomeric analogues we envisioned a short synthetic sequence to the S-aryl SMAC monomer **33** which would be amenable to subsequent chemical modification and allow access to numerous additional compounds for testing. Compounds containing substituted amino acid residues, including **34** and **36**, would have to be synthesized *de-novo*.



Scheme 2. Synthesis of aryl sulfide **39** via direct substitution of prolinol **37**.

The synthesis towards **33** began with Boc-L-Proline **37** which was reduced under lewis acidic conditions to yield prolinol **38** (Scheme 2). Several approaches were considered for the subsequent thiolation step to give **39**. While a two-step tosylation/thiolation procedure seemed reasonable a more efficient transformation was desired. Attempts to thiolate using variants of

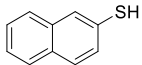
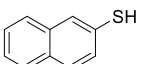
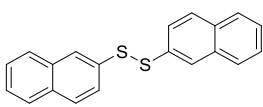
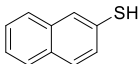
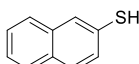


Scheme 3. Phosphonium salt proposed by Hata and co-workers.⁴

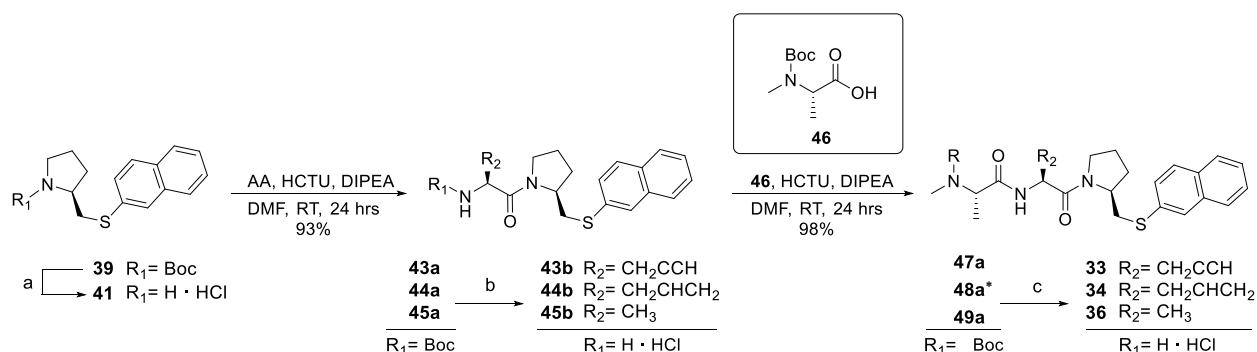
Mitsunobu's conditions² gave poor yields (Table 2). Application of Hata's conditions for aryl-thiolation provided enhanced yields but suffered from lengthy reaction times.³ Hata proposed that the reaction proceeded *via* a sulfur-phosphonium salt **40** which served to activate the alcohol and facilitate the ensuing thiolation (Scheme 3).^{1,4,5} In an attempt to generate the disulfide (from naphthalene-2-thiol) required for the Hata reaction DIAD was added as an *in-situ* oxidant (Table 2, entry D). No formation of the desired disulfide was observed, however upon treatment with n-tributylphosphine an exothermic reaction took place and an orange precipitate formed in the reaction flask. Addition of alcohol **38** clarified the mixture and TLC analysis indicated complete conversion to the desired product **39**. We reasoned that the n-tributylphosphine reacted with the DIAD to form a phosphonium salt which subsequently reacted

with the nucleophilic aryl thiol to afford complex **40**. This complex subsequently reacted with the added alcohol to give the thiolated product **39**. Attempts to replicate the results using triphenylphosphine in-place of n-tributylphosphine produced sluggish reaction conditions and poor yield (Table 2, entry E). It was noted that during the reaction, following the addition of triphenylphosphine a precipitate formed analogous to entry D, however upon addition of the alcohol **2** the mixture did not resolve, even after several days of stirring. One could imagine how the phenyl rings of triphenylphosphine might help stabilize a phosphonium salt similar to **40** *via* charge delocalization. It is reasonable to suggest that n-tributylphosphine, which does not possess such stabilizing characteristics, would form a more reactive intermediate than its aromatic counterpart. This, perhaps, explains the differences in reaction rate observed between entries D and E. A literature search yielded a plethora of articles which used Hata's method to effect aryl thiolations, often at the expense of time and chemical yield.^{6,7,8} This simple modification to Hata's conditions could serve as a new, efficient alternative.

Table 2. Experimental conditions for the thiolation of **38**.

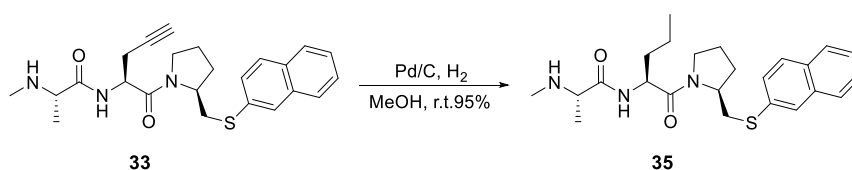
Entry	Reagents	Solvent	Temperature (°C)	Time	Yield 3 (%)
A	PPh ₃ , DIAD, Et ₃ N, 	Toluene	0 → RT	24 hrs	8%
B	PPh ₃ , DIAD, Et ₃ N, 	Toluene	RT → 80	24 hrs	37%
C	n-Bu ₃ P, 	THF	RT	72 hrs	85%
D	n-Bu ₃ P, DIAD, 	Toluene	RT	15 min	98%
E	PPh ₃ , DIAD, 	Toluene	RT	72 hrs	30%

With an economical route to **39** in-hand we continued the synthesis of **33-36**. Standard peptide coupling using HCTU and Hunig's base with propargyl glycine **42** and N-methyl alanine **46** (prepared from alanine in 2-steps) provided Boc-protected monomeric SMAC mimetics **43-45a** (Scheme 4).



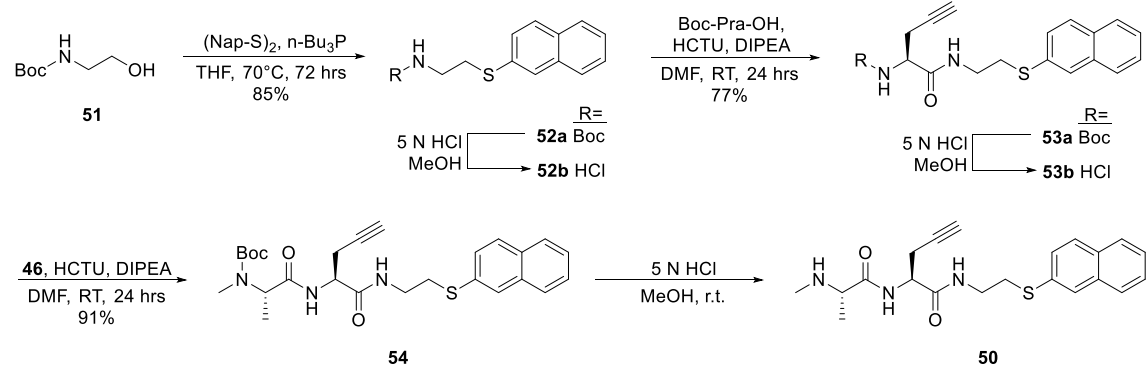
Scheme 4. Synthesis of SMAC monomers **33**, **34** and **36**. Reagents and conditions: AA represents the commercially available amino acid coupling partner used, **43a** = Boc-Pra-OH, **44a** = Boc-allyl-Gly-OH, **45a** = Boc-Gly-OH; (a-c) 5 N HCl, MeOH, r.t. * = **48a** was synthesized with an Fmoc-protecting group and de-protected using 20% piperidine in DMF at r.t.

Compound **35** was made *via* the hydrogenation of **33** using palladium on activated carbon (Scheme 5).



Scheme 5. Synthesis of **35**.

Another monomeric SMAC mimetic **50** with a glycine residue substituted for the P3 proline was synthesized as a negative control compound using a similar synthetic sequence to Scheme 4 (Scheme 6).



Scheme 6. Synthesis of P3 glycine insert **50** as negative control.

We tested our first set of monomers *in-vitro* against MDA-MB-231 breast cancer cells and obtained IC₅₀ values for each compound.

Table 3. Properties of compounds **33-36** and **50**. cLogP and polar surface area (PSA) values were obtained computationally from Marvin Sketch v.15.3.30.

Compound	Structure	IC ₅₀ (μM)	cLogP	PSA
33		11.9	-0.50	86.74
34		5.58	0.00	86.74
35		13.6	0.31	86.74
36		12.3	-1.23	86.74
37		31.2	-1.19	95.53

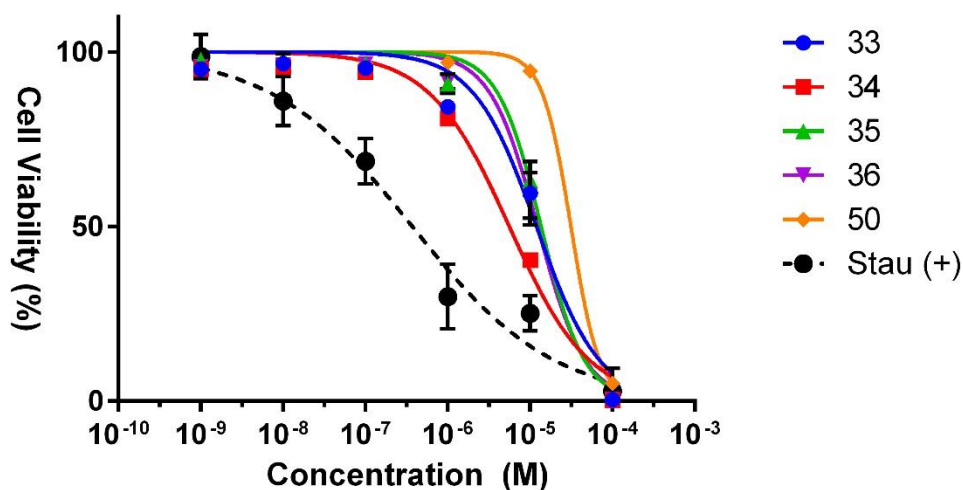


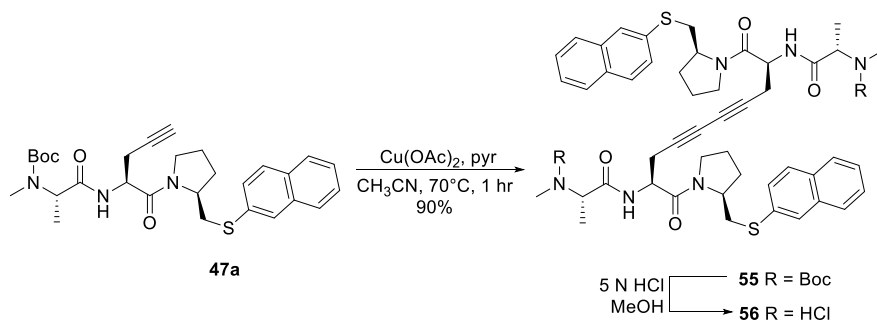
Figure 25. Functional antagonism of SMAC mimetics **33-36** and **50** against MDA-MB-231 breast cancer cells in a dose-responsive manner. Data shown in the figure are averages with standard error of duplicate wells in assay plates. Experiments were performed in-triplicate. A staurosporine positive control (black) was used as a reference standard for cell death. Non-linear regression was used to generate a line of best fit which was used to calculate IC_{50} values.

Our results show that compounds **33-36** and **50** exhibit modest cytotoxicity towards the MDA-MB-231 breast cancer cell line (Figure 25). Statistical analysis indicated that the IC_{50} value of the most potent analogue **34** was significantly higher than other monomers (* $P < 0.05$, 95% CI) and that monomers **33-36** were significantly more potent than **50** (minimum * $P < 0.05$, 95% CI). Interestingly compounds **33**, **35**, and **36** all had statistically similar IC_{50} values (ns $P > 0.05$, 95% CI) indicating that perhaps substitution at the P2 position contributes very little to IAP binding in cells. Calculated LogP and polar surface area (PSA) showed that compounds **33-36** and **50** are all reasonably lipophilic and should be capable of passively entering cells. This conclusion is supported by the enhanced killing efficiency of **34** over **35** despite its lower clogP value. It appears that SP_2 hybridization of a non-branched P2 linker is modestly favoured for IAP binding however it is difficult to speculate the exact mechanism without access to *in-silico* modeling. The unbranched alkyl chains at P2 in **33-35** may lead to reduced XIAP binding relative to a branched chain, as was reported by Condon.⁹ Perhaps the lack of β -branching at P2 could explain the modest efficiency of **33-36** relative to other SMAC monomers with P2 branching which have been reported in the literature and have achieved IC_{50} values as low as 100 nM.¹⁰ Compound **50** with a glycine residue in place of proline showed reduced potency against MDA-MB-231 cells, this

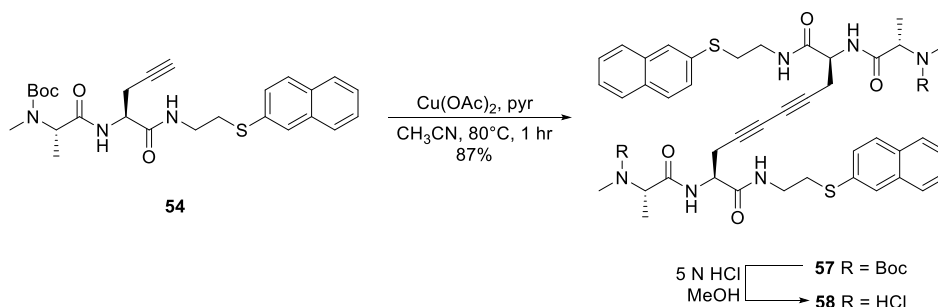
result was consistent with findings by other groups and served as an effective negative control for IAP interaction.^{11,12}

3.3 P2 Linker Strategies– Compounds **56**, **58**, **64**, **66**

Synthesis of the P2 linked bivalent compound series began with **47a**. Subjection of **47a** to a Glaser coupling¹³ and Boc-deprotection easily afforded the bis-alkyne SMAC mimetic dimer **55** (Scheme 7). A similar procedure applied to the P3 glycine substituted analogue **54** yielded dimer **58** (Scheme 8). The bis-alkyne linker style has been used successfully in numerous other SMAC mimetics.^{14,15}



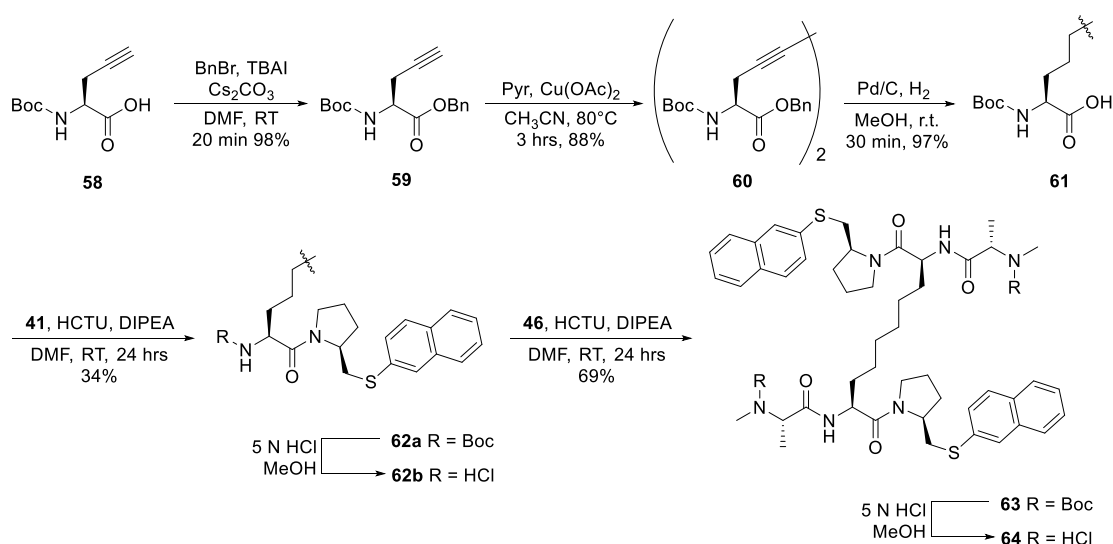
Scheme 7. Synthesis of bivalent SMAC mimetic **56**.



Scheme 8. Synthesis of bivalent SMAC mimetic **58**.

To probe linker flexibility we sought to synthesize a dimer connected through a saturated aliphatic linker. Hydrogenation of **56** seemed to be the obvious means of effecting this transformation. Frustratingly, catalytic hydrogenation using of **56** in the presence of palladium on carbon under hydrogen atmosphere proved ineffective, event at pressures up to 100 bar. It was believed that perhaps the crowded structure surrounding the bis-alkyne linker was

preventing adsorption onto the solid catalyst surface. Wilkinson's and Crabtree's homogeneous catalysts were tried but they too failed.¹⁶ A heterogeneous rhodium on carbon catalyst was able to partially reduce the bis-alkyne linker (above stoichiometric catalyst loading), however it generated a complex mixture of semi-hydrogenation products which were inseparable by HPLC. Sulfur is known to poison transition metal catalysts¹⁷ and we hypothesized that this effect, combined with the steric bulk of **56** hindered the desired transformation. Compound **64** would have to be synthesized *de-novo*, a short synthetic sequence was employed to achieve this goal (Scheme 9).

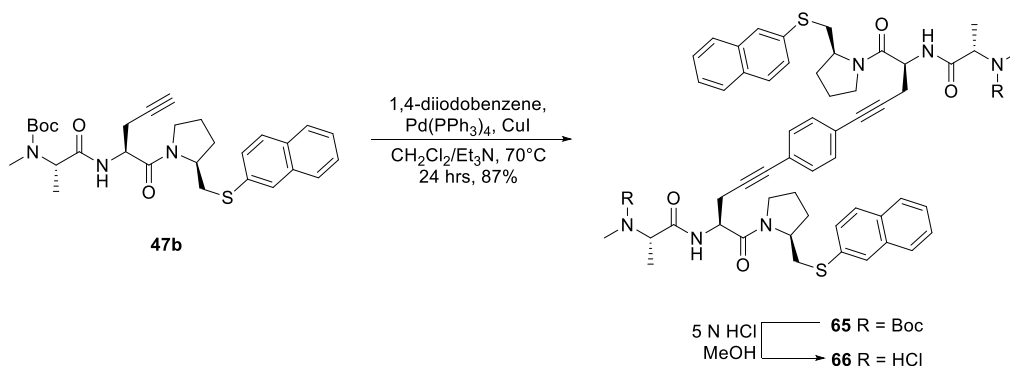


Scheme 9. Synthesis of bivalent SMAC mimetic **64** bearing a saturated alkyl linker.

To minimize steric occlusion and negate the effects of sulfur, the saturated P2 linker **61** was assembled prior to peptide coupling. Boc-L-Propargylglycine **58** was benzylated to improve its chromatographic and provide a chromophore for easy detection; a cesium counter ion was used in the reaction to suppress N-benzylation.¹⁸ The benzylated peptide **59** was cross-linked *via* a Glaser coupling to give **60** which was subjected to a palladium catalyzed hydrogenation/hydrogenolysis to give the de-benzylated, saturated dimer **61**. Two successive peptide coupling reactions with intermediate Boc-deprotection steps gave the desired bivalent SMAC mimetic **64**.

We were also interested in testing how linker length would affect the potency of our SMAC mimetic analogues. To test this we prepared **66**, which is analogous to **56** but contains an aryl

spacer. Compound **66** was easily prepared from a Sonogashira cross coupling between **47b** and 1,4-diiodobenzene (Scheme 10).¹⁹



Scheme 10. Synthesis of bivalent SMAC mimetic **66** possessing a long, rigid linker.

We tested our P2 dimerized SMAC mimetics *in-vitro* against MDA-MB-231 breast cancer cells and obtained IC₅₀ values for each compound.

Table 4. Properties of bivalent SMAC mimetics **56**, **58**, **64**, **66**. cLogP and polar surface area (PSA) values were obtained computationally from Marvin Sketch v.15.3.30.

Compound	Structure	IC ₅₀ (μM)	cLogP	PSA
56		0.631	-0.68	183
58		19.5	-2.06	200

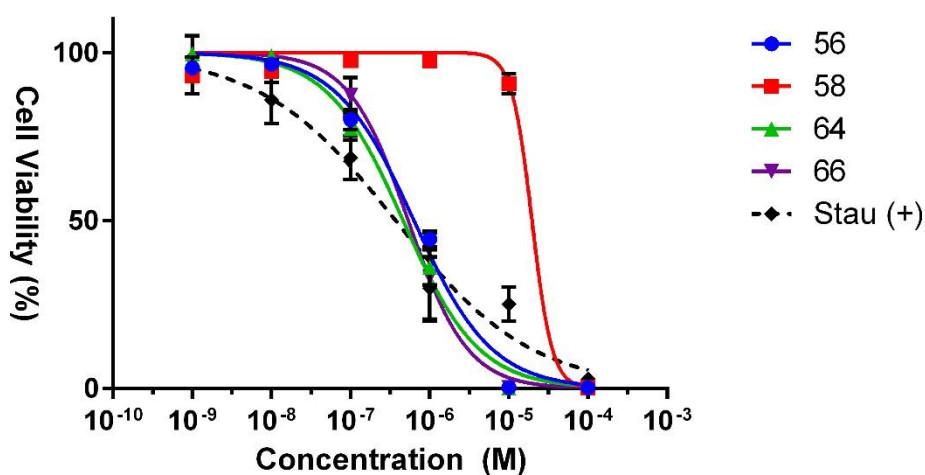
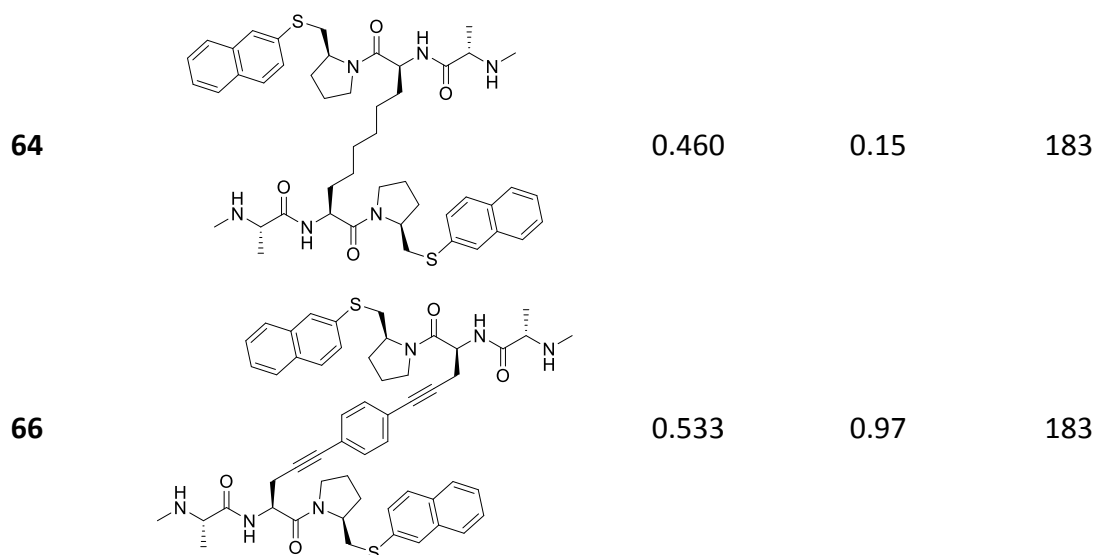


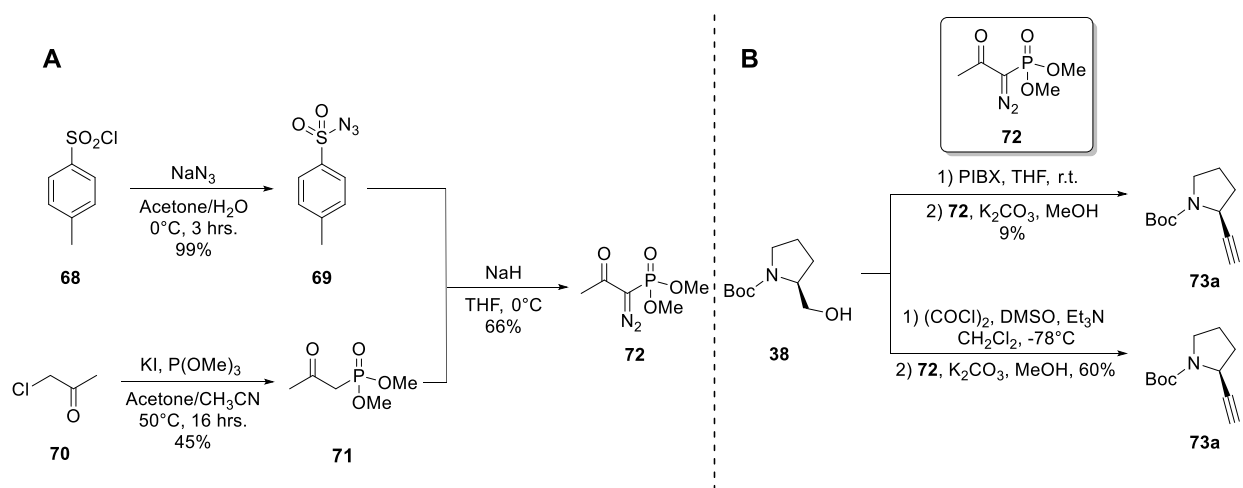
Figure 26. Functional antagonism of SMAC mimetics **56**, **58**, **64** and **66** against MDA-MB-231 breast cancer cells in a dose-responsive manner. Data points shown in the figure are averages with standard error bars of duplicate wells in assay plates. Experiments were performed in-triplicate. A staurosporine positive control (black) was used as a reference standard for cell death. Non-linear regression was used to generate a line of best fit which was used to calculate IC_{50} values.

The data shows that the bivalent SMAC mimetics **56**, **64** and **66** have reasonable potency against MDA-MB-231 breast cancer cells while **58** does not (Figure 26). Statistical analysis of **56**, **64** and **66** indicates that the IC_{50} values obtained are not statistically different (ns $P > 0.05$, 95% CI) however all three have inhibitory values much lower than **58** (** $P < 0.001$, 95% CI). Additionally, **56**, **64** and **66** do not show inhibitory concentrations which are significantly different from the staurosporine control ($IC_{50} = 371$ nM). Based on our data it seems that linker flexibility/length

does not have a significant effect on IAP binding and activation of apoptosis in the tested compounds. This result is consistent with findings by Wang, who also tested P2 linked SMAC mimetic dimers and found only short, cyclic linkers of 4 atoms or less reduced binding affinity to the BIR3 domains of XIAP and cIAP-1/2.²⁰ It is reasonable to suggest that the modest enhancement in ant-tumor cell potency for **64** is a result of its flexible highly lipophilic linker region, which has been shown to produce improved cellular permeability over more constrained ones.²¹ The bis-alkyne P3 glycine insert **58** was expected to perform poorly for reasons stated above (see section 3.2) and in addition, the low cLogP of **58** probably impaired cell permeability relative to the other less polar dimers tested.

3.4 Exploring P4 Linker Strategies

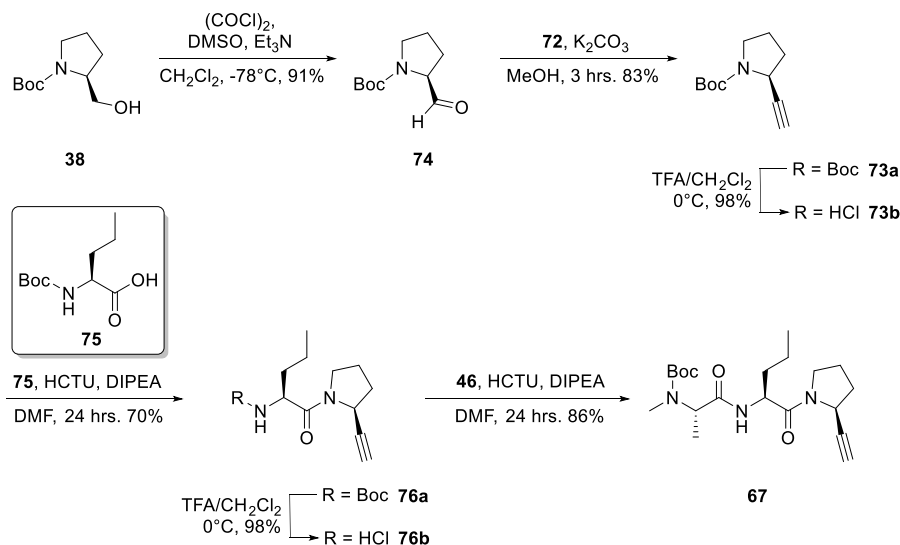
To prepare our propargylic common precursor **67** the Ohira-Bestman reagent **72** was chosen to install the alkyne through a Seyferth-Gilbert homologation²², **72** was prepared in 3 steps from literature procedures (Scheme 11A).²³



Scheme 11. (A) preparation of the Ohira-Bestman reagent **72**, (B) Attempts at a one pot oxidation-homologation reaction.

We synthesized **67** beginning with Boc-L-prolinol **38**. A one-pot oxidation homologation was attempted using different oxidants (Scheme 11B) however the two step procedure consistently provided better yields and was selected for scale-up. With **73a** in-hand, standard peptide

coupling with **75** (prepared from Boc-Pra-OH in 1 step, see experimental) followed by **46** gave the tripeptide intermediate **67** in good overall yield (Scheme 12).

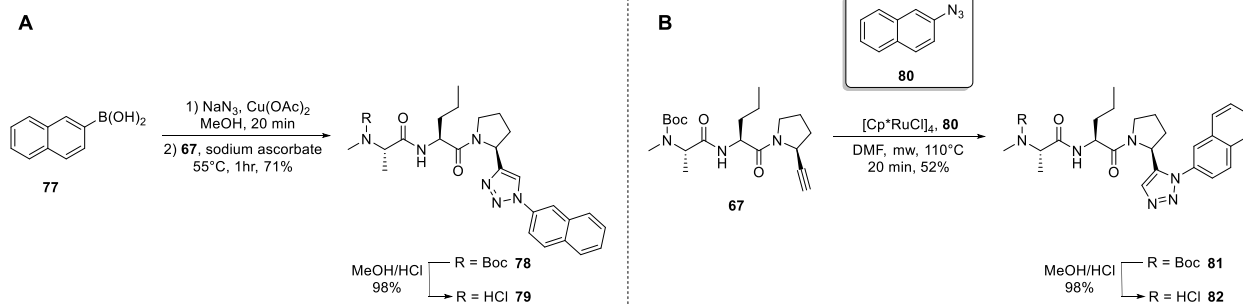


Scheme 12. Synthesis of intermediate **67**.

We used **67** as a launch-pad prepare derivatives using divergent P4 linker strategies. The naphthalene P4 residue itself was left untouched in this series to facilitate comparison between the compounds which were tested.

3.4.1 Triazole P4 Linkers – Compounds **79** and **82**

Triazoles **79** and **82** were prepared from alkyne **67** *via* the Huisgen 1,3-dipolar cycloaddition, commonly referred to as “click-chemistry”.²⁴ Triazole **79** was accessed from the reaction of **67** with a 2-naphthylazide which was pre-formed *in-situ* from a Chan-Lam cross-coupling²⁵ between boronic acid **77** and sodium azide (Scheme 13A).²⁶ Compound **82** was prepared from **67** using a pentamethylcyclopentadienyl ruthenium(II) chloride tetramer and microwave radiation which gave the desired 1,5-substituted triazole selectively (Scheme 13B).



Scheme 13. Synthesis of triazoles **79** and **82**.

We tested the triazole containing compounds *in-vitro* against MDA-MB-231 breast cancer cells and obtained IC₅₀ values for each compound.

Table 5. Properties of P4 triazole-linked monovalent SMAC mimetics **79** and **82**. cLogP and polar surface area (PSA) values were obtained computationally from Marvin Sketch v.15.3.30.

Compound	Structure	IC ₅₀ (μM)	cLogP	PSA
79		33.6	-0.20	96.7
82		> 100	-0.51	96.7

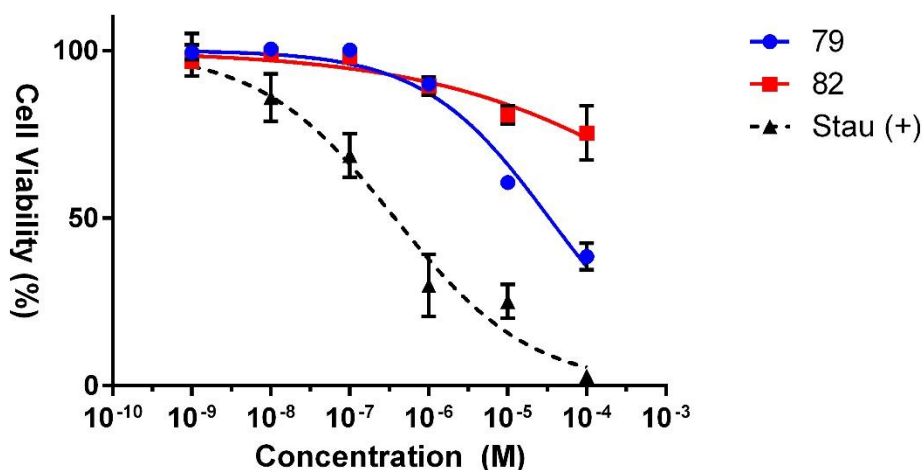


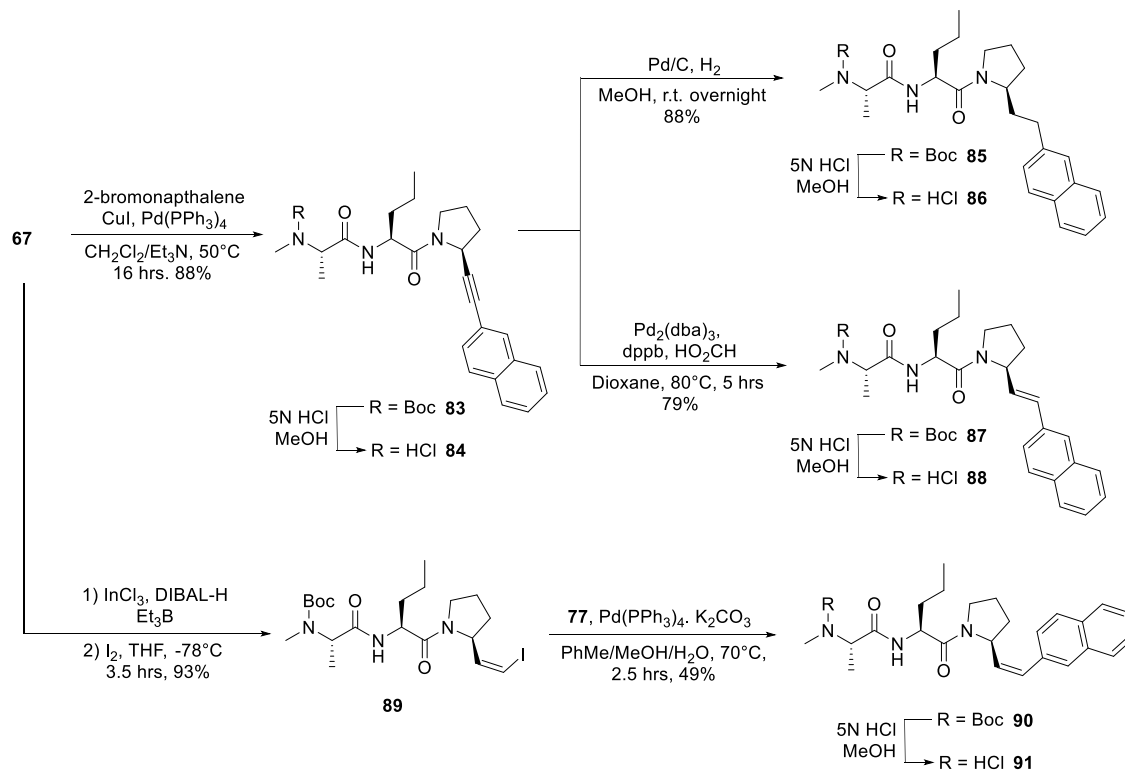
Figure 27. Functional antagonism of SMAC mimetics **79** and **82** against MDA-MB-231 breast cancer cells in a dose-responsive manner. Data points shown in the figure are averages with standard error bars of duplicate wells in assay plates. Experiments were performed in-triplicate. A staurosporine positive control (black) was used as a reference standard for cell death. Non-linear regression was used to generate a line of best fit which was used to calculate IC₅₀ values.

Surprisingly, both triazole linked monomers **79** and **82** performed quite poorly in the inhibition assay versus MDA-MB-231 breast cancer cells (Figure 27). Statistical analysis of the results indicates that the IC₅₀ values are significantly different between the monomers tested (***) P<0.001, 95% CI). Our prediction that **79** would perform better than **82** was correct however given the results it appears that the use of P4 linked 1,2,3-triazoles is not a beneficial strategy in the design of SMAC mimetics.

3.4.2 C-linked P4 linkers – Compounds **84**, **86**, **88** and **91**

The C-linked compounds **84-91** were synthesized according to Scheme 14. The alkylnaphthalene **84** was easily prepared *via* a Sonigashira cross coupling between alkyne **67** and 2-bromonaphthalene. The Boc-protected version **83** was used to access **86** by heterogeneous palladium hydrogenation. Compound **88** was also prepared from **83** through a palladium catalysed transfer semi-hydrogenation using formic acid as the reductant (E/Z = 84:14).²⁷ Attempts to synthesize **91** from **83** using Lindlar's catalyst proved ineffective and produced a complex mixture of over-reduction product and starting material. Instead, an indium mediated, (Z)-selective radical hydroindination of **67** was employed to generate a carbo-indium

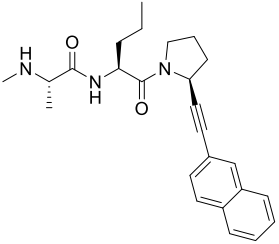
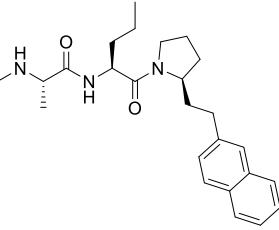
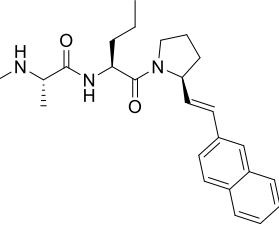
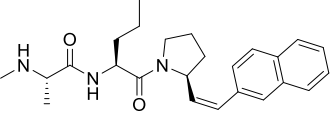
intermediate which was quenched with iodine to provide the vinyl-iodide **89** as a mixture of the E/Z isomers (4:96).²⁸ The vinyl iodide was subsequently coupled to 2-bromonaphthalene using a Suzuki cross-coupling.²⁹



Scheme 14. Synthesis of C-linked analogues **84**, **86**, **88**, **91**.

We tested the C-linked monomeric compounds *in-vitro* against MDA-MB-231 breast cancer cells and obtained IC₅₀ values for each compound.

Table 6. Properties of C-linked monovalent SMAC mimetics **84**, **86**, **88** and **91**. cLogP and polar surface area (PSA) values were obtained computationally from Marvin Sketch v.15.3.30.

Compound	Structure	IC ₅₀ (μM)	cLogP	PSA
84		13.7	0.34	66.0
86		12.5	0.60	66.0
88		15.0	0.47	66.0
91		8.04	0.47	66.0

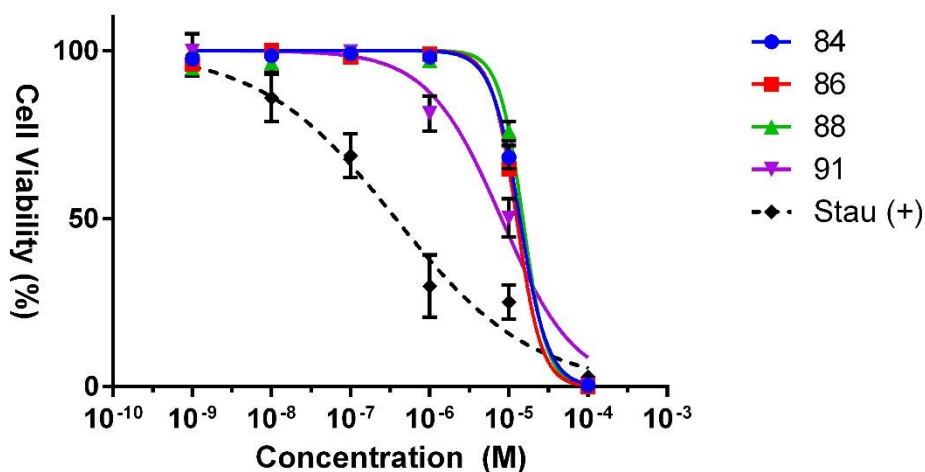


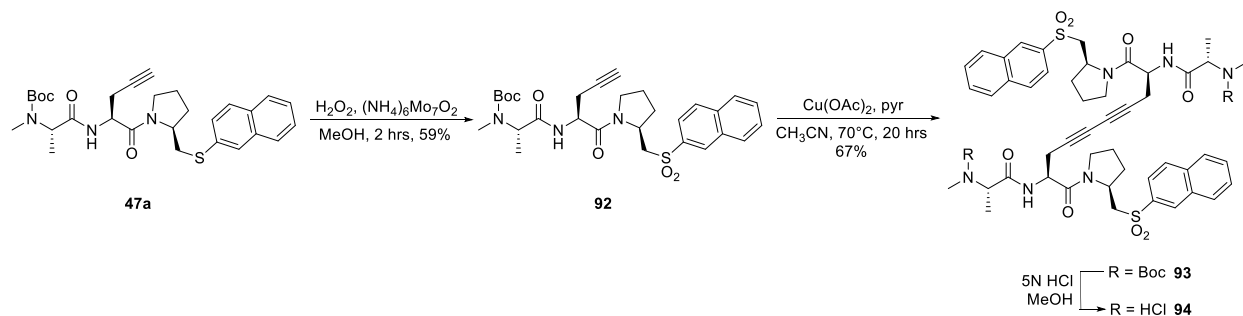
Figure 28. Functional antagonism of SMAC mimetics **84**, **86**, **88** and **91** against MDA-MB-231 breast cancer cells in a dose-responsive manner. Data points shown in the figure are averages with standard error bars of duplicate wells in assay plates. Experiments were performed in-triplicate. A staurosporine positive control (black) was used as a reference standard for cell death. Non-linear regression was used to generate a line of best fit which was used to calculate IC_{50} values.

The C-linked SMAC derivatives exhibited cytotoxicity comparable to the first set of monomeric compounds tested (Figure 28). Statistical analysis of the results for **84-91** indicated that the IC_{50} values obtained were not significantly different (ns $P > 0.05$, 95% CI). This result is somewhat surprising given the prolific placement of a polar atom or amide isostere at the P4 linker position in other reported SMAC mimetics. Despite this, binding studies have demonstrated that the leucine portion of the SMAC backbone does not form any hydrogen bonds with residues in the BIR3 IBM binding groove.^{30,31} Additionally, Fesik and Oost showed that N-methylation of the P3-P4 amide does not significantly affect binding affinities to IAPs¹¹ such a modification would disrupt the rigid SP_2 amide conformation producing a flexible linker. Taken together this may indicate that both flexible and rigid lipophilic linkers are able to orient the P4 substituent in a way which is amenable to hydrophobic interactions with the P4 hydrophobic binding pocket of the IBM binding motif.

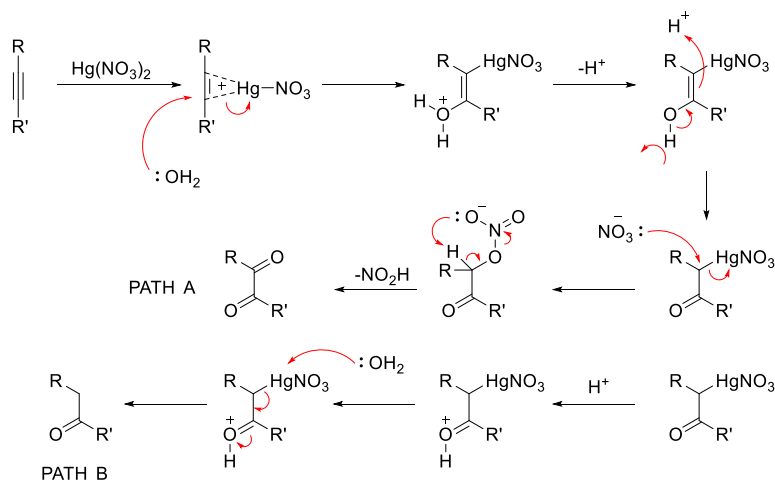
3.4.3 Oxidized P4 Linkers – Compounds 94 and 97

Compound **94** was prepared by oxidizing the sulfide in **47a** to the sulfone **92** using a molybdenum catalyst in the presence of hydrogen peroxide.³² The sulfone **92** was then subjected

to a Glaser coupling and subsequent Boc-deprotection to yield the bivalent sulfone **94** (Scheme 15).



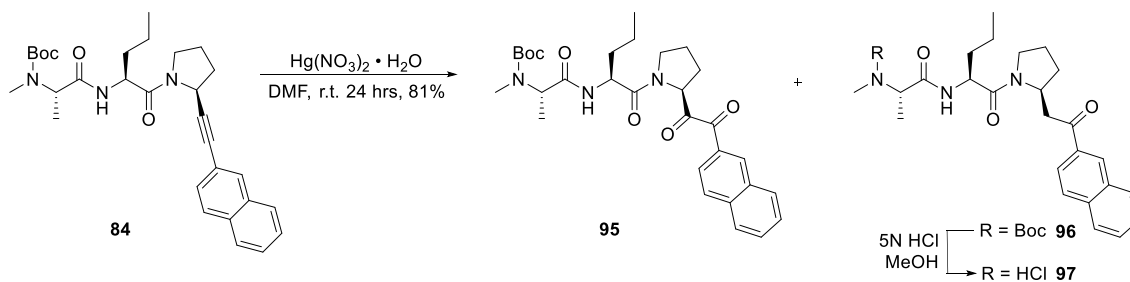
Scheme 15. Synthesis of bivalent sulfone **94**.



Scheme 16. Mercury nitrate mediated oxidation of internal alkynes. The alkyne reacts to form a mercurium ion which is trapped by water and tautomerized to give an α -keto mercuric nitrate which can either be attacked by water to provide the mono-keto product following tautomerization (path B) or can react with a nitrate to form the α -keto nitrate which oxidizes the attached carbon to produce the diketone (path A).

(Scheme 17).³⁴ The authors noted that some substrates produced the mono-oxidation product following mercuric catalysed hydration (Scheme 16, path B). In the desired reaction the α -keto mercuric nitrate is intercepted by a nitrate which is reductively eliminated to provide the 1,2-diketone oxidation product and nitrous acid (Scheme 16, path A).

We initially envisioned using the alkyne functionality of **83** to perform a Wacker style oxidation using PdBr_2 and CuBr_2 under aerobic conditions to form 1,2-diketone **95**, however in our hands this reaction was not able to achieve the stated transformation.³³ A prep utilizing mercuric nitrate was attempted which furnished the mono-oxidation product **97** (following deprotection) with trace amounts of the 1,2-diketone **95** recovered



Scheme 17. Synthesis of ketone **97** + side product **95**.

We tested the C-linked oxidized compounds *in-vitro* against MDA-MB-231 breast cancer cells and obtained IC_{50} values for each compound.

Table 7. Properties of P4 oxidized linker SMAC mimetics **94** and **96**. cLogP and polar surface area (PSA) values were obtained computationally for the hydrochloride salt of each compound using Marvin Sketch v.15.3.30.

Compound	Structure	IC_{50} (μM)	cLogP	PSA
94		14.8	-3.43	217.1
97		> 100	-0.39	83.1

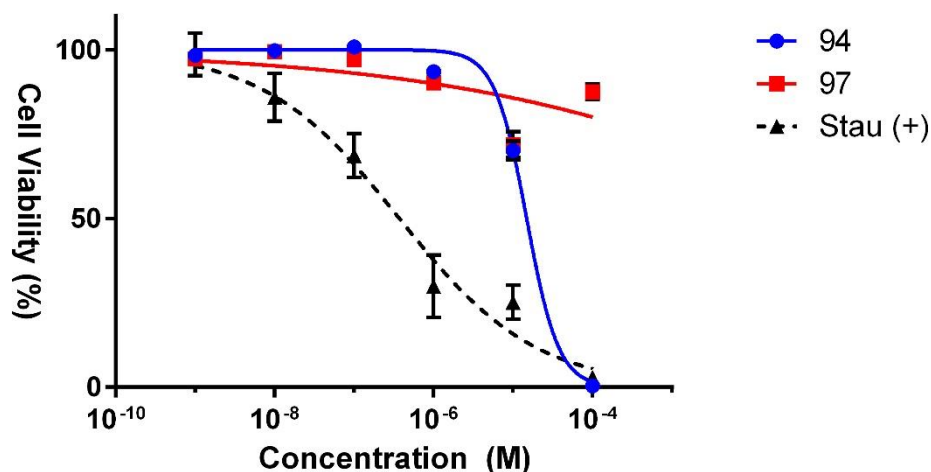


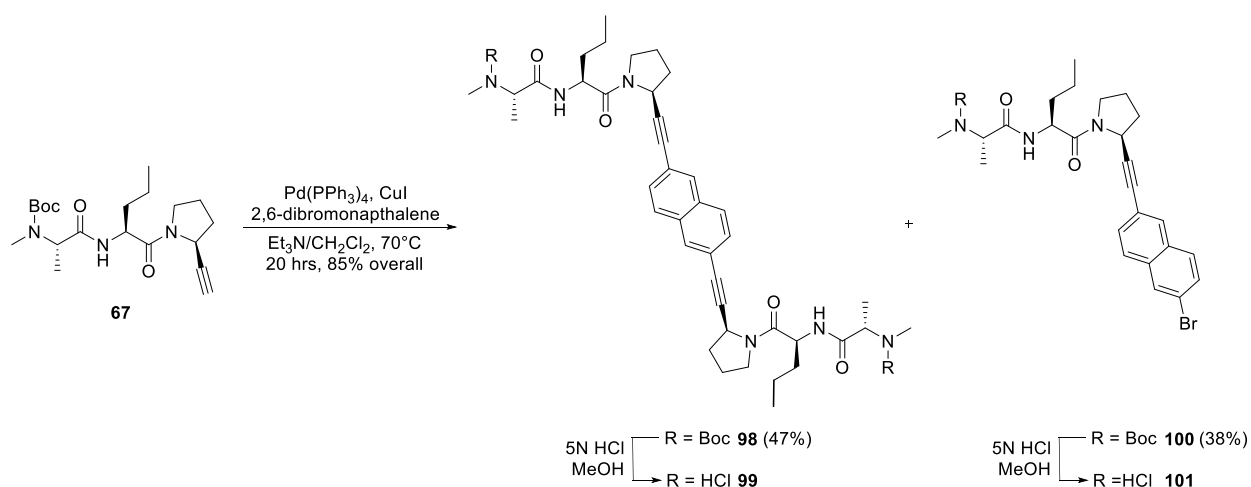
Figure 29. Functional antagonism of SMAC mimetics **94** and **97** against MDA-MB-231 breast cancer cells in a dose-responsive manner. Data points shown in the figure are averages with standard error bars of duplicate wells in assay plates. Experiments were performed in-triplicate. A staurosporine positive control (black) was used as a reference standard for cell death. Non-linear regression was used to generate a line of best fit which was used to calculate IC₅₀ values.

The results from the cell based assay for compounds **94** and **97** suggest that additional oxidation in the P4 linker is detrimental to IAP binding affinity and induction of apoptosis (Figure 29). Statistical analysis showed that **94** had an IC₅₀ which was significantly higher than its non-oxidized counterpart **56** (***) P<0.001, 95% CI) however, despite this drop in activity **94** was still more potent than the most potent monomeric SMAC mimetic tested **34** (** P<0.01). Compound **97** showed virtually no cytotoxic activity, the 100 μM cell treatment was repeated in triplicate (total n=6) and similar values were obtained. This likely means that the transient increase in potency at the 10 μM treatment level is an outlier. Without kinetic binding data for the pure IAP proteins it is difficult to ascertain whether these decreases in cell-killing efficiency are the result of decreased membrane permeability or reduced IAP binding efficiency. In the case of **94** it is reasonable to speculate that the sharp enhancement in polarity relative to **56** (decrease of nearly 3 log units) may have hindered its ability to cross the plasma membrane of the MDA-MB-231 cells and thus induce cell death. Compound **97** does not inherit the same degree of polar character relative to its un-oxidized form **86** and would be expected to cross the membrane with reasonable efficiency. Therefore it is more likely that the ketone incorporated in **97** alpha to the naphthyl ring is engaging in lone pair repulsion with a polar amino acid residue in the BIR3 IBM

binding groove. These results convey that oxidation of the P4 linker may not be an effective strategy to generate more efficient SMAC mimetics, although a broader substrate scope is required to draw more definitive conclusions.

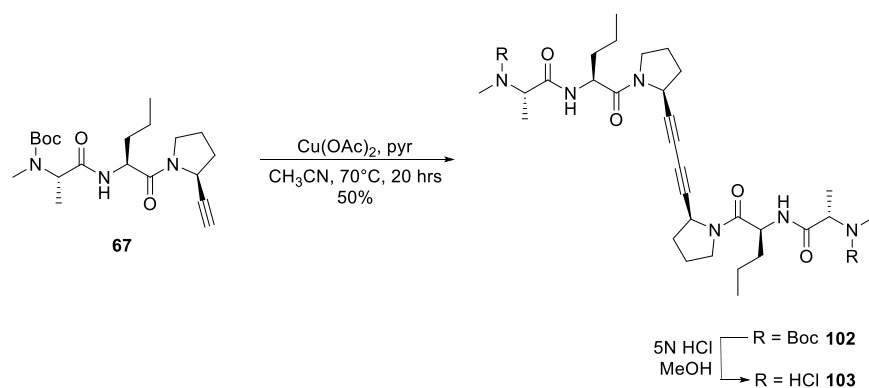
3.4.4 Dimerization at the P4 residue – Compounds **99**, **101** and **103**

Compound **99** was synthesized from **67** in one step *via* a Sonigashira cross-coupling using a bivalent 2,6-dibromonaphthalene donor (scheme 18).³⁵ Analogue **101** was the mono-coupling by-product which was testing as well.



Scheme 18. Synthesis of P4 linked bivalent SMAC mimetic **99** and 6-bromo monomer **101**.

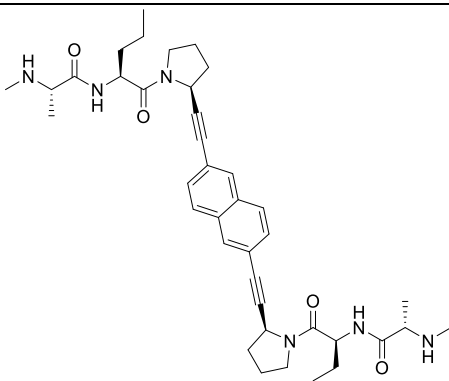
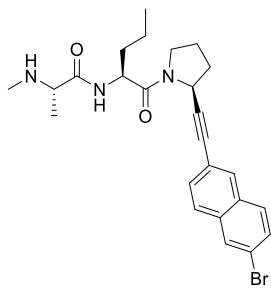
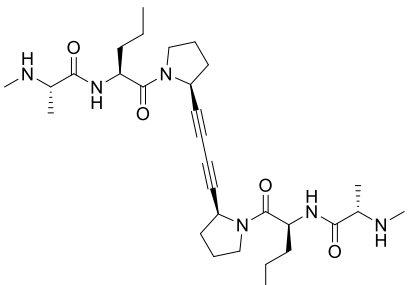
The negative control **103** was made in one step from **67** through the use of a Glaser coupling (Scheme 19).



Scheme 19. Synthesis of P4 linked negative control **103**.

We tested the P4 dimers compounds *in-vitro* against MDA-MB-231 breast cancer cells and obtained IC₅₀ values for each compound.

Table 8. Properties of P4 linked SMAC mimetics **99**, **101** and **103**. cLogP and polar surface area (PSA) values were obtained computationally for the hydrochloride salt of each compound using Marvin Sketch v.15.3.30.

Compound	Structure	IC ₅₀ (μM)	cLogP	PSA
99		0.846	-2.73	132.0
101		14.4	1.10	66.0
103		> 100	-4.93	132.0

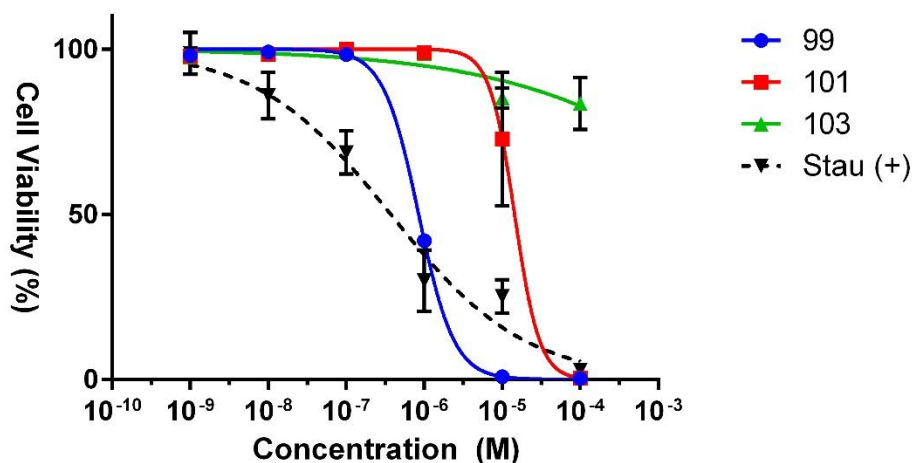


Figure 30. Functional antagonism of SMAC mimetics **99**, **101** and **103** against MDA-MB-231 breast cancer cells in a dose-responsive manner. Data points shown in the figure are averages with standard error bars of duplicate wells in assay plates. Experiments were performed in-triplicate. A staurosporine positive control (black) was used as a reference standard for cell death. Non-linear regression was used to generate a line of best fit which was used to calculate IC_{50} values.

The results obtained for this series of compounds demonstrated that bivalent SMAC mimetic linkage through P4 is an effective strategy for the design of potent inhibitors of IAPs. Statistical analysis showed that **99** had an IC_{50} value which was not significantly different from any of the other bivalent SMAC mimetics tested, with the exception of **58** (Table 8) (ns $P > 0.05$, 95% CI). Brominated monomer **101** had significant error associated with the 10 μ M cell treatment and produced a broad IC_{50} range causing it to be not statistically different from any of the other monomers (ns, $P > 0.05$, 95% CI). The negative control **103** performed as expected and exhibited limited toxicity towards the MDA-MB-231 cell line. There is a significant difference between the growth inhibition properties of **99** and **103** with the former being 5 orders of magnitude more potent at promoting death in the cell based assay. This result is likely a combination of the lower clogP value of **103** combined with the apparent requirement for a hydrophobic P4 residue as ubiquitously found in other reported SMAC mimetic dimers. The incorporation of bromine at the C6 position of the naphthalene ring in **101** did not provide an advantage over the non-brominated version **84**, however it did significantly raise the clogP of **84**. Given the equal potencies of **84** and **101** this suggest that membrane permeability may not have been limiting for the cytotoxicity of **84**.

3.5 Caspase-3/7 Activation – Confirmation of Apoptosis as a Mechanism of Cell Death

Although many of the SMAC mimetics tested were able to promote cell death in MDA-MB-231 breast cancer cells the means by which they were achieving this remained ambiguous. To understand if our compounds were acting selectively by inducing apoptosis we conducted a caspase-3/7 activation assay to assess their mechanism of action against the cell line.

Promega's Apo-ONE® caspase-3/7 detection kit was used. It is composed of a lysis buffer and capsase-3/7 substrate which becomes fluorescent green upon cleavage by active caspases. Although this test for apoptosis is not as robust as some other more involved diagnostic tools, it has been used successfully by other research groups to confirm or deny apoptotic activity.³⁶ Thus, it was deemed an adequate test to initially confirm that our compounds were effecting cell death via their predicted mechanism of action and not through general cytotoxicity and necrosis.

Compounds **33**, **34**, **56**, **64**, **91** and **99** were tested for their ability to promote caspase activation with staurosporine, a known apoptotic agent, as a positive control (Figure 31).³⁷

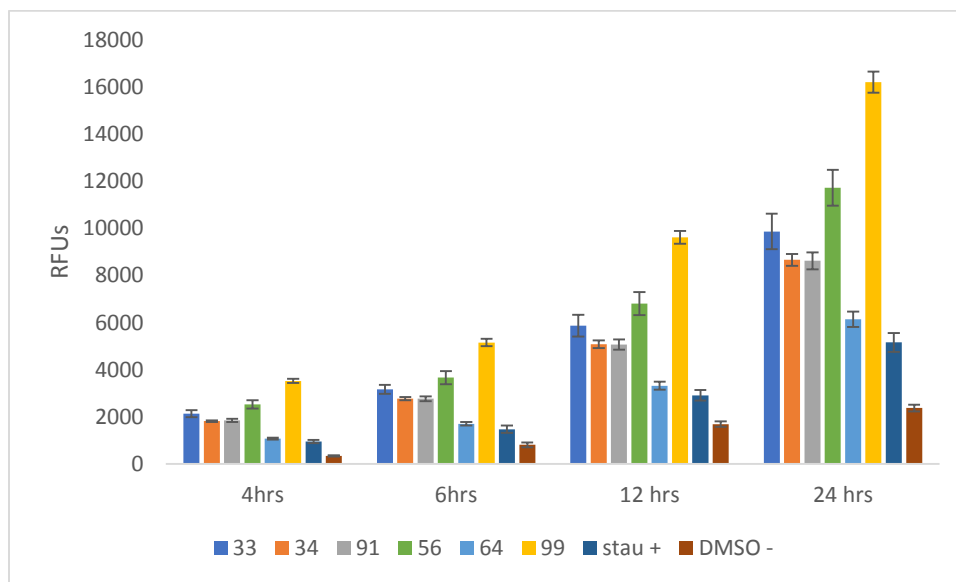


Figure 31. Functional activation ofCaspase-3/7 by the denoted compounds at 10 μ M in MDA-MB-231 breast cancer cells assessed using an Apo-ONE assay. Caspase activation was measured by fluorescence at the indicated time points and reported in relative fluorescence units (RFUs). Staurosporine (stau +) represents the positive control for apoptosis while the DMSO vehicle control represents background apoptosis.

The results from Figure 31 suggest that all compounds tested in the Apo-ONE assay were able to promote apoptosis *via* caspase-3/7 activation. This conclusion is supported by statistical analysis which determined that each data point was significantly higher than the 0.1 M DMSO control (minimum * $P < 0.05$, 95% CI). Monomers **33**, **34** and **91** all show similar activity (ns, $P > 0.05$, 95% CI) while dimers **56**, **64** and **99** are statistically different (*** $P < 0.001$, 95% CI). Compound **99** is the most active among the series (*** $P < 0.001$, 95% CI) while **64** is the least active and statistically similar to staurosporine (ns, $P > 0.05$, 95% CI). The bis-alkyne linked dimer **56** showed similar caspase-3/7 activation to its propargylic monomer **33** (ns, $P > 0.05$, 95% CI) but was more active than monomers **34** and **91** (** $P < 0.01$, 95% CI).

Due to the simplicity of this assay it is difficult to extract meaningful IAP binding affinities from the data due to the numerous variables which could skew the data. Despite this, some inferences may be gathered. The caspase-3/7 activation activity of **64** was well below that of any other compound tested in the Apo-ONE assay, yet in the cell proliferation assay it fared best among the entire library of compounds tested. One explanation for the discrepancy between cytotoxicity and caspase-3/7 activation may stem from the highly flexible, lipophilic nature of the P2 linker region in **64**. Compound **64** has similar caspase-3/7 activity to staurosporine, which is known to disrupt membrane integrity at concentrations above 6.25 μM and promote necrosis.³⁸ Perhaps the highly amphipathic hydrochloride salt of **64** is behaving as a pseudo-surfactant, disrupting the membranes of cells and increasing the ratio of necrotic to apoptotic cells. This would promote cell death by necrosis before caspase3/7 activation could occur and could help explain the potent cytotoxicity of **64**, despite its low caspase activation results. Cellular morphology appears to support this conclusion (Table 10, Appendix I), at the 10 μM treatment with staurosporine cells appear to show a combination of apoptosis (small clean spheres) and necrosis (amorphous shadowy blobs). This effect is reduced, but still present in **64** and nearly absent in **99** which would co-relate well with its high caspase-3/7 activation profile and presumably selectivity for apoptosis over necrosis.

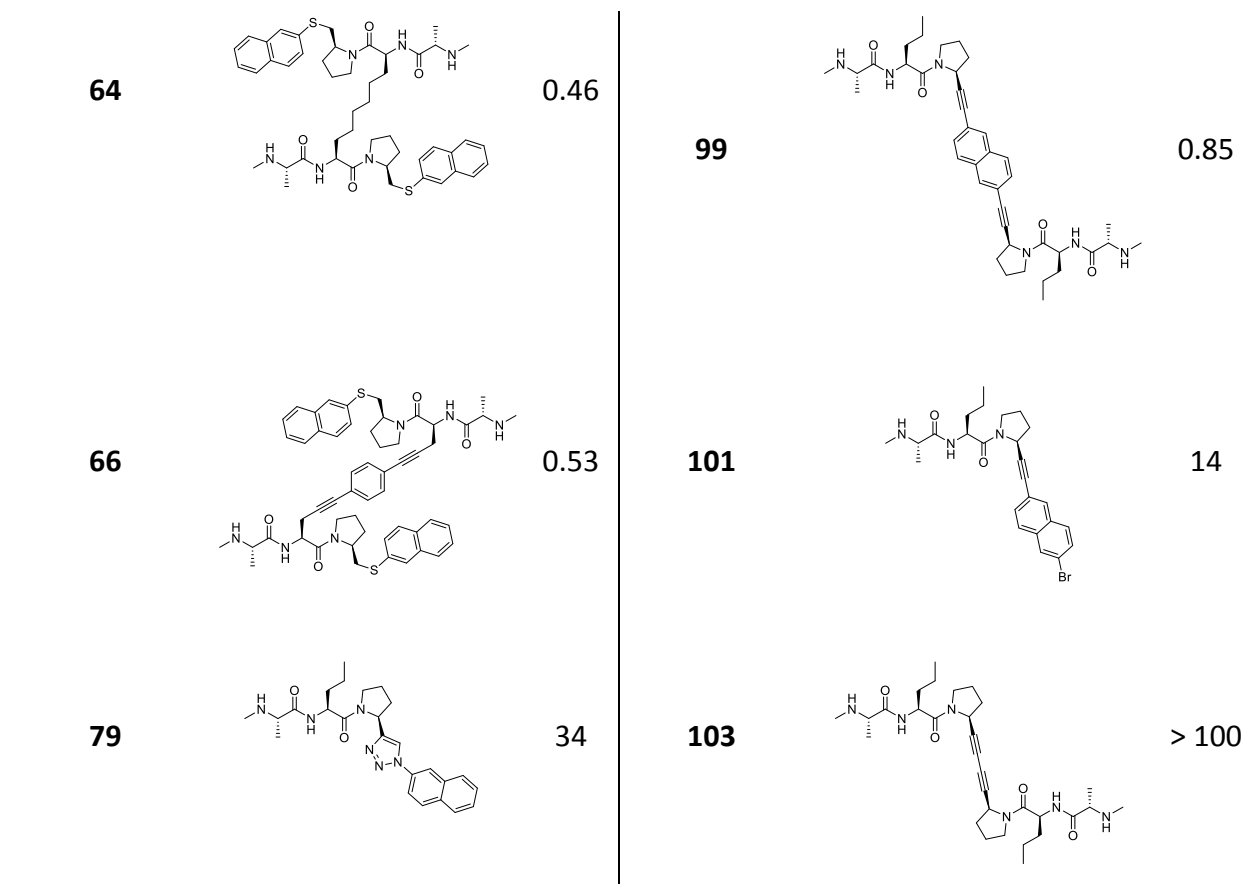
3.6 Results Summary

In total, 20 compounds were synthesized and tested against MDA-MB-231 breast cancer cells (Table 9). Of these compounds, bivalent SMAC mimetic **64** was the most potent analogue

with a calculated $IC_{50} = 460$ nM. Caspase-3/7 activation was empirically confirmed in a subset of compounds, suggesting that they were selectively promoting cell death *via* the IAP inhibition and activation of apoptosis.

Table 9. List of compounds tested with IC_{50} values against MDA-MB-231 breast cancer cells.

Compound	IC_{50} (μ M)	Compound	IC_{50} (μ M)
33	12	82	> 100
34	5.6	84	14
35	14	86	13
36	12	88	15
50	31	91	8
56	0.63	94	15
58	19.5	97	> 100



We reported chemical modifications to our general SMAC mimetic scaffold which had variable effects on their activity against MDA-MB-231 breast cancer cells, and potentially, on IAP binding affinities. Notable results include: (1) The conclusion that unbranched residues/lack of substitution at the P2 position contribute very little to gain or loss of activity in monomeric SMAC mimetics **33-36** (Table 3); (2) P2 linked bivalent SMAC mimetics benefit somewhat from a long, flexible linker (Table 4); (3) P4 1,2,3-triazole rings attached directly to the proline residue of P3 sharply reduce monomer activity (Table 5); (3) Both flexible and rigid non-polar linkers at P4 in monovalent SMAC mimetics promote cell death with equal efficiency (Table 6); (4) Oxidation of the P4 linker is detrimental in both monovalent and divalent SMAC mimetics, although this is not generalizable given the sample size (Table 7); (5) There is a structural/distance requirement for bivalent SMAC mimetics linked at P4, compounds lacking a P4 hydrophobic moiety like **103** display significantly impaired cytotoxicity relative to those that do **99** (Table 8).

3.7 Future Work

Using the data obtained from our SAR work a new series of target compounds **104-110** (Figure 32) are proposed which combine some beneficial features reported in compounds **33-103** as well as new chemical diversity.

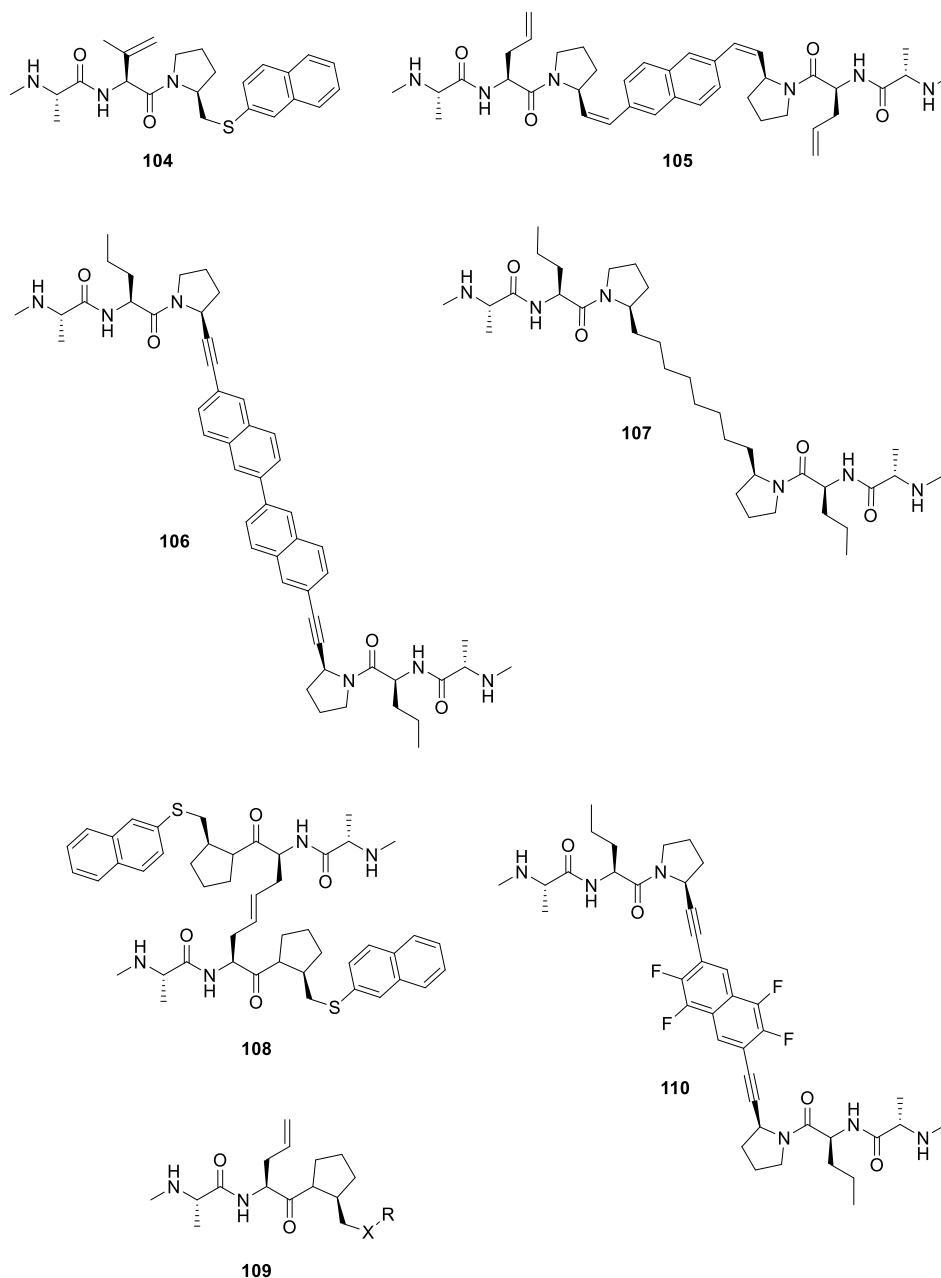


Figure 32. Proposed targets for future synthesis and testing. **109** X = (S or N), R = hydrophobic moiety.

Compound **104** incorporates α -branching common in several reported SMAC mimetics while maintaining the SP_2 character found to be beneficial for activity in our library screen. Analogues

106 and **107** are predicted to help determine the contributions of length and flexibility to P4 linked bivalent SMAC mimetic cytotoxicity. Analogue **106** maintains the rigidity of the P4 linker while extending its reach and incorporating a second hydrophobic P4 moiety. Compound **107** has a 9.04 Å flexible linker (similar in length to the 9.95 Å linker in **99**) to assess if linker rigidity/bulk dictates potency in these analogues. **108** combines the successful SP₂ P2 substituent with a shorter linker in an attempt to improve membrane permeability and reduce non-apoptotic cytotoxicity through a reduction in amphipathic character. Analogue **110** incorporates halogenation to the aryl spacer based on the observation that bromination of **101** resulted in an increase of its clogP compared to the non-brominated derivative. Fluorinated **110** is predicted to have augmented membrane permeability relative to **103**, which had a low clogP and may have had difficulty crossing the cellular membrane. In addition, the use of fluorine instead of bromine should maintain the enhancement in hydrophobicity while also providing metabolic stability.

3.8 References

1. Nakagawa, I.; Aki, K.; Hata, T., Synthesis of 5[prime or minute]-alkylthio-5[prime or minute]-deoxynucleosides from nucleosides in a one-pot reaction. *Journal of the Chemical Society, Perkin Transactions 1* **1983**, (0), 1315-1318.
2. Hughes, D. L.; Reamer, R. A.; Bergan, J. J.; Grabowski, E. J. J., A mechanistic study of the Mitsunobu esterification reaction. *Journal of the American Chemical Society* **1988**, *110* (19), 6487-6491.
3. Siedlecka, R.; Skarzewski, J., Synthesis of Homochiral N-Protected β-Amino Sulfoxides from α-Amino Alcohols. *Synlett* **1996**, *1996* (08), 757-758.
4. Kotsuki, H.; Matsumoto, K.; Nishizawa, H., High pressure-promoted transformation of alcohols into the corresponding phenylsulfides with Bu₃P-PhssPh. *Tetrahedron Letters* **1991**, *32* (33), 4155-4158.
5. Nakagawa, I.; Hata, T., A convenient method for the synthesis of 5'-S-alkylthio-5'-deoxyribonucleosides. *Tetrahedron Letters* **1975**, *16* (17), 1409-1412.
6. Kanematsu, M.; Yoshida, M.; Shishido, K., Total Synthesis of Aspergillide A and B Based on the Transannular Oxy-Michael Reaction. *Angewandte Chemie International Edition* **2011**, *50* (11), 2618-2620.
7. Gueyrard, D.; Tlegenov, R. T.; Steinbruckner, S.; Perly, B.; Rollin, P., Synthesis of new derivatives of 11-thiolupinine. *Journal of Sulfur Chemistry* **2010**, *31* (6), 493-498.

8. (a) Fletcher, S. R.; Burkamp, F.; Blurton, P.; Cheng, S. K. F.; Clarkson, R.; O'Connor, D.; Spinks, D.; Tudge, M.; van Niel, M. B.; Patel, S.; Chapman, K.; Marwood, R.; Sheppard, S.; Bentley, G.; Cook, G. P.; Bristow, L. J.; Castro, J. L.; Hutson, P. H.; MacLeod, A. M., 4-(Phenylsulfonyl)piperidines: Novel, Selective, and Bioavailable 5-HT_{2A} Receptor Antagonists. *Journal of Medicinal Chemistry* **2002**, *45* (2), 492-503; (b) Zielińska-Błajet, M.; Kucharska, M.; Skarzewski, J., Simple Enantiospecific Synthesis of Sulfides of Cinchona Alkaloids. *Synthesis* **2006**, *2006* (07), 1176-1182.
9. Condon, S. M.; Mitsuuchi, Y.; Deng, Y.; LaPorte, M. G.; Rippin, S. R.; Haimowitz, T.; Alexander, M. D.; Kumar, P. T.; Hendi, M. S.; Lee, Y.-H.; Benetatos, C. A.; Yu, G.; Kapoor, G. S.; Neiman, E.; Seipel, M. E.; Burns, J. M.; Graham, M. A.; McKinlay, M. A.; Li, X.; Wang, J.; Shi, Y.; Feltham, R.; Bettjeman, B.; Cumming, M. H.; Vince, J. E.; Khan, N.; Silke, J.; Day, C. L.; Chunduru, S. K., Birinapant, a Smac-Mimetic with Improved Tolerability for the Treatment of Solid Tumors and Hematological Malignancies. *Journal of Medicinal Chemistry* **2014**, *57* (9), 3666-3677.
10. Weisberg, E.; Ray, A.; Barrett, R.; Nelson, E.; Christie, A. L.; Porter, D.; Straub, C.; Zawel, L.; Daley, J. F.; Lazo-Kallanian, S.; Stone, R.; Galinsky, I.; Frank, D.; Kung, A. L.; Griffin, J. D., Smac mimetics: implications for enhancement of targeted therapies in leukemia. *Leukemia* **2010**, *24* (12), 2100-2109.
11. Oost, T. K.; Sun, C.; Armstrong, R. C.; Al-Assaad, A.-S.; Betz, S. F.; Deckwerth, T. L.; Ding, H.; Elmore, S. W.; Meadows, R. P.; Olejniczak, E. T.; Oleksijew, A.; Oltersdorf, T.; Rosenberg, S. H.; Shoemaker, A. R.; Tomaselli, K. J.; Zou, H.; Fesik, S. W., Discovery of Potent Antagonists of the Antiapoptotic Protein XIAP for the Treatment of Cancer. *Journal of Medicinal Chemistry* **2004**, *47* (18), 4417-4426.
12. Kipp RA, C. M., Wist AD, Cresson CM, Carrell M, Griner E, Wiita A, Albinia PA, Chai J, ShiY, Semmelhack MF, McLendon GL., Molecular targeting of inhibitors of apoptosis proteins based on small molecule mimics of natural binding partners. *Biochemistry* **2002**, *41*, 7344-7349.
13. Balaraman, K.; Kesavan, V., Efficient Copper(II) Acetate Catalyzed Homo- and Heterocoupling of Terminal Alkynes at Ambient Conditions. *Synthesis* **2010**, *2010* (20), 3461-3466.
14. Hennessy, E. J.; Adam, A.; Aquila, B. M.; Castriotta, L. M.; Cook, D.; Hattersley, M.; Hird, A. W.; Huntington, C.; Kamhi, V. M.; Laing, N. M.; Li, D.; MacIntyre, T.; Omer, C. A.; Oza, V.; Patterson, T.; Repik, G.; Rooney, M. T.; Saeh, J. C.; Sha, L.; Vasbinder, M. M.; Wang, H.; Whitston, D., Discovery of a Novel Class of Dimeric Smac Mimetics as Potent IAP Antagonists Resulting in a Clinical Candidate for the Treatment of Cancer (AZD5582). *Journal of Medicinal Chemistry* **2013**, *56* (24), 9897-9919.
15. Flygare, J. A.; Cohen, F.; Deshayes, K.; Koehler, M. F. T.; Gazzard, L. J.; Wang, L.; Ndubaku, C., Inhibitors of iap. Google Patents: 2008.
16. Del Valle, J. R.; Goodman, M., Stereoselective Synthesis of Boc-Protected cis and trans-4-Trifluoromethylprolines by Asymmetric Hydrogenation Reactions. *Angewandte Chemie International Edition* **2002**, *41* (9), 1600-1602.
17. Rodriguez, J. A.; Hrbek, J., Interaction of Sulfur with Well-Defined Metal and Oxide Surfaces: Unraveling the Mysteries behind Catalyst Poisoning and Desulfurization. *Accounts of Chemical Research* **1999**, *32* (9), 719-728.
18. Salvatore, R. N.; Nagle, A. S.; Jung, K. W., Cesium Effect: High Chemoselectivity in Direct N-Alkylation of Amines. *The Journal of Organic Chemistry* **2002**, *67* (3), 674-683.

19. Caldarelli, S. A.; El Fangour, S.; Wein, S.; Tran van Ba, C.; Périgaud, C.; Pellet, A.; Vial, H. J.; Peyrottes, S., New Bis-thiazolium Analogues as Potential Antimalarial Agents: Design, Synthesis, and Biological Evaluation. *Journal of Medicinal Chemistry* **2013**, *56* (2), 496-509.
20. Sheng, R.; Sun, H.; Liu, L.; Lu, J.; McEachern, D.; Wang, G.; Wen, J.; Min, P.; Du, Z.; Lu, H.; Kang, S.; Guo, M.; Yang, D.; Wang, S., A Potent Bivalent Smac Mimetic (SM-1200) Achieving Rapid, Complete, and Durable Tumor Regression in Mice. *Journal of Medicinal Chemistry* **2013**, *56* (10), 3969-3979.
21. Sun, H.; Liu, L.; Lu, J.; Bai, L.; Li, X.; Nikolovska-Coleska, Z.; McEachern, D.; Yang, C.-Y.; Qiu, S.; Yi, H.; Sun, D.; Wang, S., Potent Bivalent Smac Mimetics: Effect of the Linker on Binding to Inhibitor of Apoptosis Proteins (IAPs) and Anticancer Activity. *Journal of Medicinal Chemistry* **2011**, *54* (9), 3306-3318.
22. Müller, S.; Liepold, B.; Roth, G. J.; Bestmann, H. J., An Improved One-pot Procedure for the Synthesis of Alkynes from Aldehydes. *Synlett* **1996**, *1996* (06), 521-522.
23. Pietruszka, J.; Witt, A., Synthesis of the Bestmann-Ohira Reagent. *Synthesis* **2006**, *2006* (24), 4266-4268.
24. Kolb, H. C.; Finn, M. G.; Sharpless, K. B., Click Chemistry: Diverse Chemical Function from a Few Good Reactions. *Angewandte Chemie International Edition* **2001**, *40* (11), 2004-2021.
25. Chan, D. M. T.; Monaco, K. L.; Wang, R.-P.; Winters, M. P., New N- and O-arylations with phenylboronic acids and cupric acetate. *Tetrahedron Letters* **1998**, *39* (19), 2933-2936.
26. Grimes, K. D.; Gupte, A.; Aldrich, C. C., Copper(II)-Catalyzed Conversion of Aryl/Heteroaryl Boronic Acids, Boronates, and Trifluoroborates into the Corresponding Azides: Substrate Scope and Limitations. *Synthesis* **2010**, *2010* (09), 1441-1448.
27. Shen, R.; Chen, T.; Zhao, Y.; Qiu, R.; Zhou, Y.; Yin, S.; Wang, X.; Goto, M.; Han, L.-B., Facile Regio- and Stereoselective Hydrometalation of Alkynes with a Combination of Carboxylic Acids and Group 10 Transition Metal Complexes: Selective Hydrogenation of Alkynes with Formic Acid. *Journal of the American Chemical Society* **2011**, *133* (42), 17037-17044.
28. Takami, K.; Mikami, S.; Yorimitsu, H.; Shinokubo, H.; Oshima, K., Triethylborane-Mediated Hydrogallation and Hydroindation: Novel Access to Organogalliums and Organoindiums. *The Journal of Organic Chemistry* **2003**, *68* (17), 6627-6631.
29. Ashley, E. R.; Cruz, E. G.; Stoltz, B. M., The Total Synthesis of (-)-Lemonomycin. *Journal of the American Chemical Society* **2003**, *125* (49), 15000-15001.
30. Liu, Z.; Sun, C.; Olejniczak, E. T.; Meadows, R. P.; Betz, S. F.; Oost, T.; Herrmann, J.; Wu, J. C.; Fesik, S. W., Structural basis for binding of Smac/DIABLO to the XIAP BIR3 domain. *Nature* **2000**, *408* (6815), 1004-1008.
31. Wu, G.; Chai, J.; Suber, T. L.; Wu, J.-W.; Du, C.; Wang, X.; Shi, Y., Structural basis of IAP recognition by Smac/DIABLO. *Nature* **2000**, *408* (6815), 1008-1012.
32. Jeyakumar, K.; Chakravarthy, R. D.; Chand, D. K., Simple and efficient method for the oxidation of sulfides to sulfones using hydrogen peroxide and a Mo(VI) based catalyst. *Catalysis Communications* **2009**, *10* (14), 1948-1951.
33. Ren, W.; Xia, Y.; Ji, S.-J.; Zhang, Y.; Wan, X.; Zhao, J., Wacker-Type Oxidation of Alkynes into 1,2-Diketones Using Molecular Oxygen. *Organic Letters* **2009**, *11* (8), 1841-1844.
34. Jung, M. E.; Deng, G., Synthesis of α -Diketones from Alkylaryl- and Diarylalkynes Using Mercuric Salts. *Organic Letters* **2014**, *16* (8), 2142-2145.

35. Hanamoto, T.; Shimomoto, N.; Kikukawa, T.; Inanaga, J., Efficient synthesis of enantiomerically pure trans-2,5-bis(arylethynyl)pyrrolidines. A new entry into C2-symmetric chiral secondary amines. *Tetrahedron: Asymmetry* **1999**, *10* (15), 2951-2959.
36. Flygare, J. A.; Beresini, M.; Budha, N.; Chan, H.; Chan, I. T.; Cheeti, S.; Cohen, F.; Deshayes, K.; Doerner, K.; Eckhardt, S. G.; Elliott, L. O.; Feng, B.; Franklin, M. C.; Reisner, S. F.; Gazzard, L.; Halladay, J.; Hymowitz, S. G.; La, H.; LoRusso, P.; Maurer, B.; Murray, L.; Plise, E.; Quan, C.; Stephan, J.-P.; Young, S. G.; Tom, J.; Tsui, V.; Um, J.; Varfolomeev, E.; Vucic, D.; Wagner, A. J.; Wallweber, H. J. A.; Wang, L.; Ware, J.; Wen, Z.; Wong, H.; Wong, J. M.; Wong, M.; Wong, S.; Yu, R.; Zobel, K.; Fairbrother, W. J., Discovery of a Potent Small-Molecule Antagonist of Inhibitor of Apoptosis (IAP) Proteins and Clinical Candidate for the Treatment of Cancer (GDC-0152). *Journal of Medicinal Chemistry* **2012**, *55* (9), 4101-4113.
37. Zhang, X. D.; Gillespie, S. K.; Hersey, P., Staurosporine induces apoptosis of melanoma by both caspase-dependent and -independent apoptotic pathways. *Molecular Cancer Therapeutics* **2004**, *3* (2), 187-197.
38. Hoffman, R. Cell Fate Without a Crystal Ball.
<http://www.promega.ca/~media/files/resources/promega%20notes/82/in%20vitro%20toxicology%20and%20cellular%20fate%20determination%20using%20promega%20cell-based%20assays.pdf?la=en>.

Experimental Protocols and Characterization Data

General Materials and Methods for Chemical Synthesis

Reagents were purchased from Sigma-Aldrich and used as received or purified from existing stock prior to use. All anhydrous reactions were performed in flame-dried glassware under a positive pressure of dry argon. Air or moisture-sensitive reagents and anhydrous solvents were transferred with oven-dried syringes or cannulae. All flash chromatography was performed with ZEOprep 60 HYD (230-400 mesh) silica gel. All solution phase reactions were monitored using analytical thin layer chromatography (TLC) with 0.2 mm pre-coated silica gel aluminum plates 60 F254 (E. Merck). Components were visualized by illumination with a short-wavelength (254 nm) ultra-violet light and/or staining (ceric ammonium molybdate, potassium permanganate, or Ninhydrin). Alkylamine bases were distilled from calcium hydride directly before use. All solvents used for anhydrous reactions were distilled. tetrahydrofuran, dichloromethane, acetonitrile and toluene were dispensed from a SPBT- Bench Top Solvent Purification System (LC Technology Solutions inc.) and stored under argon. N,Ndimethylformamide (DMF), pyridine and dioxane were purchased from Fisher Scientific and stored over activated 4Å molecular sieves under argon. Solvents were degassed *via* 5 cycles of freeze-pump-thaw or sparging with argon for 1 hour. ¹H (300, 400 or 500 MHz) and ¹³C NMR (75, 100 or 125 MHz) spectra were recorded at ambient temperature (unless otherwise noted) on a Bruker Avance 300, Avance 400, Bruker Avance 500, or Varian Inova 500 spectrometer. Deuterated chloroform (CDCl₃), methanol (CD₃OD), dimethylsulfoxide((CD₃)₂SO), acetone ((CD₃)₂CO), benzene (C₆D₆) and water (D₂O) were used as NMR solvents, unless otherwise stated. Chemical shifts are reported in ppm downfield from trimethylsilane (TMS) or the solvent residual peak as an internal standard. Splitting patterns are designated as follows: s, singlet; d, doublet; t, triplet; q, quartet; quint, quintet; m, multiplet and br, broad. Low resolution mass spectrometry (LRMS) was performed on a Micromass Quatro-LC Electrospray spectrometer with a pump rate of 10 µL/min using electrospray ionization (ESI). Final compounds were purified by HPLC (Varian, PrepStar 218/ProStar 330 DAD) using acetonitrile (Fisher, HPLC grade) and Mili-Q water with 0.1 % trifluoroacetic acid as modifier. Chromatography was performed using reversed phase C18

analytical (Varian, Polaris C18 5 μm 4.16 x 250 mm) and preparative (Varian, Polaris C18 5 μm 21.2 x 250 mm) columns. Compounds were lyophilized using a Labconco FreeZone lyophilizer with 0.1 M aqueous HCl prior to testing in cells.¹

General Peptide Coupling Procedure

A flame dried flask is flushed with argon and fitted with a magnetic stir bar. Amino acid and HCTU are transferred to the flask and suspended in dry DMF to a concentration of 0.1 M; the mixture is left to stir for 45 minutes. In a separate dry flask, the amine coupling partner is dissolved in dry DMF and DIPEA is added. The amine coupling partner is transferred *via* cannula to the initial flask and allowed to stir at room temperature overnight. Solvent is removed under reduced pressure until a thick oil results, which is re-suspended in methylene chloride and allowed to sit for 30 minutes. A white precipitate forms which is removed by filtration and the filtrate is transferred to a separatory funnel. The organic layer was washed with saturated aqueous sodium bicarbonate (3x), Water (1x) and brine (1x). Volatiles are dried with sodium sulfate, filtered and concentrated *in-vacuo* to provide a crude product which is subsequently purified by flash chromatography.

General Boc-deprotection Procedure

The Boc protected amino acid is placed in a round bottom flask with stir bar. Anhydrous methanolic hydrochloric acid (titrated to 5 N) or a 1:1 mixture of trifluoroacetic acid in dichloromethane (run at 0 °C) are added and the mixture is stirred until starting material consumption by TLC. Solvent is removed under a stream of air or by rotary evaporation.

General Methods and Materials for Cell Based Viability Assays

General Cell Culture

MDA-MB-231 cells, from the mammary gland of a human breast, were obtained from the American Type Culture Collection as ATCC number HTB-26. Cells were grown in Eagle's Medium (MEM) containing 10% heat-inactivated fetal bovine serum (FBS) (Fisher, 361015856, supplier number SH30397-3C), 1% penicillin-streptomycin (Sigma, P4333) in 75 cm² T-75 flasks (Fisher,

10-126-37) and maintained at 37°C with 5% CO₂. All cells were removed from the plates using a trypsin-EDTA solution (Sigma, T4174) for use in experiments.

AlamarBlue® Viability Assay

Sterile polycarbonate 96-well flat-bottom culture plates (Costar 3596) were used in the Alamar Blue assay. To minimize edge-related anomalies, only the inner wells of each plate were inoculated with medium containing 10,000 cells/well; the remaining perimeter wells contained 100 µL of media. The plates were placed in a humidity-controlled incubator at 37°C with 5% CO₂ and cells were allowed to adhere over 24 hours. The supernatant was aspirated out carefully and 100 µL solution of the compound as an HCl salt in media containing 0.1M DMSO was added to the appropriate cell. Cells were allowed to incubate with the added compounds for 48 hours before a 30 µL of a 0.01 % resazurin solution was added to each compound-cell containing well. The 96-well plates were incubated as mentioned above for an additional 22 hours. Fluorescence measurements were made on a SpectraMax Absorbance Micro plate reader, set at 560 nm excitation and 590 nm emission. Readings from blank wells with media were subtracted from each test well. Wells containing only 0.01 % resazurin with media served as the positive control, wells containing cells and media without added compounds served as the negative control; cell viability was assessed relative to these controls. All experiments were performed in-triplicate.

Apo-ONE® Homogeneous Caspase-3/7 Assay

Opaque, sterile polycarbonate 96-well flat-bottom culture plates (Corning® Costar® 3596) were used in the Apo-ONE® assay. To minimize edge-related anomalies, only the inner wells of each plate were inoculated with medium containing 10,000 cells/well; the remaining perimeter wells contained 100 µL of media. The plates were placed in a humidity-controlled incubator at 37 °C with 5% CO₂ and cells were allowed to reach confluence over 48 hours. The supernatant was aspirated out carefully and 100 µL solution of the compound in media containing 0.1 M DMSO was added to the appropriate cell; cells were incubated for an additional 48 hours. The substrate/buffer solution was prepared according to the procedure supplied by Promega® and 100 µL was added to each cell-containing well for a final cell volume of 200 µL. The 96-well plate was covered and placed on a plate shaker at ambient temperature, fluorescence measurements

were taken at 4, 8, 12, 24 and 48 hour time points using a SpectraMax Absorbance Micro plate reader, set at 485 nm excitation and 530 nm emission.

Data Plotting and IC₅₀ Calculations

Cell viability data was plotted using GraphPad Prism® v. 6.05 for Windows, GraphPad Software, La Jolla California USA, www.graphpad.com. Non-linear regression was used to obtain a line of best fit from which IC₅₀ data was calculated. Apo-ONE caspase-3/7 activation data was plotted using Microsoft Excel 2013.

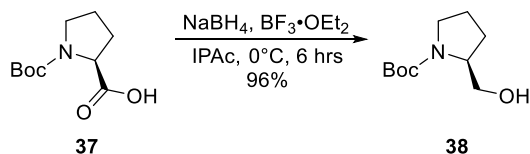
Statistical Analysis

One-way ANOVA with Turkey's post test was performed using GraphPad InStat version 3.10 for Windows, GraphPad Software, San Diego California USA, www.graphpad.com. A 95% confidence interval was applied, compared data sets with P values greater than 0.05 were considered not significantly different while P values below 0.05 were considered more significantly different than expected by chance.

Cryopreservation of Cell line

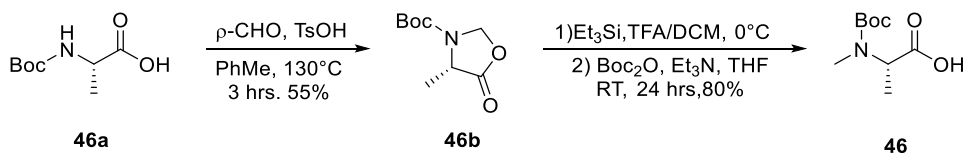
MDA-MB-231 cells, from the mammary gland of a human breast, were cultured and trypsinized as described above. Cells were diluted with MEM and counted using a haemocytometer (VWR, 15170-172). Aliquots containing 5x10⁶ cells were added to 15 mL centrifuge tubes and cells were pelleted by centrifugation for 10 min at 2000 rpm. The supernatant was removed and the cells were re-suspended in 1.5 mL MEM. Cell suspensions were transferred to 2 mL cryogenic vials (VWR, CA16001-102) and placed in a Mr. Frosty|| freezing container (Nalgene, 5100-0001, Sigma, C1562). The container was placed in an ultra-cold freezer (-80 °C) for 24 h. Samples were transferred to a dewar containing liquid nitrogen (-196 °C) for long term storage. To initiate cell culture, samples were rapidly thawed in a 37 °C water bath with gentle agitation. Thawed samples were transferred to 15 mL centrifuge tubes (Diamed, STK3217P) and slowly diluted to 3 mL by drop wise addition of Eagle's MEM (Sigma, M4655) cell culture medium. After 3 min samples were further diluted to 9 mL. Cells were pelleted by centrifugation for 10 min at 2000 rpm. The supernatant was decanted and the pellet re-suspended in 10 mL MEM and transferred to a growth plate.

Experimental Protocols and Characterization Data for Chemical Compounds



tert-butyl (2S)-2-(hydroxymethyl)pyrrolidine-1-carboxylate [38]. **38** was prepared according to the prep by Zhao.² A solution of sodium borohydride (1.7 g, 44.6 mmol, 1.60 equiv.) in isopropyl acetate (100 mL) was cooled to 0 °C in a 250 mL round bottom flask. L-Boc-Pro-OH **37** (6.0 g, 27.9 mmol, 1.00 equiv.) was added to the solution and allowed to stir for 1 hour. A dropping funnel was fitted to the reaction flask and borontrifluoride diethyletherate (7.0 mL, 56.9 mmol, 2.04 equiv.) was added dropwise over 1.5 hours; the mixture was then allowed to stir for an additional 2 hours. The reaction was gradually quenched using 200 mL 0.5 N NaOH over 30 minutes before the mixture was heated to 45 °C and stirred vigorously for 10 min to afford a biphasic solution. The aqueous phase was separated and extracted with 60 mL isopropyl acetate, volatiles were combined and washed with 100 mL saturated aqueous sodium chloride. The organic layer was concentrated azeotropically to afford the alcohol **38** as a clear, colourless oil which was re-crystallized from heptane (5.41 g 26.9 mmol, 96 % yield). Spectral data consistent with previously reported values.³

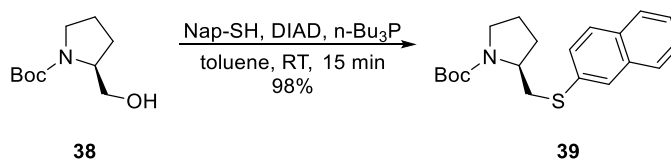
R_f = 0.34 (silica gel, 1:1 ethyl acetate/hexanes); ¹H NMR (500MHz, CDCl₃) δ 3.95 (br, OH), 3.64 (dd, J = 11.0, 3.2 Hz, 1H), 3.58 (dd, J = 11.0, 7.7 Hz, 1H), 3.46 (dt, J = 11.0, 6.8 Hz, 1H), 3.31 (dt, J = 10.7, 6.8 Hz, 1H), 1.97-2.04 (m, 1H), 1.73-1.88 (m, 2H), 1.60 (br, 1H), 1.47 (br, 1H); ¹³C NMR (100 MHz, CDCl₃) δ 156.7, 80.2, 67.3, 60.0, 47.5, 28.8, 28.5, 24.0; ESI-LRMS m/z calcd for C₁₀H₁₉NO₃[M+Na]⁺: 224.1, Found: 224.0.



Tert-butyl (4S)-4-methyl-5-oxo-1,3-oxazolidine-3-carboxylate [46a]. Prepared according to the procedure reported by Paleo.⁴ Boc protected alanine **46a** (12.0 g, 63.4 mmol, 1.00 equiv.) was added to a 1 L round bottom flask and dissolved in 630 mL of toluene. *Para*-formaldehyde (2.47 g, 82.5 mmol, 1.30 equiv.) and *p*-toluenesulfonic acid (0.6 g, 3.17 mmol, 0.05 equiv.) were added while stirring and the flask was fitted with a Dean-Stark trap and condenser. The mixture was heated to 130 °C and allowed to stir for 3 hours, until the production of water ceased. The flask contents were cooled to room temperature and transferred to a separatory funnel. The organic phase was washed with saturated aqueous sodium bicarbonate (3 x 200 mL) and brine (200 mL); the organic layer was dried with sodium sulfate, filtered, and concentrated under reduced pressure to give an oil. The crude product was suspended in heptanes (65 mL) and heated to 40 °C, upon cooling the title compound **46b** crystalized from solution as long, spiny crystals (7.02 g, 35.1 mmol, 55 % yield). Characterization consistent with the reported literature.⁴

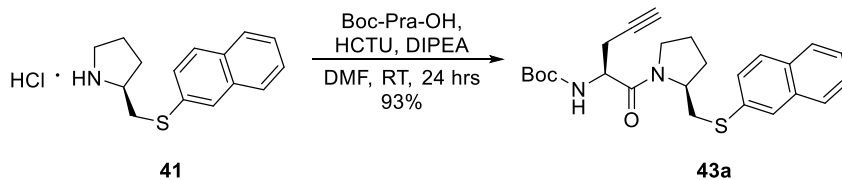
(2S)-2-(((tert-butoxy)carbonyl)(methyl)amino)propanoic acid [46]. Prepared according to the procedure reported by Perrone.⁵ A round bottom flask was charged with **46b** (6.28 g, 31.2 mmol, 1.00 equiv.) and equipped with a stir bar. A 1:1 mixture of TFA/DCM was added at 0 °C followed by slow addition of triethylsilane (15.0 mL, 93.6 mmol, 3.00 equiv.). The mixture was stirred until gas evolution ceased and solvent was removed using a rotary evaporator. The white residue was re-suspended in 100 mL anhydrous THF and triethylamine (9.40 mL, 67.4 mmol, 2.15 equiv.) was added. Boc anhydride (6.84 g, 31.3 mmol, 1.00 equiv.) was dissolved in 50 mL THF and added to a dropping funnel. The reaction mixture was cooled to 0 °C and the Boc anhydride was added dropwise over an hour, followed by overnight stirring at room temperature. The mixture was heated to 50 °C for 3 hours to destroy excess Boc anhydride before solvent was removed *in vacuo*. The remaining residue was suspended in ethyl acetate (200 mL) and extracted with water (2 x 125 mL). The organic layer was dried with sodium sulfate, filtered and concentrated to afford

a crude white solid, the product was recrystallized from *n*-heptane to afford **46** (5.12 g, 25.2 mmol) as spiny white crystals in 80 % yield over 2 steps. Spectra consistent with the reported literature.⁶



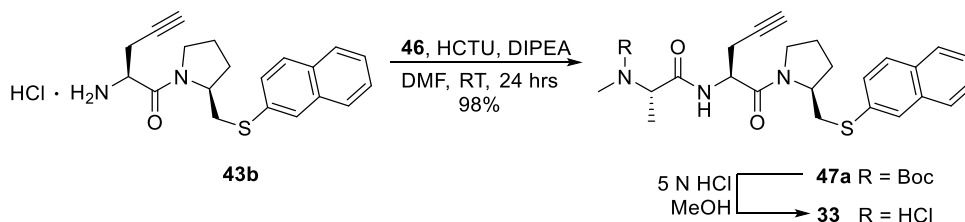
tert-butyl (2S)-2-[(naphthalen-2-ylsulfanyl)methyl]pyrrolidine-1-carboxylate [39]. A flame dried round bottomed flask was charged with 2-naphthalenethiol (2.39 g, 14.9 mmol, 3.00 equiv.) under an atmosphere of argon. Anhydrous toluene (40 mL) was added followed by diisopropyl azidodicarboxylate (2.92 mL, 14.9 mmol, 3.00 equiv.). Tributylphosphine (4.90 mL, 19.9 mmol, 4.00 equiv.) was then added dropwise while stirring resulting in the production of heat; after 10 minutes the initially clear yellow solution became an orange slurry. To this, **38** (1.00 g, 4.97 mmol, 1.00 equiv.) was cannulated which caused the reaction mixture to quickly regain pellucidity. After an additional 5 minutes of stirring the reaction was diluted with diethyl ether and transferred to a separatory funnel. The organic phase was washed with 2 M NaOH (2 x 50 mL) and brine (1 x 75 mL) then dried using sodium sulfate, filtered and concentrated under reduced pressure to afford the crude product as a yellow oil. Purification by flash chromatography (silica gel, gradient 7-15 % ethyl acetate in hexanes) provided the title compound **39** as a colourless oil (1.62 g, 4.72 mmol, 98 % yield). Spectra matched published values.⁷

R_f = 0.5 (silica gel, 15 % ethyl acetate in hexanes); ¹H NMR (CDCl₃, 400 MHz) δ 7.90 (brs, 1H), 7.73-7.79 (m, 3H), 7.49 (dd, *J* = 1.9, 8.6 Hz, 1H), 7.40-7.47 (m, 2H), 4.03 (s, 1H), 3.54 (d, *J* = 12.3 Hz, 1H), 3.38 (m, 2H), 2.85 (dd, *J* = 10.5, 12.4 Hz, 1H), 1.78-2.05 (m, 4H), 1.44 (s, 9H); ¹³C NMR (100 MHz, CDCl₃) δ 154.5, 133.9, 133.8, 131.9, 128.5, 127.8, 127.2, 126.6, 125.7, 79.6, 56.7, 47.0, 37.3, 30.0, 28.7, 23.3; **ESI-LRMS** *m/z* calcd for C₂₀H₂₅NO₂S[M+Na]⁺: 366.1, Found: 366.0.



tert-butyl N-[(2S)-1-[(2S)-2-[(naphthalen-2-ylsulfanyl)methyl]pyrrolidin-1-yl]-1-oxopent-4-yn-2-yl]carbamate [43a]. Refer to general peptide coupling procedure. **Reagents:** L-Boc-Pra-OH (0.457 g, 2.14 mmol, 3.00 equiv.), HCTU (0.887 g, 2.14 mmol, 3.00 equiv.) **41** (0.200 g, 0.715 mmol, 1.00 equiv.), DIPEA (0.250 mL, 1.43 mmol, 2.00 equiv.). Purified via flash chromatography (silica gel, 25 % ethyl acetate in hexanes + 1 % triethylamine) to give the title compound **43a** in 93 % yield (0.292 g, 0.666 mmol).

R_f = 0.31 (silica gel, 25 % ethyl acetate in hexanes + 1 % triethylamine); **$^1\text{H NMR}$** (400 MHz, C_6D_6) δ 8.31 (s, 1H), 7.86 (d, J = 8.2 Hz, 1H), 7.54-7.56 (m, 3H), 7.18 (ddd, J = 1.1, 6.9, 8.1 Hz, 2H), 5.97 (brs, 1H), 4.62 (q, J = 7.1 Hz, 1H), 4.28-4.32 (m, 1H), 3.83 (dd, J = 2.6, 13.8 Hz, 1H), 2.89-3.00 (m, 2H), 2.62 (ddd, J = 2.4, 7.3, 16.6 Hz, 1H), 2.41-2.49 (m, 1H), 2.37 (dd, J = 10.6, 13.9 Hz, 1H), 1.75 (t, J = 2.3 Hz, 1H), 1.55-1.62 (m, 1H), 1.40 (s, 9H), 1.33-1.43 (m, 1H), 1.18-1.29 (m, 1H), 1.03-1.10 (m, 1H); **$^{13}\text{C NMR}$** (100 MHz, C_6D_6) δ 169.3, 155.4, 134.8, 134.4, 131.9, 128.7, 128.0, 127.7, 126.8, 126.4, 125.6, 125.2, 79.6, 79.4, 71.3, 56.2, 51.0, 47.2, 33.8, 28.7, 28.4, 23.7, 23.4; **ESI-LRMS** m/z calcd for $\text{C}_{25}\text{H}_{30}\text{N}_2\text{O}_3[\text{M}+\text{Na}]^+$: 461.2, Found: 461.2.

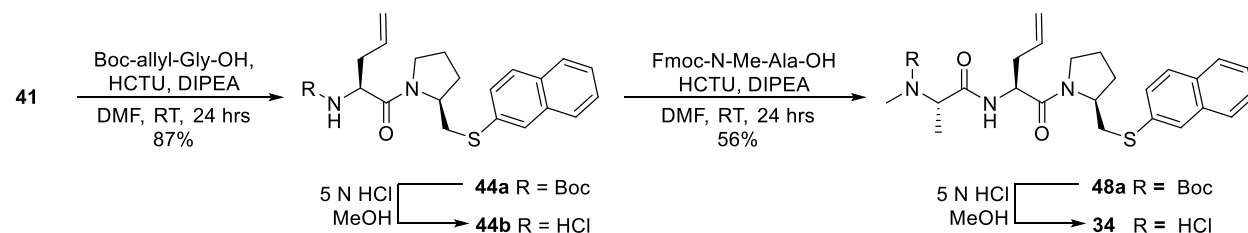


tert-butyl N-methyl-N-[(1S)-1-[(2S)-1-[(2S)-2-[(naphthalen-2-ylsulfanyl)methyl]pyrrolidin-1-yl]-1-oxopent-4-yn-2-yl]carbamoyl]ethyl]carbamate [47a]. Refer to general peptide coupling procedure. **Reagents:** Boc-N-Me-Ala-OH **46** (0.598 g, 2.94 mmol, 3.50 equiv.) HCTU (1.22 g, 2.94 mmol, 3.50 equiv.), **43b** (0.315 g, 0.840 mmol, 1.00 equiv.), DIPEA (0.292 mL, 1.68 mmol, 2.00

equiv.). Purified via flash chromatography (silica gel, 50 % ethyl acetate in hexanes + 2 % triethylamine) to give the title compound **47a** in 98 % yield (0.434 g, 0.829 mmol).

$R_f = 0.69$ (silica gel, 5 % methanol in dichloromethane); $^1\text{H NMR}$ (300 MHz, CDCl_3) δ 7.96 (d, $J = 1.6$ Hz, 1H), 7.73 (d, $J = 8.8$ Hz, 1H), 7.72-7.79 (m, 2H), 7.47 (dd, $J = 1.9, 8.6$ Hz, 1H), 7.35-7.45 (m, 2H), 6.93 (d, $J = 7.0$ Hz, 1H), 4.83 (q, $J = 7.0$, 1H), 4.33-4.40 (m, 2H), 3.68 (dd, $J = 3.0, 13.5$ Hz, 1H), 3.56-3.64 (m, 2H), 2.78 (s, 3H), 2.75 (dd, $J = 9.9, 13.5$ Hz, 1H), 2.56-2.63 (m, 2H), 1.85-2.03 (m, 5H), 1.49 (s, 9H), 1.31 (d, $J = 7.0$ Hz, 3H); $^{13}\text{C NMR}$ (75 MHz, CDCl_3) δ 171.1, 168.6, 156.3, 133.9, 133.4, 131.6, 128.4, 127.7, 127.2, 126.5, 126.4, 125.7, 125.5, 80.7, 78.7, 71.1, 56.9, 49.3, 47.7, 46.0, 34.3, 30.1, 28.8, 28.4, 24.0, 22.8, 13.6; **ESI-LRMS** m/z calcd for $\text{C}_{29}\text{H}_{37}\text{N}_3\text{O}_4[\text{M}+\text{H}]^+$: 524.3, Found: 524.1.

(2S)-2-(methylamino)-N-[(2S)-1-[(2S)-2-[(naphthalen-2-ylsulfanyl)methyl]pyrrolidin-1-yl]-1-oxopent-4-en-2-yl]propanamide hydrochloride [33]. $^1\text{H NMR}$ (500 MHz, d-DMSO) δ 9.01 (d, $J = 8.2$ Hz, 1H), 8.84 (brs, 2H), 8.08 (s, 1H), 7.80-7.88 (m, 3H), 7.44-7.59 (m, 3H), 4.71 (q, $J = 7.1$ Hz, 1H), 4.20 (brs, 1H), 3.86 (brs, 1H), 3.65-3.71 (m, 1H), 3.51-3.56 (m, 2H), 2.96 (s, 1H), 2.84-2.90 (m, 1H), 2.58-2.65 (m, 2H), 2.00-2.08 (m, 1H), 1.84-1.93 (m, 3H), 1.35 (d, $J = 6.8$ Hz, 3H); $^{13}\text{C NMR}$ (75 MHz, d-DMSO) δ 168.5, 167.9, 133.7, 133.5, 131.0, 128.4, 127.7, 126.7, 126.6, 125.9, 125.5, 124.5, 80.0, 73.4, 56.3, 55.9, 50.0, 46.9, 33.0, 30.8, 28.3, 23.4, 21.4, 15.8; **ESI-HRMS** m/z calcd for $\text{C}_{24}\text{H}_{29}\text{N}_3\text{O}_2\text{S}[\text{M}+\text{H}]^+$: 424.2059, Found: 424.2059.



tert-butyl N-[(2S)-1-[(2S)-2-[(naphthalen-2-ylsulfanyl)methyl]pyrrolidin-1-yl]-1-oxopent-4-en-2-yl]carbamate [44a]. See general peptide coupling procedure. **Reagents:** **41** (0.128 g, 0.457 mmol, 1.00 equiv.), Boc-L-allylglycine (0.526 g, 2.44 mmol, 5.34 equiv.), HCTU (1.01 g, 2.44 g, 5.34

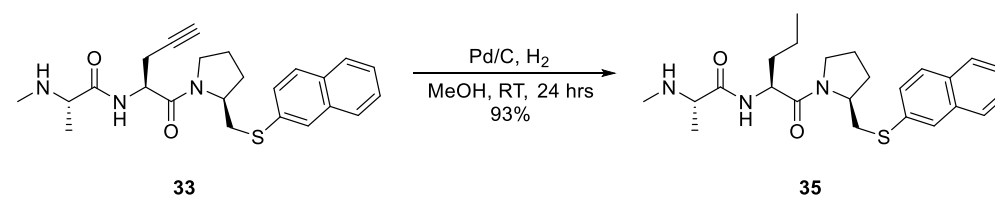
equiv.), DIPEA (0.239 mL, 1.37 mmol, 3.00 equiv.). Purified by flash chromatography (silica gel, 15 % ethyl acetate in hexanes + 1 % AcOH) to give **44a** (0.175 g, 0.397 mmol, 87% yield).

R_f = 0.3 (silica gel, 15 % ethyl acetate in hexanes + 1 % acetic acid); $^1\text{H NMR}$ (500 MHz, CDCl_3) δ 7.95 (s, 1H), 7.79 (d, J = 8.4 Hz, 1H), 7.76 (d, J = 8.6 Hz, 1H), 7.49 (dd, J = 1.8, 8.6 Hz, 1H), 7.45 (ddd, J = 8.1, 6.9, 1.2 Hz, 2H), 5.76 (dddd, J = 7.2, 10.1, 12.2, 16.9 Hz, 1H), 5.40 (d, J = 8.5 Hz, 1H), 4.72 (q, J = 7.1 Hz, 1H), 4.37-4.42 (m, 1H), 3.51-3.68 (m, 3H), 2.81 (dd, J = 9.7, 13.5 Hz, 1H), 2.45 (dt, J = 6.8, 13.9 Hz, 1H), 2.33 (dt, J = 7.0, 13.9 Hz, 1H), 1.88-2.09 (m, 4H), 1.42 (s, 9H); $^{13}\text{C NMR}$ (125 MHz, CDCl_3) δ 170.6, 155.4, 134.0, 133.5, 132.8, 131.6, 128.5, 127.7, 127.3, 126.6, 126.5, 125.9, 125.6, 118.8, 79.7, 56.8, 51.7, 47.6, 46.0, 37.6, 34.7, 28.8, 28.4, 24.2, 21.4; **ESI-LRMS** m/z calcd for $\text{C}_{25}\text{H}_{32}\text{N}_2\text{O}_3\text{S}[\text{M}+\text{K}]^+$: 479.1, Found: 479.1.

(9H-fluoren-9-yl)methylN-methyl-N-[(1S)-1-[(2S)-1-[(2S)-2-[(naphthalen-2-ylsulfanyl)methyl]pyrrolidin-1-yl]-1-oxopent-4-en-2-yl]carbamoyl]ethyl]carbamate [48a]. See general peptide coupling procedure. **Reagents:** **44b** (0.175 g, 0.464 mmol, 1.00 equiv.), Fmoc-N-Me-Ala-OH (0.755 g, 2.32 mmol, 5.00 equiv.), HCTU (0.961 g, 2.32 mmol, 5.00 equiv.), DIPEA (0.243 mL, 1.39 mmol, 2.00 equiv.). Purified by flash chromatography (silica gel, 1:1 ether/hexanes + 2 % acetic acid) to give **48a** (0.167 g, 0.258 mmol, 58 % yield).

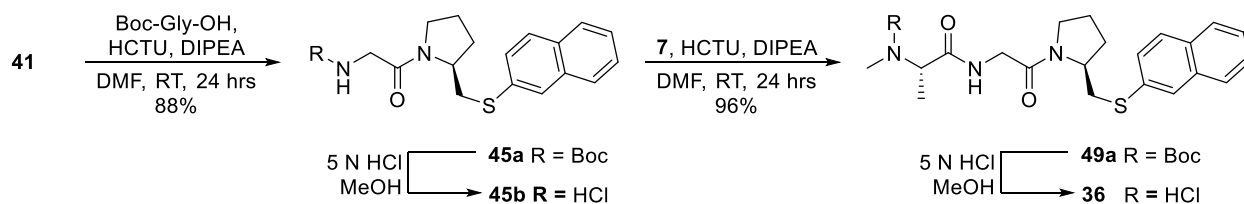
R_f = 0.37 (silica gel, 60 % ethyl acetate in hexanes + 1 % acetic acid); $^1\text{H NMR}$ (500 MHz, CDCl_3) δ 7.02-7.93 (m, 17H), 5.70 (dddd, J = 7.2, 8.6, 10.1, 17.1 Hz, 1H), 4.68-5.08 (m, 4H), 4.38-4.47 (m, 2H), 4.28 (t, J = 7.0 Hz, 1H), 3.54-3.83 (m, 3H), 2.86 (s, 3H), 2.47 (dt, J = 7.0, 14.1 Hz, 1H), 2.32-2.37 (m, 2H), 1.90-2.06 (m, 5H), 1.34 (d, J = 7.1 Hz, 3H); $^{13}\text{C NMR}$ (125 MHz, CDCl_3) δ 175.4, 170.2, 144.0, 141.4, 138.0, 134.0, 131.7, 129.1, 128.6, 128.3, 127.8, 127.7, 127.3, 127.2, 127.1, 126.6, 126.5, 125.9, 125.6, 125.4, 125.1, 120.1, 68.0, 57.0, 50.4, 47.8, 47.4, 37.0, 34.7, 28.8, 24.2, 21.6, 20.8.

(2S)-2-(methylamino)-N-[(2S)-1-[(2S)-2-[(naphthalen-2-ylsulfanyl)methyl]pyrrolidin-1-yl]-1-oxopent-4-en-2-yl]propanamide hydrochloride [34]. $^1\text{H NMR}$ (400 MHz, d-DMSO) δ 8.78-8.94 (m, 3H), 8.07 (s, 1H), 7.79-7.91 (m, 3H), 7.43-7.51 (m, 3H), 5.79 (dddd, $J = 7.2, 8.8, 10.3, 17.1$ Hz, 1H), 5.12 (dd, $J = 1.3, 17.1$ Hz, 1H), 5.07 (dd, $J = 1.2, 10.3$ Hz, 1H), 4.19-4.61 (m, 2H), 3.82-3.87 (m, 2H), 2.94 (dd, $J = 10.0, 13.5$ Hz, 1H), 1.82-2.35 (m, 5H), 1.35 (d, $J = 7.0$ Hz, 3H); $^{13}\text{C NMR}$ (75 MHz, d-DMSO) δ 169.1, 168.4, 133.8, 133.6, 133.6, 131.0, 128.4, 127.7, 126.8, 126.7, 126.0, 125.6, 124.5, 118.3, 56.2, 56.0, 50.8, 46.9, 35.7, 33.3, 30.8, 28.4, 23.6, 15.8; **ESI-HRMS** m/z calcd for $\text{C}_{24}\text{H}_{31}\text{N}_3\text{O}_2\text{S}[\text{M}+\text{H}]^+$: 426.2215, Found: 426.2209.



(2S)-2-(methylamino)-N-[(2S)-1-[(2S)-2-[(naphthalen-2-ylsulfanyl)methyl]pyrrolidin-1-yl]-1-oxopentan-2-yl]propanamide hydrochloride [35]. Alkyne **33** (0.0136 g, 0.0296 mmol, 1.00 equiv.) was added to a round bottom flask in methanol (0.1 M). Palladium on activated carbon (0.0015 g, 10 %/wt) was added before the flask was sealed and fitted with a balloon containing hydrogen. After stirring at room temperature overnight the reaction mixture was filtered through a pad of celite to give **35** in 93 % yield (0.0127 g, 0.0275 mmol).

$^1\text{H NMR}$ (500 MHz, d-DMSO) δ 8.54-8.63 (m, 3H), 8.03 (s, 1H), 7.08-7.87 (m, 3H), 7.58-7.72 (m, 1H), 7.45-7.50 (m, 2H), 4.51-4.52 (m, 1H), 4.23 (brs, 1H), 3.82 (q, $J = 6.9$ Hz, 1H), 3.62 (dd, $J = 8.8, 16.6$ Hz, 1H), 3.53-3.57 (m, 1H), 3.47 (dd, $J = 2.0, 13.4$ Hz, 1H), 3.03-3.08 (m, 1H), 2.55 (s, 3H), 1.84-2.12 (m, 4H), 1.53-1.62 (m, 2H), 1.36 (d, $J = 6.9$ Hz, 3H), 1.20-1.34 (m, 3H), 0.87 (t, $J = 7.2$ Hz, 3H); $^{13}\text{C NMR}$ (125 MHz, d-DMSO) δ 170.0, 157.7, 133.9, 133.5, 131.0, 128.4, 127.7, 126.8, 126.7, 126.0, 125.5, 124.5, 56.2, 56.0, 50.8, 46.9, 33.5, 33.3, 30.8, 28.3, 23.7, 18.5, 15.7, 13.6; **ESI-HRMS** m/z calcd for $\text{C}_{24}\text{H}_{33}\text{N}_3\text{O}_2\text{S}[\text{M}+\text{H}]^+$: 428.2372, Found: 428.2374.



tert-butyl-N-{2-[(2S)-2-[(naphthalen-2-ylsulfanyl)methyl]pyrrolidin-1-yl]-2-

oxoethyl}carbamate [45a]. See general peptide coupling procedure. **Reagents:** Boc-L-glycine (0.576 g, 3.29 mmol, 4.00 equiv.), HCTU was added (1.36 g, 3.29 mmol, 4.00 equiv.), **41** (0.200 g, 0.822 mmol, 1.00 equiv.), DIPEA (0.286 mL, 1.64 mmol, 2.00 equiv.). Flash chromatography (silica gel, 35% ethyl acetate in hexanes + 1% triethylamine) yielded the coupling product **45a** as a colourless crystalline solid (0.289 g, 0.722 mmol, 88 % yield).

$R_f = 0.42$ (silica gel, 40 % ethyl acetate in hexanes +1 % triethylamine); $^1\text{H NMR}$ (500 MHz, C_6D_6) δ 8.19 (s, 1H), 7.79 (d, $J = 8.1$ Hz, 1H), 7.51-7.56 (m, 3H), 7.18-7.26 (m, 2H), 5.63 (s, 1H), 4.20 (t, $J = 8.6$ Hz, 1H), 3.59 (dd, $J = 2.0, 13.6$ Hz, 1H), 3.46-3.56 (m, 2H), 2.51-2.56 (m, 2H), 2.40 (q, $J = 8.3$ Hz, 1H), 1.60-1.64 (m, 1H), 1.48 (s, 9H), 1.27-1.42 (m, 2H), 1.08-1.11 (m, 1H); $^{13}\text{C NMR}$ (75 MHz, C_6D_6) δ 167.2, 156.0, 134.8, 134.3, 131.9, 128.7, 128.6, 127.7, 126.9, 126.3, 125.6, 125.1, 79.1, 56.7, 45.4, 43.6, 33.6, 28.5, 28.4, 23.3; **ESI-LRMS** m/z calcd for $\text{C}_{22}\text{H}_{28}\text{N}_2\text{O}_3\text{S}[\text{M}+\text{Na}]^+$: 423.2, Found: 423.2.

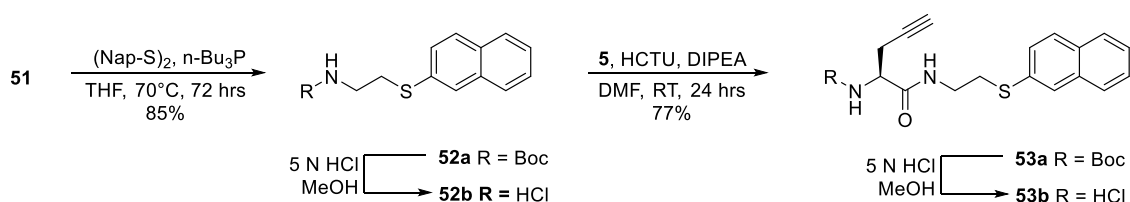
tert-butyl N-methyl-N-[(1S)-1-({2-[(2S)-2-[(naphthalen-2-ylsulfanyl)methyl]pyrrolidin-1-yl]-2-

oxoethyl}carbamoyl)ethyl}carbamate [49a]. Refer to general peptide coupling protocol. **Reagents:** **15b** (0.142 g, 0.422 mmol, 1.00 equiv.), **45b** (0.300 g, 1.48 mmol, 3.50 equiv.), HCTU (0.610 g, 1.48 mmol, 3.50 equiv.), DIPEA (0.147 mL, 0.843 mmol, 2.00 equiv.). Purified *via* flash chromatography (silica gel, 50 % ethyl acetate in hexanes + 2 % triethylamine) to give **49a** (0.197 g, 0.406 mmol, 96 % yield).

$R_f = 0.57$ (silica gel, 4 % methanol in dichloromethane); $^1\text{H NMR}$ (400 MHz, CDCl_3) δ 7.98 (d, $J = 1.1$ Hz, 1H), 7.72-7.79 (m, 3H), 7.38-7.49 (m, 3H), 6.90 (brs, 1H), 4.58-4.83 (brs, 1H), 4.38 (dd, $J = 7.2, 9.2$ Hz, 2H), 3.75-3.92 (m, 2H), 3.62 (d, $J = 9.2$ Hz, 1H), 3.59 (dd, $J = 2.0, 15.7$ Hz, 1H), 3.32-3.47 (m, 2H), 2.93 (dd, $J = 9.4, 13.6$ Hz, 1H), 2.81 (s, 3H), 1.92-2.10 (m, 5H), 1.51 (s, 9H), 1.35 (d, J

= 7.2 Hz, 3H); ^{13}C NMR (100 MHz, C_6D_6) δ 171.6, 166.9, 156.6, 134.8, 134.3, 132.0, 128.8, 128.6, 127.6, 126.9, 126.4, 125.6, 125.3, 80.2, 72.8, 61.9, 56.8, 45.6, 42.5, 33.7, 30.1, 28.5, 28.5, 23.4, 14.2; ESI-LRMS m/z calcd for $\text{C}_{26}\text{H}_{35}\text{N}_3\text{O}_4\text{S}[\text{M}+\text{Na}]^+$: 508.2 Found: 508.0.

(2S)-2-(methylamino)-N-{2-[(2S)-2-[(naphthalen-2-ylsulfanyl)methyl]pyrrolidin-1-yl]-2-oxoethyl}propanamide hydrochloride [36]. (Characterized as the free amine) ^1H NMR (500 MHz, d-DMSO) δ 8.12 (d, $J = 1.7$ Hz, 1H), 7.98 (t, $J = 5.0$ Hz, 1H), 7.80-7.87 (m, 3H), 7.47-7.51 (m, 2H), 7.44 (ddd, $J = 1.3, 6.9, 7.7$ Hz, 1H), 4.18-4.20 (m, 1H), 3.95 (dd, $J = 5.6, 17.2$ Hz, 1H), 3.76 (dd, $J = 4.9, 17.3$ Hz, 1H), 3.48-3.52 (m, 2H), 3.40-3.43 (m, 1H), 2.93-2.99 (m, 2H), 2.27 (s, 3H), 1.86-2.07 (m, 5H), 1.14 (d, $J = 7.0$ Hz, 3H); ^{13}C NMR (125 MHz, d-DMSO) δ 174.7, 167.4, 133.9, 133.6, 130.9, 128.3, 127.6, 126.7, 126.6, 125.8, 125.4, 124.4, 59.5, 56.3, 45.7, 41.1, 34.5, 33.1, 28.2, 23.2, 19.1; ESI-LRMS m/z calcd for $\text{C}_{21}\text{H}_{27}\text{N}_3\text{O}_2\text{S}[\text{M}+\text{H}]^+$: 386.2 Found: 386.0.

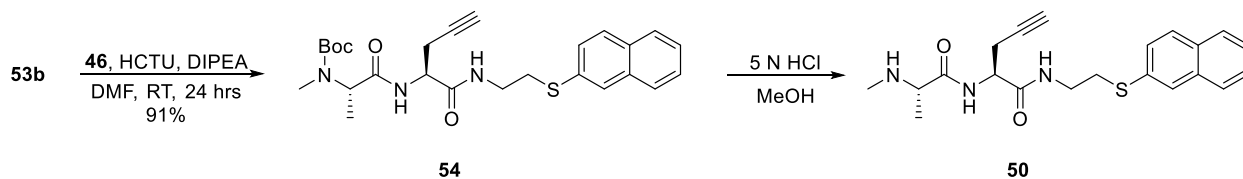


tert-butyl N-[2-(naphthalen-2-ylsulfanyl)ethyl]carbamate [52a]. **52a** was prepared according to a modified procedure by Skarzewski.⁸ An oven dried thick walled glass tube was charged with N-Boc-ethanolamine **51** (0.202 g, 1.25 mmol, 1.00 equiv.), 2-naphthyl disulfide (1.20 g, 3.76 mmol, 3.00 equiv.) and anhydrous THF (7.5 mL). Freshly distilled n-tributylphosphine (1.23 mL, 5.01 mmol, 4.00 equiv.) was added before the tube was sealed and heated to 70°C while stirring for 3 days. The reaction mixture was diluted with diethyl ether, transferred to a separatory funnel and washed with 2 N NaOH (2 x 20 mL) and brine. The organic phase was dried with sodium sulfate, filtered and solvent was removed prior to flash chromatography (silica gel, 10 % ethyl acetate in hexanes). The product **52a** was isolated in 85 % yield as a colourless oil (0.325 g, 1.07 mmol).

R_f = 0.55 (silica gel, 20 % ethyl acetate in hexanes); $^1\text{H NMR}$ (400 MHz, CDCl_3) δ 7.82 (d, J = 1.0 Hz, 1H), 7.78 (d, J = 7.9 Hz, 1H), 7.75 (d, J = 8.2 Hz, 1H), 7.42-7.49 (m, 3H), 5.02 (s, 1H), 3.38 (m, 2H), 3.13 (t, J = 6.5 Hz, 2H), 1.44 (s, 9H); $^{13}\text{C NMR}$ (100 MHz, CDCl_3) δ 155.8, 133.8, 132.7, 131.9, 128.7, 127.7, 127.6, 127.2, 126.7, 125.9, 79.5, 39.8, 34.0, 28.4; **ESI-LRMS** m/z calcd for $\text{C}_{17}\text{H}_{21}\text{NO}_2\text{S}[\text{M}+\text{Na}]^+$: 302.1, Found: 302.0.

tert-butyl N-[(1S)-1-[[2-(naphthalen-2-ylsulfanyl)ethyl]carbamoyl]but-3-yn-1-yl]carbamate [53a]. Refer to general peptide coupling protocol. **Reagents:** **52b** (0.258 g, 1.26 mmol, 1.00 equiv.), Boc-L-Propargylglycine (0.808 g, 3.79 mmol, 3.00 equiv.), HCTU (1.57 g, 3.79 mmol, 3.00 equiv.), DIPEA (0.440 mL, 2.53 mmol, 2.00 equiv.). Purified by flash chromatography (silica gel, 30 % ethyl acetate in hexanes + 3% triethylamine), isolated **53a** in 77 % yield as a colourless solid (0.389 g, 0.977 mmol).

R_f = 0.41 (silica gel, 30 % ethyl acetate in hexanes + 1 % AcOH); $^1\text{H NMR}$ (400 MHz, CDCl_3) δ 7.83 (d, J = 1.5 Hz, 1H), 7.75-7.80 (m, 3H), 7.43-7.50 (m, 3H), 6.76 (m, 1H), 5.26 (brs, 1H), 4.27 (d, J = 2.9 Hz, 1H), 3.50-3.55 (m, 2H), 3.15 (t, J = 3.5 Hz, 2H), 2.77 (ddd, J = 2.6, 5.4, 16.9 Hz, 1H), 2.58 (ddd, J = 2.6, 6.7, 16.9 Hz, 1H), 2.05 (t, J = 2.6 Hz, 1H), 1.46 (s, 9H); $^{13}\text{C NMR}$ (100 MHz, CDCl_3) δ 170.4, 155.5, 133.8, 132.3, 132.1, 128.8, 128.2, 127.8, 127.7, 127.3, 126.8, 126.1, 80.7, 79.5, 71.8, 53.0, 38.7, 33.5, 28.4, 22.6; **ESI-LRMS** m/z calcd for $\text{C}_{22}\text{H}_{25}\text{N}_2\text{O}_3\text{S}[\text{M}+\text{H}]^+$: 397.2, Found: 397.1.

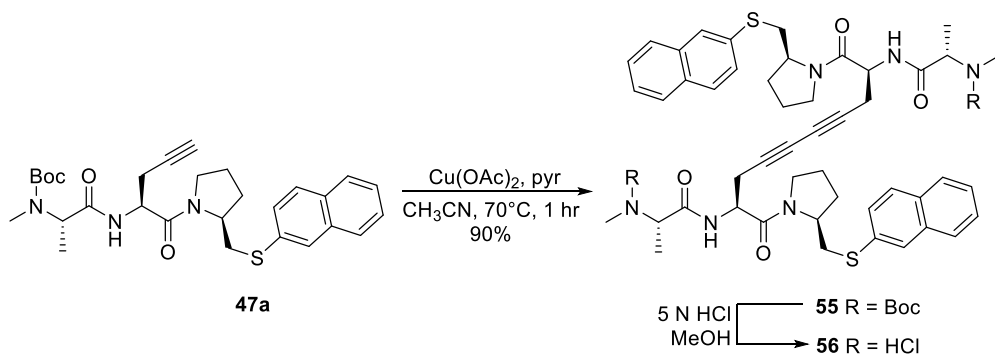


tert-butylN-methyl-N-[(1S)-1-[[[(1S)-1-[[2-(naphthalen-2-ylsulfanyl)ethyl]carbamoyl]but-3-yn-1-yl]carbamoyl]ethyl]carbamate [54]. Refer to general peptide coupling protocol. **Reagents:** **53b** (0.255 g, 0.762 mmol, 1.00 equiv.), **46** (0.619 g, 3.05 mmol, 4.00 equiv.), HCTU (1.26 g, 3.05 mmol, 4.00 equiv.), DIPEA (0.270 mL, 1.52 mmol, 2.00 equiv.). Column chromatography (silica gel, 40 %

ethyl acetate in hexanes + 1 % triethylamine) gave the title compound **54** (0.335 g, 0.693 mmol, 91 % yield).

R_f = 0.25 (silica gel, 40 % ethyl acetate in hexanes + 1 % triethylamine); $^1\text{H NMR}$ (500MHz, $(\text{CD}_3)_2\text{CO}$) δ 7.95 (d, J = 0.8 Hz, 1H), 7.85 (t, J = 8.1 Hz, 2H), 7.75 (brs, 2H), 7.44-7.52 (m, 3H), 7.30-7.32 (m, 1H), 4.66 (brs, 1H), 4.53-4.54 (m, 1H), 3.47-3.51 (m, 2H), 3.18-3.21 (m, 2H), 2.74 (ddd, J = 2.7, 5.7, 17.0 Hz, 1H), 2.73 (s, 3H), 2.67 (ddd, J = 2.7, 6.9, 17.0 Hz, 1H), 2.45 (t, J = 2.7 Hz, 1H), 1.46 (s, 9H), 1.30 (d, J = 7.0 Hz, 3H); $^{13}\text{C NMR}$ (75 MHz, $(\text{CD}_3)_2\text{CO}$) δ 172.1, 170.8, 156.5, 135.0, 134.4, 132.7, 129.4, 128.6, 128.0, 127.9, 127.5, 127.1, 126.6, 80.8, 80.5, 72.4, 55.3, 52.6, 39.7, 38.8, 32.7, 38.6, 22.7, 14.3; **ESI-LRMS** m/z calcd for $\text{C}_{26}\text{H}_{33}\text{N}_3\text{O}_4\text{S}[\text{M}+\text{Na}]^+$: 506.2, Found: 506.2.

(2S)-2-[(2S)-2-(methylamino)propanamido]-N-[2-(naphthalen-2-ylsulfanyl)ethyl]pent-4-ynamide hydrochloride [50]. $^1\text{H NMR}$ (400 MHz, d-DMSO) δ 9.18 (brs, 2H), 9.00 (d, J = 8.2 Hz, 1H), 8.58 (t, J = 5.8 Hz, 1H), 7.84-7.92 (m, 4H), 7.44-7.53 (m, 3H), 4.45 (ddd, J = 5.3, 8.1, 8.1 Hz, 1H), 3.83 (q, J = 6.9 Hz, 1H), 3.26-3.40 (m, 2H), 3.11-3.16 (m, 2H), 2.92 (t, J = 2.6 Hz, 1H), 2.63 (ddd, J = 2.6, 5.7, 16.9 Hz, 1H), 2.55 (ddd, J = 2.6, 8.2, 16.8 Hz, 1H), 2.46 (s, 3H), 1.39 (d, J = 6.9 Hz, 3H); $^{13}\text{C NMR}$ (100 MHz, d-DMSO) δ 169.2, 168.5, 133.5, 133.3, 131.1, 128.4, 127.6, 126.9, 126.7, 126.5, 125.6, 125.2, 80.4, 73.2, 56.1, 51.9, 38.2, 31.1, 30.7, 22.0, 15.8; **ESI-HRMS** m/z calcd for $\text{C}_{21}\text{H}_{26}\text{N}_3\text{O}_2\text{S}[\text{M}+\text{H}]^+$: 384.1746, Found: 384.1736.



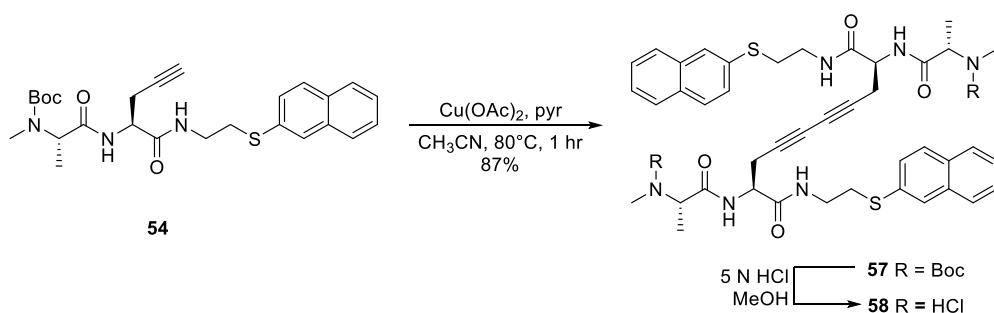
tert-butyl N-[(1S)-1-[[[(2S,9S)-9-[(2S)-2-[[[(tert-butoxy)carbonyl](methyl)amino]propanamido]-1,10-bis[(2S)-2-[(naphthalen-2-ylsulfanyl)methyl]pyrrolidin-1-yl]-1,10-dioxodeca-4,6-diyn-2-

yl]carbamoyl]ethyl]-N-methylcarbamate [55]. **55** was prepared using a modified version of the procedure described by Hennessy.⁹ Tripeptide **47a** (0.230 g, 0.439 mmol, 1.00 equiv.) was dissolved in 10 mL of acetonitrile in a 50 mL round bottom flask fitted with a condenser. Copper(II)acetate (0.614 g, 3.07 mmol, 7.00 equiv.) was added and the mixture was stirred at 70 °C for 1 hour. The acetonitrile was stripped off and the resulting green solid was re-suspended in ethyl acetate and transferred to a separatory funnel with 10 % aqueous ammonium hydroxide (100 mL). The organic layer was collected and the aqueous phase was extracted with ethyl acetate (3 x 50 mL) until the extracts were clear. The combined organic phases were washed with water (100 mL) and saturated aqueous sodium chloride (75 mL) then dried using sodium sulfate, filtered and concentrated *in-vacuo* to yield a solid yellow residue. Purification through a plug of silica (silica gel, 10 % methanol in dichloromethane) gave the bis-alkyne product **55** (0.207 g, 0.198 mmol) in 90 % yield.

$R_f = 0.43$ (silica gel, 4 % methanol in dichloromethane); $^1\text{H NMR}$ (500 MHz, C_6D_6) δ 8.19 (s, 1H), 7.81 (d, 8.1 Hz, 1H), 7.52-7.66 (m, 3H), 7.30 (dd, $J = 7.5, 7.5$ Hz, 1H), 7.20 (dd, $J = 7.5, 7.5$ Hz, 1H), 4.77 (dd, $J = 6.5, 13.3$ Hz, 1H), 4.66-4.84 (m, 1H), 4.28-4.32 (m, 1H), 3.77 (dd, $J = 2.7, 13.6$ Hz, 1H), 2.86-3.00 (m, 2H), 2.83 (s, 3H), 2.71 (dd, $J = 10.1, 13.4$ Hz, 1H), 2.65 (dd, $J = 6.7, 17.0$ Hz, 1H), 2.47 (dd, $J = 5.3, 17.0$ Hz, 1H), 1.64-1.70 (m, 1H), 1.52 (s, 9H), 1.41-1.50 (m, 3H), 1.26 (d, $J = 7.2$ Hz, 3H), 1.12-1.18 (m, 1H).

(2S)-2-(methylamino)-N-[(2S,9S)-9-[(2S)-2-(methylamino)propanamido]-1,10-bis[(2S)-2-[(naphthalen-2-ylsulfanyl)methyl]pyrrolidin-1-yl]-1,10-dioxodeca-4,6-diyne-2-yl]propanamide dihydrochloride [56].

$^1\text{H NMR}$ (300 MHz, d-DMSO) δ 9.09 (d, $J = 7.9$ Hz, 1H), 8.88 (brs, 2H), 8.07 (d $J = 1.6$ Hz, 1H), 7.79-7.88 (m, 3H), 7.42-7.56 (m, 3H), 4.66-4.74 (m, 1H), 4.16-4.24 (m, 1H), 3.32-3.85 (m, 7H), 2.61-2.89 (m, 3H), 1.75-2.04 (m, 4H), 1.35 (d $J = 6.9$ Hz, 3H); $^{13}\text{C NMR}$ (75 MHz, d-DMSO) δ 168.5, 167.5, 133.7, 133.5, 131.0, 128.4, 127.7, 126.7, 126.7, 125.9, 125.5, 124.4, 74.4, 66.5, 56.3, 56.0, 49.8, 46.9, 33.0, 30.8, 28.3, 23.4, 22.0, 15.8; **ESI-LRMS** m/z calcd for $\text{C}_{48}\text{H}_{56}\text{N}_6\text{O}_4\text{S}_2[\text{M}+\text{H}]^+$: 845.4, Found: 845.0.

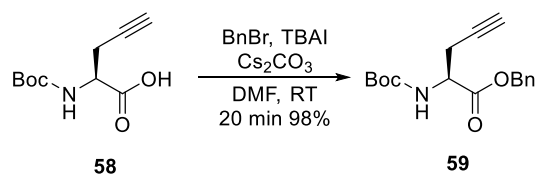


tert-butyl N-[(1S)-1-[[[(1S,8S)-8-[(2S)-2-[[[(tert-butoxy)carbonyl](methylamino)propanamido]-1,8-bis[[2-(naphthalen-2-ylsulfanyl)ethyl]carbamoyl]octa-3,5-diyne-1-yl]carbamoyl]ethyl]-N-methylcarbamate [57]. Compound **57** was prepared in accordance with the general procedure reported by Hennessey.⁹ A round bottom flask was equipped with a stir bar and charged with alkyne **54** (0.150 g, 0.310 mmol, 1.00 equiv.) dissolved in acetonitrile (2 mL). Copper(II) acetate (0.072 g, 0.360 mmol, 1.15 equiv.) and pyridine (0.150 mL, 1.86 mmol, 6.00 equiv.) were added and the reaction was allowed to stir at 80 °C overnight. The flask contents were transferred to a separatory funnel, diluted with ethyl acetate (60 mL) and washed with a 40 mL volume of 50 % aqueous ammonium hydroxide. The aqueous phase was back-extracted with ethyl acetate (2 x 25 mL) and the combined organic extracts were dried with sodium sulfate, filtered and concentrated *in vacuo*. Flash chromatography (silica gel, 30→60 % acetone in toluene) of the crude product gave **57** (0.131 g, 0.135 mmol, 87 % yield).

R_f = 0.32 (silica gel, 60 % ethyl acetate in hexanes + 1% triethylamine); **¹H NMR** (400 MHz, d-DMSO) δ 8.28 (brs, 1H), 7.94 (brs, 1H), 7.81-7.89 (m, 4H), 7.51 (ddd, J = 1.3, 6.8, 8.0 Hz, 1H), 7.44-7.48 (m, 2H), 4.43-4.61 (m, 1H), 4.37 (dd, J = 7.4, 13.3 Hz, 1H), 3.28-3.36 (m, 2H), 3.10 (t, J = 7.1 Hz, 2H), 2.71-2.75 (m, 4H), 2.63 (dd, J = 7.9, 17.1 Hz, 1H), 1.38 (s, 9H), 1.21 (brs, 3H); **¹³C NMR** (100 MHz, d-DMSO) δ 177.1, 170.0, 155.7, 133.9, 133.7, 131.6, 128.9, 128.1, 127.3, 127.2, 127.0, 126.1, 125.8, 79.6, 75.1, 67.1, 58.7, 51.7, 38.8, 31.7, 30.5, 28.5, 22.9, 15.6; **ESI-LRMS** m/z calcd for $C_{52}H_{64}N_6O_8S_2[M+K]^+$: 1003.4, Found: 1003.4.

(2S,9S)-2,9-bis[(2S)-2-(methylamino)propanamido]-N,N'-bis[2-(naphthalen-2-ylsulfanyl)ethyl]deca-4,6-diyne diamide dihydrochloride [58]. **¹H NMR** (500 MHz, d-DMSO) δ

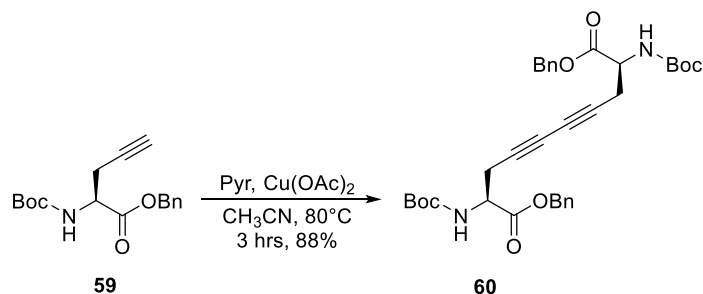
9.01 (d, $J = 7.8$ Hz, 1H), 8.73-9.20 (brs, 2H), 8.55 (t, $J = 5.4$ Hz, 1H), 7.82-7.89 (m, 4H), 7.44-7.53 (m, 3H), 4.67 (q, $J = 7.2$ Hz, 1H), 3.81 (q, $J = 6.5$ Hz, 1H), 3.13 (t, $J = 6.9$ Hz, 1H), 2.76 (dd, $J = 5.2, 17.2$ Hz, 1H), 2.67 (dd, $J = 8.2, 17.2$ Hz, 1H), 2.47 (s, 3H), 1.37 (d, $J = 6.8$ Hz, 3H); $^{13}\text{C NMR}$ (100 MHz, d-DMSO) δ 168.9, 168.6, 133.5, 133.3, 131.1, 128.5, 127.7, 126.9, 126.8, 126.5, 125.7, 125.3, 74.5, 66.7, 56.1, 51.4, 38.2, 31.2, 30.8, 22.7, 15.8; **ESI-LRMS** m/z calcd for $\text{C}_{42}\text{H}_{48}\text{N}_6\text{O}_4\text{S}_2[\text{M}+\text{H}]^+$: 765.3, Found: 765.0.



benzyl (2S)-2-(((tert-butoxy)carbonyl)amino)pent-4-ynoate [59]. A flame dried flask fitted with a stir bar was charged with L-Boc-Pra-OH **58** (0.100 g, 0.469 mmol, 1.00 equiv.), Cesium carbonate (0.168 g, 0.516 mmol, 1.10 equiv.) and tetrabutylammonium iodide (0.017 g, 0.0469 mmol, 0.10 equiv.). The flask contents were dried under vacuum before being dissolved in anhydrous DMF (3 mL). Freshly distilled benzyl bromide (0.110 mL, 0.938 mmol, 2.00 equiv.) was added *via* syringe and the mixture was stirred at room temperature until complete by TLC (silica gel, 20 % ethyl acetate in hexanes). The reaction was poured into a separatory funnel containing 30 mL saturated aqueous sodium bicarbonate and extracted with diethyl ether (50 mL). The organic layer was washed with water (4 x 25 mL), brine (30 mL), dried with sodium sulfate, filtered and concentrated under reduced pressure. The resulting colourless oil was pure enough to carry over to the next step, purification *via* flash chromatography was performed for characterization purposes (silica gel, 20 % ethyl acetate in hexanes) to provide the title compound **59** in 98 % yield (0.140 g, 0.462 mmol). Spectral data was consistent with the reported literature.¹⁰

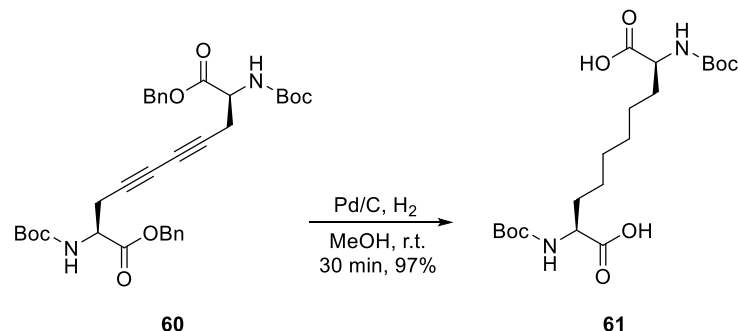
$R_f = 0.33$ (silica gel, 20 % ethyl acetate in hexanes); $^1\text{H NMR}$ (400 MHz, CDCl_3) δ 7.35 (s, 5H), 5.40 (d, $J = 8.2$ Hz, 1H), 5.22 (d, $J = 12.2$ Hz, 1H), 5.17 (d, $J = 12.2$ Hz, 1H), 4.51 (ddd, $J = 4.2, 4.6, 8.2$ Hz, 1H), 2.75 (ddd, $J = 2.3, 4.2, 16.8$ Hz, 1H), 2.72 (ddd, $J = 2.3, 4.6, 16.8$ Hz, 1H), 2.01 (t, $J = 2.3$ Hz,

1H), 1.44 (s, 9H); $^{13}\text{C NMR}$ (100 MHz, CDCl_3) δ 170.6, 155.1, 135.3, 128.6, 128.5, 128.3, 80.1, 78.6, 71.8, 67.4, 52.1, 28.3, 22.8; **ESI-LRMS** m/z calcd for $\text{C}_{17}\text{H}_{21}\text{NO}_4[\text{M}+\text{Na}]^+$: 326.1, Found: 326.0.



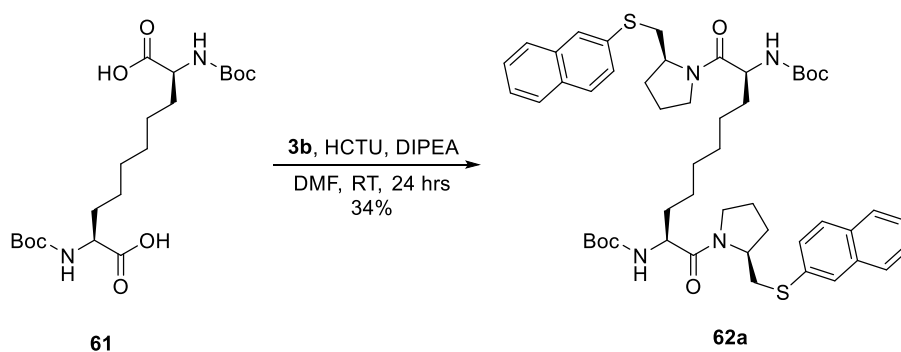
1,10-dibenzyl (2S,9S)-2,9-bis({[(tert-butoxy)carbonyl]amino})deca-4,6-diynedioate [60]. Bis-alkyne **60** was prepared using a modified version of the procedure reported by Hennessey.⁹ A round bottom flask was equipped with a stir bar and charged with alkyne **59** (0.140 g, 0.462 mmol, 1.00 equiv.) dissolved in acetonitrile (3 mL). Copper(II) acetate (0.106 g, 0.531 mmol, 1.15 equiv.) and pyridine (22 μL , 0.277 mmol, 6.00 equiv.) were added and the reaction was allowed to stir at 70 °C overnight. The flask contents were transferred to a separatory funnel, diluted with ethyl acetate (60 mL) and washed with a 40 mL volume of 50 % aqueous ammonium hydroxide. The aqueous phase was back-extracted with ethyl acetate (2 x 25 mL) and the combined organic extracts were dried with sodium sulfate, filtered and concentrated *in-vacuo*. Flash chromatography (silica gel, 30% ethyl acetate in hexanes) gave the bis-alkyne dimer **60** (0.122 g, 0.203 mmol) in 88 % yield.

R_f = 0.41 (silica gel, 30 % ethyl acetate in hexanes); $^1\text{H NMR}$ (100 MHz, CDCl_3) δ 7.36 (s, 5H), 5.35 (d, J = 7.6 Hz, 1H), 5.23 (d, J = 12.3 Hz, 1H), 5.18 (d, J = 12.3 Hz, 1H), 4.48-4.51 (m, 1H), 2.86 (dd, J = 3.9, 17.5 Hz, 1H), 2.81 (dd, J = 4.6, 17.5 Hz, 1H), 1.45 (s, 9H); $^{13}\text{C NMR}$ (100 MHz, CDCl_3) δ 170.3, 155.1, 135.2, 128.7, 128.6, 128.4, 80.4, 72.6, 68.0, 67.7, 52.1, 28.4, 23.8; **ESI-LRMS** m/z calcd for $\text{C}_{34}\text{H}_{40}\text{N}_2\text{O}_8[\text{M}+\text{Na}]^+$: 627.3, Found: 627.1.



1,10-dibenzyl (2S,9S)-2,9-bis(((tert-butoxy)carbonyl)amino)decanedioate [61]. A flask containing dimer **60** (0.122 g, 0.202 mmol, 1.00 equiv.) was diluted with 3 mL of methanol. Palladium 5 %/wt on activated carbon (0.013 g, 10 %/wt) was added and the reaction vessel was sealed under a positive pressure of hydrogen. Stirring for 30 minutes afforded the desired transformation and upon filtration through a pad of celite, **61** (0.085 g, 0.197 mmol, 97 % yield) was isolated as a pure colourless flask residue.

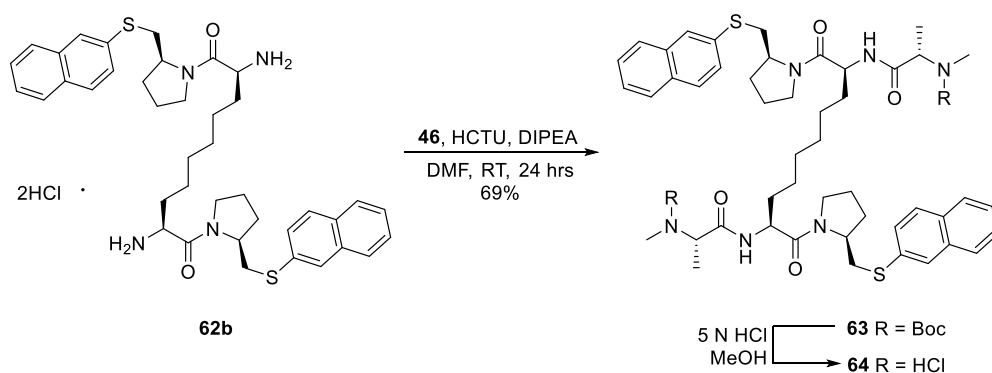
$R_f = 0.09$ (silica gel, 2 % methanol in dichloromethane + 1 % acetic acid); $^1\text{H NMR}$ (400 MHz, CDCl_3) δ 4.05 (dd, $J = 4.6, 8.3$ Hz, 1H), 1.75-1.82 (m, 1H), 1.58-1.67 (m, 1H), 1.28-1.44 (m, 13H); $^{13}\text{C NMR}$ (100 MHz, CDCl_3) δ 176.5, 158.1, 80.4, 54.9, 32.8, 30.0, 28.7, 26.8; **ESI-LRMS** m/z calcd for $\text{C}_{20}\text{H}_{36}\text{N}_2\text{O}_8[\text{M}+\text{Na}]^+$: 455.2, Found: 455.1.



tert-butylN-[(2S,9S)-9-(((tert-butoxy)carbonyl)amino)-1,10-bis((2S)-2-((naphthalen-2-ylsulfanyl)methyl)pyrrolidin-1-yl)-1,10-dioxodecan-2-yl]carbamate [62a]. Refer to general peptide coupling procedure. **Reagents:** **61** (0.160 g, 0.370 mmol, 1.00 equiv.), HCTU (0.153 g, 0.370 mmol, 1.00 equiv.), **41** (0.310 g, 1.11 mmol, 3.00 equiv.), DIPEA (0.387 mL, 2.22 mmol, 6.00

equiv.). Purified via flash chromatography (silica gel, 2 % methanol in dichloromethane + 1 % acetic acid) to give the title compound **62a** in 34 % yield (0.110 g, 0.125 mmol).

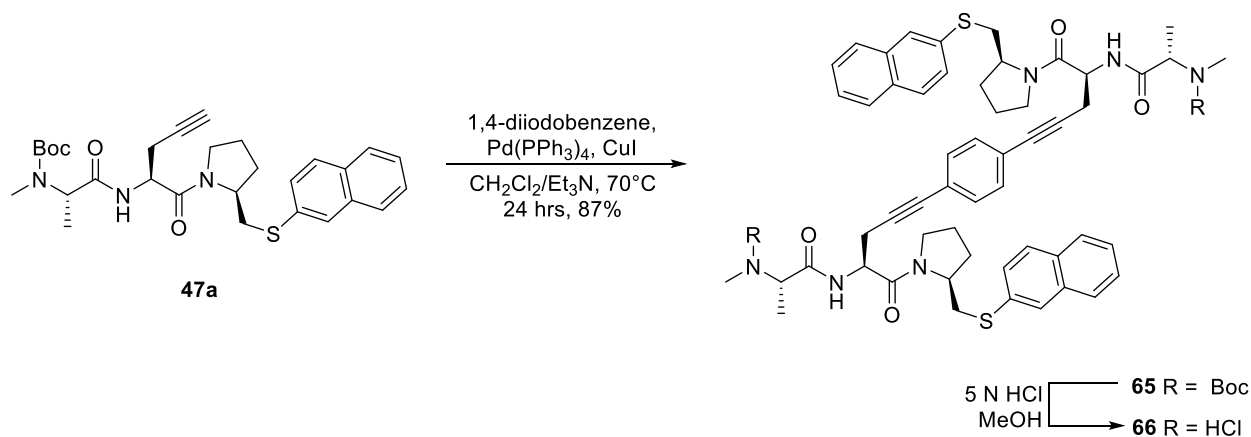
R_f = 0.69 (silica gel, 4 % methanol in dichloromethane); $^1\text{H NMR}$ (300 MHz, C_6D_6) δ 8.15 (s, 1H), 7.75 (d, J = 7.7 Hz, 1H), 7.54-7.56 (m, 3H), 7.18-7.26 (m, 2H), 5.52 (d, J = 8.2 Hz, 1H), 4.43-4.50 (m, 1H), 4.32-4.38 (m, 1H), 3.63 (dd, J = 2.8, 13.4 Hz, 1H), 3.14-3.22 (m, 1H), 2.98-3.05 (m, 1H), 2.74 (dd, J = 9.5, 13.4 Hz, 1H), 1.60-1.72 (m, 2H), 1.37-1.51 (m, 14H), 1.14-1.23 (m, 3H); $^{13}\text{C NMR}$ (100 MHz, CDCl_3) δ 171.7, 155.7, 134.0, 133.6, 131.7, 128.6, 127.8, 127.3, 126.7, 126.6, 126.0, 125.6, 79.6, 56.8, 52.1, 47.6, 34.9, 33.4, 29.5, 28.9, 28.5, 25.5, 24.3; **ESI-LRMS** m/z calcd for $\text{C}_{50}\text{H}_{66}\text{N}_4\text{O}_6\text{S}_2[\text{M}+\text{Na}]^+$: 905.4, Found: 905.1.



(2S)-2-(methylamino)-N-[(2S,9S)-9-[(2S)-2-(methylamino)propanamido]-1,10-bis[(2S)-2-[(naphthalen-2-ylsulfanyl)methyl]pyrrolidin-1-yl]-1,10-dioxodecan-2-yl]propanamide dihydrochloride [63]. Refer to general peptide coupling. **Reagents:** N-methyl-alanine **46** (0.100 g, 0.492 mmol, 6.00 equiv.), HCTU (0.204 g, 0.492 mmol, 6.00 equiv.), **62b** (0.062 g, 0.082 mmol, 1.00 equiv.), DIPEA (0.028 mL, 0.164 mmol, 2.00 equiv.) The crude product **63** was treated with 5 N HCl to provide **64** which was free-based to the diamine using triethylamine and purified by HPLC (gradient, 50-90 % acetonitrile in water + 0.1 % TFA, 20→25 mL/min, 40 min). Subsequent treatment of the pure material with methanolic HCl gave **64** in 69 % isolated yield (0.052 g, 0.0563 mmol).

$^1\text{H NMR}$ (500 MHz, d-DMSO) δ 8.82-9.41 (m, 3H), 8.06 (d, J = 1.6 Hz, 1H), 7.82-7.89 (m, 2H), 7.79 (d, J = 8.1 Hz, 1H), 7.48-7.52 (m, 2H), 7.42-7.45 (m, 1H), 4.43-4.47 (m, 1H), 3.83 (q, J = 6.8 Hz, 1H),

3.54-3.63 (m, 2H), 3.44 (dd, $J = 3.1, 13.4$ Hz, 1H), 3.01 (dd, $J = 9.5, 13.5$ Hz, 1H), 2.46 (s, 3H), 1.80-2.12 (m, 4H), 1.62-0.36 (m, 9H); ^{13}C NMR (100 MHz, d-DMSO) δ 170.0, 168.4, 133.8, 133.5, 130.9, 128.3, 127.6, 126.7, 126.6, 125.9, 125.4, 124.5, 55.6, 51.0, 46.9, 33.5, 31.1, 30.7, 30.6, 28.3, 25.2, 23.6, 15.9, 15.8; ESI-HRMS m/z calcd for $\text{C}_{48}\text{H}_{64}\text{N}_6\text{O}_4[\text{M}+\text{Na}]^+$: 875.4328, Found: 875.4292.

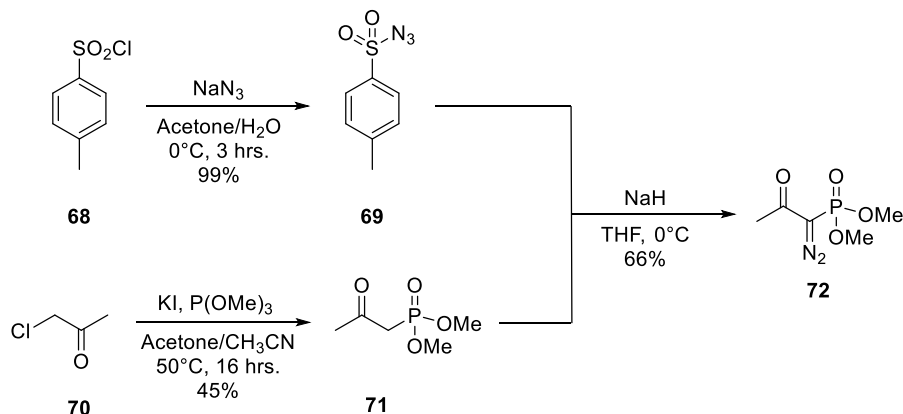


tert-butylN-[(1S)-1-[(2S)-5-{4-[(4S)-4-[(2S)-2-[(tert-butoxy)carbonyl](methyl)amino]propanamido]-5-[(2S)-2-[(naphthalen-2-ylsulfanyl)methyl]pyrrolidin-1-yl]-5-oxopent-1-yn-1-yl]phenyl}-1-[(2S)-2-[(naphthalen-2-ylsulfanyl)methyl]pyrrolidin-1-yl]-1-oxopent-4-yn-2-yl]carbamoyl]ethyl]-N-methylcarbamate [65]. **65** was prepared using a modified version of the procedure described by Peyrottes.¹¹ A flame dried round bottom flask was charged with 1,4-diiodobenzene (0.0189 g, 0.0573 mmol, 1.00 equiv.), Copper(I) iodide (0.001 g, 0.00573 mmol, 0.10 equiv.) and tetrakis(triphenylphosphine)palladium (0.0033 g, 0.00286 mmol, 0.05 equiv.). The flask was evacuated and backfilled with argon three times before a solution of **47a** (0.075 g, 0.143 mmol, 2.50 equiv.) dissolved in 3:1 triethylamine/dichloromethane (0.1 M, degassed) was cannulated over. The flask was fitted with a condenser and heated to 70 °C for 24 hours. The reaction mixture was transferred to a separatory funnel containing 30 mL saturated aqueous ammonium chloride and extracted with ethyl acetate (3 x 20 mL). The combined organic extracts were washed with water, brine, dried with sodium sulfate and concentrated under reduced pressure to provide an orange residue which was subjected to flash chromatography (silica gel, 2 % methanol in

dichloromethane + 0.5 % triethylamine). Subsequent HPLC purification (isocratic, 80 % acetonitrile in water + 0.1 % TFA, 13 mL/min, 60 min) gave **65** as a colourless solid (0.070 g, 0.0624 mmol, 87 % yield).

R_f = 0.26 (silica gel, 2% methanol in dichloromethane); $^1\text{H NMR}$ (300 MHz, C_6D_6) δ 8.11 (s, 1H), 7.46-7.77 (m, 4H), 7.18-7.31 (m, 5H), 4.91 (q, J = 6.9 Hz, 1H), 4.76-4.78 (m, 1H), 4.30-4.35 (m, 1H), 3.71 (dd, J = 3.0, 13.5 Hz, 1H), 2.84-3.06 (m, 3H), 2.75 (s, 3H), 2.54-2.73 (m, 2H), 1.60-1.61 (m, 1H), 1.48 (s, 9H), 1.24 (d, J = 7.1 Hz, 3H), 1.09-1.36 (m, 3H); **ESI-LRMS** m/z calcd for $\text{C}_{64}\text{H}_{76}\text{N}_6\text{O}_8\text{S}_2$ $[\text{M}+\text{Na}]^+$: 1143.5, Found: 1143.5.

(2S)-2-(methylamino)-N-[(2S)-5-{4-[(4S)-4-[(2S)-2-(methylamino)propanamido]-5-[(2S)-2-[(naphthalen-2-ylsulfanyl)methyl]pyrrolidin-1-yl]-5-oxopent-1-yn-1-yl]phenyl}-1-[(2S)-2-[(naphthalen-2-ylsulfanyl)methyl]pyrrolidin-1-yl]-1-oxopent-4-yn-2-yl]propanamide dihydrochloride [66]. $^1\text{H NMR}$ (500 MHz, d-DMSO) δ 8.88-9.31 (m, 3H), 8.02 (d, J = 1.5 Hz, 1H), 7.86 (d, J = 8.6 Hz, 1H), 7.76-7.83 (m, 2H), 7.41-7.52 (m, 3H), 6.99-7.34 (m, 2H), 4.77-4.82 (m, 1H), 4.17-4.24 (m, 1H), 3.86-3.87 (m, 1H), 3.69-3.75 (m, 1H), 3.56-3.61 (m, 1H), 3.50 (dd, J = 2.5, 13.3 Hz, 1H), 2.83-2.91 (m, 2H), 2.77 (dd, J = 10.3, 13.5 Hz, 1H), 2.45 (m, 3H), 1.59-2.06 (m, 4H), 1.37 (d, J = 6.8 Hz, 3H); $^{13}\text{C NMR}$ (75 MHz, d-DMSO) δ 168.1, 167.6, 133.2, 133.1, 131.1, 131.0, 130.9, 130.6, 128.0, 127.3, 126.3, 125.5, 125.1, 124.1, 122.0, 87.7, 81.2, 55.9, 55.5, 49.6, 46.6, 32.8, 30.3, 27.9, 23.1, 22.1, 15.4; **ESI-HRMS** m/z calcd for $\text{C}_{54}\text{H}_{60}\text{N}_6\text{O}_4\text{S}_2$ $[\text{M}+\text{H}]^+$: 921.4196, Found: 921.4227.

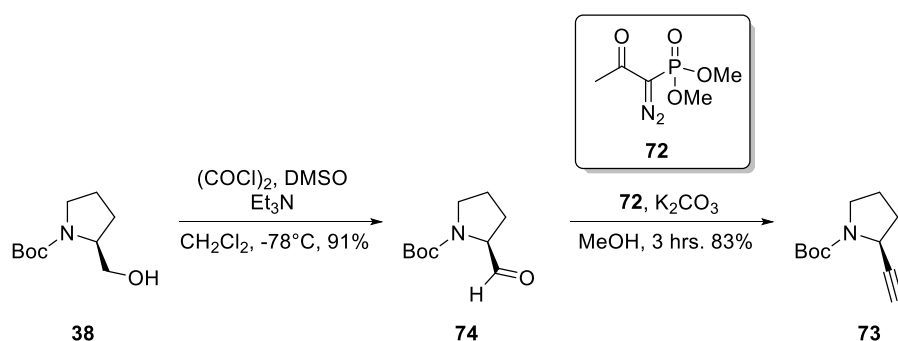


Toluenesulfonyl azide [69]. Prepared according to the procedure described by Katritzky.¹² A round bottom flask equipped with stir bar was charged with sodium azide (3.72 g, 57.2 mmol, 1.00 equiv.) then suspended in a mixture of water (120 mL)/acetone (60 mL) and cooled to 0°C . Freshly re-crystallized tosyl chloride **68** (10.9 g, 57.2 mmol, 1.00 equiv.) in 60 mL dry acetone was transferred to an addition funnel fitted to the reaction flask. The tosyl chloride was added to the reaction mixture over 30 minutes and the reaction was allowed to stir for an additional 2 hours. Acetone was removed *in-vacuo* (no heating) and the flask contents were transferred to a separatory funnel and extracted with diethyl ether (3 x 300 mL). The combined organic extracts were dried using sodium sulfate, filtered and concentrated to give a clear, colourless oil which crystallized to a white solid upon storage at -20°C (11.1 g, 56.4 mmol, 99 % yield). Obtained spectra were consistent with the reported literature.¹²

Dimethyl-2-oxopropylphosphonate [71]. Compound **71** prepared according to the procedure described by Pietruska.¹³ A flame dried round bottom flask was charged with potassium iodide (dried *in-vacuo*) and dissolved in 1:1 acetone/acetonitrile (75 mL). While stirring, chloroacetone **70** (15 mL, 182 mmol, 1.00 equiv.) was added dropwise, the orange slurry was allowed to stir for 1 hour at room temperature. Trimethylphosphite (21.5 mL, 182 mmol, 1.00 equiv.) was added in portions and the mixture was allowed to stir overnight, producing a cloudy white suspension. A condenser was fitted and the reaction was heated to 50°C for 3 hours. The reaction was allowed to cool and the flask contents were filtered through a pad of celite and concentrated *in-vacuo* to afford a dark red oil. Fractional vacuum distillation at 1.2 mmHg gave the product **71** (13.7 g, 82.3

mmol) in the fraction which collected at 93 °C in 45 % yield. The colourless oil gave spectroscopic data consistent with the literature.¹³

Dimethyl-1-diazo-2-oxopropylphosphonate (Ohira-Bestmann reagent) [72]. Prepared according to the procedure described.¹³ Sodium hydride (60 %/wt in mineral oil) (2.57 g, 64.1 mmol, 1.25 equiv.) was added to a flame dried round bottom flask, dissolved in anhydrous tetrahydrofuran (180 mL) and cooled to 0 °C. Phosphonate **71** (8.52 g, 51.3 mmol, 1.00 equiv.) in THF was cannulated into the reaction flask and allowed to stir for 1 hour. Toluenesulfonyl azide **69** (11.1 g, 56.4 mmol, 1.10 equiv.) was dissolved in THF and added dropwise to the reaction mixture *via* cannula. The mixture was allowed to stir for one hour before being warmed to room temperature. Water was added (5 mL) and the mixture was filtered through a pad of celite and concentrated under reduced pressure. The resultant crude orange oil was purified *via* flash chromatography (silica gel, gradient 1:1 to 7:3 ethyl acetate in hexanes) to afford the Ohira-Bestmann reagent **72** as a yellow oil (6.55 g, 34.1 mmol, 66 % yield). Observed spectroscopic properties were consistent with the literature.¹³



Tert-butyl (2S)-2-formylpyrrolidine-1-carboxylate [74]. Aldehyde **74** was prepared according to a modified procedure from Ireland.¹⁴ A flame dried round bottom flask was charged with 100 mL anhydrous dichloromethane and cooled to -78°C . Oxalyl chloride (2.14 mL, 25.0 mmol, 1.30 equiv.) was added followed by dropwise addition of dimethylsulfoxide (3.41 mL, 48.1 mmol, 2.50 equiv.). After stirring for 10 minutes the starting alcohol **38** (3.87 g, 19.2 mmol, 1.00 equiv.) was added dropwise in DCM down the side of the flask and the cloudy white mixture was allowed to stir for 15 minutes. Triethylamine (10.2 mL, 73.0 mmol, 3.80 equiv.) was added dropwise and the reaction was stirred at -78°C for 20 minutes, then warmed to room temperature. The reaction

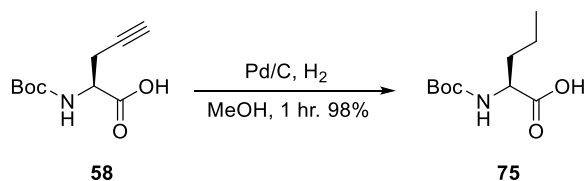
was quenched with saturated aqueous ammonium chloride and the flask contents were transferred to a separatory funnel where the organic phase was washed with brine (3 x 100 mL), dried with sodium sulfate, filtered and concentrated under reduced pressure. The resulting oil was re-suspended in diethyl ether and the oxalic acid present was allowed to crystallize out of solution. The ethereal supernatant was collected, concentrated and purified *via* flash chromatography (silica gel, 30 % ethyl acetate in hexanes) to give the desired aldehyde **74** in 91 % yield (3.47 g, 17.4 mmol). Spectral data was consistent with published values.¹⁵

R_f = 0.4 (silica gel, 30 % ethylacetate in hexanes); $^1\text{H NMR}$ (400 MHz, CDCl_3) δ 9.56 (s, 1H), 4.05 (m, 1H), 3.42-3.59 (m, 2H), 1.84-2.17 (m, 4H), 1.43 (s, 9H); $^{13}\text{C NMR}$ (100 MHz, CDCl_3) δ 200.5, 154.0, 80.7, 65.1, 46.8, 28.4, 28.1, 24.0; **ESI-LRMS** m/z calcd for $\text{C}_{10}\text{H}_{17}\text{NO}_3$ $[\text{M}+\text{H}]^+$: 199.12; $[\text{M}+\text{Na}]^+$: 222.1. Found: 222.1.

Tert-butyl (2S)-2-ethynylpyrrolidine-1-carboxylate [73]. **73** was prepared using a modified version of the procedure reported by Pietruszka.¹³ A flame dried round bottom flask was charged with the Ohira-Bestmann reagent **72** (4.32 g, 22.5 mmol, 1.20 equiv.), potassium carbonate (4.78 g, 34.6 mmol, 2.00 equiv.) and dissolved in 100 mL anhydrous methanol. The mixture was allowed to stir at room temperature for 5 minutes before aldehyde **74** (3.45 g, 17.3 mmol, 1.00 equiv.) in methanol was added dropwise *via* cannula. The reaction was allowed to stir for 3 hours, on completion by TLC analysis (silica gel, 30 % ethylacetate in hexanes) saturated aqueous sodium chloride was added (10 mL) and the flask contents were concentrated *in-vacuo* then re-suspended in diethylether. The organic phase was extracted with saturated aqueous sodium carbonate (100 mL), water (100 mL) and brine (100 mL) before being dried with sodium sulfate, filtered and concentrated. The resulting yellow oil was purified using flash chromatography (silica gel, 30% diethylether in hexanes) to provide the alkyne **73** in 83 % yield as a colourless oil (2.80 g, 14.4 mmol). Characterization consistent with the reported literature.¹⁶

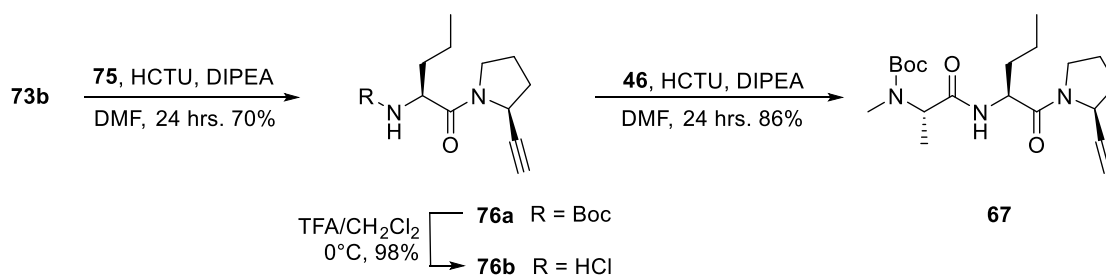
R_f = 0.40 (silica gel, 30 % diethylether in hexanes); $^1\text{H NMR}$ (400 MHz, CDCl_3) δ 4.36-4.44 (m, 1H), 3.40 (m, 1H), 3.25 (m, 1H), 2.17 (s, 1H), 1.83-2.01 (m, 4H), 1.42 (s, 9H); $^{13}\text{C NMR}$ (100 MHz, CDCl_3)

δ 154.0, 84.3, 79.7, 69.6, 47.9, 45.6, 33.7, 28.5, 23.6; **ESI-LRMS** m/z calcd for $C_{11}H_{17}NO_2[M+Na]^+$: 218.1, Found: 218.0.



(2S)-2-[[[(tert-butoxy)carbonyl]amino]pentanoic acid [75]. A round bottom flask fitted with a stir bar was charged with L-Boc-propargylglycine **58** (0.307 g, 1.44 mmol, 1.00 equiv.) and 8 mL methanol. Palladium on carbon (0.03 g, 10 %/wt) was added and the flask was fitted with a rubber septum and balloon containing hydrogen. The flask was purged with hydrogen while stirring vigorously and allowed to continue stirring under hydrogen atmosphere for 1 hour. The flask contents were filtered through a pad of celite and concentrated *in-vacuo* to afford the product **75** as a pale yellow oil (0.312 g, 1.144 mmol, 100 % yield). Spectra matched reported values.¹⁷

¹H NMR (400, CDCl₃) δ 5.00 (d, $J = 7.4$ Hz, 1H), 4.30 (dd, $J = 12.8, 7.4$ Hz, 1H), 1.80-1.87 (m, 1H), 1.60-1.69 (m, 1H), 1.37-1.44 (m, 11H), 0.94 (t, $J = 7.3$ Hz, 3H); ¹³C NMR (100 MHz, CDCl₃) δ 177.7, 155.8, 80.3, 53.4, 34.6, 28.4, 18.8, 13.8; **ESI-LRMS** m/z calcd for $C_{10}H_{19}NO_4[M+Na]^+$: 240.1, Found: 240.0.



tert-butyl N-[(2S)-1-[(2S)-2-ethynylpyrrolidin-1-yl]-1-oxopentan-2-yl]carbamate [76a]. Refer to general peptide coupling procedure. **Reagents:** L-Boc-Norvaline (0.449 g, 2.07 mmol, 2.50 equiv.), HCTU (0.856 g, 2.07 mmol, 2.50 equiv.), **73b** (0.173 g, 0.827 mmol, 1.00 equiv.), DIPEA

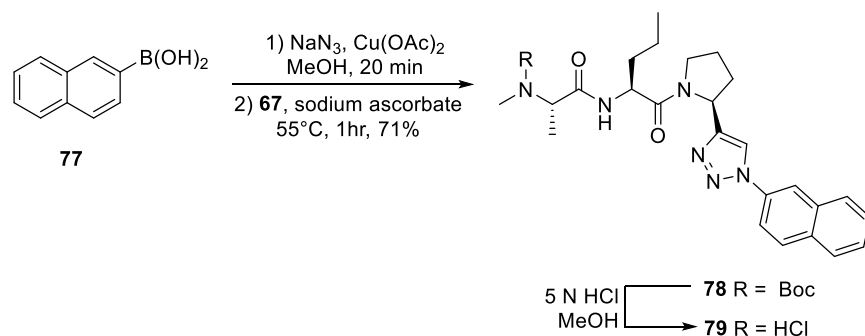
(0.29 mL, 1.65 mmol, 2.00 equiv.). Purified by flash chromatography (silica gel, 60% ether in hexanes) to afford **76a** (0.171 g, 1.65 mmol, 70% yield).

R_f = 0.3 (silica gel, 60 % ether in hexanes); ¹H NMR (300 MHz, CDCl₃) δ 5.26 (d, *J* = 8.6 Hz, 1H), 4.73-4.76 (m, 1H), 4.31-4.38 (m, 1H), 3.52-3.67 (m, 2H), 2.19 (d, *J* = 2.12 Hz, 1H), 2.00-2.18 (m, 4H), 1.39 (s, 9H), 1.22-1.73 (m, 5H), 0.91 (t, *J* = 7.2 Hz, 3H); ¹³C NMR (300 MHz, CDCl₃) δ 173.05, 157.6, 85.1, 81.5, 72.2, 53.6, 49.5, 48.2, 37.4, 34.0, 30.4, 26.9, 20.6, 16.0; ESI-LRMS *m/z* calcd for C₁₆H₂₆N₂O₃[M+Na]⁺: 317.2. Found: 317.1.

tert-butyl-N-[(1S)-1-[[[(2S)-1-[(2S)-2-ethynylpyrrolidin-1-yl]-1-oxopentan-2-

yl]carbamoyl]ethyl]-N-methylcarbamate [67]. Refer to general peptide coupling. **Reagents** Boc-N-methyl-L-Alanine **46** (0.280, 1.38 mmol, 2.50 equiv.), HCTU (0.570 g, 1.38 mmol, 2.50 equiv.), **76b** (0.170 g, 0.551 mmol, 1.00 equiv.), DIPEA (0.193 mL, 1.10 mmol, 2.00 equiv.) Flash chromatography (silica gel, 60 % ethyl acetate in hexanes + 1 % triethylamine) provided **67** as a colourless oil in 86 % yield (0.179 g, 0.472 mmol).

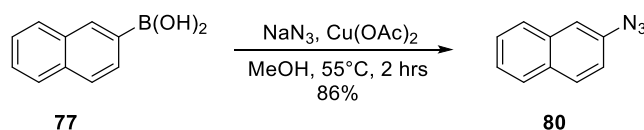
R_f = 0.28 (silica gel, 60 % ethyl acetate in hexanes); ¹H NMR (400 MHz, CDCl₃) δ 6.70 (s, 1H), 4.68-4.71 (m, 1H), 4.59 (q, *J* = 7.9 Hz, 1H), 4.47-4.50 (m, 1H), 3.52-3.62 (m, 2H), 2.71 (s, 3H), 2.18 (d, *J* = 2.2 Hz, 1H), 1.86-2.16 (m, 4H), 1.48-1.70 (m, 2H), 1.41 (s, 9H), 1.25 (d, *J* = 7.1 Hz, 3H), 0.85 (t, *J* = 7.3 Hz, 3H); ¹³C NMR (100 MHz, CDCl₃) δ 171.1, 170.1, 155.8, 82.9, 80.5, 70.2, 50.2, 48.0, 47.5, 46.2, 34.8, 31.9, 30.1, 28.3, 24.9, 18.4, 13.8, 13.7; ESI-LRMS *m/z* calcd for C₂₀H₃₃N₃O₄[M+Na]⁺: 402.2. Found: 402.1.



tert-butyl-N-methyl-N-[(1S)-1-[(2S)-1-[(2S)-2-[1-(naphthalen-2-yl)-1H-1,2,3-triazol-4-yl]pyrrolidin-1-yl]-1-oxopentan-2-yl]carbamoyl]ethyl]carbamate [78]. Compound **78** was prepared according to a modified procedure by Grimes.¹⁸ A round bottom flask equipped with stir bar was charged with starting boronic acid **77** (0.150 g, 0.395 mmol, 1.00 equiv.) and 2 mL of methanol (0.2 M). Sodium azide (0.025 g, 0.395 mmol, 1.00 equiv.) and copper acetate (0.008 g, 0.0395 mmol, 0.1 equiv.) were added and the brown mixture was stirred at 55 °C for 20 minutes. Sodium ascorbate (0.0156 g, 0.0791 mmol, 0.2 equiv.) was added, followed by alkyne **67** dissolved in 1.2 mL dichloromethane. The reaction was complete after one hour, solvent was stripped off and the residue was re-suspended in 75 mL of ethyl acetate. The organic layer was washed with 20% aqueous ammonium hydroxide (50 mL) and the aqueous washing was back-extracted with 50 mL ethyl acetate. Combined organic layers were washed with water (50 mL), brine (50 mL), dried using sodium sulfate and concentrated under reduced pressure to provide a residue which was purified *via* flash chromatography to afford the 1,4-1,2,3 triazole **78** in 71 % yield (0.124 g, 0.226 mmol).

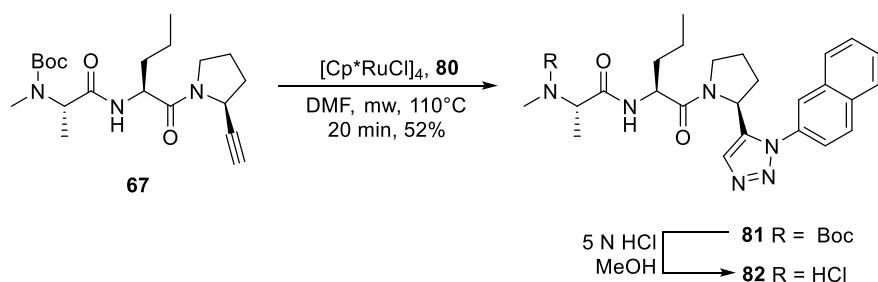
$R_f = 0.36$ (silica gel, 3 % methanol in dichloromethane); $^1\text{H NMR}$ (400 MHz, CDCl_3) δ 8.12 (d, $J = 2$ Hz, 1H), 8.09 (s, 1H), 7.87-7.99 (m, 4H), 7.53-7.59 (m, 2H), 6.73 (brs, 1H), 5.39 (dd, $J = 2.8, 8.1$ Hz, 1H), 4.75 (ddd, $J = 5.0, 8.1, 8.1$ Hz, 1H), 4.50-4.70 (brs, 1H), 3.70-3.85 (m, 2H), 2.78 (s, 3H), 2.55-2.61 (m, 1H), 2.40-2.49 (m, 1H), 1.63-2.29 (m, 4H), 1.49-1.55 (m, 1H), 1.47 (s, 9H), 1.34 (d, $J = 7.0$ Hz, 3H), 1.25-1.30 (m, 2H), 0.86 (t, $J = 7.1$ Hz, 3H); $^{13}\text{C NMR}$ (100 MHz, CDCl_3) δ 171.3, 170.8, 148.8, 134.6, 133.3, 133.0, 130.1, 128.4, 128.1, 127.5, 127.1, 121.0, 119.0, 118.4, 80.7, 52.7, 51.3, 50.5, 47.3, 46.4, 34.9, 30.2, 28.5, 25.2, 18.7, 13.9, 13.8; **ESI-LRMS** m/z calcd for $\text{C}_{30}\text{H}_{40}\text{N}_6\text{O}_4[\text{M}+\text{Na}]^+$: 571.3 Found: 571.2.

(2S)-2-(methylamino)-N-[(2S)-1-[(2S)-2-[1-(naphthalen-2-yl)-1H-1,2,3-triazol-4-yl]pyrrolidin-1-yl]-1-oxopentan-2-yl]propanamide hydrochloride [79]. $^1\text{H NMR}$ (400 MHz, d-DMSO) δ 8.82 (brs, 2H), 8.73 (d, $J = 7.5$ Hz, 1H), 8.72 (s, 1H), 8.43 (d, $J = 2.0$ Hz, 1H), 8.2 (d, $J = 8.9$ Hz, 1H), 8.02-8.11 (m, 3H), 7.59-7.66 (m, 2H), 5.26-5.32 (m, 1H), 4.56-4.61 (m, 1H), 3.79-3.86 (m, 1H), 3.41-3.75 (m, 2H), 2.51 (t, $J = 5.2$ Hz, 3H), 1.48-2.24 (m, 6H), 1.36 (d, $J = 7.0$ Hz, 3H), 1.26-1.42 (m, 2H), 0.87-0.93 (m, 3H); $^{13}\text{C NMR}$ (100 MHz, d-DMSO) δ 169.5, 168.5, 150.1, 134.1, 132.9, 132.3, 130.0, 128.2, 127.9, 127.5, 126.9, 118.5, 117.5, 114.3, 55.9, 52.7, 50.6, 46.4, 32.8, 31.3, 30.7, 24.0, 18.4, 15.7, 13.5; **ESI-LRMS** m/z calcd for $\text{C}_{25}\text{H}_{33}\text{N}_6\text{O}_2[\text{M}+\text{H}]^+$: 449.3 Found: 449.2.



Naphthalene-2-azide [80]. Prepared in accordance with the procedure reported by Grimes.¹⁸ A round bottom flask equipped with stir bar was charged with starting boronic acid **77** (0.400 g, 2.33 mmol, 1.00 equiv.) and 9 mL of methanol (0.25 M). Sodium azide (0.166 g, 2.56 mmol, 1.10 equiv.) and copper acetate (0.046 g, 0.233 mmol, 0.1 equiv.) were added and the brown mixture was stirred at 55 °C for 2 hours until completion by TLC (silica gel, 5 % Et₂O in hexanes). The flask contents were transferred to a separatory funnel and diluted with diethyl ether (100 mL). The organic layer was washed with 75 mL of 20 % aqueous ammonium hydroxide and the blue aqueous phase was back extracted with 50 mL diethyl ether. The combined organics were washed with water (75 mL), brine (75 mL), dried with sodium sulfate and concentrated *in-vacuo* to afford **80** as a brown oil which solidified upon storage at 0 °C (0.339 g, 2.00 mmol, 86 %). Spectral data consistent with reported values.¹⁸

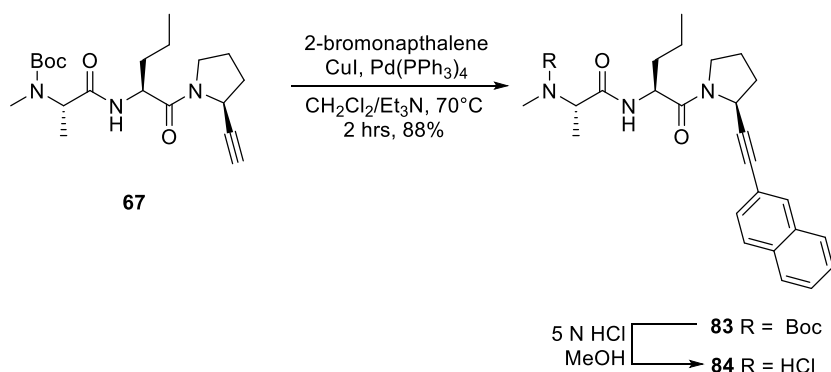
$R_f = 0.69$ (silica gel, 5 % Et₂O in hexanes); $^1\text{H NMR}$ (400 MHz, CDCl₃) δ 7.81-7.84 (m, 2H), 7.76 (d, $J = 8.2$ Hz, 1H), 7.50 (ddd, $J = 1.2, 6.9, 8.2$, 1H), 7.42-7.46 (m, 2H), 7.16 (dd, $J = 2.3, 8.8$ Hz, 1H); $^{13}\text{C NMR}$ (100 MHz, CDCl₃) δ 137.6, 134.1, 131.2, 130.0, 128.0, 127.1, 127.1, 125.5, 118.8, 115.9.



tert-butylN-methyl-N-[(1S)-1-[[[(2S)-1-[(2S)-2-[1-(naphthalen-2-yl)-1H-1,2,3-triazol-5-yl]pyrrolidin-1-yl]-1-oxopentan-2-yl]carbamoyl]ethyl]carbamate [81]. Prepared using a modified version of a procedure reported by Fokin.¹⁹ A 5 mL flame dried vial was charged with starting alkene **67** (0.086 g, 0.226 mmol, 1.00 equiv.) and purged with argon. 2-naphthaleneazide (0.042 g, 0.248 mmol, 1.10 equiv.) was dissolved in 2 mL DMF (0.1 M) and added to the vial followed by chloro(pentamethylcyclopentadienyl)ruthenium(II)tetramer (0.025 g, 0.0226 mmol, 0.10 equiv.). The vial was sealed under argon atmosphere and placed in a microwave reactor to stir for 20 minutes at 110 °C. The vial contents were partitioned between water and ethyl acetate, the aqueous phase was extracted with ethyl acetate (2 x 20 mL). The combined organic layers were washed with brine (3 x 20 mL), dried with sodium sulfate and concentrated *in-vacuo* to give a crude black residue which was purified twice by flash chromatography (silica gel, gradient 20-25 % acetone in toluene + 1 % triethylamine) affording the 1,5-1,2,3 triazole **81** (0.0642 g, 0.117 mmol, 52 % yield).

$R_f = 0.36$ (silica gel, 3 % methanol in dichloromethane); 1H NMR (500 MHz, $CDCl_3$) δ 8.10 (d, $J = 2.0$ Hz, 1H), 8.00 (d, $J = 8.7$ Hz, 1H), 7.92-7.94 (m, 2H), 7.71 (dd, $J = 2.1, 8.7$ Hz, 1H), 7.57-7.60 (m, 2H), 7.49 (s, 1H), 6.72 (brs, 1H), 5.33 (dd, $J = 3.5, 7.8$ Hz, 1H), 4.72 (ddd, $J = 8.0, 8.0, 5.5$ Hz, 1H), 4.40-4.60 (brs, 1H), 3.75-3.84 (m, 2H), 2.76 (s, 3H), 2.00-2.16 (m, 3H), 1.68-1.76 (m, 2H), 1.53-1.60 (m, 1H), 1.46 (s, 9H), 1.31-1.38 (m, 2H), 1.29 (d, $J = 7.1$ Hz, 3H), 0.94 (t, $J = 7.4$, 3H); ^{13}C NMR (125 MHz, $CDCl_3$) δ 171.3, 171.0, 149.6, 140.6, 133.6, 133.5, 133.1, 130.8, 129.9, 128.6, 128.0, 127.6, 127.4, 124.8, 123.2, 80.7, 51.9, 50.4, 47.1, 34.9, 32.1, 30.1, 28.4, 24.4, 18.6, 13.9; **ESI-LRMS** m/z calcd for $C_{30}H_{40}N_6O_4[M+Na]^+$: 571.3 Found: 571.3.

(2S)-2-(methylamino)-N-[(2S)-1-[(2S)-2-[1-(naphthalen-2-yl)-1H-1,2,3-triazol-5-yl]pyrrolidin-1-yl]-1-oxopentan-2-yl]propanamide hydrochloride [82]. $^1\text{H NMR}$ (400 MHz, d-DMSO) δ 8.76 (brs, 2H), 8.69 (d, $J = 7.7$ Hz, 1H), 8.21 (d, $J = 1.9$ Hz, 1H), 8.18 (d, $J = 8.8$ Hz, 1H), 8.08-8.10 (m, 2H), 7.83 (s, 1H), 7.74 (dd, $J = 2.1, 8.7$ Hz, 1H), 7.67-7.69 (m, 2H), 5.06 (m, 1H), 4.51-4.57 (m, 1H), 3.62-3.87 (m, 3H), 2.48 (t, $J = 5.2$ Hz, 3H), 1.65-2.23 (m, 5H), 1.43-1.52 (m, 1H), 1.26-1.38 (m, 2H), 1.29 (d, $J = 6.9$ Hz, 3H), 0.91 (t, $J = 7.4$ Hz, 3H); $^{13}\text{C NMR}$ (100 MHz, d-DMSO) δ 169.7, 168.4, 141.2, 133.4, 132.8, 132.6, 130.8, 129.6, 128.4, 127.9, 127.6, 127.4, 124.3, 123.2, 55.8, 51.3, 50.5, 46.5, 32.7, 31.7, 30.7, 24.1, 18.4, 15.6, 13.5; **ESI-LRMS** m/z calcd for $\text{C}_{25}\text{H}_{33}\text{N}_6\text{O}_2[\text{M}+\text{H}]^+$: 449.3 Found: 449.1.

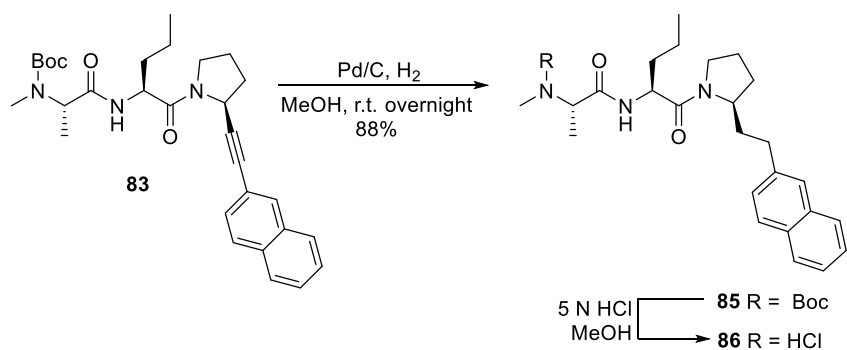


tert-butylN-methyl-N-[(1S)-1-[[[(2S)-1-[(2S)-2-[2-(naphthalen-2-yl)ethynyl]pyrrolidin-1-yl]-1-oxopentan-2-yl]carbamoyl]ethyl]carbamate [83]. Prepared according to a modified procedure by Hanamoto.²⁰ A flame dried round bottom flask with stir bar was charged with 2-bromonaphthalene (0.109 g, 0.527 mmol, 2.00 equiv.), tetrakis(triphenylphosphine)palladium (0.030 g, 0.026 mmol, 0.1 equiv.) and Copper(I) Iodide (0.005 g, 0.026 mmol, 0.1 equiv.). The flask was placed under vacuum and backfilled with argon three times. A 3:1 mixture of trimethylamine/dichloromethane was sparged with argon for 45 minutes and 2.5 mL (0.1 M) was added to a flame dried vial containing starting alkyne **67** (0.100 g, 0.264 mmol, 1.00 equiv.). The alkyne was cannulated into the reaction flask, a condenser was fitted and the reaction was allowed to stir at 70 °C for two hours. Solvent was removed *in-vacuo* and the residue was re-suspended in EtOAc (30 mL). The organic layer was washed with saturated aqueous ammonium chloride (2 x 25 mL), water (25 mL), brine (30 mL), dried with sodium sulfate and concentrated.

Purification *via* flash chromatography (15 % acetone in toluene + 1 % triethylamine) afforded the coupling product **83** in 63 % yield as a light yellow solid (0.091 g, 0.170 mmol).

R_f = 0.33 (silica gel, 15 % acetone in toluene + 1% triethylamine); $^1\text{H NMR}$ (400 MHz, CDCl_3) δ 7.88 (s, 1H), 7.71-7.78 (m, 3H), 7.39-7.49 (m, 3H), 6.79 (s, 1H), 5.06 (dd, J = 3.5, 6.7 Hz, 1H), 4.82 (dd, J = 2.5, 6.6 Hz, 1H), 4.72 (q, J = 7.7 Hz, 1H), 3.67-3.76 (m, 2H), 2.79 (s, 3H), 2.00-2.34 (m, 4H), 1.58-1.82 (m, 2H), 1.48 (s, 9H), 1.36-1.45 (m, 1H), 1.33 (d, J = 7.1 Hz, 3H), 0.93 (t, J = 7.4 Hz, 3H); $^{13}\text{C NMR}$ (100 MHz, CDCl_3) δ 171.2, 170.2, 156.1, 133.0, 132.8, 132.3, 131.65, 128.6, 127.9, 127.8, 126.6, 126.5, 120.3, 88.8, 82.5, 80.7, 50.5, 49.1, 48.5, 46.3, 35.0, 32.3, 30.2, 28.5, 25.1, 18.5, 14.0, 13.9; **ESI-MS** m/z calcd for $\text{C}_{30}\text{H}_{39}\text{N}_3\text{O}_4[\text{M}+\text{Na}]^+$: 528.2838. Found: 528.2495.

(2S)-2-(methylamino)-N-[(2S)-1-[(2S)-2-[2-(naphthalen-2-yl)ethynyl]pyrrolidin-1-yl]-1-oxopentan-2-yl]propanamide hydrochloride [84]. $^1\text{H NMR}$ (300 MHz, d-DMSO) δ 8.93 (brs, 2H), 8.81 (dd, J = 7.7 Hz, 1H), 7.96 (d, J = 1.0 Hz, 1H), 7.87-7.96 (m, 3H), 7.50-7.57 (m, 2H), 7.39 (dd, J = 1.6, 8.5 Hz, 1H), 4.91 (dd, J = 2.5, 7.6 Hz, 1H), 4.54 (ddd, J = 5.8, 7.9 Hz, 1H), 3.82-3.90 (m, 1H), 3.65-3.69 (m, 1H), 3.30-3.59 (m, 1H), 2.51 (s, 3H), 1.95-2.36 (m, 4H), 1.55-1.73 (m, 2H), 1.36 (d, J = 7.0 Hz, 3H), 1.37-1.44 (m, 2H), 0.88-0.96 (m, 3H); $^{13}\text{C NMR}$ (75 MHz, d-DMSO) δ 169.3, 168.4, 132.5, 132.5, 132.4, 132.3, 131.4, 130.9, 128.3, 128.2, 128.1, 127.7, 127.6, 127.0, 126.9, 126.9, 90.2, 81.4, 55.9, 50.6, 47.9, 46.0, 33.2, 31.9, 30.7, 24.8, 18.2, 15.7, 13.6; **ESI-LRMS** m/z calcd for $\text{C}_{25}\text{H}_{31}\text{N}_3\text{O}_2[\text{M}+\text{H}]^+$: 406.2. Found: 406.1.

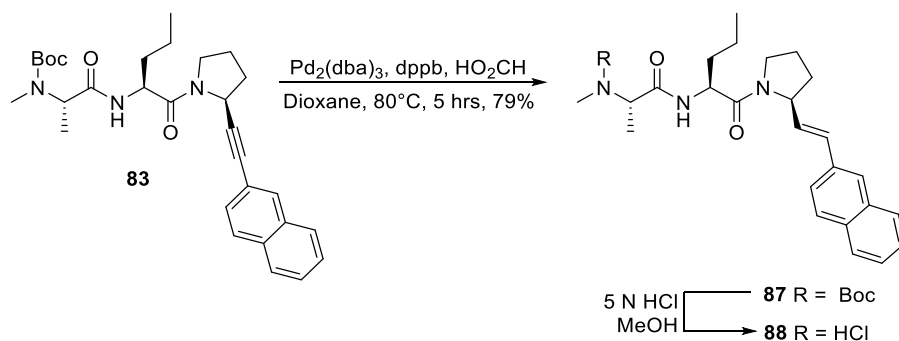


tert-butyl N-methyl-N-[(1S)-1-[[[(2S)-1-[(2R)-2-[2-(naphthalen-2-yl)ethyl]pyrrolidin-1-yl]-1-oxopentan-2-yl]carbonyl]ethyl]carbamate [85]. A round bottom flask was charged with **83** (0.065 g, 0.129 mmol, 1.00 equiv.), palladium on activated carbon (0.006 g, 10 %/wt) and methanol, 1.5 mL. The reaction mixture was placed under an atmosphere of hydrogen and stirred vigorously for 30 minutes before being filtered through a pad of celite and concentrated *in-vacuo*. The product was purified by flash chromatography (silica gel, 20 % acetone in toluene + 1 % triethylamine) to give **85** (0.058 g, 0.1139 mmol, 88 % yield).

R_f = 0.4 (silica gel, 20 % acetone in toluene + 1% triethylamine); $^1\text{H NMR}$ (500 MHz, CDCl_3) δ 7.77-7.79 (m, 1H), 7.76 (d, J = 8.1 Hz, 1H), 7.62 (s, 1H), 7.38-7.45 (m, 2H), 7.34 (dd, J = 1.7, 8.4 Hz, 1H), 6.77 (brs, 1H), 4.71 (ddd, J = 5.3, 7.8, 7.8, 1H), 4.42-4.60 (brs, 1H), 4.19-4.23 (m, 1H), 3.65-3.70 (m, 1H), 3.46-3.50 (m, 1H), 2.72-2.80 (m, 5H), 2.20-2.26 (m, 1H), 1.53-2.04 (m, 7H), 1.48 (s, 9H), 1.34-1.36 (m, 2H), 1.32 (d, J = 7.0 Hz, 3H), 0.90 (t, J = 7.5 Hz, 3H); $^{13}\text{C NMR}$ (100 MHz, CDCl_3) δ 171.0, 170.4, 139.2, 133.6, 132.0, 127.9, 127.6, 127.4, 127.2, 126.3, 125.9, 125.2, 80.5, 57.3, 50.5, 50.3, 46.8, 35.2, 35.0, 32.9, 30.2, 30.0, 29.2, 28.4, 24.3, 18.5, 13.9, 13.7; **ESI-LRMS** m/z calcd for $\text{C}_{30}\text{H}_{43}\text{N}_3\text{O}_4[\text{M}+\text{Na}]^+$: 532.3 Found: 571.2.

(2S)-2-(methylamino)-N-[(2S)-1-[(2R)-2-[2-(naphthalen-2-yl)ethyl]pyrrolidin-1-yl]-1-oxopentan-2-yl]propanamide hydrochloride [86]. $^1\text{H NMR}$ (400 MHz, $d\text{-DMSO}$) δ 8.70-8.94 (m, 3H), 7.81-7.87 (m, 3H), 7.69 (s, 1H), 7.42-7.49 (m, 2H), 7.37 (dd, J = 1.6, 8.39 Hz, 1H), 4.51 (ddd, J = 5.1, 8.0, 8.0 Hz, 1H), 3.25-4.05 (m, 4H), 2.65-2.79 (m, 2H), 2.50 (s, 3H), 1.76-2.09 (m, 5H), 1.49-1.71 (m, 2H), 1.33 (d, J = 7.0 Hz, 3H), 1.27-1.41 (m, 2H), 0.88 (t, J = 7.2 Hz, 3H); $^{13}\text{C NMR}$ (100 MHz,

d-DMSO) δ 169.4, 168.3, 139.5, 133.2, 131.6, 127.8, 127.7, 127.5, 127.3, 127.2, 126.0, 125.9, 125.2, 56.6, 55.9, 50.7, 46.3, 34.2, 33.4, 31.9, 30.7, 28.6, 24.0, 18.4, 15.7, 13.6; **ESI-LRMS** m/z calcd for $C_{25}H_{35}N_3O_2[M+Na]^+$: 410.3 Found: 410.1.

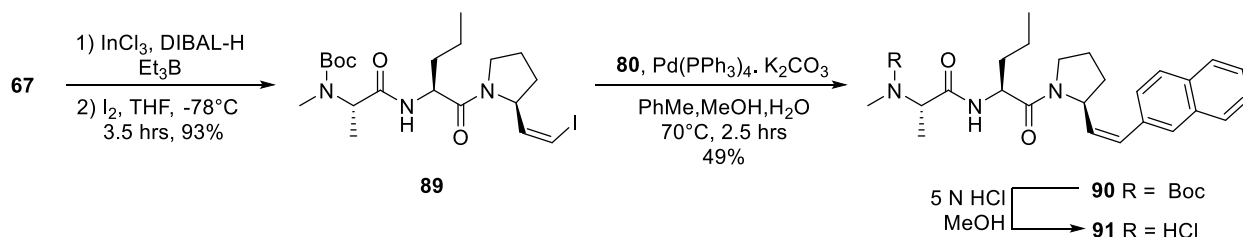


tert-butyl N-methyl-N-[(1S)-1-[[[(2S)-1-[(2S)-2-[(E)-2-(naphthalen-2-yl)ethenyl]pyrrolidin-1-yl]-1-oxopentan-2-yl]carbamoyl]ethyl]carbamate [87]. Compound **87** was prepared according to a modified version of the procedure reported by Han.²¹ A flame dried round bottom flask was fitted with a stir bar and charged with starting alkyne **83** (0.103 g, 0.204 mmol, 1.00 equiv.), Tris(dibenzylideneacetone)dipalladium(0) (0.0037 g, 0.0041 mmol, 0.02 equiv.) and 1,4-Bis(diphenylphosphino)butane (0.0035 g, 0.0081 mmol, 0.04 equiv.); the flask was evacuated and backfilled with argon three times. A 0.5 mL volume of dioxane (degassed *via* argon sparge) was added and the mixture was allowed to stir for 15 minutes before 65 μ L (2.00 equiv.) of 25 % aqueous formic acid (degassed) was added. The mixture was heated to 80 $^\circ$ C for 3 hours at which point an additional 65 μ L (2.00 equiv.) 25% aqueous formic acid was added and the reaction was allowed to stir for another 2 hours. Solvent was removed under a stream of air and the brown residue was purified *via* flash chromatography (silica gel, gradient, 10-15 % acetone in toluene + 1 % triethylamine) to give the product **87** (0.082 g, 0.162 mmol, 79 %) as an isomeric mixture (E/Z = 86:14). Subsequent preparative HPLC purification provided the E-isomer exclusively (RP C18, gradient 50-90 % CH_3CN in water with 0.1 % TFA, 40 min, 25 mL/min).

R_f = 0.39 (silica gel, 20 % acetone in toluene + 1 % triethylamine); $^1\text{H NMR}$ (500 MHz, CDCl_3) δ 7.67-7.79 (m, 4H), 7.54 (ddd, J = 1.6, 8.8, 9.1 Hz, 1H), 7.41-7.47 (m, 2H), 6.98 (brs, 1H), 6.57 (d, J

= 15.8 Hz, 1H), 6.19 (dd, $J = 6.0, 15.8$ Hz, 1H), 4.67-4.91 (m, 2H), 4.79 (ddd, $J = 5.3, 8.1, 8.1$ Hz, 1H), 3.53-3.84 (m, 2H), 2.80 (s, 3H), 1.91-2.24 (m, 4H), 1.59-1.82 (m, 2H), 1.47 (s, 9H), 1.32-1.42 (m, 2H), 1.35 (d, $J = 7.2$ Hz, 3H), 0.92-0.98 (m, 3H); ^{13}C NMR (100 MHz, CDCl_3) δ 171.8, 171.2, 156.2, 134.2, 133.7, 133.1, 130.5, 128.9, 128.3, 128.1, 127.8, 126.9, 126.4, 126.0, 123.7, 80.9, 58.9, 50.9, 50.7, 47.2, 34.9, 33.1, 30.8, 28.5, 24.2, 18.8, 14.0, 13.6; **ESI-LRMS** m/z calcd for $\text{C}_{30}\text{H}_{41}\text{N}_3\text{O}_4[\text{M}+\text{Na}]^+$: 530.3 Found: 530.3.

(2S)-2-(methylamino)-N-[(2S)-1-[(2S)-2-[(E)-2-(naphthalen-2-yl)ethenyl]pyrrolidin-1-yl]-1-oxopentan-2-yl]propanamide hydrochloride [88]. ^1H NMR (500 MHz, d-DMSO) δ 8.47 (d, $J = 7.7$ Hz, 2H), 8.39 (d, $J = 7.8$ Hz, 1H), 7.84-7.87 (m, 4H), 7.78 (s, 1H), 7.64 (dd, $J = 1.4, 8.5$ Hz, 1H), 7.46-7.51 (m, 2H), 6.50 (d, $J = 15.9$ Hz, 1H), 6.36 (dd, $J = 5.8, 15.8$ Hz, 1H), 4.63-4.71 (m, 1H), 4.59 (ddd, $J = 4.7, 8.3, 8.3$ Hz, 1H), 3.65-3.67 (m, 1H), 3.49-3.53 (m, 2H), 2.38 (s, 3H), 1.52-2.03 (m, 6H), 1.27 (d, $J = 6.8$ Hz, 3H), 1.21-1.41 (m, 3H), 0.92 (ddd, $J = 7.4, 7.4, 9.9$ Hz, 3H); **ESI-LRMS** m/z calcd for $\text{C}_{25}\text{H}_{34}\text{N}_3\text{O}_2[\text{M}+\text{H}]^+$: 408.3 Found: 408.3.



[tert-butylN-[(1S)-1-[[2S)-1-[(2S)-2-[(Z)-2-iodoethenyl]pyrrolidin-1-yl]-1-oxopentan-2-yl]carbamoyl]ethyl]-N-methylcarbamate [89]. Vinyl iodide **89** was prepared *via* a modified version of the procedure reported by Oshima.²² A round bottom containing indium(III) chloride (0.094 g, 0.427 mmol, 1.35 equiv.) was placed under vacuum (1.2 mmHg) and heated in bursts using a heat gun for 2 minutes. Upon cooling, anhydrous THF (2 mL) was added and the mixture was cooled to -78°C . 1M Diisobutylaluminum hydride in hexanes (0.41 mL, 0.411 mmol, 1.30 equiv.) was added dropwise and the dark brown suspension was allowed to stir 30 minutes. Alkyne **67** (0.120 g, 0.316 mmol, 1.00 equiv.) and triethylborane (0.063 mL, 0.0632 mmol, 0.2

equiv.) were added and the flask contents were allowed to stir for 2.5 hours at -78 °C. In a dry vial, iodine (0.481 g, 1.90 mmol, 6.00 equiv.) was dissolved in 1 mL THF and cannulated into the reaction mixture. After 30 minutes the reaction mixture was poured into a separatory funnel containing saturated aqueous sodium bicarbonate (10 mL), 50 mL 60 % aqueous sodium thiosulfate was added and the aqueous phase was extracted with diethyl ether (75 mL). The organic phase was dried with sodium sulfate, filtered and concentrated *in-vacuo* to provide a colourless oil which was purified by flash chromatography to give the (Z)-vinyl iodide **89** (0.149 g, 0.294 mmol) as a colourless oil in 93 % yield (E/Z = 96:4).

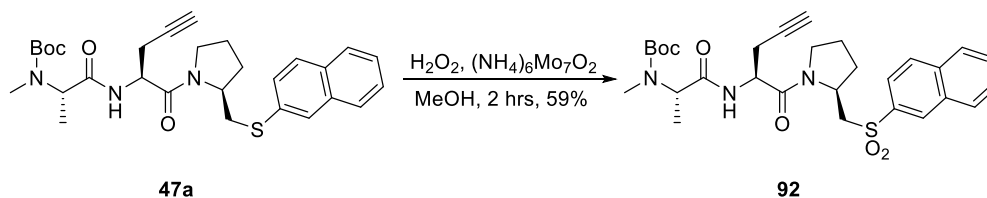
R_f = 0.24 (silica gel, 60 % ethyl acetate in hexanes + 1 % triethylamine); $^1\text{H NMR}$ (400 MHz, CDCl_3) δ 6.67 (brs, 1H), 6.28 (dd, 1.1, 7.7 Hz, 1H), 6.08 (dd, 7.6, 7.7 Hz, 1H), 4.49-4.71 (m, 3H), 3.48-3.56 (m, 2H), 2.73 (s, 3H), 2.15-2.27 (m, 1H), 1.78-1.98 (m, 2H), 1.48-1.69 (m, 2H), 1.43 (s, 9H), 1.25-1.39 (m, 5H), 0.85-0.90 (m, 3H); $^{13}\text{C NMR}$ (100 MHz, CDCl_3) δ 171.0, 170.6, 156.0, 141.4, 83.5, 80.6, 61.8, 50.7, 50.5, 47.5, 35.2, 33.2, 30.6, 28.4, 25.0, 18.6, 14.1, 13.9; **ESI-LRMS** m/z calcd for $\text{C}_{20}\text{H}_{34}\text{IN}_3\text{O}_4[\text{M}+\text{Na}]^+$: 530.1 Found: 530.0.

tert-butyl N-methyl-N-[(1S)-1-[[[(2S)-1-[(2S)-2-[(Z)-2-(naphthalen-2-yl)ethenyl]pyrrolidin-1-yl]-1-oxopentan-2-yl]carbamoyl]ethyl]carbamate [90]. Compound **90** was prepared using a modified version of the procedure reported by Stoltz.²³ Naphthalene-2-boronic acid (0.0854 g, 0.497 mmol, 2.00 equiv.) and tetrakis(triphenylphosphine)palladium (0.029 g, 0.0248 mmol, 0.10 equiv.) were added to a flame dried round bottom flask. The flask was evacuated and backfilled with argon three times before a degassed mixture of toluene, methanol and 2 M K_2CO_3 (5:1:0.125 mL respectively) containing vinyl iodide **89** (0.126 g, 0.248 mmol, 1.00 equiv.) was cannulated over. The yellow mixture was stirred at 70 °C for 2.5 hours before being poured into a separatory funnel containing a 60 mL saturated aqueous sodium chloride. The aqueous layer was extracted with dichloromethane (2 x 50 mL), the combined organic extracts were dried with sodium sulfate, filtered and concentrated under reduced pressure. The resulting orange resin was purified using flash chromatography (silica gel, 20 % acetone in toluene + 1 % triethylamine) to give product **90**

(0.0621 g, 0.122 mmol, 49 % yield). Preparative HPLC purification furnished the Z-alkene exclusively (RP C18, gradient 50-90 % CH₃CN in water with 0.1 % TFA, 40 min, 25 mL/min).

R_f = 0.46 (silica gel, 3 % methanol in dichloromethane); ¹H NMR (400 MHz, CDCl₃) δ 7.73-7.85 (m, 4H), 7.43-7.50 (m, 3H), 6.85 (brs, 1H), 6.63 (d, J = 11.6 Hz, 1H), 5.55 (dd, J = 9.0, 11.6 Hz, 1H), 4.53-5.15 (m, 3H), 3.53-3.66 (m, 2H), 2.76 (s, 3H), 1.57-2.46 (m, 5H), 1.45 (s, 9H), 1.10-1.41 (m, 3H), 1.31 (d, J = 7.1 Hz, 3H), 0.95 (t, J = 7.2 Hz, 3H); ¹³C NMR (100 MHz, CDCl₃) δ 171.4, 170.9, 156.0, 134.5, 133.2, 133.1, 132.5, 132.3, 131.1, 128.2, 127.9, 127.7, 126.4, 126.2, 80.7, 56.0, 50.8, 50.6, 47.5, 35.2, 32.5, 30.4, 28.5, 25.0, 18.8, 14.0, 13.3; ESI-MS m/z calcd for C₃₀H₄₁N₃O₄[M+Na]⁺: 530.2995 Found: 530.3012.

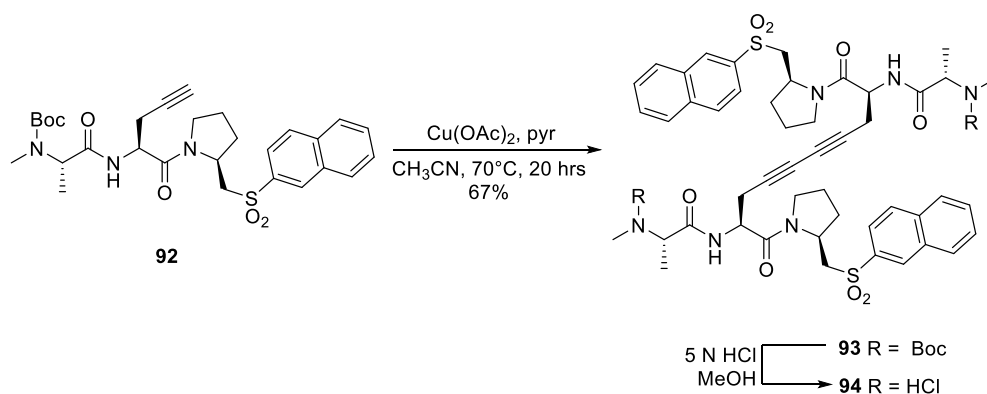
(2S)-2-(methylamino)-N-[(2S)-1-[(2S)-2-[(Z)-2-(naphthalen-2-yl)ethenyl]pyrrolidin-1-yl]-1-oxopentan-2-yl]propanamide hydrochloride [91]. ¹H NMR (400 MHz, d-DMSO) δ 9.14 (brs, 2H), 8.72 (d, J = 7.3, 1H), 7.81-7.96 (m, 4H), 7.45-7.63 (m, 3H), 6.53 (d, J = 11.8 Hz, 1H), 5.60 (dd, J = 9.1, 11.7 Hz, 1H), 5.01 (ddd, J = 4.5, 8.4, 8.4 Hz, 1H), 4.52 (ddd, J = 5.1, 8.0, 8.0 Hz, 1H), 3.60-3.81 (m, 2H), 3.41-3.47 (m, 1H), 2.44 (s, 3H), 1.50-2.25 (m, 5H), 1.31 (d, J = 6.9 Hz, 3H), 1.13-1.43 (m, 2H), 0.91 (t, J = 7.4 Hz, 3H); ¹³C NMR (100 MHz, d-DMSO) δ 169.9, 168.2, 134.3, 133.4, 132.9, 131.8, 128.0, 127.9, 127.6, 127.4, 127.3, 127.1, 126.2, 126.0, 55.9, 54.9, 50.7, 46.5, 33.8, 33.4, 30.7, 24.5, 18.4, 15.7, 13.7; ESI-MS m/z calcd for C₂₅H₃₄N₃O₂[M+Na]⁺: 408.3 Found: 408.1.



tert-butyl N-methyl-N-[(1S)-1-[(2S)-1-[(2S)-2-[(naphthalene-2-sulfonyl)methyl]pyrrolidin-1-yl]-1-oxopent-4-yn-2-yl]carbamoyl]ethyl]carbamate [92]. **92** was prepared according to a modified version of the procedure reported by Chand.²⁴ A 1 dram vial equipped with a stir bar was charged with aryl sulfide **47a** (0.0771 g, 0.147 mmol, 1.00 equiv.), ammonium

heptamolybdate tetrahydrate (0.018 g, 0.0147 mmol, 0.10 equiv.) and methanol (0.4 M). A solution of 30 % aqueous hydrogen peroxide (60 μ L, 0.589 mmol, 4.00 equiv.) was added and the mixture was stirred vigorously at room temperature for 2 hours. Solvent was removed under a stream of air and the residue was partitioned between ethyl acetate (50 mL) and saturated aqueous sodium bicarbonate (25 mL). The organic layer was washed with water (25 mL), brine (30 mL) then dried with sodium sulfate and concentrated *in-vacuo*. Sulfone **92** (0.0481 g, 0.0866 mmol, 59 % yield) was isolated following flash chromatography of the crude residue (silica gel, 10 % acetone in dichloromethane + 1 % triethylamine).

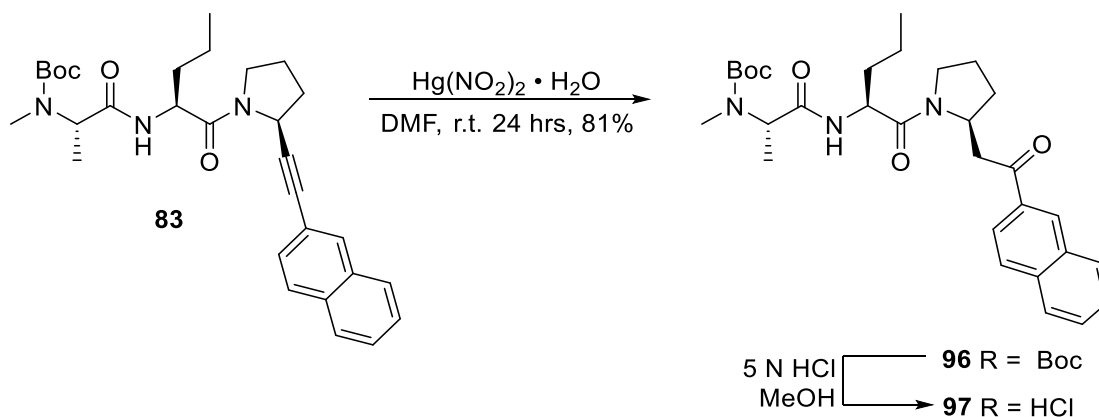
R_f = 0.53 (silica gel, 15 % acetone in dichloromethane + 1% triethylamine); $^1\text{H NMR}$ (400 MHz, CDCl_3) δ 8.49 (s, 1H), 8.00 (t, J = 8.8 Hz, 2H), 7.90 (ddd, J = 1.8, 8.7 9.2 Hz, 2H), 7.59-7.67 (m, 2H), 6.75 (d, J = 4.6 Hz, 1H), 4.76 (q, J = 7.0 Hz, 1H), 4.17-4.72 (m, 2H), 3.91 (dd, J = 2.5, 13.8 Hz, 1H), 3.54-3.65 (m, 2H), 3.09 (dd, J = 10.2, 13.8 Hz, 1H), 2.72 (s, 3H), 2.51-2.58 (m, 3H), 2.30-2.38 (m, 1H), 1.89-2.08 (m, 3H), 1.41 (s, 9H), 1.26 (d, J = 7.1 Hz, 3H); $^{13}\text{C NMR}$ (100 MHz, CDCl_3) δ 171.1, 168.6, 155.9, 136.5, 135.5, 132.2, 129.9, 129.8, 129.6, 129.4, 128.1, 127.8, 122.6, 80.8, 78.6, 71.1, 56.5, 53.2, 49.3, 47.3, 46.3, 30.2, 29.3, 28.4, 24.3, 22.7, 11.5; **ESI-LRMS** m/z calcd for $\text{C}_{29}\text{H}_{37}\text{N}_3\text{O}_6\text{S}[\text{M}+\text{Na}]^+$: 578.2 Found: 578.2.



tert-butyl N-[(1S)-1-[[[(2S,9S)-9-[(2S)-2-[[[(tert-butoxy)carbonyl](methyl)amino]propanamido]-1,10-bis[(2S)-2-[(naphthalene-2-sulfonyl)methyl]pyrrolidin-1-yl]-1,10-dioxodeca-4,6-diyn-2-yl]carbamoyl]ethyl]-N-methylcarbamate [93]. See preparation of **60**.

$R_f = 0.26$ (silica gel, 90 % ethyl acetate in hexanes + 1% triethylamine; $^1\text{H NMR}$ (400 MHz, CDCl_3) δ 8.51 (d, $J = 0.8$ Hz, 1H), 8.02 (m, 2H), 7.93 (d, $J = 7.8$ Hz, 1H), 7.89 (dd, $J = 1.7, 8.7$ Hz, 1H), 7.60-7.69 (m, 2H), 6.74 (d, $J = 5.2$ Hz, 1H), 4.75 (q, $J = 7.0$ Hz, 1H), 4.24-4.61 (m, 2H), 3.89 (dd, $J = 2.4, 13.9$ Hz, 1H), 3.50-3.63 (m, 2H), 3.18 (dd, $J = 10.3, 13.9$ Hz, 1H), 2.73 (s, 3H), 2.43-2.62 (m, 2H), 2.29-2.37 (m, 1H), 1.87-2.16 (m, 3H), 1.42 (s, 9H), 1.28 (d, $J = 7.1$ Hz, 3H); $^{13}\text{C NMR}$ (75 MHz, CDCl_3) δ 171.2, 168.3, 156.4, 136.4, 135.5, 132.3, 129.9, 129.8, 129.7, 129.4, 128.2, 127.8, 122.7, 80.7, 73.1, 67.4, 56.3, 53.3, 49.3, 47.3, 46.0, 30.3, 29.3, 28.4, 24.4, 23.6, 13.7; **ESI-LRMS** m/z calcd for $\text{C}_{58}\text{H}_{72}\text{N}_6\text{O}_{12}\text{S}_2[\text{M}+\text{Na}]^+$: 1131.4 Found: 1131.3.

(2S)-2-(methylamino)-N-[(2S,9S)-9-[(2S)-2-(methylamino)propanamido]-1,10-bis[(2S)-2-[(naphthalene-2-sulfonyl)methyl]pyrrolidin-1-yl]-1,10-dioxodeca-4,6-diyne-2-yl]propanamide dihydrochloride [94]. $^1\text{H NMR}$ (400 MHz, d-DMSO) δ 8.80-9.01 (m, 3H), 8.59 (d, 2.7 Hz, 1H), 8.17-8.25 (m, 2H), 8.07-8.11 (m, 1H), 7.89 (dd, $J = 1.6, 8.4$ Hz, 1H), 7.69-7.78 (m, 2H), 4.57-4.65 (m, 1H), 3.14-4.18 (m, 6H), 2.54-2.76 (m, 2H), 2.47 (t, $J = 5.1$ Hz, 3H), 1.82-2.01 (m, 4H), 1.26-1.32 (m, 3H); $^{13}\text{C NMR}$ (100 MHz, d-DMSO) δ 168.4, 167.0, 136.3, 134.9, 131.7, 129.7, 129.6, 129.5, 129.3, 128.0, 127.8, 122.6, 74.5, 66.3, 55.9, 55.8, 52.4, 49.6, 46.1, 30.8, 28.7, 23.5, 15.7, 15.4; **ESI-LRMS** m/z calcd for $\text{C}_{48}\text{H}_{56}\text{N}_6\text{O}_8\text{S}_2[\text{M}+\text{Na}]^+$: 931.3 Found: 931.2.

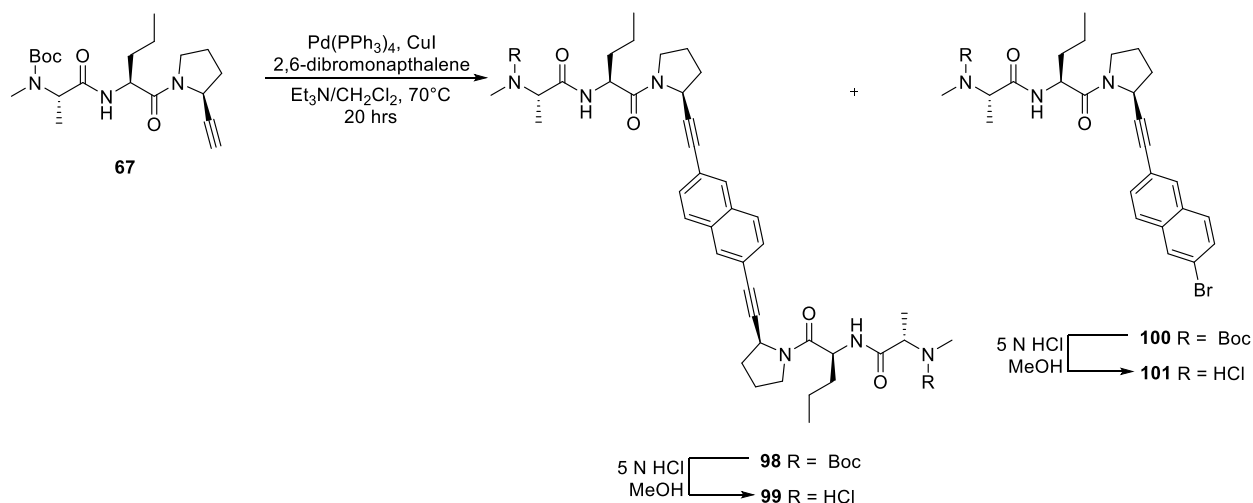


tert-butyl N-methyl-N-[(1S)-1-[(2S)-1-[(2S)-2-[2-(naphthalen-2-yl)-2-oxoethyl]pyrrolidin-1-yl]-1-oxopentan-2-yl]carbamoyl]ethyl]carbamate [96]. Prepared using a modified procedure of that reported by Jung.²⁵ A dry flask was charged with starting material **83** (0.0775 g, 0.153 mmol,

1.00 equiv.) dissolved in 1.5 mL anhydrous DMF. Mercuric nitrate monohydrate (0.105 g, 0.307 mmol, 2.00 equiv.) was added in two portions and the reaction was allowed to stir under argon for 24 hours at room temperature. The mixture was diluted with water (30 mL) and extracted with ethyl acetate (3 x 40 mL). The combined organic extracts were washed with water, brine, dried with sodium sulfate and concentrated *in-vacuo*. Flash chromatography (silica gel, 20 % acetone in toluene + 1 % triethylamine) gave **96** (0.048 g, 0.0917 mmol) in 81 % yield.

R_f = 0.36 (silica gel, 20 % acetone in toluene + 1% triethylamine); $^1\text{H NMR}$ (400 MHz, CDCl_3) δ 8.64 (s, 1H), 8.06 (dd, J = 1.7, 8.6 Hz, 1H), 8.00 (d, J = 8.0 Hz, 1H), 7.84-7.89 (m, 2H), 7.52-7.61 (m, 2H), 6.75 (brs, 1H), 4.73 (ddd, J = 5.2, 8.0, 8.0 Hz, 1H), 4.58-4.63 (m, 2H), 3.85 (dd, J = 3.3, 14.8 Hz, 1H), 3.67-3.74 (m, 1H), 3.54-3.60 (m, 1H), 2.91 (dd, J = 9.8, 14.8 Hz, 1H), 2.79 (s, 3H), 1.86-2.12 (m, 4H), 1.52-1.74 (m, 2H), 1.49 (s, 9H), 1.33 (d, J = 7.1 Hz, 3H), 1.29-1.37 (m, 2H), 0.92 (t, J = 7.3 Hz, 3H); $^{13}\text{C NMR}$ (100 MHz, CDCl_3) δ 198.6, 171.2, 170.8, 156.2, 135.8, 134.0, 132.7, 130.6, 129.9, 128.6, 128.5, 127.8, 126.8, 124.0, 80.7, 55.2, 54.2, 50.6, 47.2, 42.3, 35.2, 30.2, 29.7, 28.5, 24.4, 18.7, 14.0, 13.9; **ESI-LRMS** m/z calcd for $\text{C}_{30}\text{H}_{41}\text{N}_3\text{O}_5[\text{M}+\text{Na}]^+$: 546.3 Found: 546.2.

(2S)-2-(methylamino)-N-[(2S)-1-[(2S)-2-[2-(naphthalen-2-yl)-2-oxoethyl]pyrrolidin-1-yl]-1-oxopentan-2-yl]propanamide hydrochloride [97]. $^1\text{H NMR}$ (400 MHz, d-DMSO) δ 8.70-8.91 (m, 4H), 7.99-8.12 (m, 4H), 7.60-7.70 (m, 2H), 4.45-4.53 (m, 2H), 3.47-3.82 (m, 3H), 3.50 (dd, J = 4.0, 15.9 Hz, 1H), 3.20 (dd, J = 9.0, 15.9 Hz), 2.49 (s, 3H), 1.33 (d, J = 6.9 Hz, 3H), 1.24-2.09 (m, 8H), 0.85-0.91 (m, 3H); $^{13}\text{C NMR}$ (100 MHz, d-DMSO) δ 198.42, 169.5, 168.4, 135.1, 134.0, 132.2, 130.0, 129.6, 128.7, 128.3, 127.7, 126.9, 123.6, 55.9, 54.2, 50.7, 46.4, 41.6, 33.2, 30.7, 29.6, 23.7, 18.5, 15.6, 13.6; **ESI-LRMS** m/z calcd for $\text{C}_{25}\text{H}_{34}\text{N}_3\text{O}_3[\text{M}+\text{H}]^+$: 424.3 Found: 424.1.



tert-butylN-[(1S)-1-[(2S)-1-[(2S)-2-[2-(6-{2-[(2S)-1-[(2S)-2-[(2S)-2-[(tert-butoxy)carbonyl](methyl)amino]propanamido]pentanoyl]pyrrolidin-2-yl]ethynyl]naphthalen-2-yl)ethynyl]pyrrolidin-1-yl]-1-oxopentan-2-yl]carbamoyl]ethyl]-N-methylcarbamate [98]. Compounds **98/100** were prepared using a modified version of the procedure reported by Caldarelli.¹¹ A flame dried round bottom flask was charged with 2,6-dibromonaphthalene (0.0663 g, 0.232 mmol, 1.00 equiv.), Copper(I) iodide (0.0044 g, 0.023 mmol, 0.10 equiv.) and tetrakis(triphenylphosphine)palladium (0.0134 g, 0.0116 mmol, 0.05 equiv.). The flask was evacuated and backfilled with argon three times before a solution of **67** (0.220 g, 0.580 mmol, 2.50 equiv.) dissolved in 3:1 triethylamine/dichloromethane (0.1 M, degassed) was cannulated over. The flask was fitted with a condenser and heated to 70°C for 20 hours. The reaction mixture was transferred to a separatory funnel containing 50 mL saturated aqueous ammonium chloride and extracted with ethyl acetate (3 x 40 mL). The combined organic extracts were washed with water, brine, dried with sodium sulfate and concentrated under reduced pressure to provide a yellow residue which was subjected to flash chromatography (silica gel, 20 % acetone in dichloromethane + 1 % triethylamine). Dimer **98** (0.097 g, 0.110 mmol) and monomer **100** (0.052 g, 0.0892 mmol) were isolated in 47 % and 38 % yields respectively.

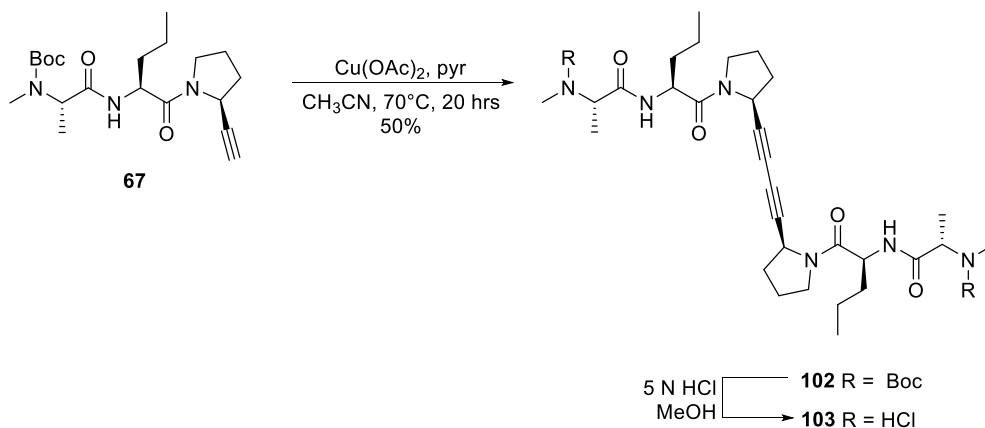
$R_f = 0.32$ (silica gel, 20 % acetone in dichloromethane + 1 % triethylamine); $^1\text{H NMR}$ (400 MHz, CDCl_3) δ 7.82 (s, 1H), 7.62-7.68 (m, 1H), 7.38 (d, $J = 8.4$ Hz, 1H), 6.74 (brs, 1H), 5.03-5.06 (m, 1H), 4.81 (dd, $J = 2.7, 6.3$ Hz, 1H), 4.69-4.74 (m, 1H), 3.41-3.75 (m, 2H), 2.78 (s, 3H), 1.99-2.32 (m, 4H),

1.56-1.81 (m, 2H), 1.48 (s, 9H), 1.32 (d, $J = 7.1$ Hz, 3H), 1.24-1.42 (m, 2H), 0.90-0.96 (m, 3H); ^{13}C NMR (100 MHz, CDCl_3) δ 171.2 170.3, 156.4, 132.2, 131.4, 129.3, 127.8, 127.6, 121.1, 89.5, 82.3, 80.7, 50.5, 49.1, 48.5, 46.4, 35.0, 32.3, 30.2, 28.5, 25.1, 18.5, 14.1, 14.0; ESI-LRMS m/z calcd for $\text{C}_{50}\text{H}_{70}\text{N}_6\text{O}_8[\text{M}+\text{Na}]^+$: 905.5 Found: 905.4.

tert-butyl N-[(1S)-1-[(2S)-1-[(2S)-2-[2-(6-bromonaphthalen-2-yl)ethynyl]pyrrolidin-1-yl]-1-oxopentan-2-yl]carbamoyl]ethyl]-N-methylcarbamate [100]. $R_f = 0.5$ (silica gel, 20 % acetone in dichloromethane + 1 % triethylamine), ^1H NMR (400 MHz, CDCl_3) δ 7.94 (d, $J = 0.9$, 1H), 7.84 (s, 1H), 7.64 (dd, $J = 3.1, 8.6$ Hz, 1H), 7.61 (d, $J = 9.7$ Hz, 1H), 7.53 (dd, $J = 1.9, 8.8$ Hz, 1H), 7.42 (dd, $J = 1.6, 8.5$ Hz, 1H), 6.76 (brs, 1H), 5.05 (dd, $J = 4.8, 5.8$ Hz, 1H), 4.72 (ddd, $J = 5.6, 7.8, 7.8$ Hz, 1H), 3.36-3.72 (m, 2H), 2.79 (s, 3H), 2.26-2.31 (m, 1H), 2.07-2.18 (m, 2H), 1.99-2.01 (m, 1H), 1.63-1.82 (m, 2H), 1.48 (s, 9H), 1.40 (q, $J = 7.5$ Hz, 2H), 1.33 (d, $J = 7.2$ Hz, 3H), 0.93 (t, $J = 7.5$ Hz, 3H); ^{13}C NMR (400 MHz, CDCl_3) δ 171.1, 170.2, 156.2, 133.7, 132.2, 131.4, 129.9, 129.8, 129.6, 129.2, 126.9, 120.8, 120.6, 89.4, 82.0, 80.6, 50.4, 49.0, 48.4, 46.3, 34.9, 32.2, 30.1, 28.4, 25.1, 18.4, 13.9, 13.8; ESI-LRMS m/z calcd for $\text{C}_{30}\text{H}_{38}\text{BrN}_3\text{O}_4[\text{M}+\text{Na}]^+$: 608.2 Found: 608.1.

(2S)-2-(methylamino)-N-[(2S)-1-[(2S)-2-[2-(6-{2-[(2S)-1-[(2S)-2-[(2S)-2-(methylamino)propanamido]pentanoyl]pyrrolidin-2-yl]ethynyl}naphthalen-2-yl)ethynyl]pyrrolidin-1-yl]-1-oxopentan-2-yl]propanamide dihydrochloride [99]. ^1H NMR (400 MHz, $d\text{-DMSO}$) δ 8.96 (brs, 2H), 8.80 (d, $J = 7.5$ Hz, 1H), 7.96 (s, 1H), 7.86-7.91 (m, 1H), 7.42 (dd, $J = 1.4, 8.5$ Hz, 1H), 4.90 (dd, $J = 2.2, 7.2$ Hz, 1H), 4.53 (q, $J = 7.8$ Hz, 1H), 3.83-3.91 (m, 1H), 3.68 (d, $J = 4.9$ Hz, 1H), 3.30-3.56 (m, 1H), 2.51 (s, 3H), 2.00-2.33 (m, 4H), 1.56-1.72 (m, 2H), 1.33-1.44 (m, 2H), 1.35 (d, $J = 6.9$ Hz, 1H), 0.88-0.95 (m, 3H); ^{13}C NMR (400 MHz, $d\text{-DMSO}$) δ 169.3, 168.4, 131.8, 131.2, 130.8, 128.9, 128.1, 91.0, 81.2, 55.9, 50.6, 47.9, 46.0, 33.2, 31.8, 30.7, 24.8, 18.3, 15.7, 13.6; ESI-LRMS m/z calcd for $\text{C}_{40}\text{H}_{54}\text{N}_6\text{O}_4[\text{M}+\text{Na}]^+$: 705.4 Found: 705.1.

(2S)-N-[(2S)-1-[(2S)-2-[2-(6-bromonaphthalen-2-yl)ethynyl]pyrrolidin-1-yl]-1-oxopentan-2-yl]-2-(methylamino)propanamide hydrochloride [101]. $^1\text{H NMR}$ (400 MHz, d-DMSO) δ 8.95 (brs, 2H), 8.81 (d, $J = 7.6$ Hz, 1H), 8.22 (d, $J = 1.8$ Hz, 1H), 7.99 (s, 1H), 7.88 (dt, $J = 2.9, 8.6$ Hz, 2H), 7.66-7.69 (m, 2H), 7.45 (dd, $J = 1.6, 8.5$ Hz, 1H), 4.90 (dd, $J = 2.4, 7.4$ Hz, 1H), 4.54 (ddd, $J = 5.8, 7.9$ Hz, 1H), 3.83-3.91 (m, 1H), 3.65-3.69 (m, 1H), 3.30-3.57 (m, 1H), 2.51 (s, 3H), 1.92-2.37 (m, 4H), 1.57-1.73 (m, 2H), 1.36 (d, $J = 6.9$ Hz, 3H), 1.33-1.47 (m, 2H), 0.88-0.95 (m, 3H); $^{13}\text{C NMR}$ (100 MHz, d-DMSO) δ 169.3, 168.4, 133.4, 131.4, 131.1, 131.0, 129.9, 129.8, 129.6, 129.5, 129.2, 127.5, 90.9, 81.1, 55.9, 50.6, 47.9, 46.0, 33.2, 31.8, 30.7, 24.8, 18.3, 15.7, 13.6; **ESI-LRMS** m/z calcd for $\text{C}_{25}\text{H}_{30}\text{BrN}_3\text{O}_2[\text{M}+\text{H}]^+$: 484.2 Found: 484.0.



tert-butyl-N-[(1S)-1-[[[(2S)-1-[(2S)-2-{4-[(2S)-1-[(2S)-2-[(2S)-2-[[tert-butoxy)carbonyl](methyl)amino]propanamido]pentanoyl]pyrrolidin-2-yl]buta-1,3-diyne-1-yl]pyrrolidin-1-yl]-1-oxopentan-2-yl]carbonyl]ethyl]-N-methylcarbamate [102]. Prepared using a modified version of the procedure reported by Hennessey.⁹ A round bottom flask was equipped with a stir bar and charged with starting alkyne **67** (0.0411 g, 0.108 mmol, 1.00 equiv.) dissolved in acetonitrile (3 mL). Copper(II) acetate (0.025 g, 0.1245 mmol, 1.15 equiv.) and pyridine (50 μL , 0.650 mmol, 6.00 equiv.) were added and the reaction was allowed to stir at 70 $^\circ\text{C}$ overnight. The flask contents were transferred to a separatory funnel, diluted with ethyl acetate (50 mL) and washed with a 40 mL volume of 50 % aqueous ammonium hydroxide. The aqueous phase was back-extracted with ethyl acetate (2 x 25 mL) and the combined organic

extracts were dried with sodium sulfate, filtered and concentrated *in-vacuo*. Flash chromatography (silica gel, 95 % ethyl acetate in hexanes + 1 % triethylamine) gave the bis-alkyne dimer **102** (0.0201 g, 0.0266 mmol) in 50 % yield.

R_f = 0.22 (silica gel, 4 % methanol in dichloromethane); $^1\text{H NMR}$ (500 MHz, CDCl_3) δ 6.71 (brs, 1H), 4.61-4.80 (m, 3H), 3.54-3.65 (m, 2H), 2.77 (s, 3H), 2.01-2.20 (m, 4H), 1.66-1.73 (m, 1H), 1.52-1.61 (m, 1H), 1.47 (s, 9H), 1.32-1.39 (m, 2H), 1.30 (d, J = 7.2 Hz, 3H), 0.87-0.93 (m, 3H); $^{13}\text{C NMR}$ (125 Hz, CDCl_3) δ 171.3, 170.4, 156.2, 80.7, 66.7, 50.4, 48.9, 48.3, 46.3, 35.0, 31.9, 30.2, 28.5, 25.1, 18.7, 14.0, 13.7; **ESI-LRMS** m/z calcd for $\text{C}_{40}\text{H}_{64}\text{N}_6\text{O}_8[\text{M}+\text{Na}]^+$: 779.5 Found: 779.3.

(2S)-2-(methylamino)-N-[(2S)-1-[(2S)-2-{4-[(2S)-1-[(2S)-2-[(2S)-2-(methylamino)propanamido]pentanoyl]pyrrolidin-2-yl]buta-1,3-diyne-1-yl}pyrrolidin-1-yl]-1-oxopentan-2-yl]propanamide dihydrochloride [103]. $^1\text{H NMR}$ (400 MHz, $d\text{-DMSO}$) δ 9.10 (brs, 2H), 8.79 (d, J = 7.5 Hz, 1H), 4.66-4.69 (m, 1H), 4.43-4.48 (m, 1H), 3.79 (q, J = 3.79 Hz, 1H), 3.56-3.59 (m, 2H), 2.44 (s, 3H), 1.88-2.06 (m, 4H), 1.53-1.63 (m, 2H), 1.34 (d, J = 6.8 Hz, 3H), 1.26-1.37 (m, 2H), 0.89 (t, J = 7.3 Hz, 1H); $^{13}\text{C NMR}$ (100 MHz, $d\text{-DMSO}$) δ 169.6, 168.6, 79.2, 65.6, 56.0, 50.6, 47.7, 46.0, 33.1, 31.5, 30.8, 25.0, 18.5, 15.9, 13.7; **ESI-LRMS** m/z calcd for $\text{C}_{30}\text{H}_{49}\text{N}_6\text{O}_4[\text{M}+\text{H}]^+$: 557.4 Found: 557.1.

References

1. Andrushchenko, V. V.; Vogel, H. J.; Prenner, E. J., Optimization of the hydrochloric acid concentration used for trifluoroacetate removal from synthetic peptides. *Journal of Peptide Science* **2007**, *13* (1), 37-43.
2. Zhao, D.; Kuethe, J. T.; Journet, M.; Peng, Z.; Humphrey, G. R., Efficient and Practical Synthesis of (R)-2-Methylpyrrolidine. *The Journal of Organic Chemistry* **2006**, *71* (11), 4336-4338.
3. Reed, P. E.; Katzenellenbogen, J. A., Synthesis of proline-valine pseudodipeptide enol lactones, serine protease inhibitors. *The Journal of Organic Chemistry* **1991**, *56* (8), 2624-2634.
4. Paleo, M. R.; Calaza, M. I.; Graña, P.; Sardina, F. J., Stanna-Brook Rearrangement of Carboxylic Acid Derivatives. Synthetic Utility and Mechanistic Studies. *Organic Letters* **2004**, *6* (6), 1061-1063.
5. Perrone, A. D. a. D., SYNTHESIS OF 1,1-DIMETHYLETHYL (S)-4-FORMYL-2,2-DIMETHYL-3-OXAZOLIDINECARBOXYLATE BY OXIDATION OF THE ALCOHOL. *Organic Syntheses* **2000**, *77*, 64.

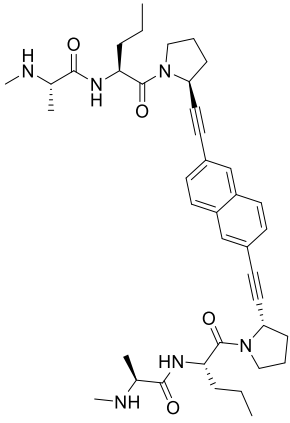
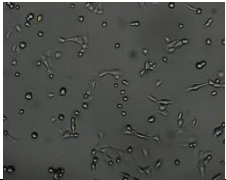
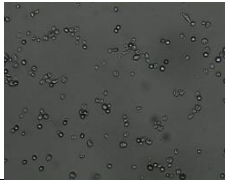
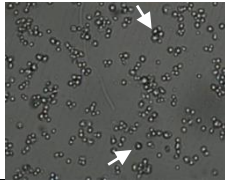
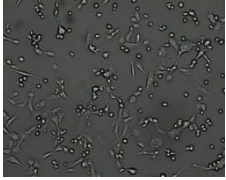
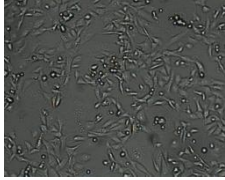
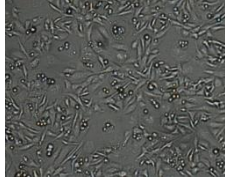
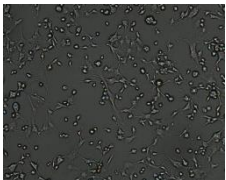
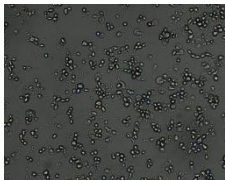
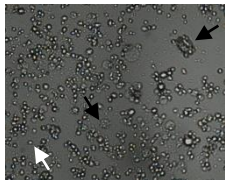
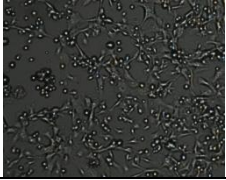
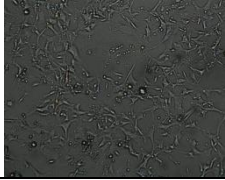
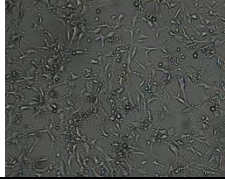
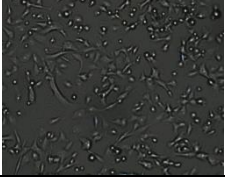
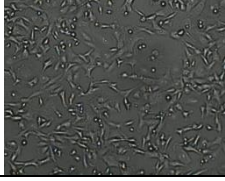
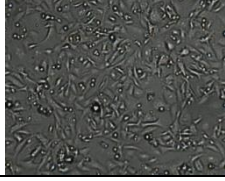
6. Malkov, A. V.; Stončius, S.; MacDougall, K. N.; Mariani, A.; McGeoch, G. D.; Kočovský, P., Formamides derived from N-methyl amino acids serve as new chiral organocatalysts in the enantioselective reduction of aromatic ketimines with trichlorosilane. *Tetrahedron* **2006**, *62* (2–3), 264-284.
7. Syu, S.-e.; Kao, T.-T.; Lin, W., A new type of organocatalyst for highly stereoselective Michael addition of ketones to nitroolefins on water. *Tetrahedron* **2010**, *66* (4), 891-897.
8. Siedlecka, R.; Skarzewski, J., Synthesis of Homochiral N-Protected β -Amino Sulfoxides from α -Amino Alcohols. *Synlett* **1996**, *1996* (08), 757-758.
9. Hennessy, E. J.; Adam, A.; Aquila, B. M.; Castriotta, L. M.; Cook, D.; Hattersley, M.; Hird, A. W.; Huntington, C.; Kamhi, V. M.; Laing, N. M.; Li, D.; MacIntyre, T.; Omer, C. A.; Oza, V.; Patterson, T.; Repik, G.; Rooney, M. T.; Saeh, J. C.; Sha, L.; Vasbinder, M. M.; Wang, H.; Whitston, D., Discovery of a Novel Class of Dimeric Smac Mimetics as Potent IAP Antagonists Resulting in a Clinical Candidate for the Treatment of Cancer (AZD5582). *Journal of Medicinal Chemistry* **2013**, *56* (24), 9897-9919.
10. Usuki, T.; Yamada, H.; Hayashi, T.; Yanuma, H.; Koseki, Y.; Suzuki, N.; Masuyama, Y.; Lin, Y. Y., Total synthesis of COPD biomarker desmosine that crosslinks elastin. *Chemical Communications* **2012**, *48* (26), 3233-3235.
11. Caldarelli, S. A.; El Fangour, S.; Wein, S.; Tran van Ba, C.; Périgaud, C.; Pellet, A.; Vial, H. J.; Peyrottes, S., New Bis-thiazolium Analogues as Potential Antimalarial Agents: Design, Synthesis, and Biological Evaluation. *Journal of Medicinal Chemistry* **2013**, *56* (2), 496-509.
12. Katritzky, A.; Widyan, K.; Gyanda, K., Synthesis of Sulfonyl Azides. *Synthesis* **2008**, *2008* (08), 1201-1204.
13. Pietruszka, J.; Witt, A., Synthesis of the Bestmann-Ohira Reagent. *Synthesis* **2006**, *2006* (24), 4266-4268.
14. Ireland, R. E.; Norbeck, D. W., Application of the Swern oxidation to the manipulation of highly reactive carbonyl compounds. *The Journal of Organic Chemistry* **1985**, *50* (12), 2198-2200.
15. Uyanik, M.; Akakura, M.; Ishihara, K., 2-Iodoxybenzenesulfonic Acid as an Extremely Active Catalyst for the Selective Oxidation of Alcohols to Aldehydes, Ketones, Carboxylic Acids, and Enones with Oxone. *Journal of the American Chemical Society* **2009**, *131* (1), 251-262.
16. Barrett, A. G. M.; Hopkins, B. T.; Love, A. C.; Tedeschi, L., Parallel Synthesis of Terminal Alkynes Using a ROMPgel-Supported Ethyl 1-Diazo-2-oxopropylphosphonate. *Organic Letters* **2004**, *6* (5), 835-837.
17. Agosta, E.; Caligiuri, A.; D'Arrigo, P.; Servi, S.; Tessaro, D.; Canevotti, R., Enzymatic approach to both enantiomers of N-Boc hydrophobic amino acids. *Tetrahedron: Asymmetry* **2006**, *17* (13), 1995-1999.
18. Grimes, K. D.; Gupte, A.; Aldrich, C. C., Copper(II)-Catalyzed Conversion of Aryl/Heteroaryl Boronic Acids, Boronates, and Trifluoroborates into the Corresponding Azides: Substrate Scope and Limitations. *Synthesis* **2010**, *2010* (09), 1441-1448.
19. Rasmussen, L. K.; Boren, B. C.; Fokin, V. V., Ruthenium-Catalyzed Cycloaddition of Aryl Azides and Alkynes. *Organic Letters* **2007**, *9* (26), 5337-5339.
20. Hanamoto, T.; Shimomoto, N.; Kikukawa, T.; Inanaga, J., Efficient synthesis of enantiomerically pure trans-2,5-bis(arylethynyl)pyrrolidines. A new entry into C2-symmetric chiral secondary amines. *Tetrahedron: Asymmetry* **1999**, *10* (15), 2951-2959.

21. Shen, R.; Chen, T.; Zhao, Y.; Qiu, R.; Zhou, Y.; Yin, S.; Wang, X.; Goto, M.; Han, L.-B., Facile Regio- and Stereoselective Hydrometalation of Alkynes with a Combination of Carboxylic Acids and Group 10 Transition Metal Complexes: Selective Hydrogenation of Alkynes with Formic Acid. *Journal of the American Chemical Society* **2011**, *133* (42), 17037-17044.
22. Takami, K.; Mikami, S.; Yorimitsu, H.; Shinokubo, H.; Oshima, K., Triethylborane-Mediated Hydrogallation and Hydroindation: Novel Access to Organogalliums and Organoindiums. *The Journal of Organic Chemistry* **2003**, *68* (17), 6627-6631.
23. Ashley, E. R.; Cruz, E. G.; Stoltz, B. M., The Total Synthesis of (-)-Lemonomycin. *Journal of the American Chemical Society* **2003**, *125* (49), 15000-15001.
24. Jeyakumar, K.; Chakravarthy, R. D.; Chand, D. K., Simple and efficient method for the oxidation of sulfides to sulfones using hydrogen peroxide and a Mo(VI) based catalyst. *Catalysis Communications* **2009**, *10* (14), 1948-1951.
25. Jung, M. E.; Deng, G., Synthesis of α -Diketones from Alkylaryl- and Diarylalkynes Using Mercuric Salts. *Organic Letters* **2014**, *16* (8), 2142-2145.

Appendix I: Cellular morphology Images

Table 10. Images of MDA-MB-231 breast cancer cells treated with denoted compound at either 10 μ M or 10 nM. Pictures taken at 30 min, 24 hrs and 48 hrs post inoculation using a bright field microscope. Apoptotic cells are indicated by the white arrow while necrotic cells are indicated by a black arrow.

Compound	Conc.	Time (hours)		
		0.5	24	48
<chem>CN(C)C(=O)NCCCCCN(C)C(=O)Nc1ccc2ccccc12</chem> 025	10 μ M			
	10 nM			
<chem>CN(C)C(=O)N(CC)C(=O)Nc1ccc2ccccc12</chem> 157	10 μ M			
	10 nM			
<chem>CN(C)C(=O)N(CC)C(=O)Nc1ccc2ccccc12</chem> 105	10 μ M			
	10 nM			

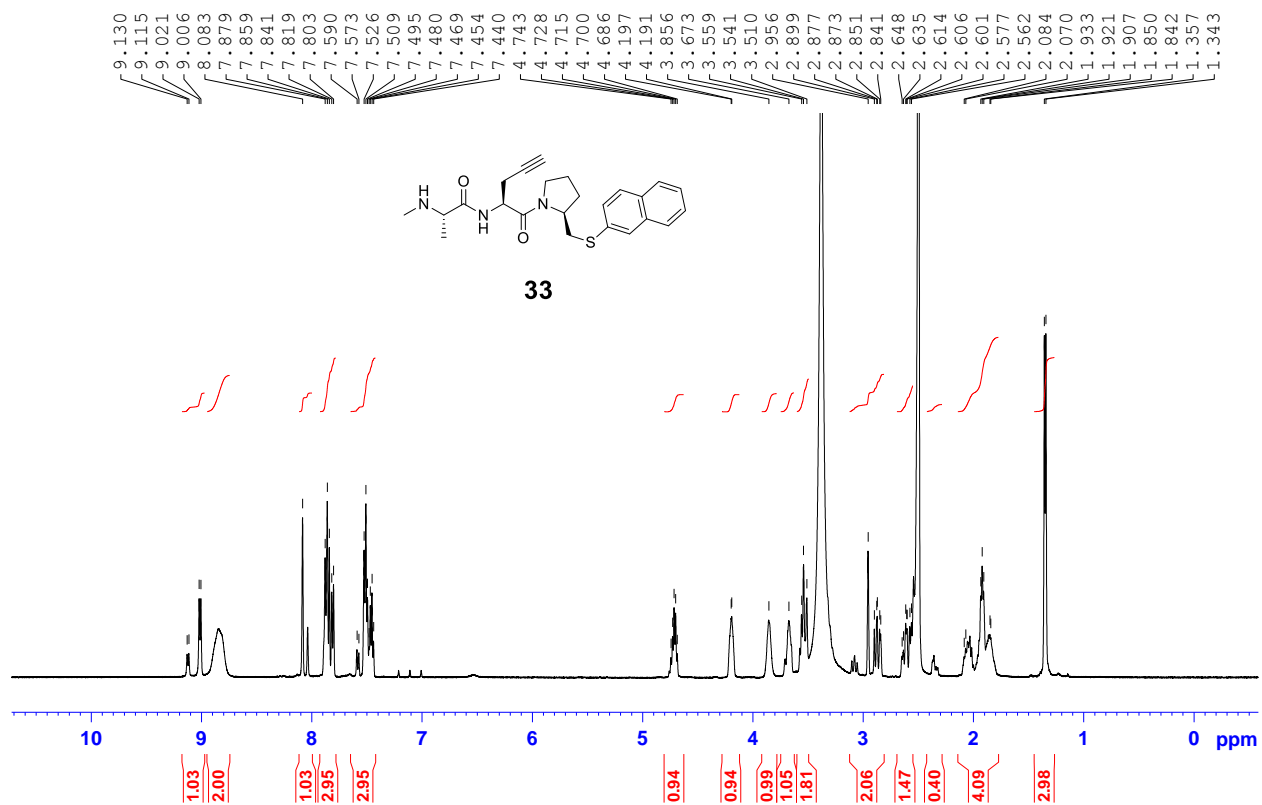
 <p>107</p>	10 μ M			
	10 nM			
Staurosporine	10 μ M			
	10 nM			
DMSO (vehicle)	0.1 M			

Supplementary Spectral Data

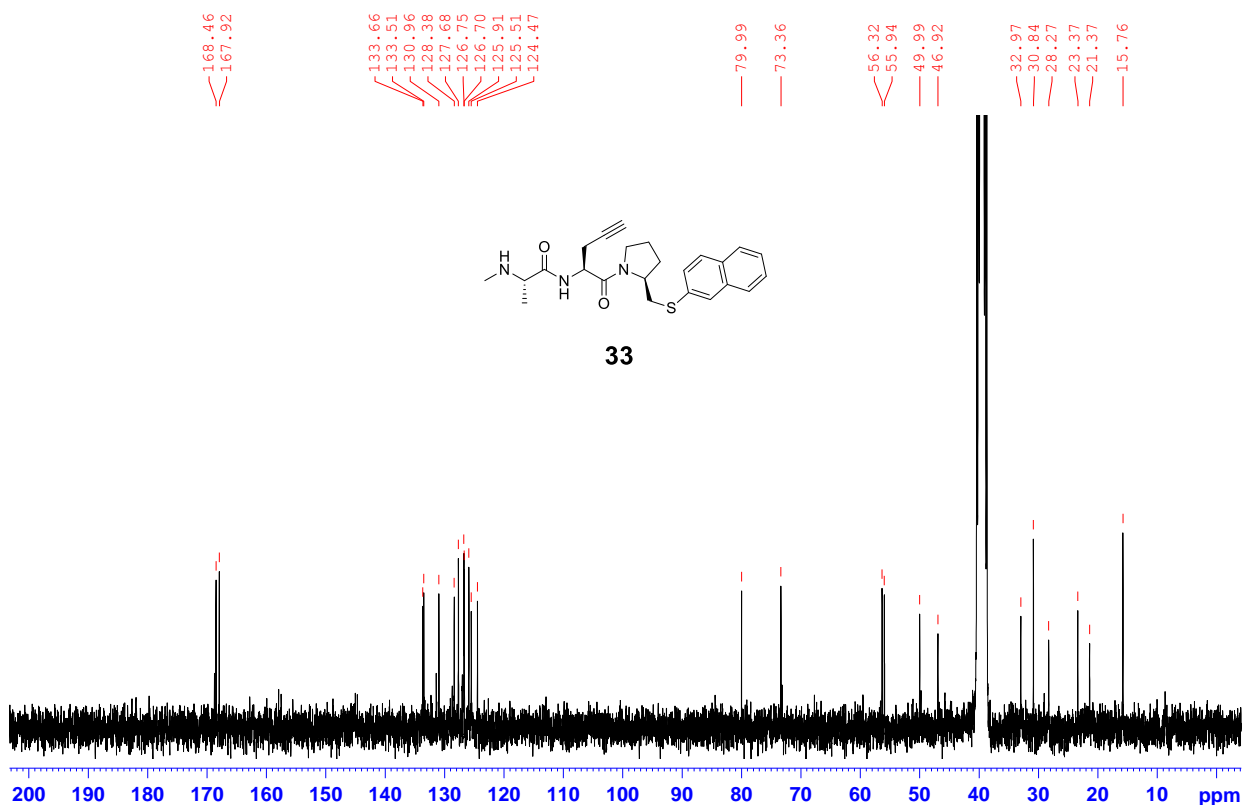
^1H and ^{13}C spectra are provided for previously unpublished compounds, published compounds with poor or no available spectral data, and key compounds; all other compounds have references to the published spectra provided in the experimental section above.

Some ^{13}C samples show residual trifluoroacetic acid peaks at 164 (q) and 116 (q) ppm. This is due to partial counter-ion exchange during HPLC purification as 0.01% TFA is present in the water eluent as a modifier. Lyophilization with 0.1 M HCl prior to testing is effective at removing this impurity (see General Materials and Methods for Chemical Synthesis).

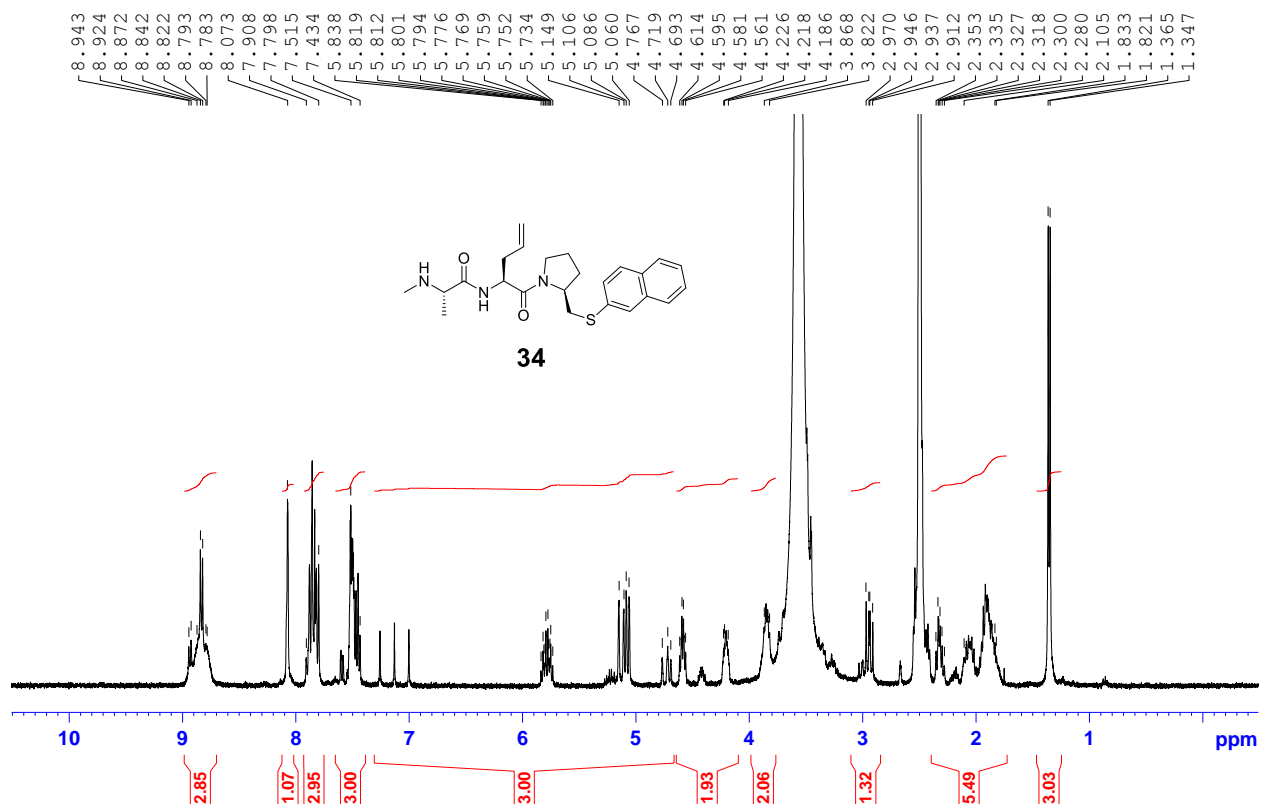
Compound 33 - ¹H NMR



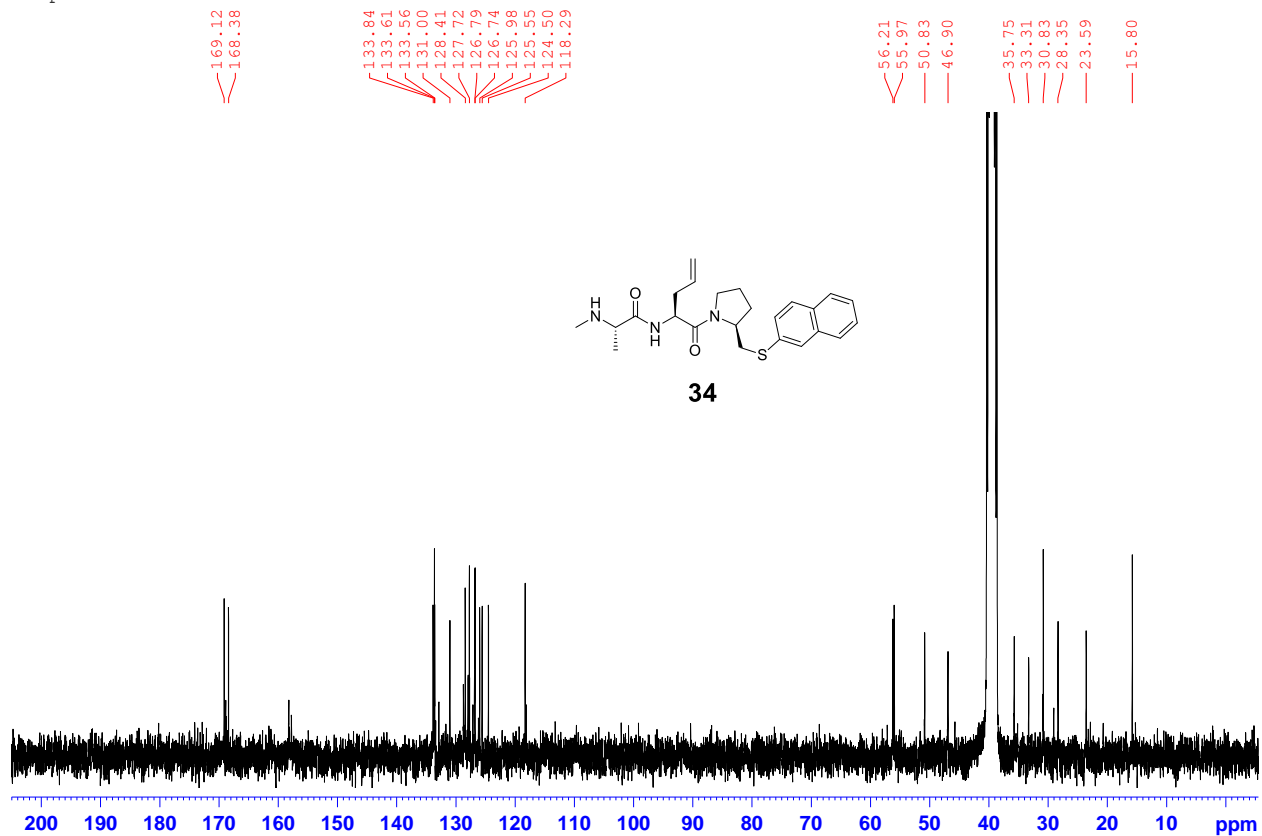
Compound 33 -¹³C



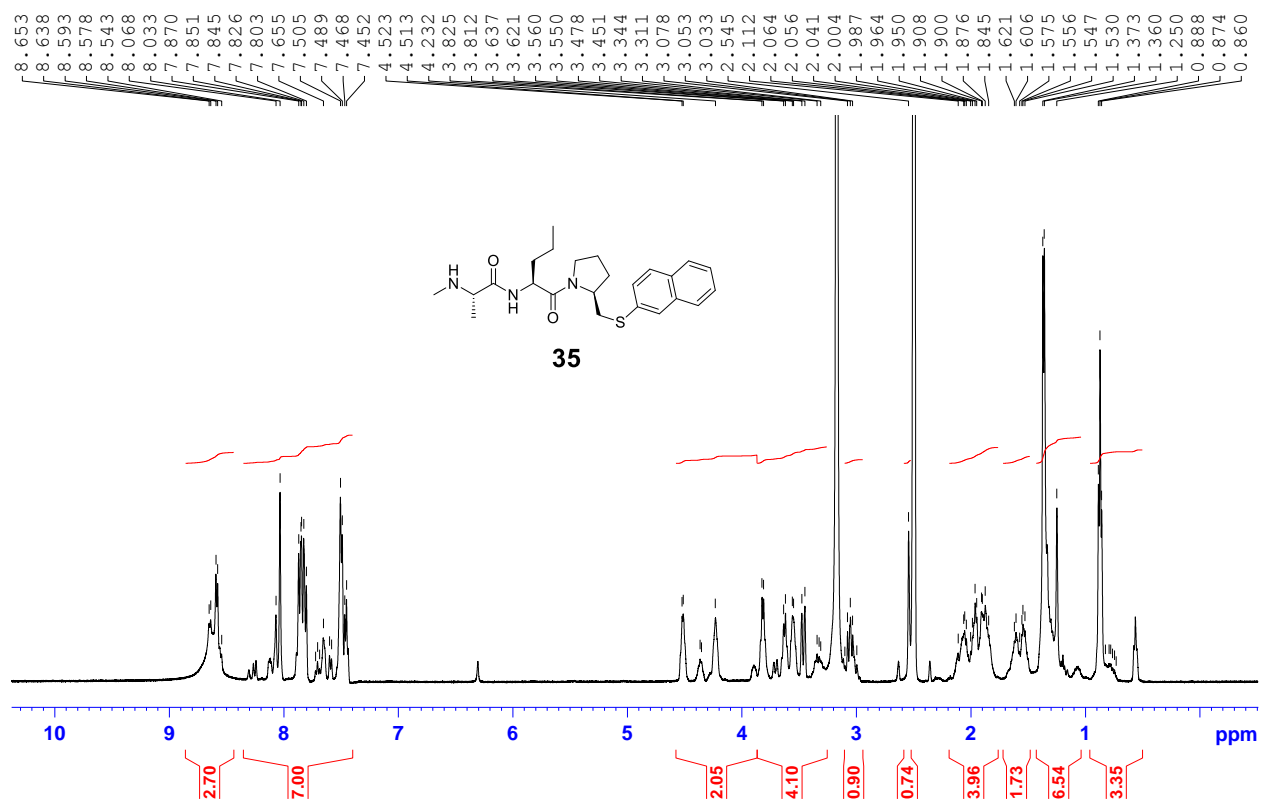
Compound 34 - ¹H



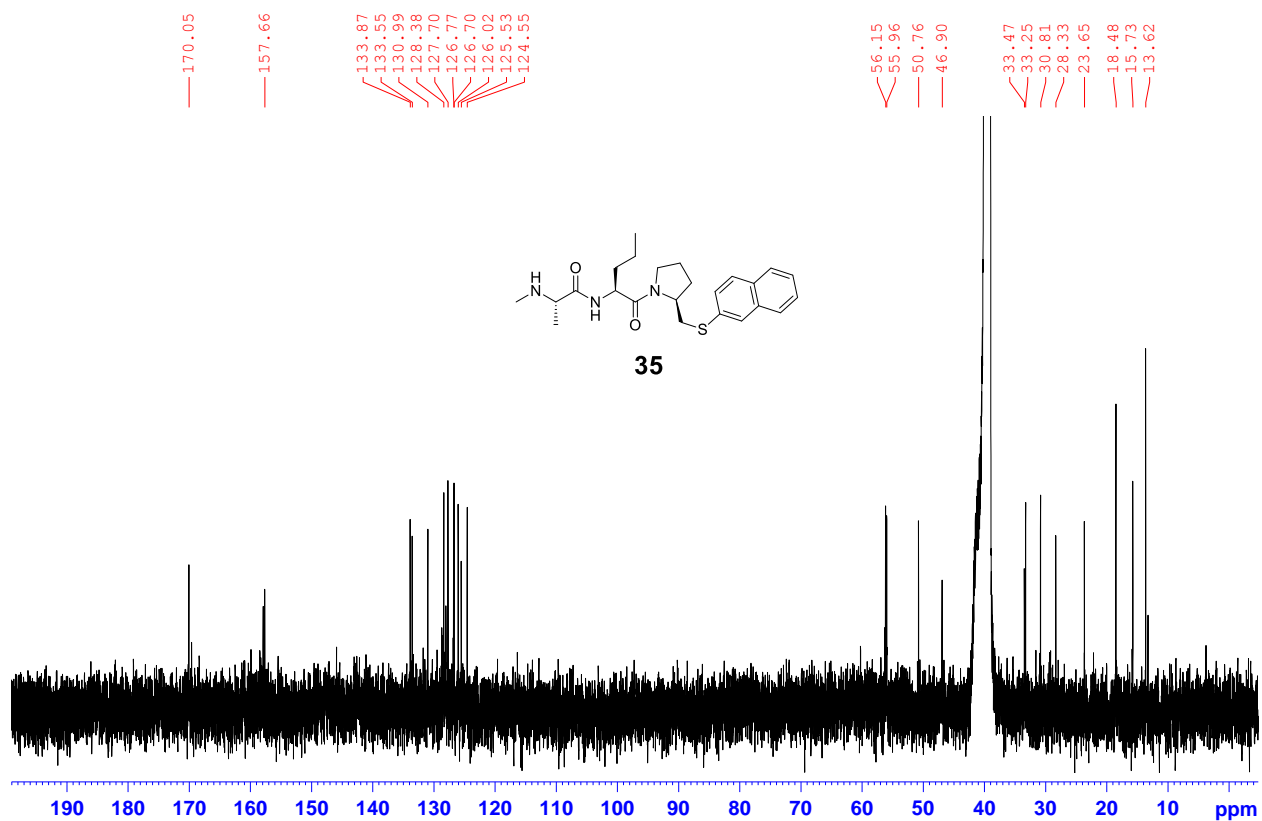
Compound 34 - ¹³C



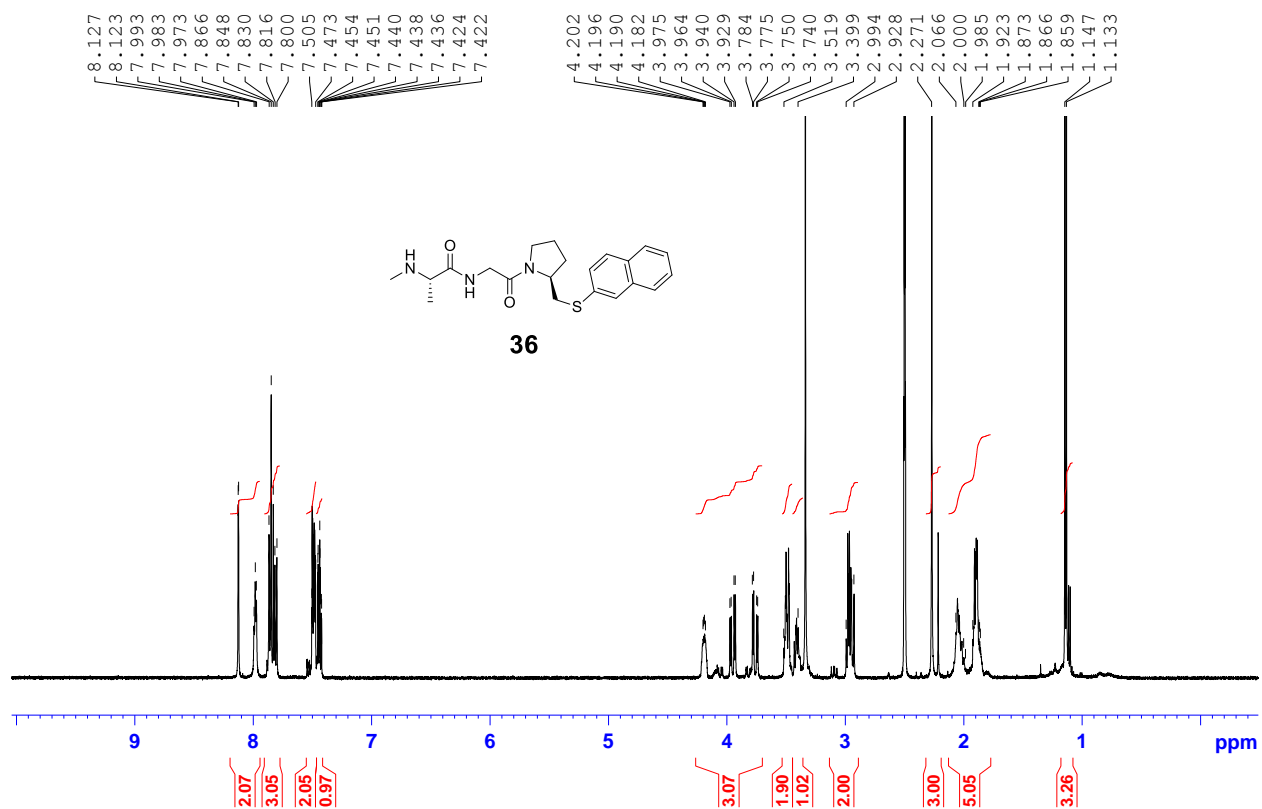
Compound 35 -1H



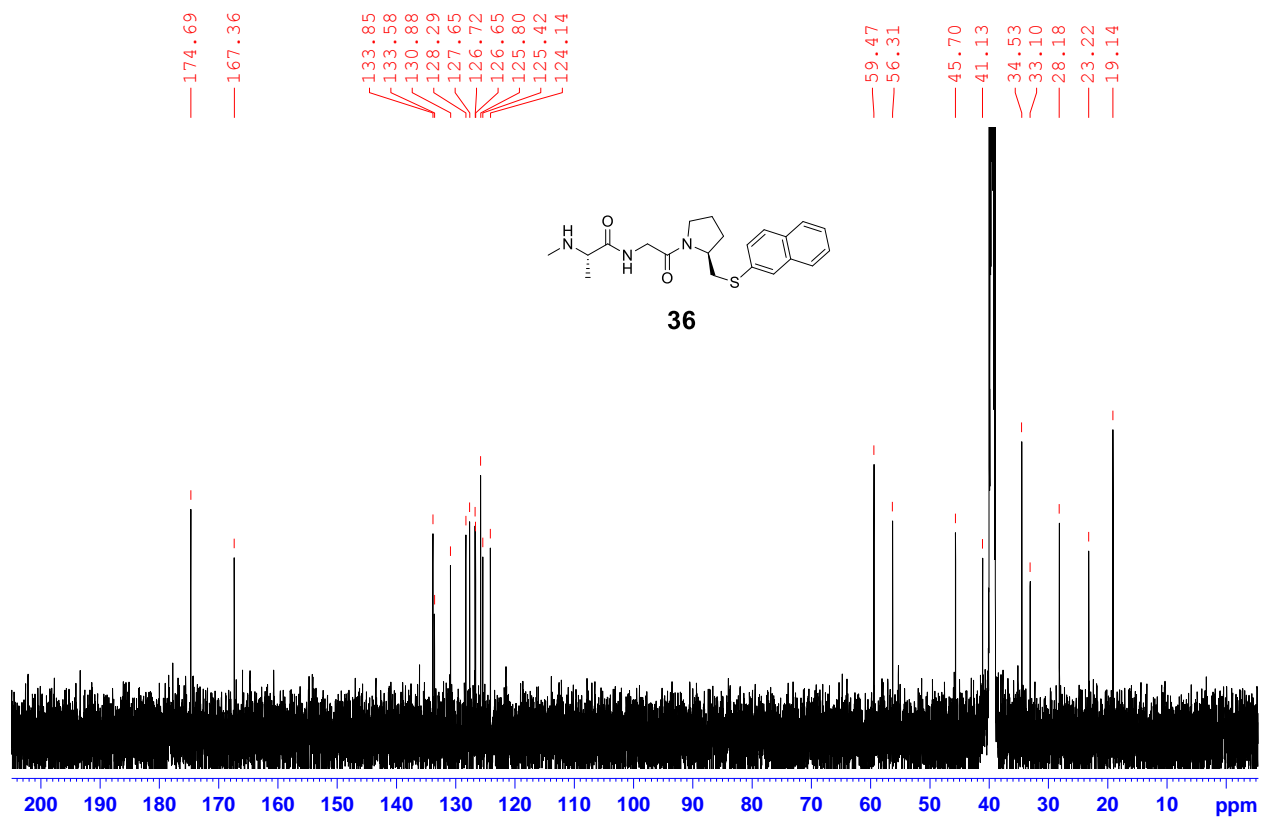
Compound 35 - 13C



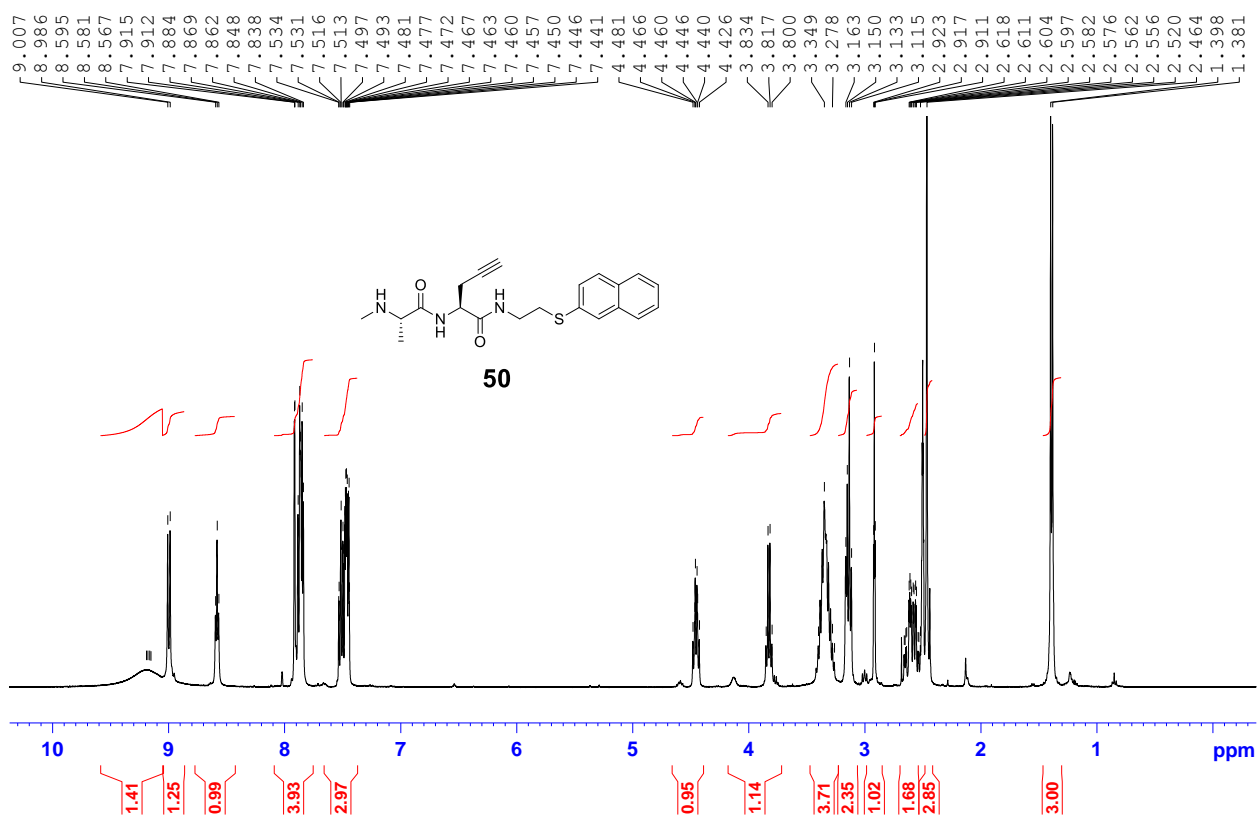
Compound 36 - ¹H NMR



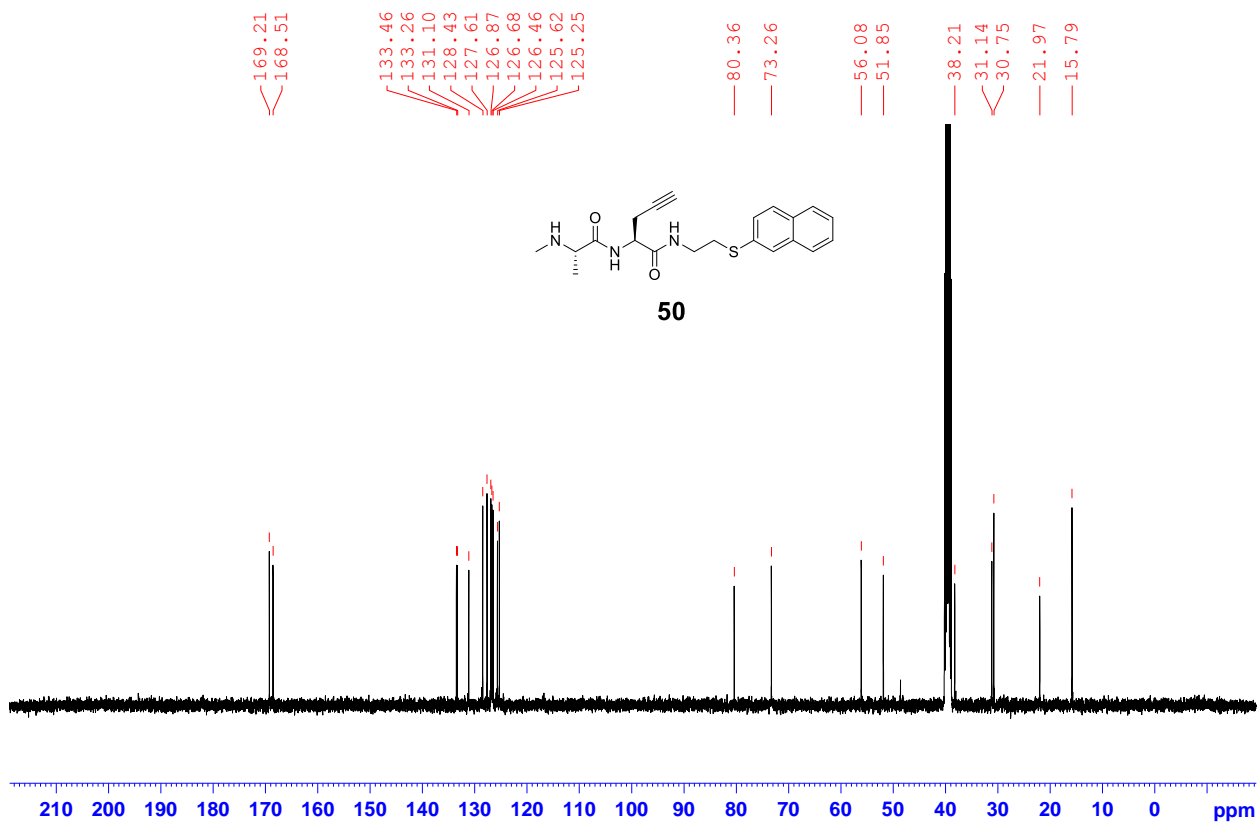
Compound 36 - ¹³C NMR



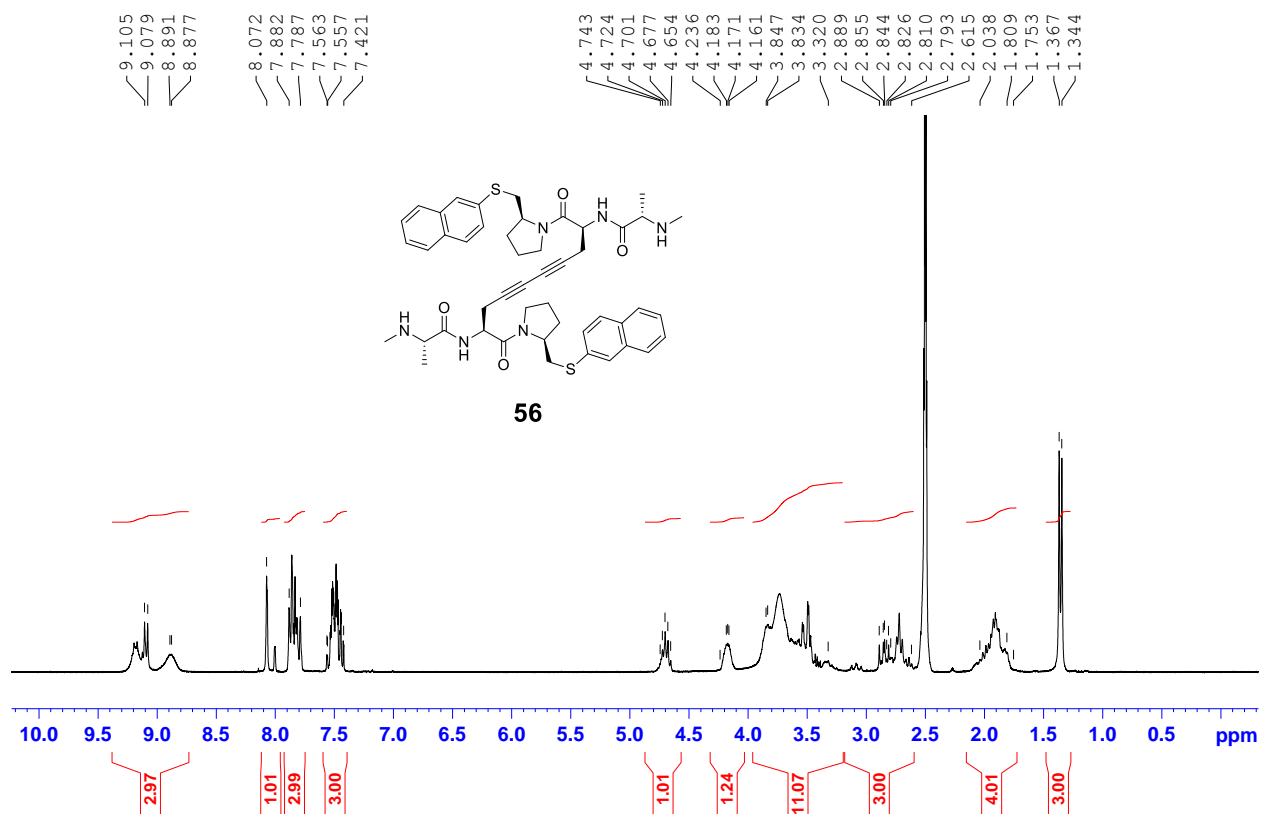
Compound 50 - 1H



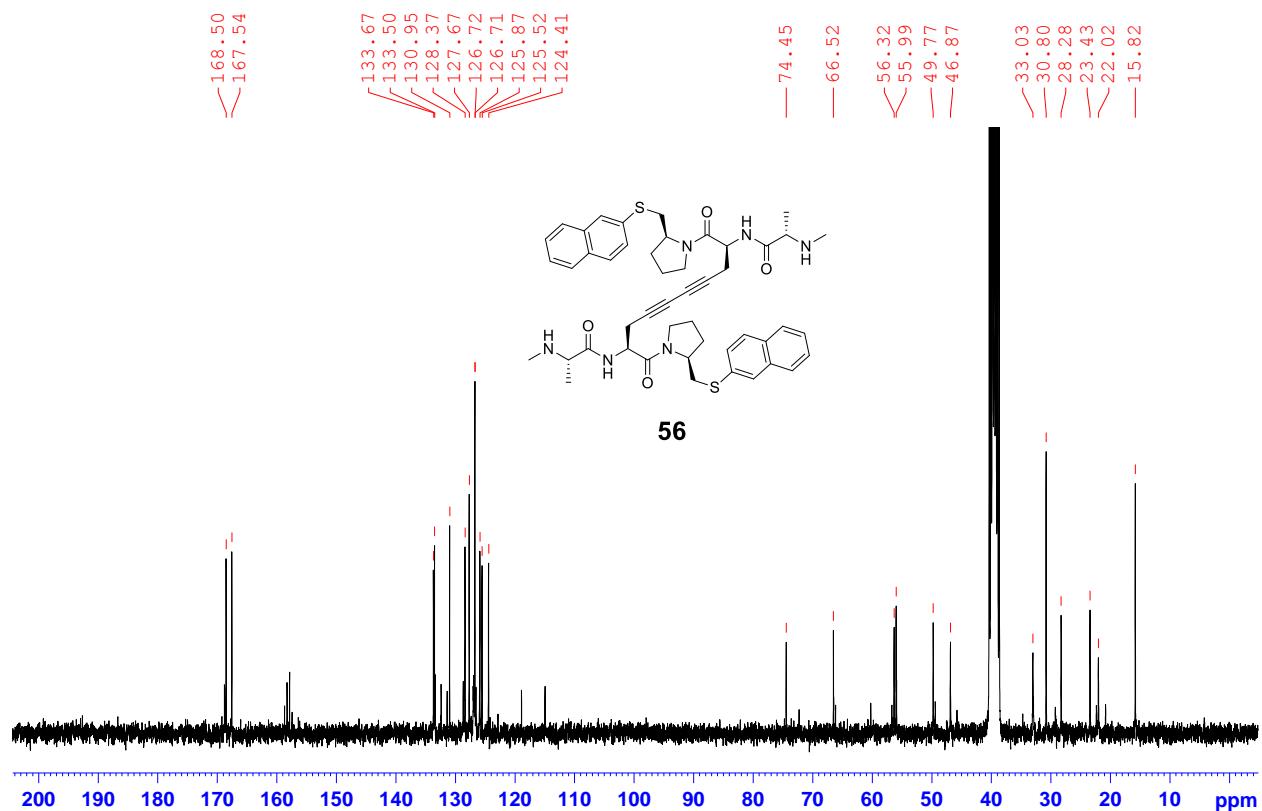
Compound 50 -13C



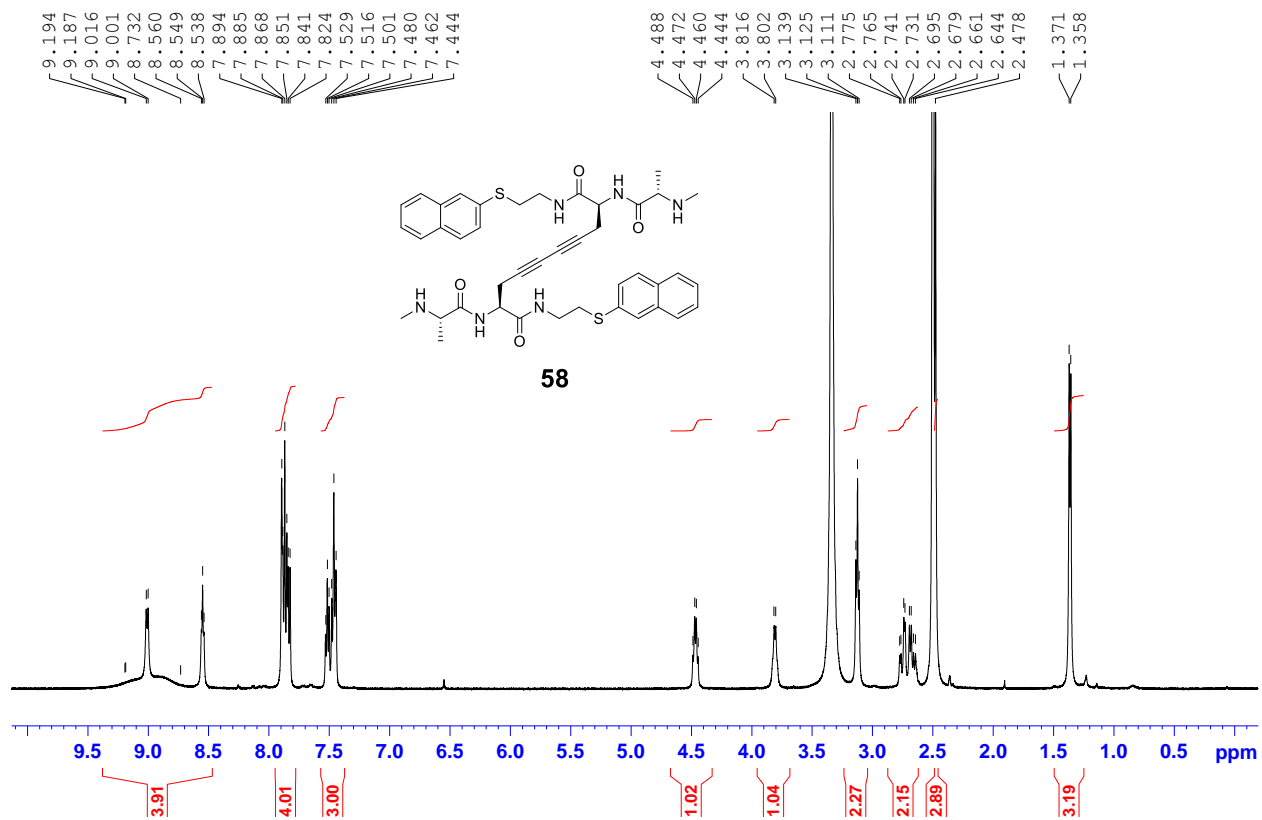
Compound 56 - 1H



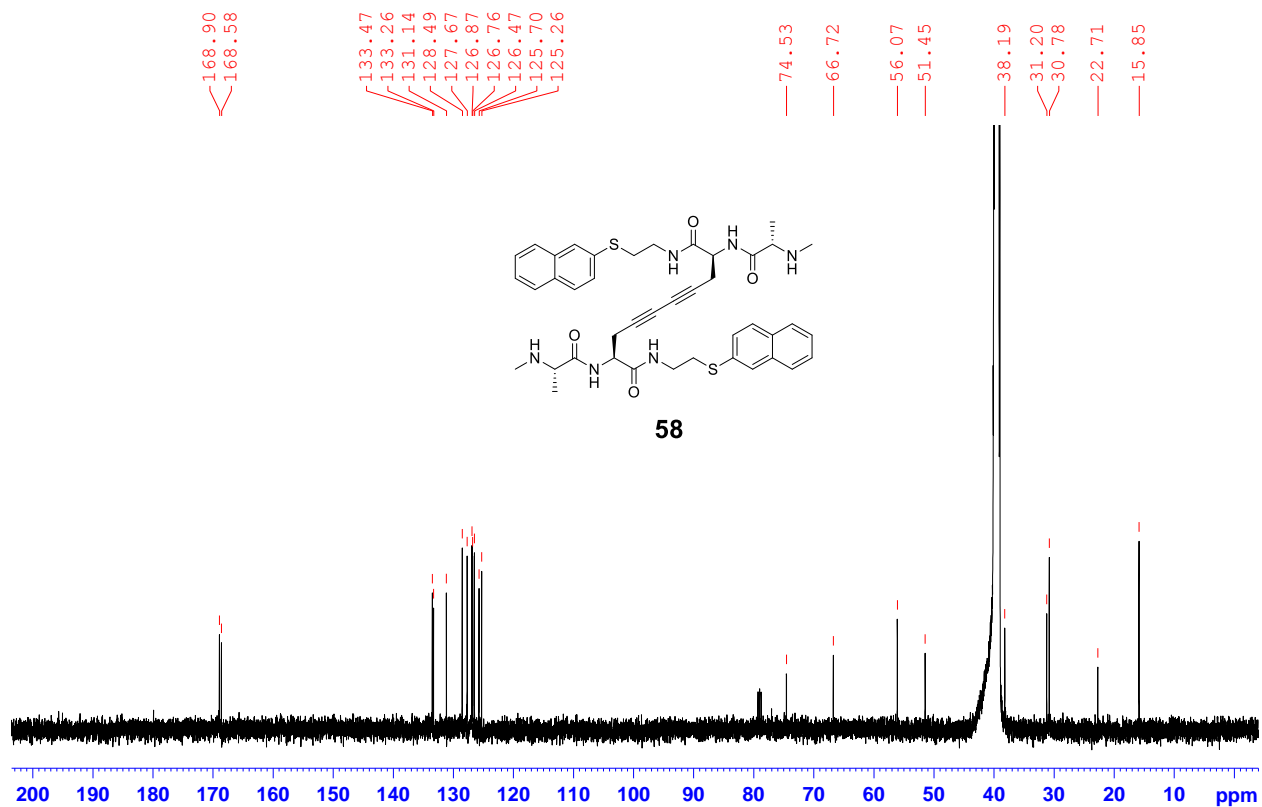
Compound 56 - 13C



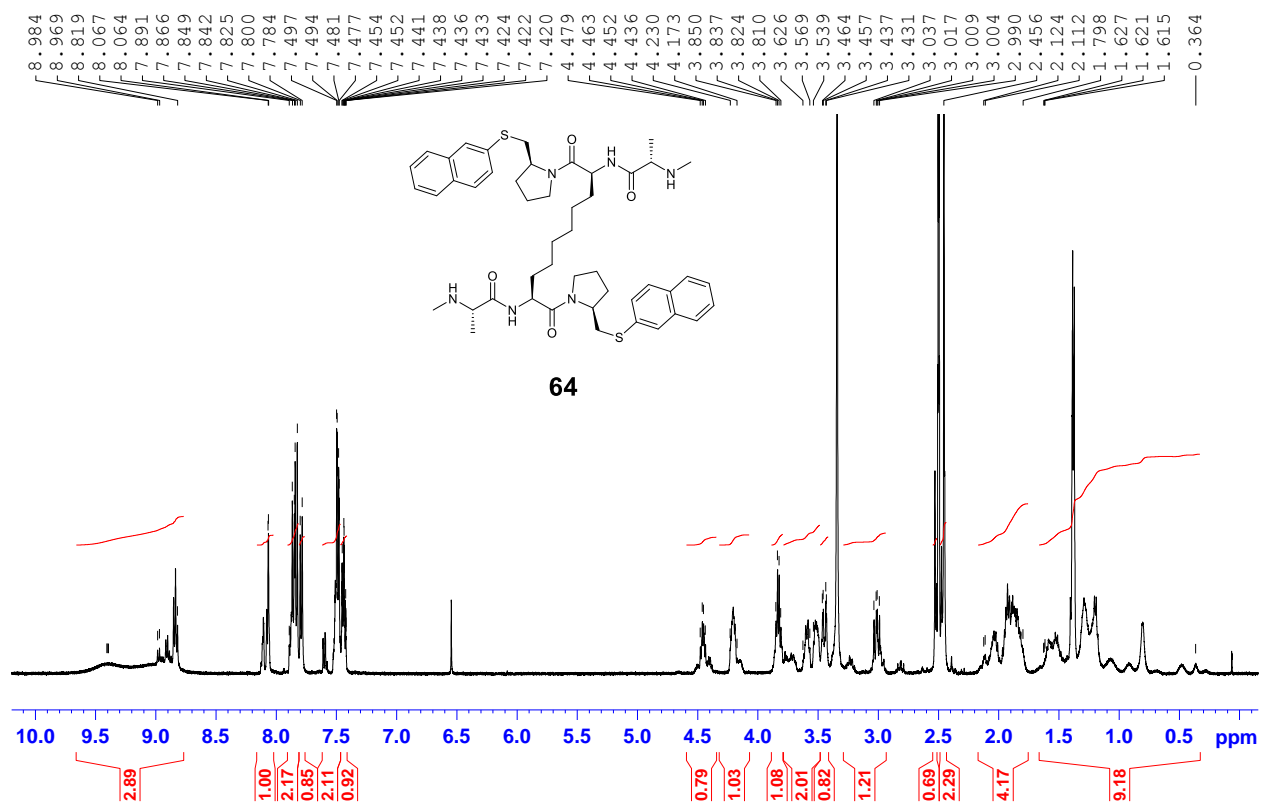
Compound 58 - 1H



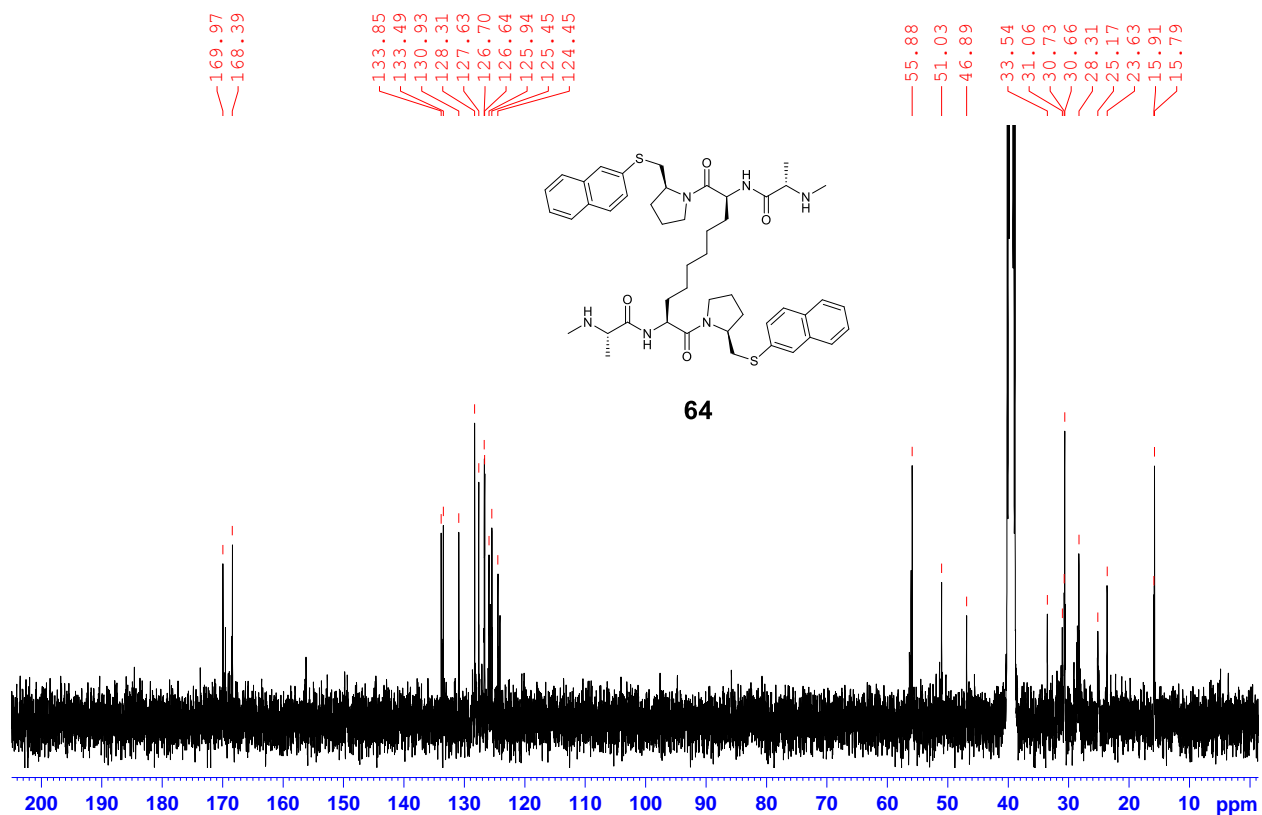
Compound 58 - 13C



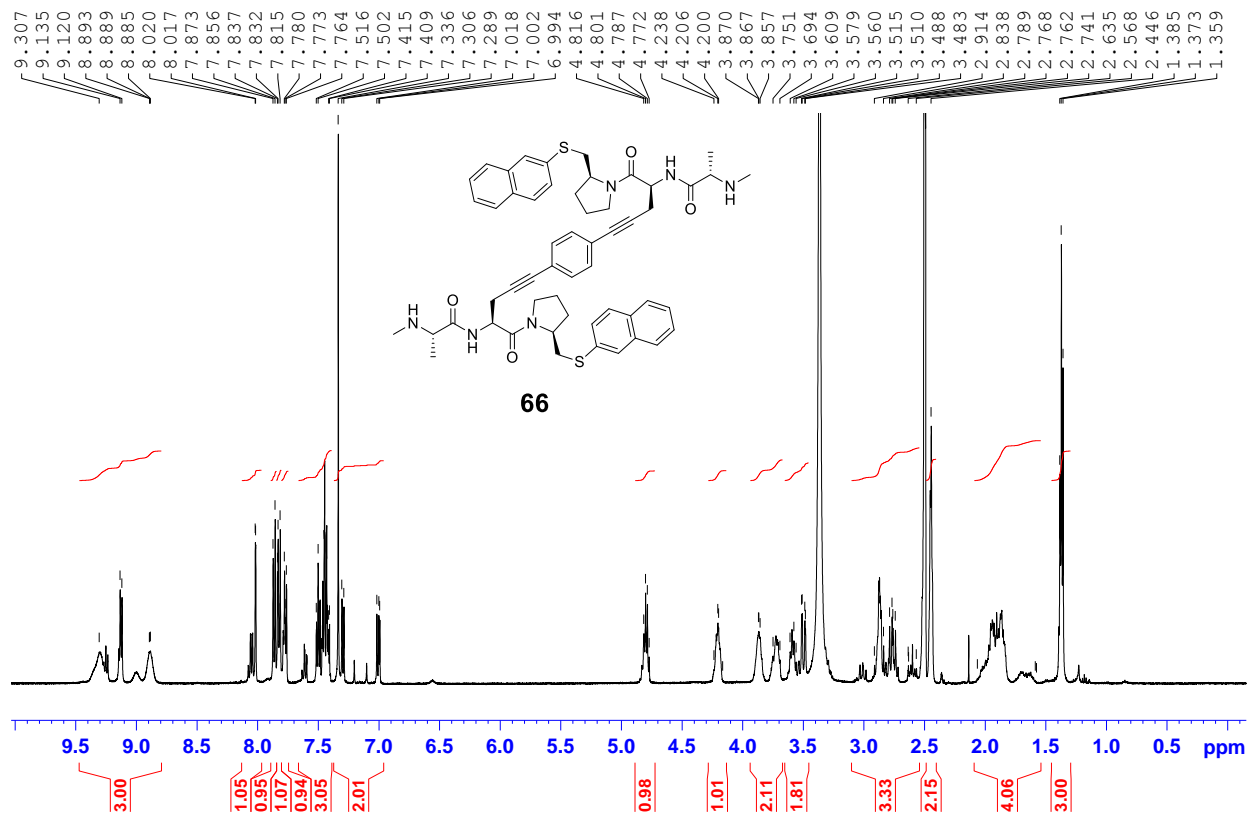
Compound 64 - ¹H



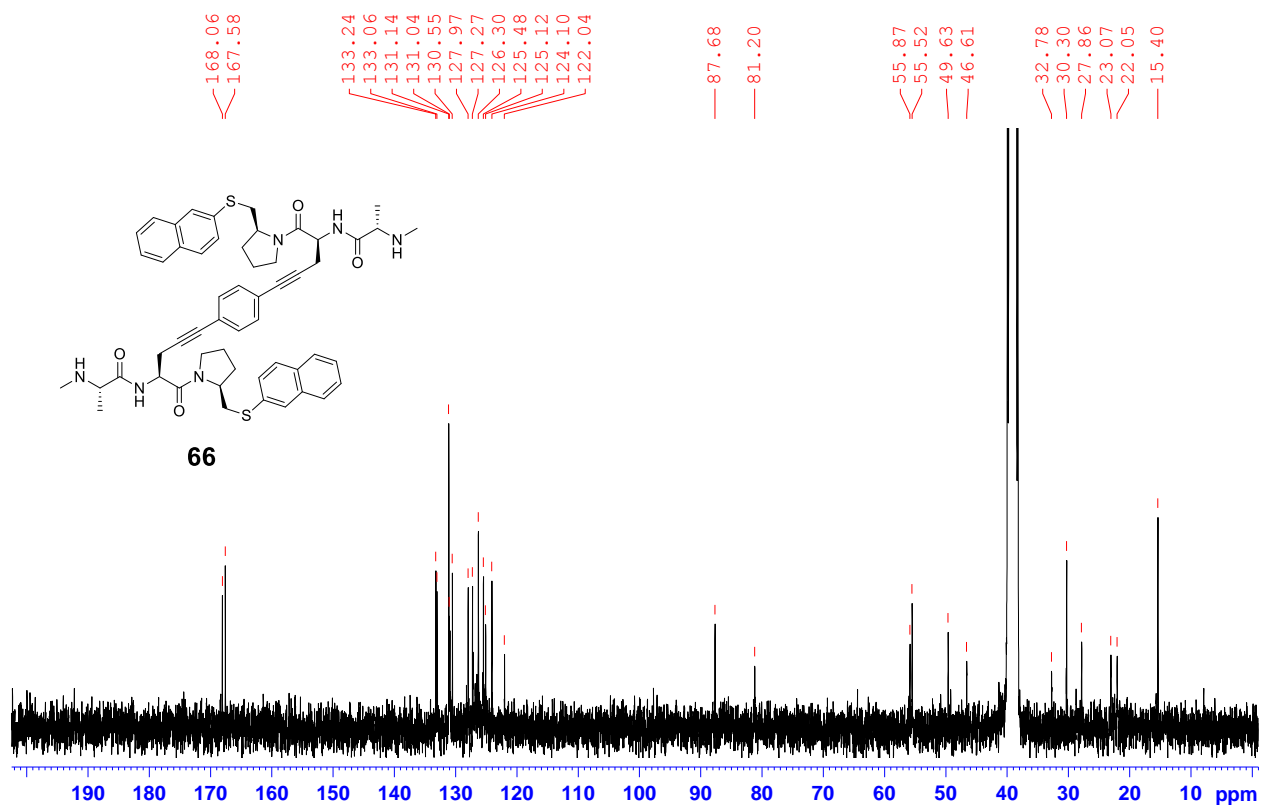
Compound 64 - ¹³C



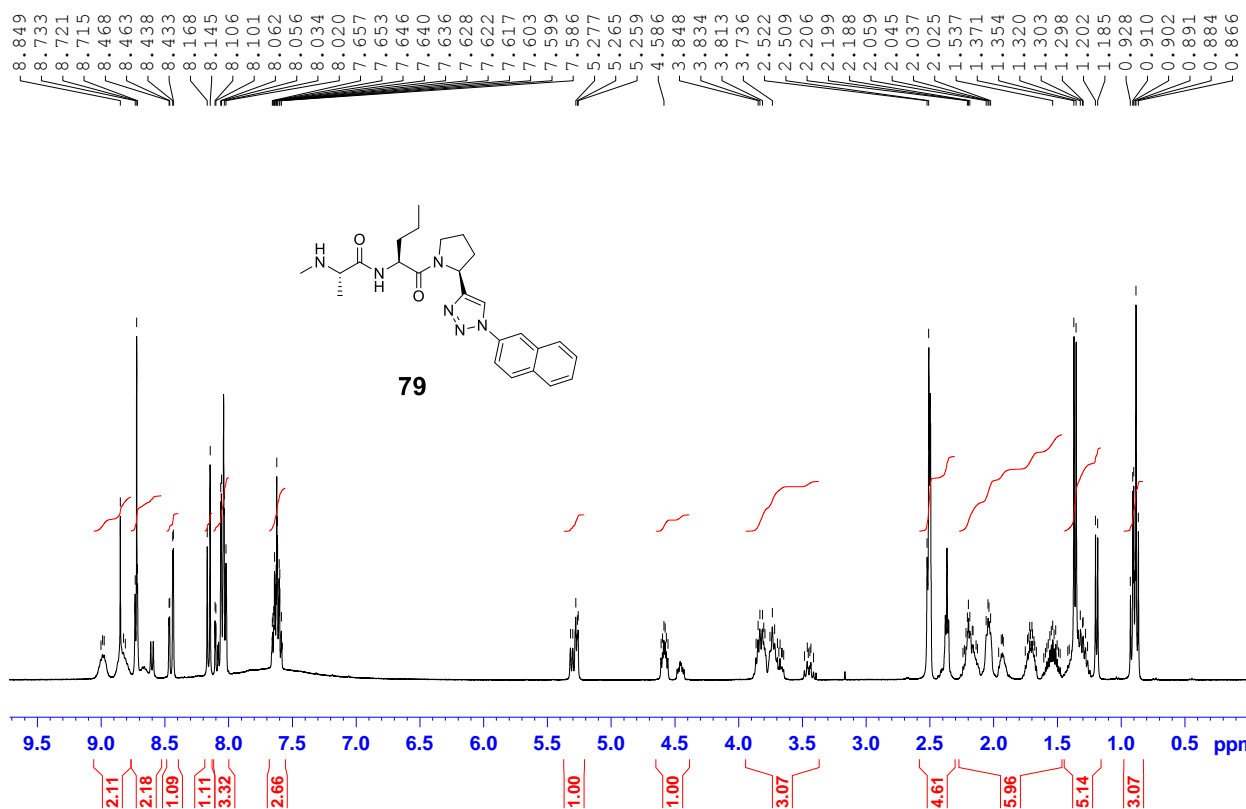
Compound 66 - ¹H



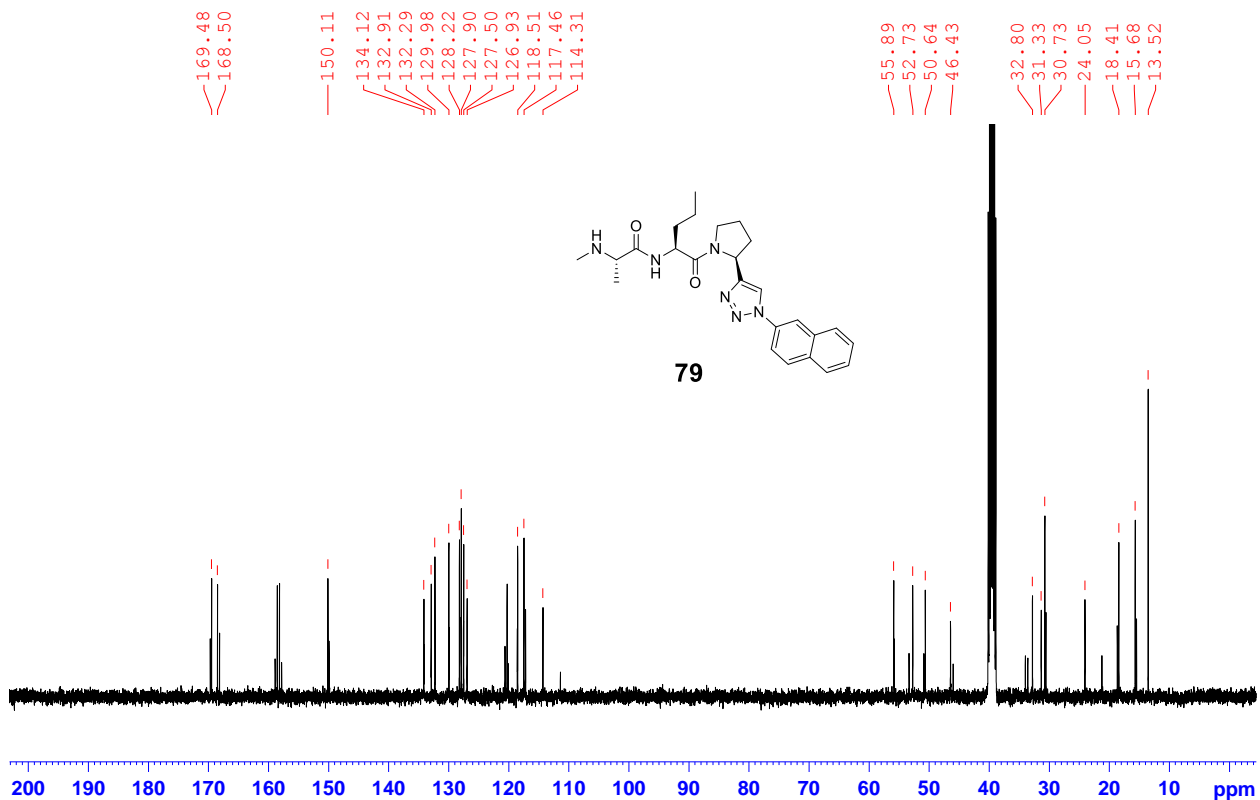
Compound 66 - ¹³C



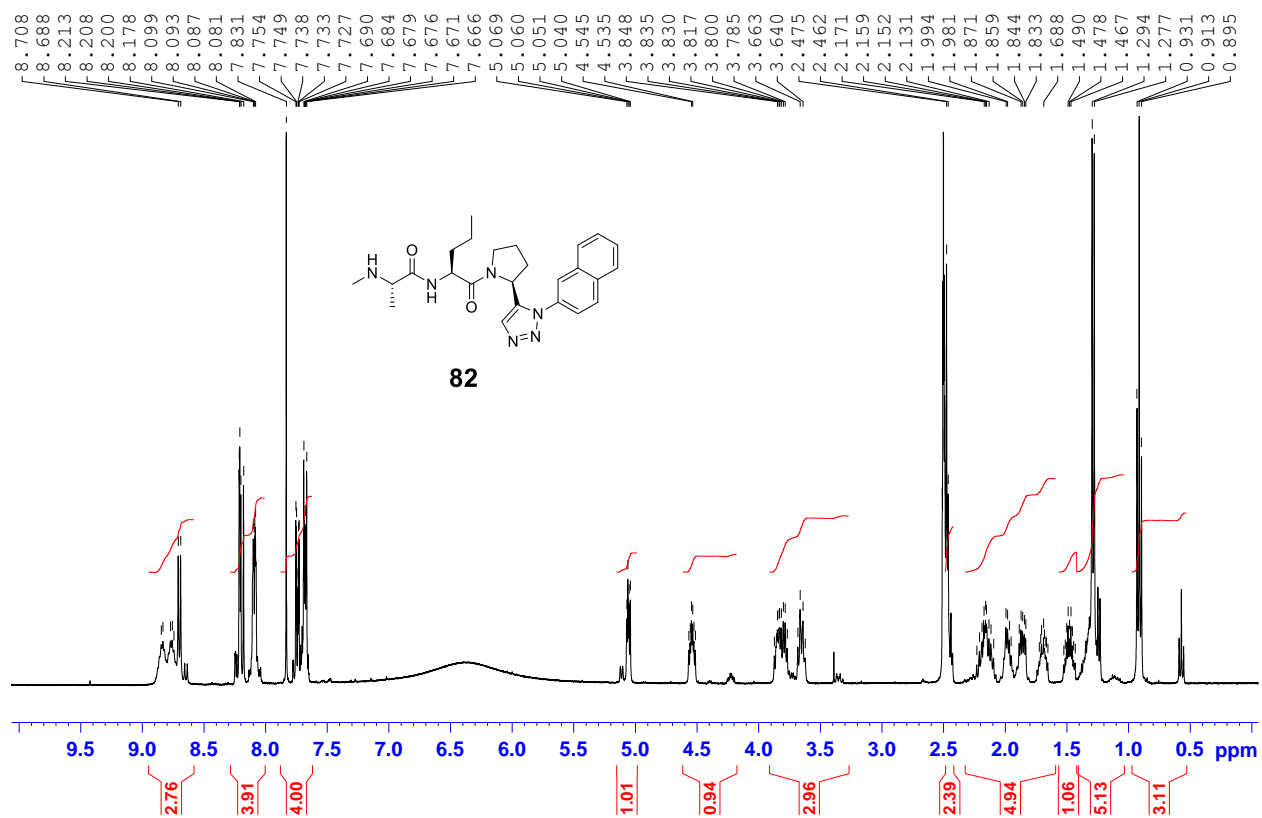
Compound 79 - ¹H



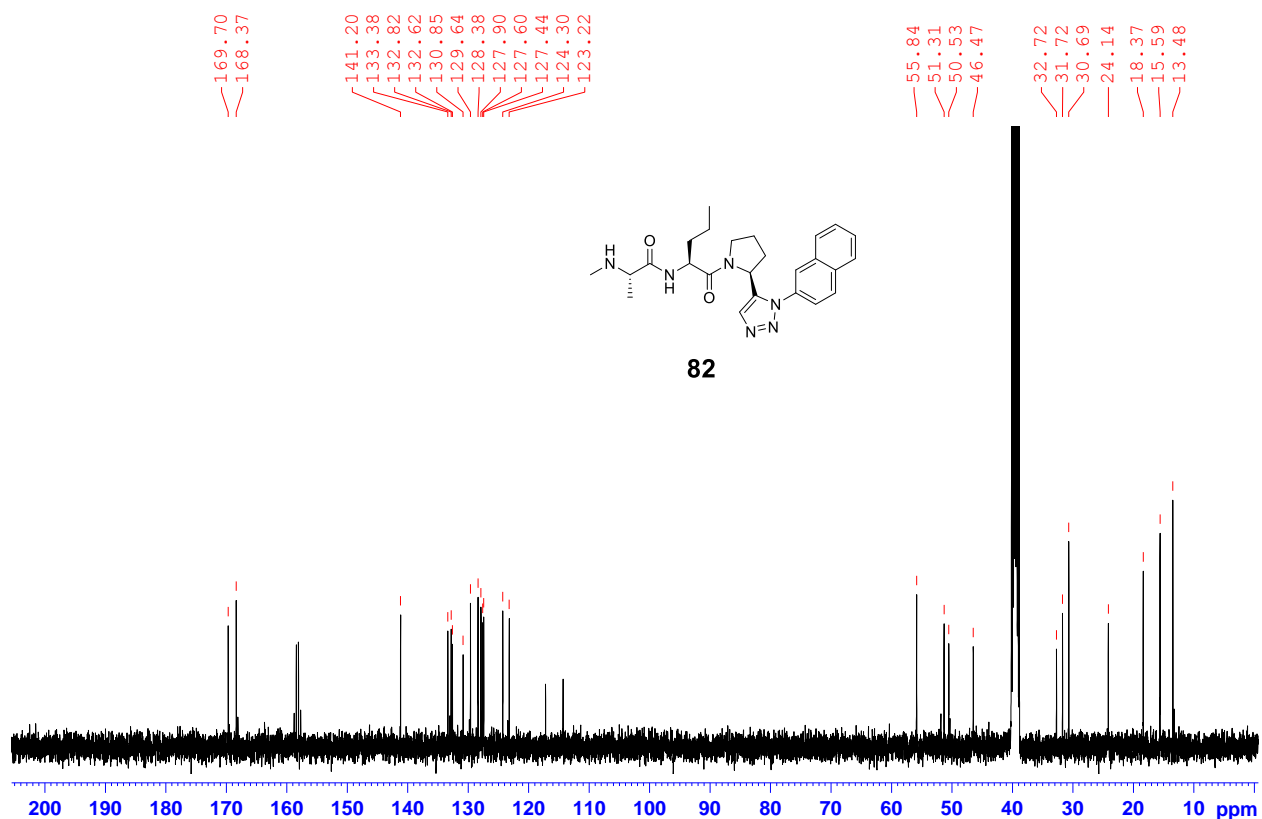
Compound 79 - ¹³C



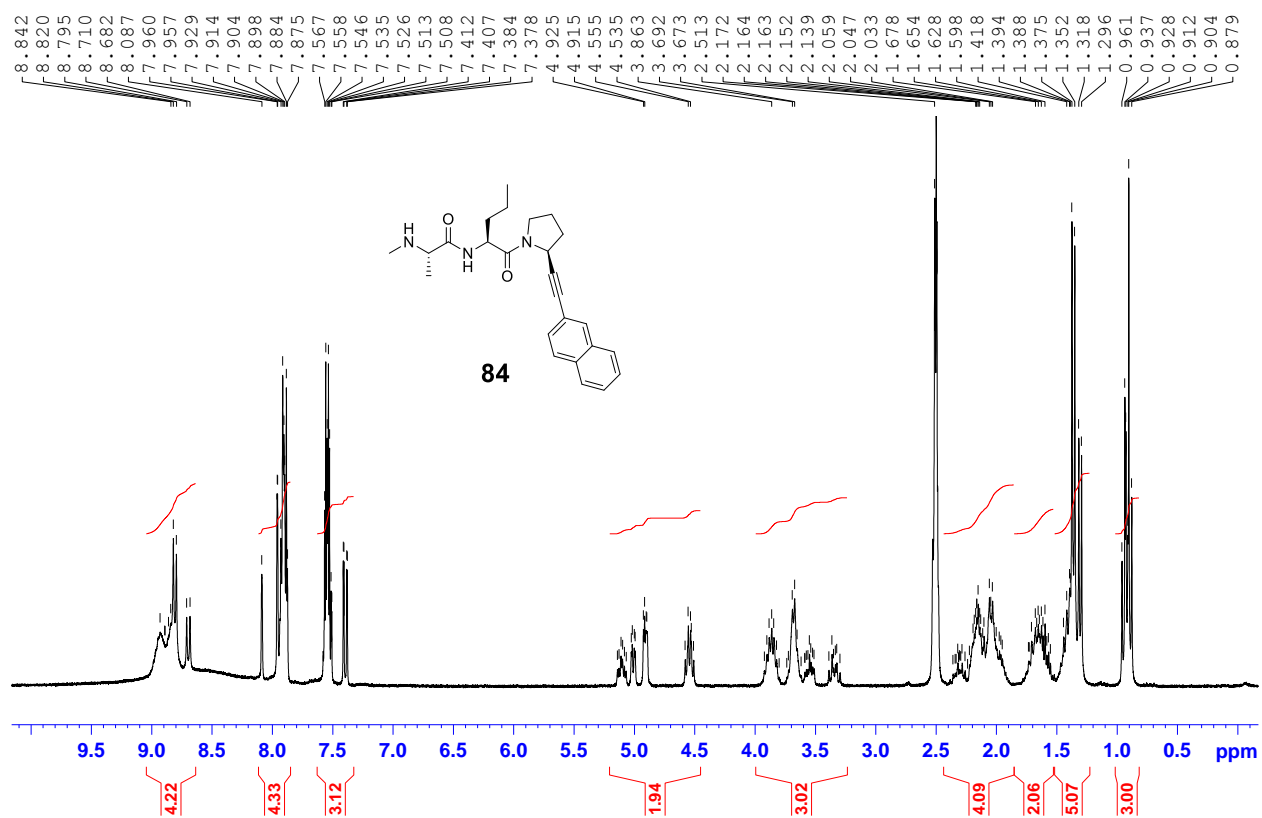
Compound 82 - ¹H



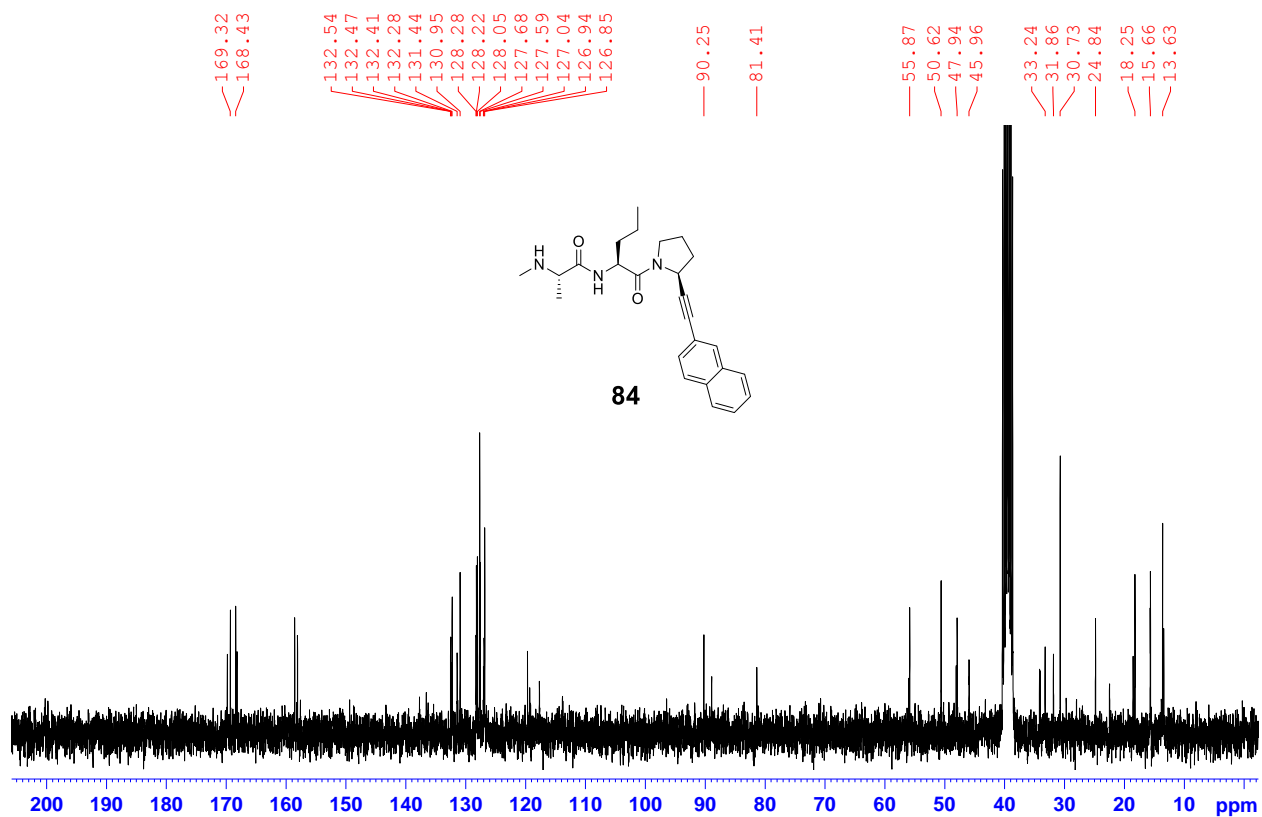
Compound 82 - ¹³C



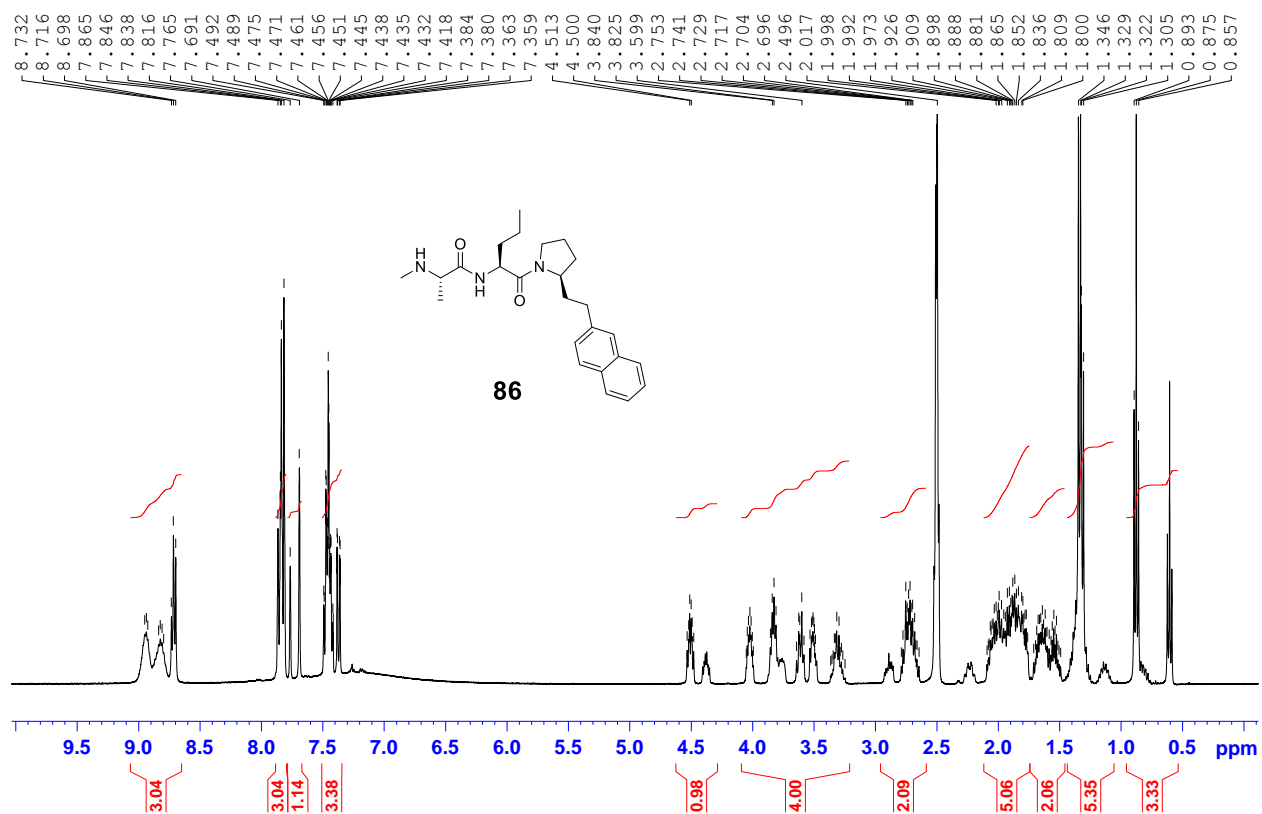
Compound 84 - ¹H



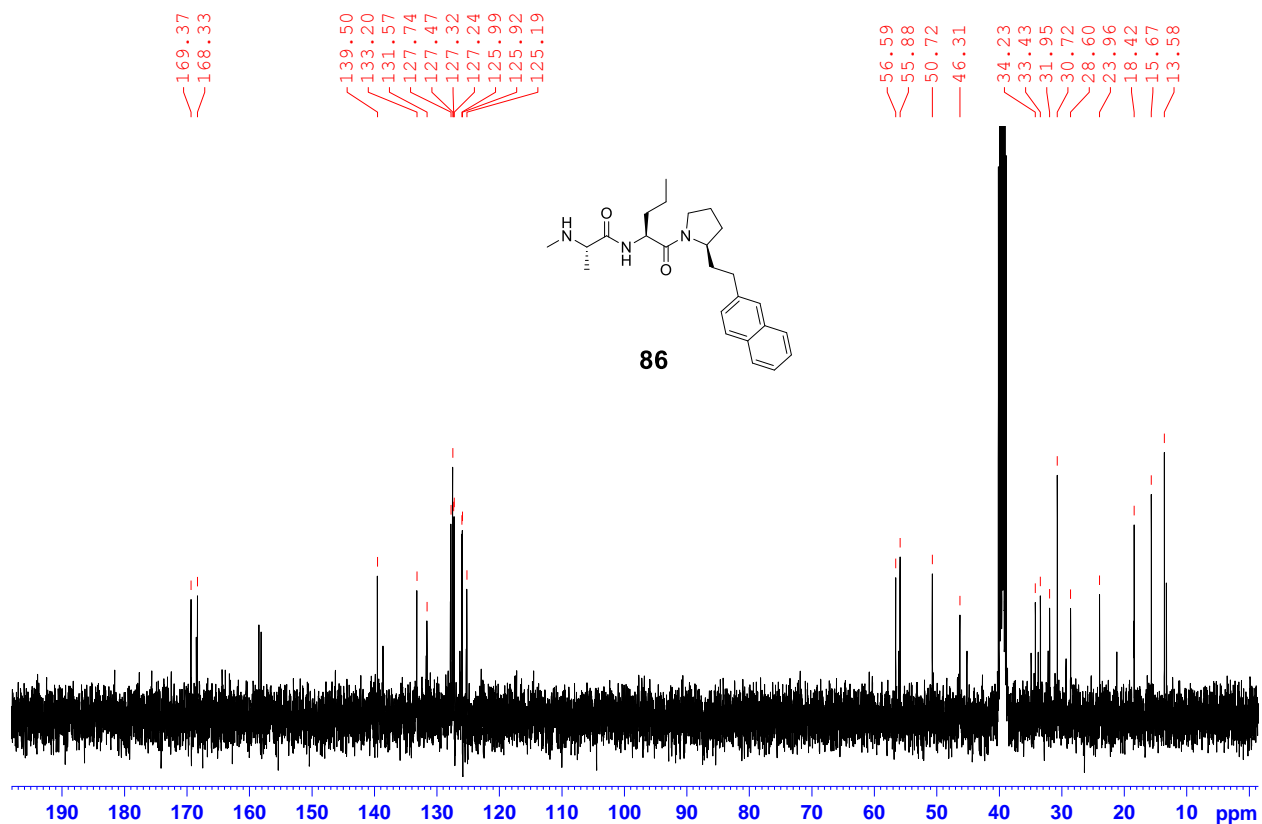
Compound 84 - ¹³C



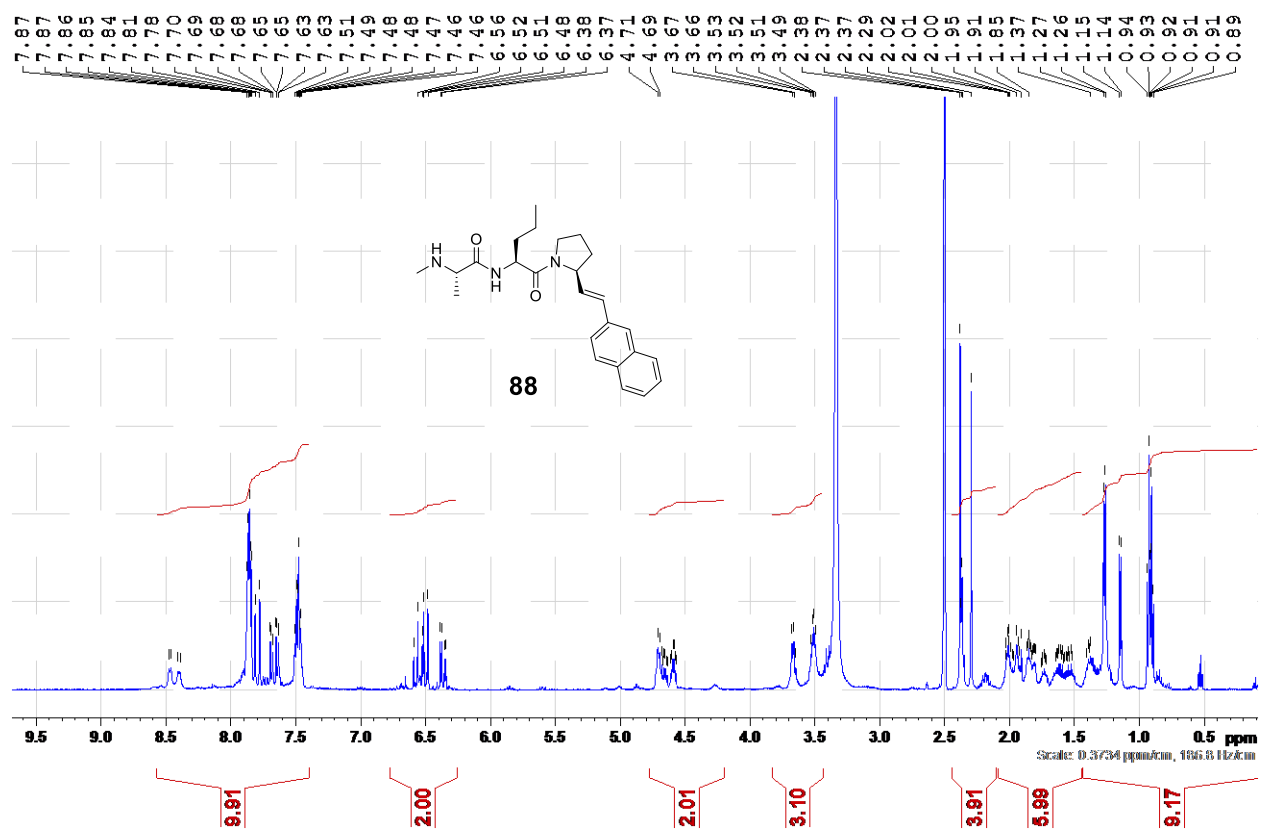
Compound 86 - ¹H



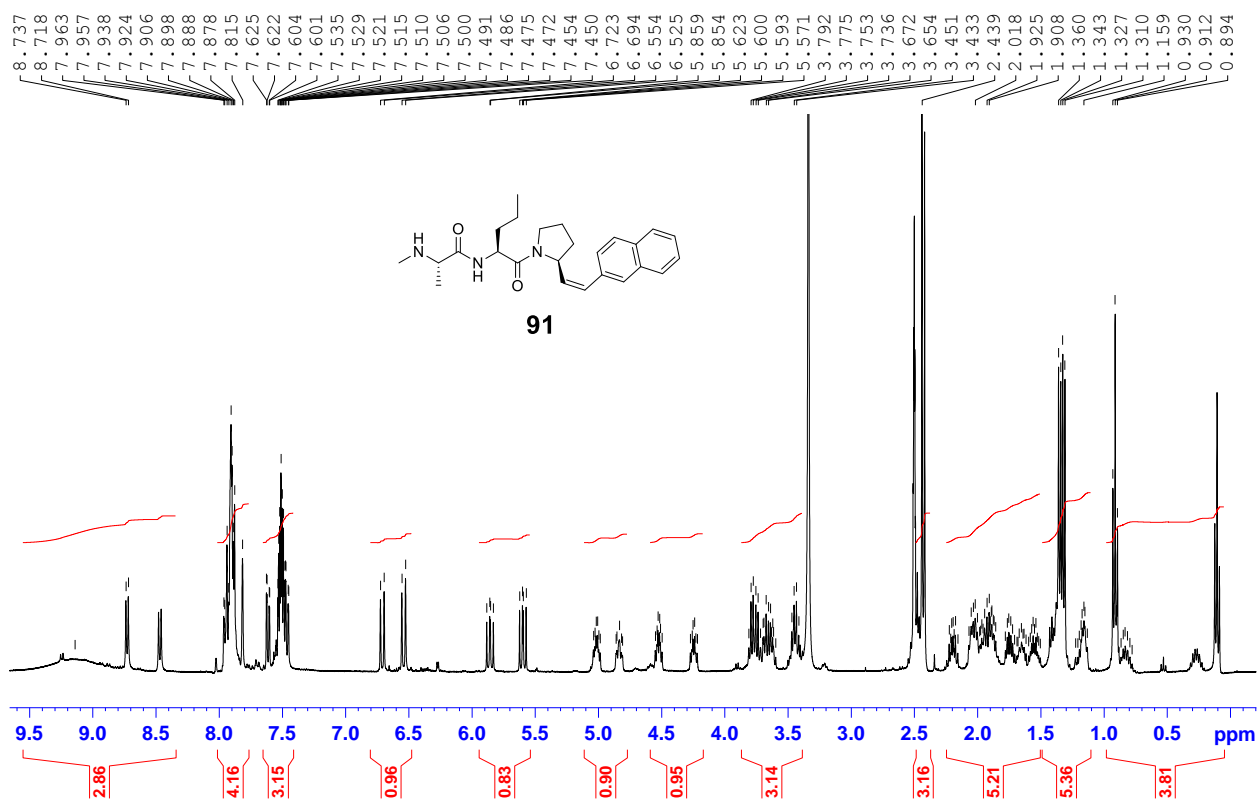
Compound 86 - ¹³C



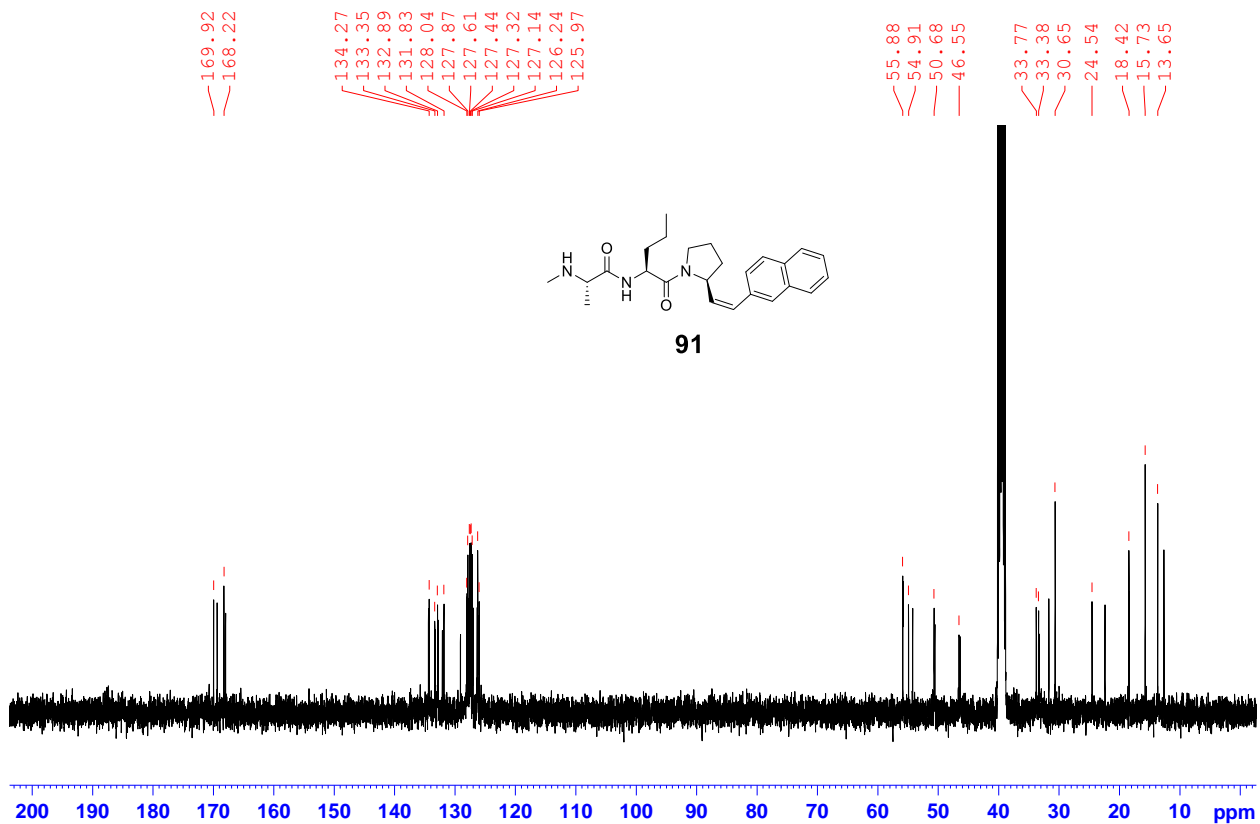
Compound 88 - 1H



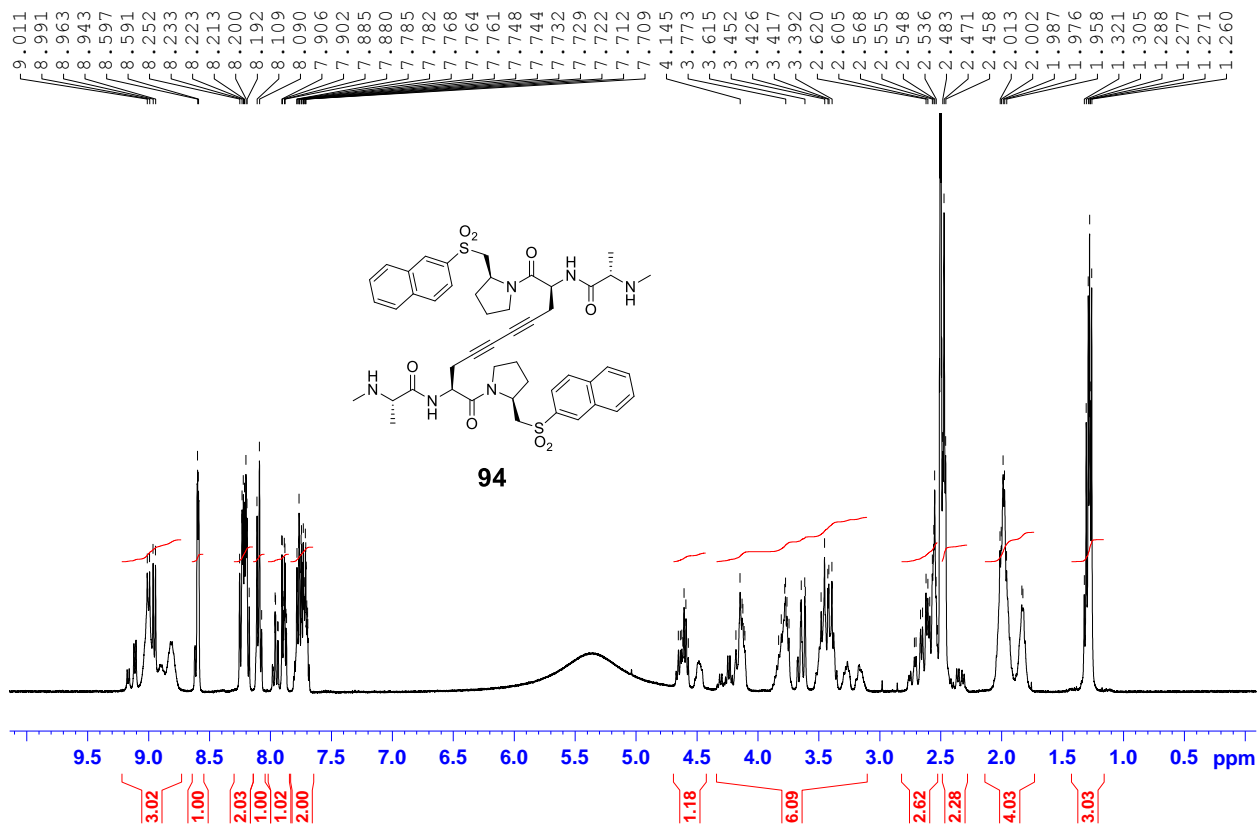
Compound 91 - ¹H



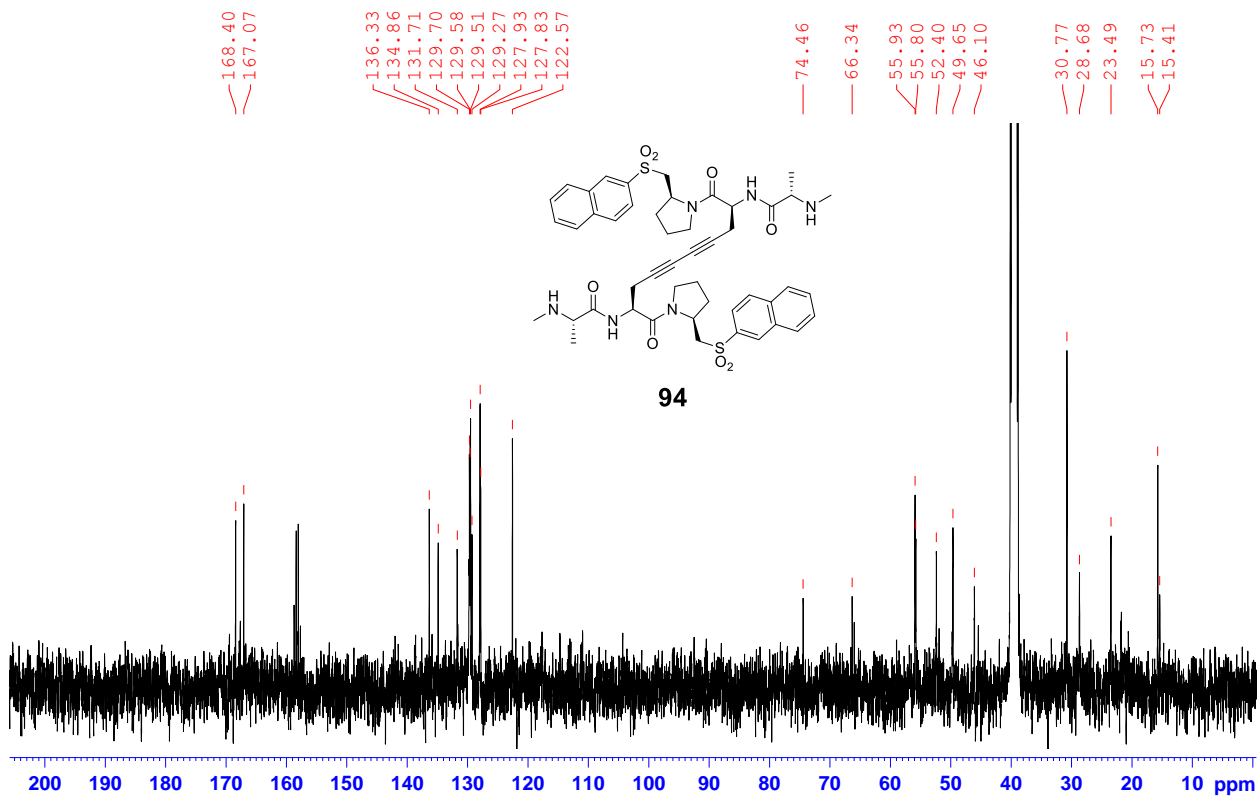
Compound 91 - ¹³C



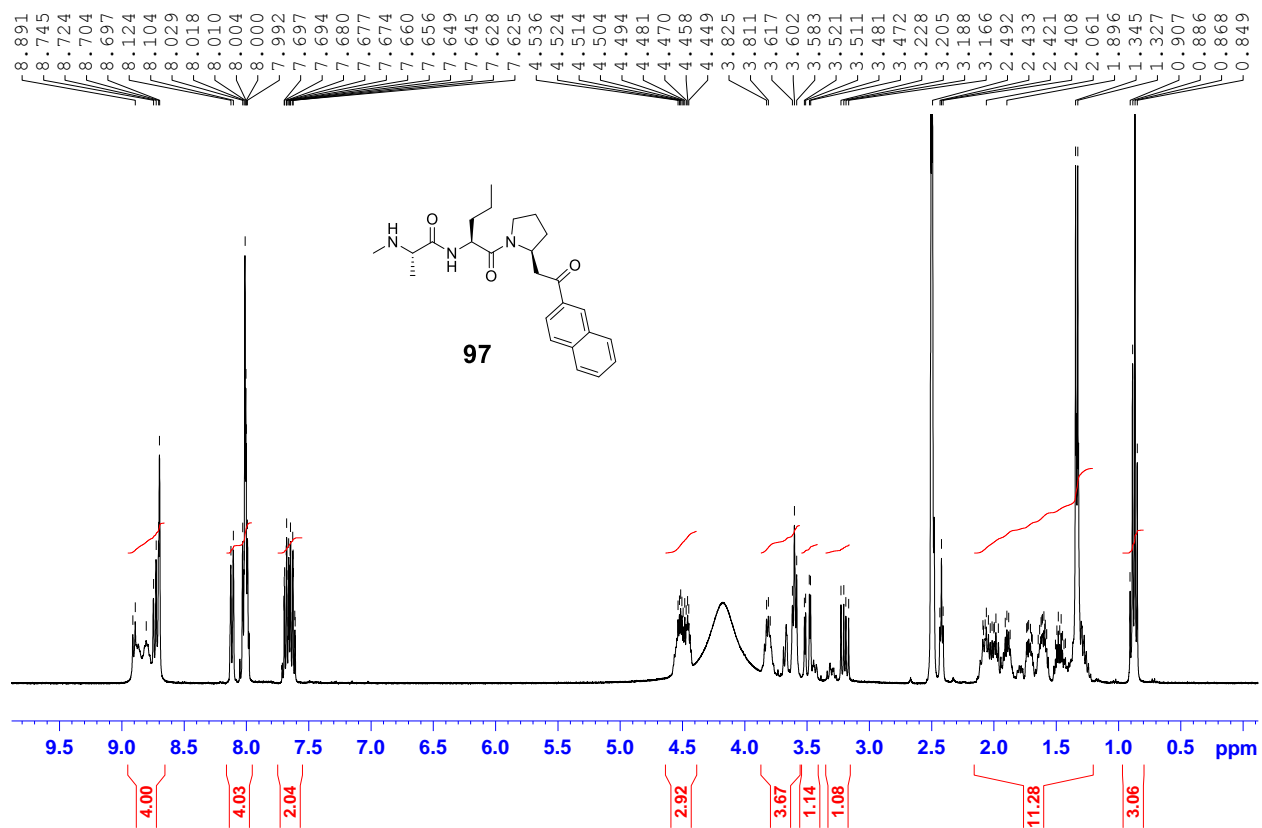
Compound 94 - 1H



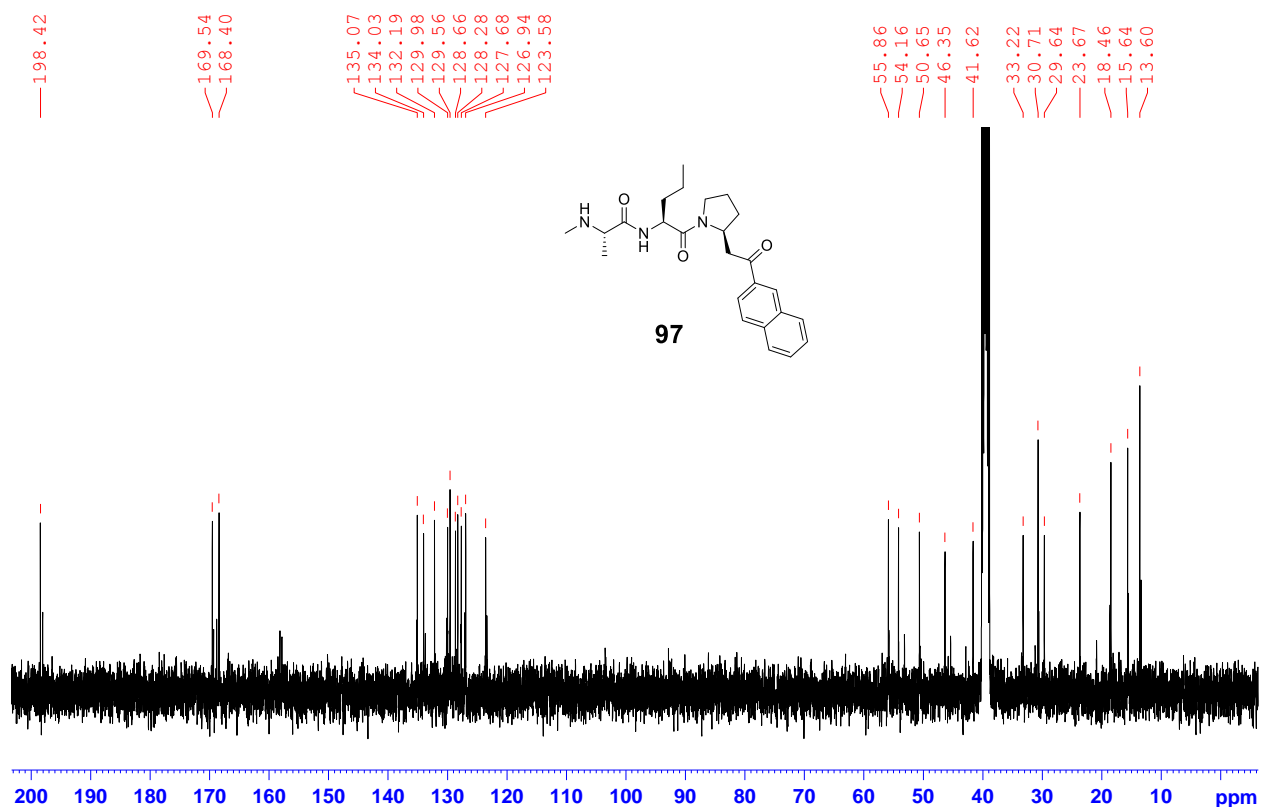
Compound 94 - 13C



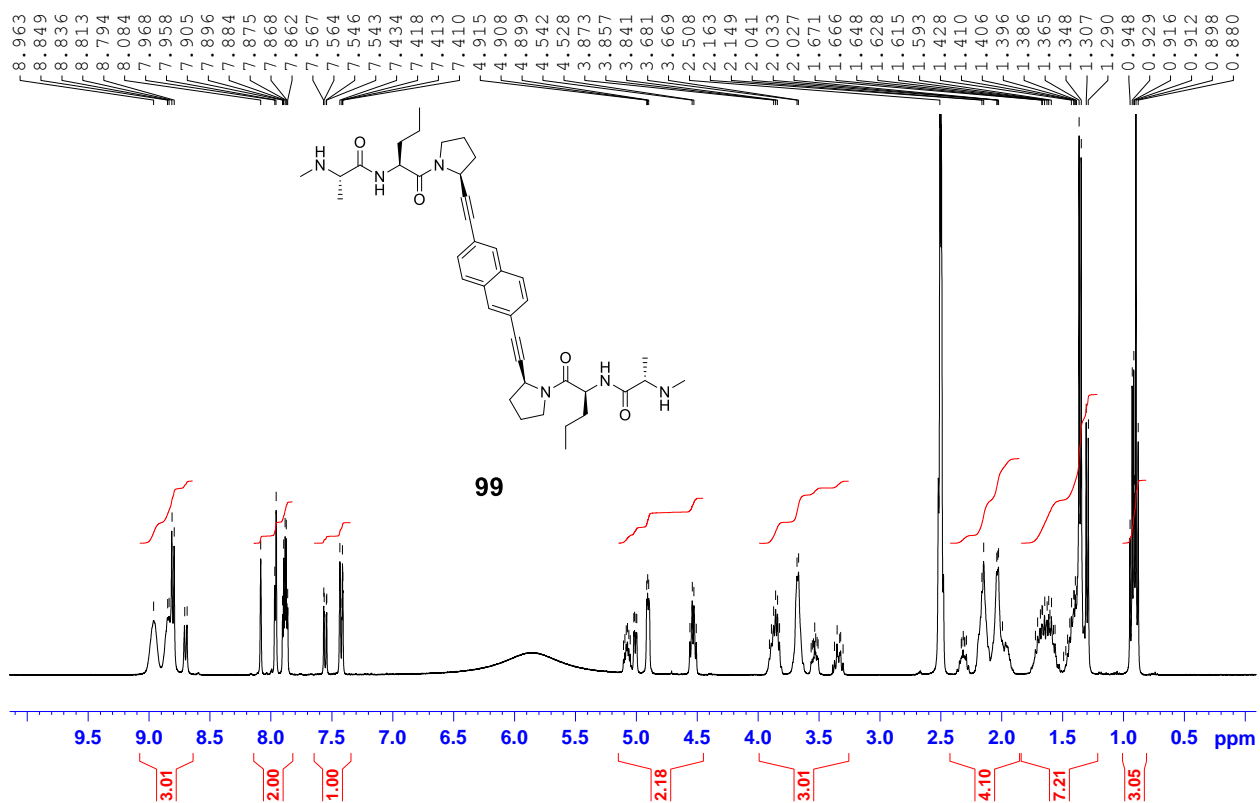
Compound 97 - ¹H



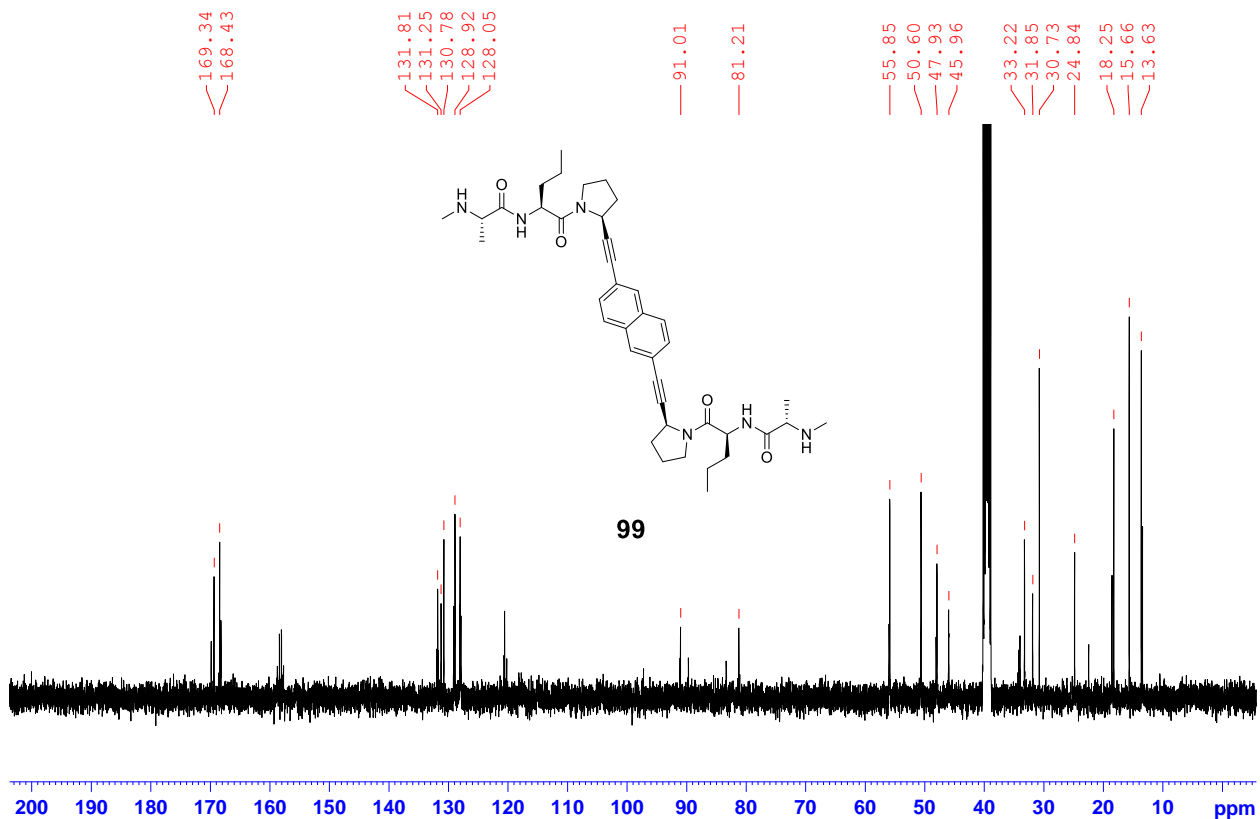
Compound 97 - ¹³C



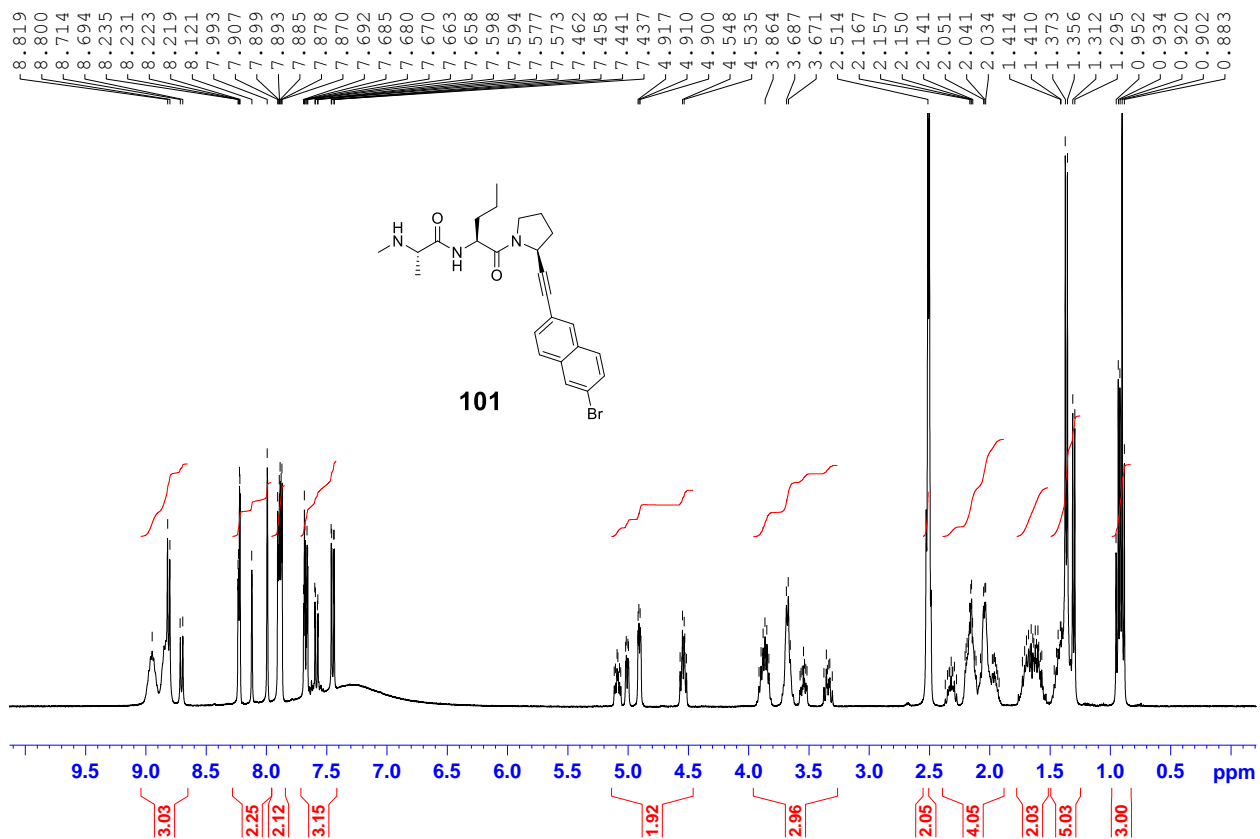
Compound 99 - ¹H



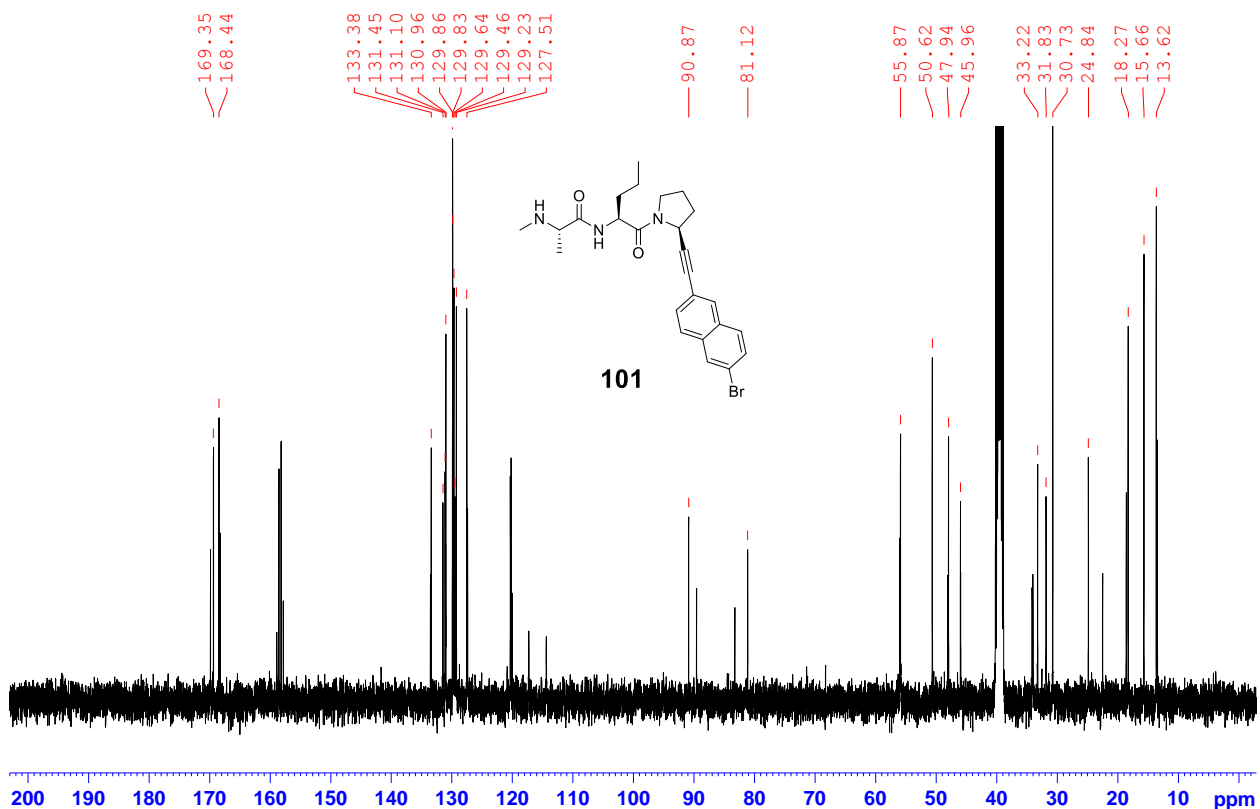
Compound 99 - ¹³C



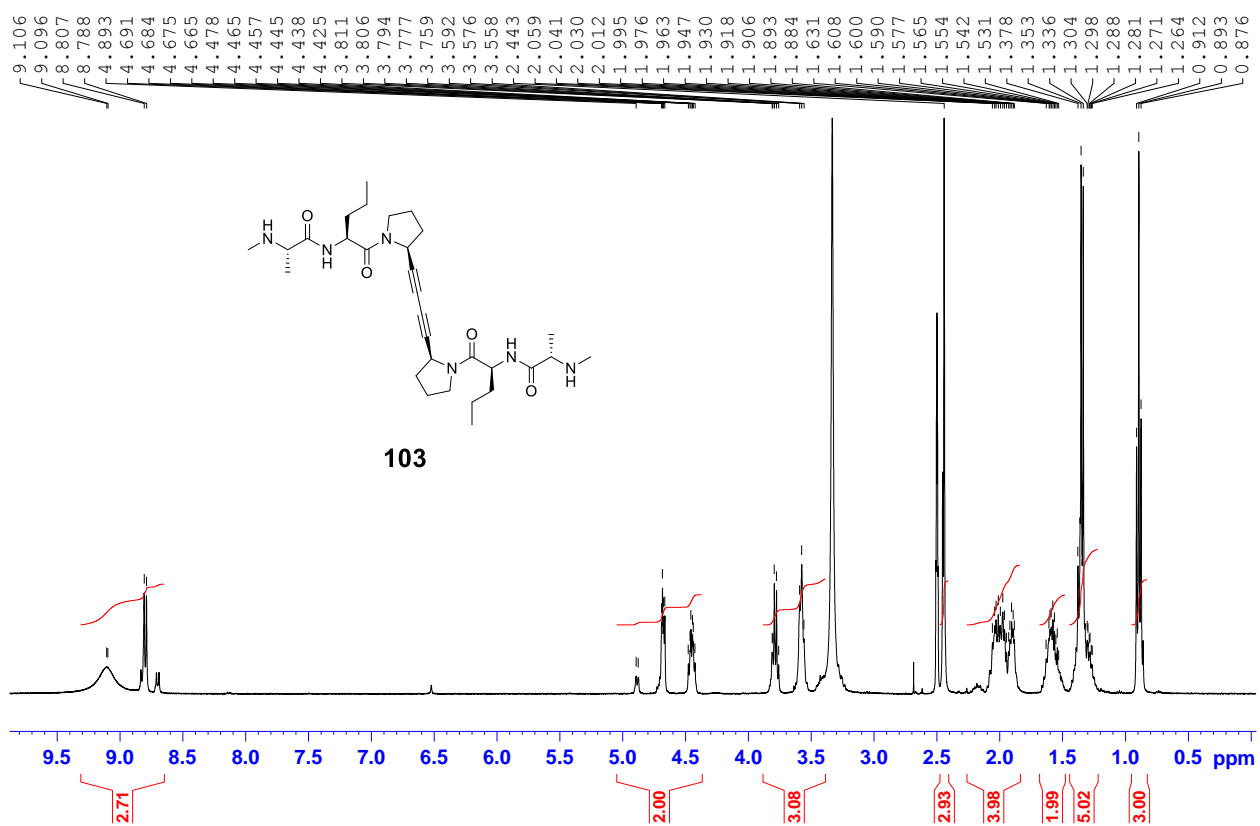
Compound 101 - ¹H



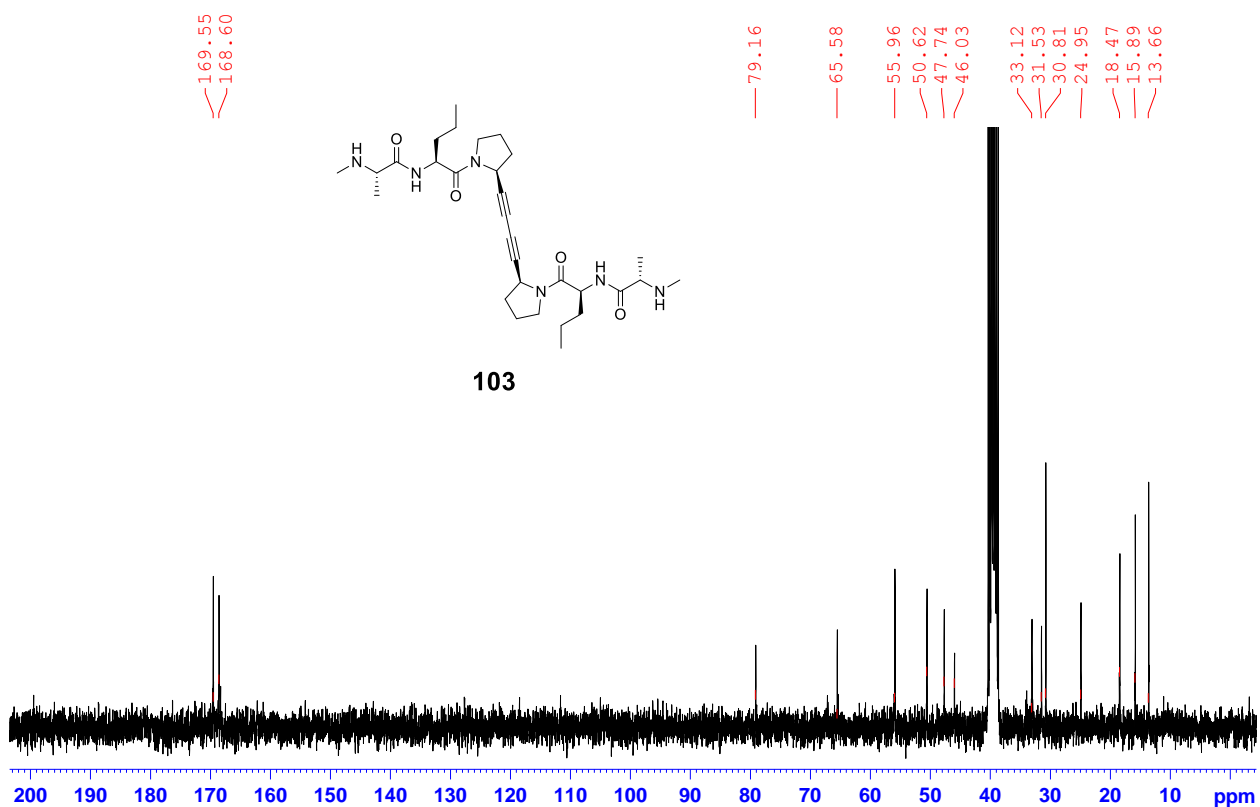
Compound 101 - ¹³C



Compound 103 -1H

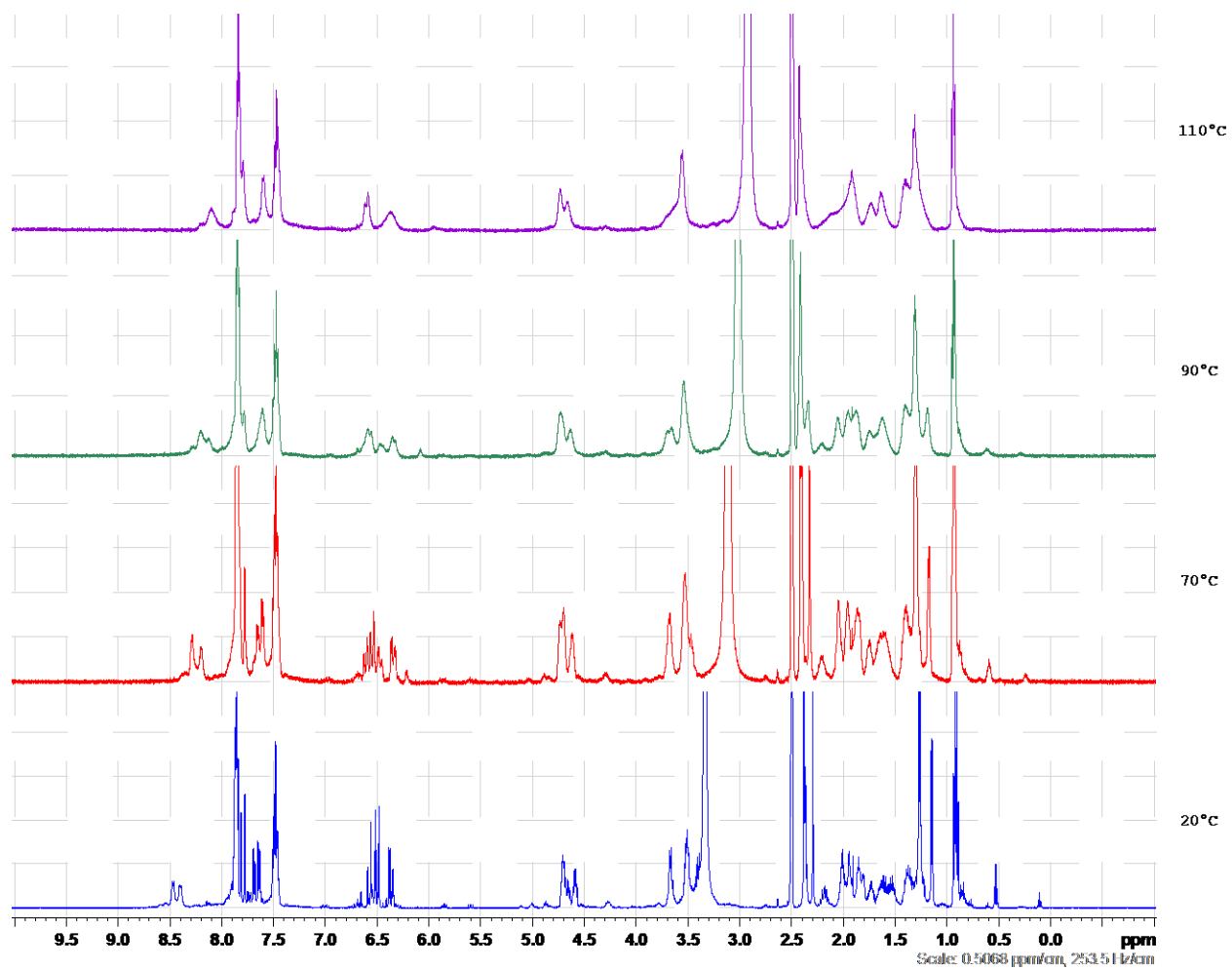


Compound 103 - 13C



Compound **88** – ^1H VT NMR to show pea coalescence

^1H NMR – KM-02-104_vTexp1



Compound **91** - ^1H VT NMR to show peak coalescence

^1H NMR - KM-02-090_HCl_VTexp1

